Gaspar Mendes do Rego

Arc-Induced Long-Period Fibre Gratings. Fabrication and Their Applications in Optical Communications and Sensing

Thesis presented to the University of Porto for the degree of Ph.D. in Engineering Sciences

Department of Electrical and Computer Engineering
Faculty of Engineering, University of Porto
July 2006

Projecto co-financiado pelo fundo Social Europeu no âmbito do concurso Público 2/5.3/PRODEP/2001, pedido de financiamento nº 1012.007, da medida 5/acção 5.3 – Formação Avançada de Docentes do Ensino Superior submetido pela Escola Superior de Tecnologia e Gestão do Instituto Politécnico de Viana do Castelo.

Arc-Induced Long-Period Fibre Gratings

Fabrication and Their Applications in Optical Communications and Sensing

Thesis approved by

José Alfredo Ribeiro da Silva Matos, Chair
Full Professor of the Department of Electrical and Computer Engineering
Faculty of Engineering, University of Porto

Oleg G. Okhotnikov, External examiner
Head of Ultrafast and Intense Optics Group
Tampere University of Technology

Paulo Miguel Nepomuceno Pereira Monteiro, External examiner
Associate Professor of the University of Aveiro

Henrique Manuel de Castro Faria Salgado, Supervisor
Associate Professor of the Department of Electrical and Computer Engineering
Faculty of Engineering, University of Porto

José Luís Campos de Oliveira Santos, Co-Supervisor
Associate Professor of the Department of Physics
Faculty of Sciences, University of Porto

Armindo Luís Vilar Soares Lage
Assistant Professor of the Department of Electrical and Computer Engineering
Faculty of Engineering, University of Porto

Date approved: July 17, 2006

It is not because things are difficult that we do not dare; it is because we do not dare that they are difficult.

Não é porque as coisas nos parecem inacessíveis que não ousamos; é porque não ousamos que elas nos parecem inacessíveis.

Lucius Annaeus Seneca

Roman Philosopher (4 BC-AD 65)

To my wife, Elda and to my sons, Rodrigo and Pedro

To my mother, Isilda and to the memory of my father, Joaquim

Acknowledgements

To my supervisors, José Luís Santos and Henrique Salgado, for their dedication, encouraging and on time help. I also would like to thank José Luís Santos for giving me the opportunity to develop this research in the Unity of Optoelectronics and Electronics Systems of INESC-Porto.

To Paulo Marques for his permanent dedication through out this project.

To Manuel Carlos Torres for his friendship, for his company during the three years that we spent commuting between Barroselas and Porto and also for his technical support. Indeed, without his interest and commitment this work would be much poorer. Therefore, thank you, thank you very much for all.

To Oleg Okhotnikov who gave the first step towards the fabrication of arc-induced gratings and to Vladimir Sulimov for his knowledge and dedication allowing me to start this project on the right foot!

To Florian Durr for his friendship and hard work regarding stress measurements. To Hans Limberger for his interest, helpful discussions and in particular, for allowing me to work at EPFL-Lausanne.

To Alberto Fernandez Fernandez and Andrei Gusarov for a fruitful collaboration regarding the study on the effect of gamma radiation on long-period fibre gratings.

To Evgeny Dianov, Sergei Semjonov, Sergei Vasiliev and Konstantini Golant for supplying most of the fibres used in this work and also for helpful discussions.

To Walter Margulis for supplying the silica capillaries used in the estimation of the fibre temperature.

To Bernd Shröder and Luís Belchior for their collaboration, interest and dedication regarding the measurement of the fibre temperature with the thermocouples.

To Filipe Pinto and Alberto Maia for their dedication concerning the development of the power supply.

To Oleg Ivanov for his help regarding the theory and simulations of long-period fibre gratings.

To Paulo Caldas for his excellent work whilst replacing me at Escola Superior de Tecnologia e Gestão de Viana do Castelo.

To José Manuel Baptista for his friendship, genuine interest, support and fruitful collaborations.

To João Ferreira for his help regarding the elaboration of the Labview programs.

To Francisco Araújo for his interest and helpful discussions. In particular, I would like to congratulate him for his interesting idea regarding the fusion between fishing and Optics!

To Modesto Morais for his friendship, interest and dedication regarding the measurement of geometrical parameters of the fibres and also on the measurement of the polarisation dependent loss of long-period gratings.

To João Chamma for his dedication regarding gratings simulations and to Rosane Falate for her collaboration in performing experimental work.

To Orlando Frazão e Rosa Romero for their collaboration concerning the applications of the electric arc technique, namely, apodisation of fibre Bragg gratings and the fabrication of sampled fibre Bragg gratings.

To Albano Costa, Ernesto Pinheiro and Joaquim Cardoso for their technical support in an initial part of this project. A special thanks to Francisco Carpinteiro for his help regarding electrode's polishing and mechanical gratings.

To João Abrantes and Vítor Leal for their interest and helpful discussions regarding the measurement of the fibre temperature.

To José Luís Costa and Luís Miguel Bernardo for their collaboration regarding the measurement of the fibre temperature based on the blackbody radiation.

To Lourenço Castro, from Cabelte S.A., for allowing using their facilities and to Nuno Pontes and Alexandre Rodrigues for measuring the refractive index profiles of the fibres.

To Ireneu Dias for his interest and help on the thermocouple's patent submission.

To my colleagues and friends from UOSE, Miguel Melo, Rui Morais, Daniel Alexandre, Joel Carvalho, Paulo Moreira, Pedro Jorge, Jaime Viegas, Susana Silva, Carla Rosa, Nuno Pinto and Dionísio Pereira for their interest, support and mainly for being so comprehensive! A special thanks to Luísa Mendonça for being so kind and professional.

To my colleagues and friends of ESTG, in particular, Joana Santos, Paulo Costa, Preciosa Pires and Paulo Fernandes. I also would like to thank Lígia Martins as far as the Prodep funding is concerned.

To my family, for their support and understanding along this project.

Finally, to the European Community through the program PRODEP III - Medida 5 - Acção 5.3. - Formação Avançada de Docentes do Ensino Superior, integrada no Eixo 3, for the grant conceded allowing me fulltime dedication to research.

Summary of the thesis

This thesis is dedicated to the fabrication, through electric arc discharges, of long-period fibre gratings and to their applications in optical communications and sensing fields.

The main theoretical aspects of long-period gratings are presented. The several mechanisms proposed in the literature for the formation of arc-induced gratings are discussed. In particular, the effect of stress relaxation is investigated for the first time through the measurement of the tomographic stress profiles of these gratings.

The temperature is a key parameter for the understanding of the formation mechanisms and, therefore, two methods to estimate the temperature reached by the fibre whilst being submitted to electric arc discharges are presented. One method is based on the blackbody radiation and the other on electrically insulated thermocouples assembled in situ. The latter technique was submitted to the Portuguese Patent Institute.

The fabrication of long-period gratings using the electric arc technique is described in detail. The several setups that were implemented during this work in order to improve the fabrication method are also presented.

The influence of the fabrication parameters on the characteristics and properties of arc-induced gratings is discussed. It was found that by changing the fabrication conditions it is possible to modify the sensitivity of the gratings to physical parameters, such as, temperature and strain. This important property of the electric arc technique has not been demonstrated, so far, by any other technique.

The thermal behaviour of the produced gratings was also investigated and it was demonstrated that the ones induced in Ge-free fibres, in particular, in Er/Al co-doped fibres show a linear behaviour on temperature up to 700 ºC. Arc-induced gratings were also shown to exhibit very high temperature stability. These are important properties for development of high temperature sensors.

The effect of gamma radiation on the properties of gratings arc-induced in pure-silica-core fibres was also studied for the first time, and the results obtained enable one to conclude that those gratings are very promising to perform sensing in radiation environments.

A new technique to mechanically induce long-period fibre gratings is presented. A fully characterisation of the produced gratings is given. Two straightforward applications of mechanical gratings are also demonstrated.

Other devices fabricated with the electric arc technique, such as, phase-shifted short and long-period gratings are briefly discussed. Special attention is given to the apodisation of fibre Bragg gratings and to the fabrication of sampled fibre Bragg gratings. The fabrication of core mode blockers to implement bandpass filters is also presented.

Finally, several applications of arc-induced gratings in optical communications and sensing are given, being of particular importance the sensor head developed for the simultaneous measurement of temperature and strain based on a single long-period grating having two sections fabricated with different parameters.

Sumário da tese

Esta tese é dedicada à fabricação de redes de período longo em fibra óptica por aplicação de descargas eléctricas e às suas aplicações em comunicações ópticas e sensores.

Os aspectos teóricos fundamentais para a compreensão das redes de período longo são aqui apresentados e são discutidos os vários mecanismos propostos na literatura subjacentes à formação das redes por arco eléctrico. Em particular, é investigado pela primeira vez o efeito da relaxação das tensões intrínsecas da fibra, através da medição dos respectivos perfis tomográficos.

A temperatura é um parâmetro fundamental para se compreender os mecanismos de formação das redes. Assim, são apresentados dois métodos para estimar a temperatura atingida pela fibra enquanto submetida a descargas eléctricas. Um método baseia-se na radiação do corpo negro e o outro em termopares isolados electricamente e fabricados *in situ*. Esta última técnica foi submetida ao Instituto Português de Patentes.

É descrita a fabricação de redes de período longo usando a técnica do arco eléctrico. As várias montagens que foram implementadas ao longo deste trabalho de forma a melhorar o método de fabricação são também apresentadas.

A influência dos parâmetros de escrita nas características e propriedades das redes induzidas por arco eléctrico é discutida. Verificou-se que por alteração das condições de fabricação é possível modificar a sensibilidade das redes a variações de parâmetros físicos como a temperatura e a deformação. Esta importante propriedade da técnica do arco eléctrico ainda não foi demonstrada por nenhuma outra técnica.

O comportamento térmico das redes produzidas foi investigado e demonstrou-se que as redes induzidas em fibras sem germânio, em particular em fibras co-dopadas com érbio e alumínio, exibem um comportamento linear com a temperatura até 700 ºC. Como as redes de período longo também suportam temperaturas elevadas estão assim reunidas duas condições importantes para o desenvolvimento de sensores a utilizar a altas temperaturas.

O efeito da radiação gama nas propriedades das redes induzidas por arco eléctrico em fibras com núcleo de sílica pura foi estudado pela primeira vez, e os resultados obtidos permitem concluir que essas redes são muito promissoras para ser usadas como sensores em ambientes radioactivos.

É apresentada uma nova técnica para fabricar mecanicamente redes de período longo, bem como uma caracterização exaustiva das redes produzidas. Duas aplicações simples destas redes são ainda analisadas.

Também são brevemente discutidos outros dispositivos fabricados pela técnica do arco eléctrico, tais como, redes de Bragg e de período longo com desvio de fase. É dada especial

atenção à apodização de redes de Bragg e à fabricação de redes de Bragg amostradas. É ainda descrita a fabricação de bloqueadores do modo fundamental a utilizar na implementação de filtros passa-banda.

Finalmente são apresentadas várias aplicações das redes produzidas por arco eléctrico quer em comunicações ópticas quer como sensores, sendo de particular importância a cabeça sensora desenvolvida para a medição simultânea de temperatura e deformação, baseada numa única rede possuindo duas secções fabricadas com diferentes parâmetros de escrita.

Sommaire de la thèse

Cette thèse est dédiquée à la fabrication de réseaux à longue période en fibre optique par des décharges d'arc électrique et à leurs applications en communications et senseurs optiques.

La théorie fondamentale pour comprendre les réseaux à longue période est présentée. Les divers mécanismes proposés dans la littérature pour la formation de ces réseaux on été discutés et les profils de contraintes résiduelles des réseaux on été mesurés pour la première fois.

La température est un paramètre très important pour comprendre les mécanismes de formation des réseaux. On présent deux méthodes pour estimer la température de la fibre pendant la décharge de l'arc électrique. Une méthode est basée sur la radiation du corps noire et l'autre sur des thermocouples isolés électriquement et assemblés in situ. La dernière technique a été soumise à l'Institut Portugais des Patents.

La fabrication de réseaux de longue périodicité par des décharges d'arc électrique est décrite. Les divers montages expérimentaux qui ont été exécutés dans ce travaille pour améliorer la méthode de fabrication sont aussi présentée.

L'influence des paramètres de fabrication sur les propriétés des réseaux est discutée. On s'est aperçu que, par le changement des paramètres de fabrication, on peut modifier la sensibilité des réseaux aux paramètres physiques, comme par exemple, la température et la déformation. Ces importantes propriétés obtenues par la technique de l'arc électrique arc n'ont pas été démontrées par d'autres techniques.

Le comportement thermique des réseaux fabriqués a été investigué et on a démontré que les réseaux en fibre optiques sans germanium, et, en particulier, en fibre optique co-dopée avec erbium et aluminium, montrent un comportement linéaire avec la température jusqu'à 700 ºC. Les réseaux fabriqués par les décharges supportent aussi les températures élevées et, pourtant, ils peuvent être utilisés comme senseurs à haute température.

L'effet de la radiation gamma sur les propriétés des réseaux, induit dans les fibres avec en noyau de pure silice a aussi été étudié pour la première fois, et les résultats obtenus permettent de conclure que ces réseaux peuvent être utilisées comme senseurs dans des environments radioactives.

Une nouvelle technique pour fabriquer mécaniquement des réseaux en fibre optique de longue périodicité et la caractérisation des réseaux produits sont présentées. Deux applications simples de ces réseaux sont analysées.

D'autres dispositifs fabriqués par les décharges d'arc électrique sont discutés superficiellement, comme par exemple, les réseaux de Bragg et à longue période avec un écart de phase. Une attention spéciale est donnée à l'apodisation de réseaux de Bragg et à la

fabrication des réseaux de Bragg échantillonné. La fabrication d’un bloqueur du mode fondamentale, pour être utilisé dans un filtre passe-bande, est aussi décrite.

Finalement, de différentes applications des réseaux gravés par arc électrique sont présentées, particulièrement, en communications optiques et en senseurs en fibre. Un senseur important a été développé pour mesurer simultanément la température et la déformation; il est basé dans un seul réseau avec deux sections fabriquées en utilisant des paramètres de gravure différents.

Table of contents

1

Introduction

1.1 Motivation

It is well known that the fibre Bragg grating technology had an enormous impact in telecommunications and in fibre sensing. Since the appearance of long-period fibre gratings that it was expected that they could play a similar role and therefore, the question for us was "Which fabrication technology can provide gratings with the best performance?"

In an early stage of this work several advantages of the electric arc technique over the most common used technique that is based on UV radiation were already identified. In particular, the flexibility of the technique, its inexpensiveness and the fact that, in principle, it could be applied to any kind of fibre were strong arguments to push us towards a more detailed study. It had also been demonstrated that these gratings could stand high temperatures. However, besides the obvious application as a high temperature sensor, little was known regarding the formation mechanisms of these gratings.

The drawbacks of this technology and the lack of knowledge regarding issues related to the gratings properties led us to define four main topics of research. First, the development of a new infrastructure that allows a higher reproducibility and flexibility. In particular, that would allow the change of the fabrication parameters from point-to-point in order to produce complex optical components and that at the same time the dimensions of the arc discharge could be controlled in order to enable the decrease of the gratings period. Second, the fabrication and the fully characterisation of arc-induced gratings. Third, to have a better understanding of the mechanisms underlying the gratings formation. Finally, to present new applications of these gratings. The degree of achievement regarding the initial goals can be assessed in this thesis. Meanwhile, it can be anticipated that other advantages of this technique and of the gratings produced have been identified during this project, some of which where already employed in the applications presented and others will be certainly used in future work.

1.2 Structure of the thesis

Chapter 1 gives the motivation and describes the structure of the thesis.

Chapter 2 presents the physical concepts linked to long-period gratings. The fabrication techniques available are briefly described and finally some examples of applications of long-period gratings are given.

Chapter 3 gives the basic theory of long-period gratings and discusses the different potential mechanisms responsible for their formation.

Chapter 4 describes the electric arc technique that was employed to produce the long-period fibre gratings. Two methods are presented to estimate the temperature reached by the fibre during the arc discharges, one method being based on theory of the blackbody radiation and the other on the use of electrically insulated thermocouples.

Chapter 5 analyses the properties of arc-induced gratings. This chapter starts by discussing the influence of the fabrication parameters on the spectra of the long-period gratings and also on their sensitivity to changes of physical parameters. Afterwards their thermal behaviour and polarisation dependent loss is addressed. The influence of exposing the gratings to uniform UV radiation is also investigated. Finally, the effect of ionising radiation on the properties of arc-induced gratings is discussed.

Chapter 6 describes a new technique to mechanically induce long-period fibre gratings. A fully characterisation of the gratings produced including the analysis of their sensitivity to temperature, strain and load is presented. The polarisation dependent loss of these gratings is also discussed. Finally, two applications of mechanical gratings are also given. The first is a EDFA’s gain flattener and the second a tunable filter for the measurement of physical parameters with a wide dynamic range.

Chapter 7 refers to applications of the electric arc technique other than the production of simple long-period gratings. Particular attention is given to the apodisation of fibre Bragg gratings, the fabrication of sampled fibre Bragg gratings based on the writing of a Bragg grating on top of a long-period grating and also to the fabrication of core mode blockers.

Chapter 8 presents several applications of long-period gratings. In the optics communications domain, the equalisation of erbium doped fibre amplifiers gain spectra and the suppression of amplified spontaneous emission in Er/Yb fibre lasers. In the sensing domain several applications are addressed namely, the use of long-period gratings for the simultaneous measurement of temperature and strain, measurements of refractive index and also the possibility of using them in the monitoring of the structural integrity in nuclear facilities.

Chapter 9 summarises the thesis and gives suggestions for future work.

1.3 Contributions

In this work, based on its practical interest, it is possible to classify the presented novelties in three different levels. Since the beginning that several minor contributions were given, such as, the apodisation of fibre Bragg gratings and the fabrication of sampled fibre Bragg gratings, both based on the interactions between UV radiation and the arc discharges, and also the new technique to mechanically induce long-period gratings. At an intermediate stage, I would highlight the tomographic stress measurements, a further step towards the understanding of the formation mechanisms of these gratings and the demonstration of the high temperature stability of arc-induced gratings as well as the linear thermal behaviour obtained in Ge-free fibres that enable the development of enhanced temperature sensors. However, there are still three issues that require special attention.

Measurement of the fibre temperature

The temperature reached by an optical fibre whilst submitted to electric arc discharges is a key parameter for determining the mechanisms underlying gratings formation since they are triggered by a thermal effect. The technique employed to achieve such goal, consisting on the fabrication of a thermocouple inside a silica capillary, is by itself a remarkable contribution

since the electrically insulated temperature microsensor assembled this way has high potential application in different areas as indicated in the Portuguese patent submitted.

Tuning the gratings sensitivities

The ability to modify the gratings spectra in terms of choosing their resonant wavelengths and their transmission loss was known since an early stage of this work. However, the possibility to tune the temperature and strain sensitivities by changing the fabrication parameters is a recent achievement. This property of the electric arc technique was not yet demonstrated by any other fabrication technique. Its potential is well patented in the sensor head developed for the simultaneous measurement of temperature and strain described in Chapter 8.

Sensors for radiation environments

A study on the effect of gamma radiation on the gratings spectra and also on the temperature and strain sensitivities revealed that gratings arc-induced in pure-silica-core fibres are insensitive to doses up to 0.5 MGy, being therefore, excellent candidates for multi-parameter measurement in radiation environments. In particular, the relative low sensitivity to temperature and high sensitivity to strain allows their use in the monitoring of the structural integrity of nuclear facilities. This result is a very important one, since nowadays people are aware of ambient issues and also of the requirement to decrease the dependence on petrol, therefore the building of non pollutant sources of energy, such as, nuclear facilities is again in debate.

1.4 List of publications

Patents

G. Rego, L. M. B. N. F. Santos, B. Schröder, P. V. S. Marques, J. L. Santos, H. M. Salgado, Micro-Sensor de Temperatura Isolado Electricamente, PAT 103160, Submitted 6th July 2004, Published 31st January 2006 and Conceded 22nd June 2006.

Papers published in international journals

1. G. Rego, H. M. Salgado, J. L. Santos, *Interrogation of a Fiber Bragg Grating using a Mechanically Induced Long-Period Fiber Grating*, *IEEE Sensors Journal* (to be published).

2. G. Rego, O. Ivanov, P. V. S. Marques, *Demonstration of Coupling to Symmetric and Antisymmetric Cladding modes in Arc-Induced Long-Period Fiber Gratings*, *Optics Express* (to be published).

3. R. Falate, O. Frazão, G. Rego, J. L. Fabris, J. L. Santos, *Refractometric Sensor Based on a Phase-Shifted Long Period Fiber Grating, Applied Optics*, vol. 45, pp. 5066-5072, July 2006.

4. G. Rego, J. L. Santos, H. M. Salgado, *Polarization Dependent Loss of Arc-Induced Long-Period Fibre Gratings, Optics Communications*, vol. 262, pp. 152-156, June 2006.

5. J. M. Baptista, S. F. Santos, G. Rego, O. Frazão, J. L. Santos, *Measurement of Micro-Displacement using a Long Period Fiber Grating in a Self-Referenced Fiber Optic Intensity Sensor, Optics Communications*, vol. 260, No.1, pp. 8-11, April 2006.

6. G. Rego, F. Dürr, P. V. S. Marques, H. G. Limberger, *Strong Asymmetric Stresses Arc-Induced in Pre-Annealed Nitrogen-doped Fibres, Electronics Letters*, vol. 42, No.6, pp. 334-335, March 2006.

7. G. Rego, P. V. S. Marques, J. L. Santos, H. M. Salgado, *Estimation of the Fibre Temperature during the Inscription of Arc-Induced Gratings, Optics Communications*, vol. 259, No.2, pp. 620-625, March 2006.

8. G. Rego, J. L. Santos, H. M. Salgado, *Refractive Index Measurement with Long-Period Gratings Arc-Induced in Pure-Silica-Core Fibres, Optics Communications*, vol. 259, No.2, pp. 598-602, March 2006.

9. F. Dürr, G. Rego, P. V. S. Marques, S. L. Semjonov, E. M. Dianov, H. G. Limberger, R. P. Salathé, *Tomographic Stress Profiling of Arc-Induced Long Period Fiber Gratings, Journal of Lightwave and Technology*, vol. 23, No.11, pp. 3947-3953, Nov. 2005.

10. G. Rego, A. Fernandez Fernandez, A. Gusarov, B. Brichard, F. Berghmans, J. L. Santos, H. M. Salgado, *Effect of Ionizing Radiation on the Properties of Long-Period Fiber Gratings, Applied Optics*, vol. 44, No.29, pp. 6258-6263, Oct. 2005.

11. G. Rego, R. Falate, J. L. Fabris, J. L. Santos, H. M. Salgado, S. L. Semjonov, E. M. Dianov, *Arc-Induced Long-Period Gratings in Aluminosilicate Glass Fibers, Optics Letters*, vol. 30, No.16, pp. 2265-2267, Aug. 2005.

12. G. Rego, P. V. S. Marques, H. M. Salgado, J. L. Santos (invited paper), *Arc-Induced Long-Period Gratings, Fiber and Integrated Optics*, vol. 24, No.3-4, pp. 245-259, May 2005.

13. G. Rego, P. V. S. Marques, H. M. Salgado, J. L. Santos, *Simultaneous Measurement of Temperature and Strain based on Arc-Induced Long-Period Fibre Gratings, Electronics Letters*, vol. 41, No.2, pp. 60-62, Jan. 2005.

14. G. Rego, L. M. B. N. F. Santos, B. Schröder, P. V. S. Marques, J. L. Santos, H. M. Salgado, *In Situ Temperature Measurement of an Optical Fiber Submitted to Electric Arc Discharges*, *IEEE Photonics Technology Letters*, vol. 16, No.9, pp. 2111-2113, Sep. 2004.

15. J. M. Baptista, S. Abad, G. Rego, L. A. Ferreira, F. M. Araújo, J. L. Santos, A. S. Lage, *Wavelength Multiplexing of Frequency Based Self-Referenced Fiber Optic Intensity Sensors*, *Optical Engineering*, vol. 43, No.3, pp. 702-707, Mar 2004.

16. G. Rego, J. R. A. Fernandes, J. L. Santos, H. M. Salgado, P. V. S. Marques, *New Technique to Mechanically Induce Long–Period Fibre Gratings*, *Optics Communications*, vol. 220, Nº 1-3, pp. 111-118, May 2003.

17. O. Frazão, R. Romero, G. Rego, P. V. S. Marques, H. M. Salgado, J. L. Santos, *Sampled Fibre Bragg Grating Sensors for Simultaneous Strain and Temperature Measurement*, *Electronics Letters*, vol. 38, No.14, pp. 693-695, July 2002.

18. G. Rego, O. Okhotnikov, E. Dianov, V. Sulimov, *High Temperature Stability of Long-Period Fiber Gratings Produced using an Electric Arc*, *Journal of Lightwave and Technology*, vol. 19, Nº 10, pp. 1574-1579, Oct. 2001.

Papers published in international conferences

1. G. Rego, O. Ivanov, P. V. S. Marques, J. L. Santos, *Investigation of Formation Mechanisms of Arc-Induced Long-Period Fiber Gratings*, *18th International Conference on Optical Fiber Sensors, Proceedings of SPIE* (to be published).

2. R. Falate, O.Frazão, G. Rego, O. Ivanov, H. J. Kalinowski, J. L. Fabris, J. L. Santos, *Bend and Temperature Sensing with Arc-Induced Phase-Shifted Long-Period Fiber Gratings*, *18th International Conference on Optical Fiber Sensors, Proceedings of SPIE* (to be published).

3. J. M. Baptista, S. F. Santos, G. Rego, O. Frazão, J. L. Santos, *Measurement of Angular Rotation using a Long Period Fiber Grating in a Self-Referenced Fiber Optic Intensity Sensor*, *Proceedings of the 18th Annual Meeting of the IEEE Laser & Electro-Optics Society*, pp. 806-807, Oct. 2005.

4. G. Rego, J. L. Santos, H. M. Salgado, *Measurement of the Salinity in Water through Long-Period Gratings Induced in Pure-Silica-Core fibers*, *Recent Advances in Multidisciplinary Applied Physics: Proceedings of the First International Meeting on Applied Physics*, pp. 439-443, Sep. 2005.

5. G. Rego, A. Fernandez Fernandez, J. L. Santos, H. M. Salgado, F. Berghmans, A. Gusarov, *Optical Fiber Sensors for Radiation Environments, Recent Advances in Multidisciplinary Applied Physics: Proceedings of the First International Meeting on Applied Physics*, pp. 433-437, Sep. 2005.

6. G. Rego, F. Dürr, J. C. C. Carvalho, A. Fernandez Fernandez, P. V. S. Marques, H. G. Limberger, *Stress Profiling of Arc-Induced Long-Period Gratings Written in Pure-Silica-Core Fibers*, *17th International Conference on Optical Fiber Sensors, Proceedings of SPIE*, Vol. 5855, pp. 884-887, May 2005.

7. G. Rego, R. Falate, H. J. Kalinowski, J. L. Fabris, P. V. S. Marques, H. M. Salgado, J. L. Santos, *Simultaneous Temperature and Strain Measurement based on Arc-Induced Long-Period Fiber Gratings, 17th International Conference on Optical Fiber Sensors, Proceedings of SPIE*, Vol. 5855, pp. 679-682, May 2005.

8. S. Cazacu, J. M. Martins, G. Rego, S. F. Santos, J. L. Santos, J. M. Baptista, *Micro-Displacement Measurement using a Long-Period Fiber Grating in a Self-Referenced Fiber Optic Intensity Sensor, Proceedings of the 17th Annual Meeting of the IEEE Laser & Electro-Optics Society*, pp. 262-263, Oct. 2004.

9. G. Rego, P. V. S. Marques, H. M. Salgado, J. L. Santos (*invited talk*), *Arc-Induced Long-Period Fiber Gratings, Proceedings of the International Symposium on Advances and Trends in Fiber Optics and Applications*, pp. 58-68, Oct. 2004.

10. G. Rego, P. V. S. Marques, H. M. Salgado, J. L. Santos, *Measurement of the Temperature of an Optical Fiber Submitted to an Electric Arc Discharge*, *Second European Workshop on Optical Fibre Sensors, Proceedings of SPIE, Vol. 5502*, pp. 374-377, June 2004.

11. A. Fernandez Fernandez, G. Rego, A. Gusarov, B. Brichard, J. L. Santos, H. M. Salgado, F. Berghmans, *Evaluation of Long-Period Fiber Grating Temperature Sensors in Nuclear Environments*, *Second European Workshop on Optical Fibre Sensors, Proceedings of SPIE, Vol. 5502*, pp. 88-91, June 2004.

12. O. Frazão, G. Rego, F. M. Araújo, L. A. Ferreira, H. M. Salgado, J. L. Santos, *Simultaneous Measurement of Strain and Temperature Based on Polarization Loss Properties of Arc-Induced Long Period Gratings*, *Second European Workshop on Optical Fibre Sensors, Proceedings of SPIE, Vol. 5502*, pp. 168-171, June 2004.

13. G. Rego, M. Morais, J. L. Santos, H. M. Salgado, *PDL and DGD Measurements of Mechanically Induced Long-Period Fiber Gratings*, *Proceedings of the London Communications Symposium 2003*, pp. 77-80, Sep. 2003.

14. G. Rego, J. L. Santos, P. V. S. Marques, H. M. Salgado, *Study of the Properties of Arc-Induced Long-Period Gratings and Bragg Gratings in B/Ge Doped Fibers, Proceedings of the Bragg Gratings, Photosensitivity and Poling in Glass Waveguides Conference, paper* MD23, pp. 121-123, Sep. 2003.

15. G. Rego, M. Melo, J. L. Santos, H. M. Salgado, *Optical Filters for Fibre Lasers and Amplifiers, Proceedings of the London Communications Symposium 2002*, pp. 49-52, Sep. 2002.

16. R. Romero, O. Frazão, G. Rego, P. V. S Marques, H. M. Salgado, *Sampled Fibre Bragg Gratings Fabrication using an Electric Arc and their Applications, Proceedings of the Course on Photosensitivity in Optical Waveguides and Glasses, paper* 43/WA5, June 2002.

17. G. Rego, R. Romero, O. Frazão, P. V. S Marques, H. M. Salgado, *Apodisation of Uniform Fibre Bragg Gratings using Electric Arc Discharges*, *Proceedings of the Workshop on Fibre and Optical Passive Components*, pp. 13-15, June 2002.

18. J. M. Baptista, S. Abad, G. Rego, L. A. Ferreira, F. M. Araújo, J. L. Santos, A. S. Lage, *Multiplexing of Self-Referenced Fibre Optic Intensity Sensors using Fibre Bragg Gratings and Wavelength Division Couplers, Proceedings of the Optical Fiber Sensors 2002 Conference, paper* TuP30, May 2002.

19. G. Rego, O. Okhotnikov, V. Sulimov, *Writing & Thermal Stability of Long-Period Fibre Gratings Produced using an Electric Arc, Proceedings of the Course on Photosensitivity in Optical Waveguides and Glasses, paper 27 RT4*, Oct. 2001.

20. O. Frazão, G. Rego, M. Lima, A. Teixeira, F. M. Araújo, P. André, J. F. Rocha, H. M. Salgado, *EDFA Gain Flattening using Long-Period Fibre Gratings Based on the Electric Arc Technique, Proceedings of the London Communications Symposium 2001*, pp. 55-57, Sep. 2001.

21. G. Rego, O. Frazão, F. Araújo, V. Sulimov, *Long-Period Fiber Gratings Produced using the Electric Arc Technique for DWDM Communication Systems, Proceedings of the 5th Conference on Systemics, Cybernetics and Informatics,* pp. 178-180, July 2001.

22. G. Rego, O. Okhotnikov, E. Dianov, V. Sulimov, *Long-Period Fiber Gratings Stable at Very High Temperatures, Proceedings of the Bragg Gratings, Photosensitivity and Poling in Glass Waveguides Conference, paper BFB4*, July 2001.

Papers published in national conferences

1. G. Rego, O. V. Ivanov, *Effect of Fiber Microdeformation on the Formation of Gratings Induced by Arc Discharges, Proceedings of the IV Symposium on Enabling Optical Networks and Sensors*, pp. 55-56, June 2006.

2. G. Rego, M. Melo, P. V. S. Marques, J. L. Santos, H. M. Salgado, *Fibre Gratings for Sensing and Communications, Proceedings of the 14th National Physics Conference*, pp. 275-276, Dec. 2005.

3. G. Rego, P. V. S. Marques, J. L. Santos, H. M. Salgado, *Arc Induced Gratings, Proceedings of the III Symposium on Enabling Optical Networks*, pp. 45-50, June 2005.

4. G. Rego, H. M. Salgado, J. L. Santos, *Interrogation of a Fiber Bragg Grating using a Mechanically Induced Long-Period Fiber Grating, Proceedings of the III Symposium on Enabling Optical Networks*, pp. 128-130, June 2005.

5. R. Falate, O. Frazão, G. Rego, J. L. Fabris, J. L. Santos, *Phase-Shifted Long-Period Fiber Gratings based on Electric Arc Discharges, Proceedings of the III Symposium on Enabling Optical Networks*, pp. 51-53, June 2005.

6. G. Rego, P. V. S. Marques, H. M. Salgado, J. L. Santos, *Temperature Measurement of an Optical Fiber Submitted to Electric Arc Discharges, Proceedings of the II Symposium on Enabling Optical Networks*, pp. 63-64, June 2004.

7. G. Rego, P. V. S. Marques, J. L. Santos, H. M. Salgado, *Simultaneous Measurement of Temperature and Strain based on Long-period Gratings written in Standard Fibers using the Arc-discharge Technique, Proceedings of the II Symposium on Enabling Optical Networks*, pp. 91-92, June 2004.

8. G. Rego, J. L. Santos, H. M. Salgado, *Applications of the Electric Arc Technique, Proceedings of the I Symposium on Enabling Optical Networks*, pp. 5-6, June 2003.

9. G. Rego, M. Morais, J. L. Santos, H. M. Salgado, *Polarization Dependent-Loss and Polarization Mode Dispersion Measurements of Mechanically Induced Long-Period Fiber Gratings, Proceedings of the I Symposium on Enabling Optical Networks*, pp. 17-18, June 2003.

10. G. Rego, V. Sulimov, E. Dianov, J. L. Santos, H. M. Salgado, *Thermal Behaviour at High Temperatures of Electric Arc Induced Long-Period Fiber Gratings, Proceedings of the 13th National Physics Conference*, pp. 496-498, Sep. 2002.

11. G. Rego, F. Dürr, H. G. Limberger, S. L. Semjonov, H. M. Salgado, J. L. Santos, *Inscription of Long-Period Gratings in Nitrogen-Doped Fibers Drawn at Different Drawing Tensions, Proceedings of the 13th National Physics Conference*, pp. 506-507, Sept. 2002.

12. G. Rego, R. Romero, O. Frazão, M. Lima, J. L. Santos, H. M. Salgado, *Apodisation of Fiber Bragg Gratings through Electric Arc Discharges*, *Proceedings of the 13th National Physics Conference*, pp. 530-531, Sep. 2002.

13. G. Rego, J. L. Santos, H. M. Salgado, *Electric Arc Induced Long-Period Fiber Gratings for EDFA's Gain Flattening*, *Proceedings of the 13th National Physics Conference*, pp. 532-533, Sep. 2002.

14. G. Rego, J. L. Santos, H. M. Salgado, *Fiber Sensors for Nuclear Environments: Part I*, *Proceedings of the 13th National Physics Conference*, pp. 534-535, Sep. 2002.

15. G. Rego, J. L. Santos, H. M. Salgado, *Fiber Sensors for Nuclear Environments: Part II*, *Proceedings of the 13th National Physics Conference*, pp. 536-537, Sept. 2002.

16. G. Rego, M. Melo, J. L. Santos, H. M. Salgado, *Filters for Fibre Lasers and Amplifiers*, *Proceedings of the 13th National Physics Conference*, pp. 538-540, Sep. 2002.

17. G. Rego, R. Romero, P. V. S. Marques, J. L. Santos, H. M. Salgado, *Influence of Hydrogen Out-Fibre Diffusion on the Resonances of Arc-Induced Long-Period Fibre Gratings*, *Proceedings of the 13th National Physics Conference*, pp. 541-542, Sep. 2002.

18. J. M. Baptista, S. Abad, G. Rego, L. A. Ferreira, F. M. Araújo, J. L. Santos, A. S. Lage, *Multiplexagem em Comprimento de Onda de Sensores de Intensidade em Fibra Óptica Auto-Referenciados*, *Proceedings of the 13th National Physics Conference*, pp. 547-548, Sep. 2002.

19. O. Frazão, R. Romero, G. Rego, P. V. S. Marques, H. M. Salgado, J. L. Santos, *Aplicações das Redes de Período Longo como Elemento Sensor*, *Proceedings of the 13th National Physics Conference*, pp. 560-561, Sep. 2002.

20. O. Frazão, R. Romero, G. Rego, P. V. S. Marques, H. M. Salgado, J. L. Santos, *Sensor Óptico para Medição Simultânea de Temperatura e Deformação*, *Proceedings of the 13th National Physics Conference*, pp. 562-563, Sep. 2002.

21. R. Romero, G. Rego, O. Frazão, P. V. S. Marques, H. M. Salgado, *New Technique for Sampled Fibre Bragg Gratings Fabrication*, *Proceedings of the 13th National Physics Conference*, pp. 580-581, Sep. 2002.

22. R. Romero, O. Frazão, G. Rego, P. V. S. Marques, H. M. Salgado, *Multiwavelength Fibre Ring Laser Source using Sampled Fibre Bragg Gratings*, *Proceedings of the 13th National Physics Conference*, pp. 582-583, Sep. 2002.

2

Long-period fibre gratings

2.1 Physical concepts

A long-period fibre grating (LPFG) is a periodic modulation in the refractive index of the fibre's core (and cladding) performed by some means, such as, an electric arc discharge. LPFGs have typically periods between 100 μm and 1 mm, being much longer than the well known fibre Bragg gratings (FBGs) that have periods lower than 1 μm (therefore, their name: long-period gratings). Another distinction between these two kind of gratings, is that FBGs couple two counter-propagating guided modes whilst, for LPFGs the core mode is coupled, at specific resonance wavelengths, to several cladding modes propagating in the same direction till being completely attenuated by scattering in the air-cladding interface, by curvature losses and in the fibre coating. The gratings spectra are characterised by dips at those wavelengths that satisfy the resonance condition, that is, the values of the resonance wavelengths equals the product grating period times the difference between the effective refractive indices of the core mode and the respective cladding mode. In general, LPFGs possess low insertion loss (<0.2 dB), low back reflection (<-80 dB), large bandwidth (10-20 nm), high coupling strength (>25 dB is achievable) and the polarisation dependent loss (that can be as high as 10 dB) depends on the fabrication technique and respective fabrication parameters. These gratings are very sensitive to changes of physical parameters, such as, temperature and strain. In other words, the gratings spectra, resonance wavelengths and coupling strengths, can be altered by heating or stretching the gratings and therefore, they behave as wavelength selective transmissive filters with applications in the fields of optical communications and sensing.

This concept of LPFG, in which the core mode is coupled to several cladding modes, appeared in 1996 [1]. The formation of these former band rejection filters was due to a periodic modulation of the core refractive index induced by UV-radiation. Gratings able to promote coupling between two core modes have been used in the past [2-4]. Regarding the context of this work, is of particular interest the two steps process used by Poole *et al.* in 1994 [5]. The method consisted in the periodic ablation of the fibre cladding using CO_2 laser radiation followed by periodic annealing using electric arc discharges. The same methodology

was used in 1997 to produce LPFGs [6]. Almost simultaneously two different approaches, where only one of the former two steps was required, have been established [7-9]. Later, several other fabrication techniques have been demonstrated.

2.2 Fabrication techniques

LPFGs are usually written by exposing, through an amplitude mask, an optical fibre to the UV-radiation from a KrF excimer laser (242-248 nm) [1, 10] or to the second harmonic radiation of a continuous-wave (CW) Ar ion laser (244 nm) [11]. Gratings inscription was also achieved through exposure to the radiation delivered by a CW Ar ion laser working in single-line (334 nm) [12] or in a multi-line regime: (300-305 nm) [13] and (333-364 nm) [14]; or through exposure to nanosecond pulses from a ArF excimer laser (193 nm) [15, 16], or from the frequency quadrupled and tripled of the Nd:YAG laser (266 nm and 355 nm) [17, 18]. High-intensity femtosecond laser radiation at several wavelengths have also been used: 211 nm [19], 264 nm [20] and 352 nm [21] corresponding respectively, to the fifth, fourth and third harmonics of a Nd:glass laser; and the second harmonic from Ti^{3+}: Al_2O_3 laser (400 nm) [22, 23]. Gratings fabrication by using a broadband UV source was also demonstrated [24]. Note that despite the different laser intensities and wavelengths, in all cases gratings were written in photosensitive fibres and/or in hydrogenated ones.

There are, however, several alternative techniques for gratings fabrication that does not require the fibre to be photosensitive. LPFGs were written in the Corning SMF-28 fibre (3 mol% Ge) using nanosecond pulses from a 157 nm F_2 laser [25]. Since this fibre usually requires hydrogen loading in order to photoimprint gratings on it, it is believed that this laser radiation be able to photoinduce gratings in germanium free fibres. Note however that the annealing at 150 ºC of gratings written in the SMF-28 fibre led to a decrease of the resonant wavelengths of about 7 nm. Femtosecond pulses from a 800 nm Ti^{3+}: Al_2O_3 laser have been used to inscribe gratings in a standard fibre [26, 27] and in a pure-silica-core fibre [27]. In this case the gratings spectra strongly depend on the ability to keep the alignment between the fibre core and the laser beam. Besides the changes in the refractive index photoinduced by laser radiation, gratings have been fabricated due to thermal effects by ~5 μm CO laser radiation [8], by 10.6 μm CO_2 laser radiation [9] and by arc discharges [8, 28]. The latter two techniques have been catching an increasing attention from the fibre gratings community. Regarding CO_2 laser radiation, it is possible to work at frequencies up to several hundreds of hertz being the gratings produced by periodic stress relaxation [29, 30]. It happens that when

going from the initial several hertz [9] to high-frequency laser pulses (5 kHz) and by focusing the beam to 1 μm, which enables the lateral sweep of the fibre cross section with the laser beam, these two effects create a thermal shock in the exposed regions giving rise to new properties of the produced gratings with applications in optical communications and sensing [31, 32]. Arc-induced gratings which can be produced by microbending [33], by glass-structure rearrangements as a result of using high electric currents (>20 mA) of short duration (<100 ms) [34], or by other mechanisms due to the use of moderate electric currents (9-10 mA) of about 1 s duration whilst applying a tension (0-40 g) to the fibre [35, 36] have also shown new and interesting properties [37-39], being probably, the kind of gratings written in a wider variety of fibres [34, 40, 41]. It is believed that LPFGs produced through exposure to CO_2 laser radiation and to arc discharges may share most of their properties. Comparatively, the major disadvantage of the electric arc technique is the limitation in the minimum period that can be written due to the dimensions of the arc which forbids the use of cladding modes of higher order, in particular, near the turning points where they exhibit higher sensitivity to physical parameters [42]. On the other hand, it is one of the most cost effective techniques.

LPFGs fabrication by using other techniques has also been demonstrated. For instance, by heating at high temperatures a standard fibre heavily twisted [43, 44] or by twisting at high rate a glass fibre with non-circular core's cross section whilst it is being heated in a miniature oven [45]. The periodic corrugation of the fibre's silica cladding through etching leads to a LPFG formation [46]. Gratings can also be produced by exposure of a fibre, through an amplitude mask, to a beam of He ions [47]. This method requires that the fibre cladding be reduced to ~53 μm by etching. Later, the etching process was overcome by exposure of a fibre to a focused beam of protons, which have a longer stopping distance [48]. It is known that gamma radiation can lead to considerable changes in the refractive index of optical fibres [49] and, therefore, it may be an alternative way to produce long-period gratings.

The techniques available to produce LPFGs can be divided in two groups: the ones that enables the fabrication of permanent gratings, as the ones described above, and the others that allow the fabrication of reversible gratings, that is, by removing the external perturbation the grating disappears. Examples of these techniques are the use of a flexure acoustic wave that periodically creates antisymmetric microbends along the fibre, promoting coupling between the core mode and the antisymmetric cladding modes [50], the periodical poling of the liquid-crystalline core in a hollow-core fibre by means of an external long-period-combed electrode [51] and the heavily twist of a high birefringent fibre that potentially causes the so called "virtual gratings" [52]. However, the most popular way to produce reversible gratings is by mechanical means, that is, by pressing the fibre periodically [53]. There is an increasing interest in mechanically induced gratings and they will be discussed in Chapter 6.

In summary, UV-induced gratings requires photosensitive fibres or hydrogen loading followed by thermal annealing being therefore difficult to predict the final position of the resonance wavelengths. Furthermore, UV-induced gratings decay and, in general, cannot stand high temperatures. Mechanically induced LPFGs are very simple, inexpensive and exhibit high flexibility, however their suitable applications are well defined: polarizers, gain equalization and load sensing. Femtosecond laser radiation at 800 nm has a huge potential allowing the writing of both LPFGs and FBGs [54]. However, a reliable assessment of this technique will require further work. Therefore, the two point-by-point techniques (which possess higher flexibility when compared to the use of amplitude masks) that have already proved their efficiency in the fabrication of gratings with unique properties are based on CO_2 laser radiation and on arc discharges, being the latter simpler, harmless and low cost.

LPFGs have been virtually written in all kind of fibres, namely, in standard singlemode telecommunications fibres [1], in two-mode (or few-mode) fibres [5, 55] for optical filtering and sensing, in polarization maintaining fibres [56], in D-fibres for enhanced RI measurements [57], in non-photosensitive fibres [35, 38, 39] for EDFAs gain equalisation and sensing, in multimode fibres [58] for chemical sensing, in single crystal sapphire fibres by a photolithographic method [59] for high temperature measurements, in specially designed fibres: dispersion shifted [1], dispersion compensating [60], depressed inner cladding [61], dual core [62], twin core [63], progressive three layered [64] with particular properties for optical communications and sensing; in hybrid fibres containing silica and polymers [65] or metal coatings [66] for sensitivity enhancement, in a microstructured polymer fibre [67] and in photonic crystal fibres [10, 34, 41, 68] making use of their new optical properties, and also in planar waveguides [69] for compactness and mass production.

A final note to emphasize that depending on the fabrication technique and respective fabrication parameters and also on the fibre type several mechanisms may contribute simultaneously for the grating formation, as will be discussed in detail for arc-induced gratings in the next chapter.

2.3 Applications in optical communications and sensing

LPFGs are band rejection filters that can be tuned in wavelength and coupling strength due to their sensitivity to various physical parameters [70]. As a result of those properties they can find application in the elimination of Stokes' orders in cascaded Raman amplifiers/lasers, in the suppression of the amplified spontaneous emission (ASE) [71] and gain equalization in

erbium doped fibre amplifiers (EDFAs) [31, 72-75]. They have also been used for temperature stabilisation of Er-doped superfluorescent fibre sources [76]. The gratings' rejection bands can be made very broad [77] being useful for polarisation dependent loss compensation, ultimately they can be made wavelength independent and therefore can act as variable optical attenuators [78]. On the other hand, by cascading two identical gratings it is possible to obtain very narrow optical filters [79-81] being therefore useful devices in wavelength division multiplexing and optical code division multiple access systems [60, 82]. The use of LPFGs as mode converters in two-mode fibres [5, 83] and as wavelength selective polarizers [15, 45, 55, 84-86] has also been demonstrated. LPFGs can be used to enhance coupling between different optical devices, such as, from a waveguide to a fibre [87], from a semiconductor laser to an optical fibre or between two fibres when a bulk optical element needs to be inserted in-between [88]. Coupling between a fibre and the free space by producing a planar wave was also demonstrated [89]. Two important applications of LPFGs in optical communications are as optical switches [90-92] and as add-drop multiplexers that can be realized by using two gratings in close proximity [93], or by a grating assisted fibre coupler [94] or be based on coupling between mismatched twin-core fibres [63]. LPFGs can act as ultrafast optical differentiators [95]. The use of LPFGs as dispersion compensators has also been investigated theoretically [96, 97]. LPFGs alone or with other gratings were used for producing multiwavelength fibre lasers [98-100]. LPFGs can also act as bandpass filters by using phase-shifted gratings [101, 102] or two concatenated gratings with a core-mode blocker in between [13, 103-105].

Long period gratings are very sensitive to changes in physical parameters, such as, temperature [106-109], strain [110], transverse load [111-113], bending [114-117], torsion [46, 118-120] and refractive index (RI) of the surrounding medium [121-127]. The sensitivity characteristics of LPFGs have been investigated by several authors [128-130]. It is known that, in general, gratings sensitivity increases with the order of the cladding modes which requires short periods. In particular, [127]as the period decreases a point is reached, called the turning point (note that periods below 100 μm may be needed), for which there is no shift of the resonant wavelengths with changes of the physical parameters, only the coupling strength changes [12]. Beyond that point, each cladding mode has two resonance bands showing different sensitivities to physical parameters, what has been used for sensing discrimination [42, 131].

In general, the gratings sense the simultaneous action of two or more parameters. Therefore, it is required that they will be able to separate the influence of different parameters acting simultaneously. That can be done by monitoring changes in more than one resonant band (wavelength or strength) belonging to the same grating [11, 17], or by monitoring

grating's diffraction from different orders [56, 132], or by writing a grating in a polarization maintaining fibre [133], or by using gratings written in different fibres [134], or written under different fabrication conditions [37]. Often, different kind of gratings: LPFGs, mechanically induced LPFGs, FBGs and sampled FBGs are used for multi-parameter sensing [111, 113, 135-137]. Some effort has been done in order to make the gratings insensitive to a particular physical parameter, such as, temperature [138], temperature and strain [139], bending [140, 141], or bending and refractive index [64]. On the other hand, the enhancement of the gratings response to temperature variations has been achieved by using special polymers and metal coatings [65, 66, 142]. The sensitivity to changes in the RI of the surrounding medium enable LPFGs to be used as chemical detectors, that is, to measure the concentration of a particular constituent in liquids, such as, sugar [57] and salt [143, 144] solutions, ethylene glycol [122], xylene [145] or hydrocarbon [146]. A biosensor based on a LPFG written in a cladding etched fibre was employed to detect the concentration of the haemoglobin protein in a sugar solution [147]. The use of LPFGs as liquid level sensors [148] and as flow sensors [149] has also been demonstrated. High relative humidity was performed by gelatine coated LPFGs [150]. By the deposition of thin film overlay materials [151-153] that exhibit changes in their refractive indices in response to their local environment, LPFGs have been used as a biosensor to detect the RI change when an antigen bonds with the antibody [154].

In conclusion, the diversity of applications of long-period fibre gratings has only parallel with the amount of fabrication techniques demonstrated.

References

[1] A. Vengsarkar, P. Lemaire, J. Judkins, V. Bhatia, T. Erdogan, and J. Sipe. *Long-period fiber gratings as band-rejection filters.* Journal of Lightwave Technology **14**(1): 58-65, 1996.

[2] R.C. Youngquist, J.L. Brooks, and H.J. Shaw. *2-Mode Fiber Modal Coupler.* Optics Letters **9**(5): 177-179, 1984.

[3] J.N. Blake, B.Y. Kim, and H.J. Shaw. *Fiberoptic Modal Coupler Using Periodic Microbending.* Optics Letters **11**(3): 177-179, 1986.

[4] H.G. Park and B.Y. Kim. *Intermodal Coupler Using Permanently Photoinduced Grating in 2-Mode Optical Fiber.* Electronics Letters **25**(12): 797-799, 1989.

[5] C.D. Poole, H.M. Presby, and J.P. Meester. *2-Mode Fiber Spatial-Mode Converter Using Periodic Core Deformation.* Electronics Letters **30**(17): 1437-1438, 1994.

[6] C. Narayanan, H.M. Presby, and A.M. Vengsarkar. *Band-rejection fibre filter using periodic core deformation.* Electronics Letters **33**(4): 280-281, 1997.

[7] S.G. Kosinski, G.A. Ten Eyck, and A.M. Vengsarkar. *Method for making long-period fiber gratings*, in *European Patent EP0840146*. 1998-05-06, 1998

[8] E.M. Dianov, V.I. Karpov, M.V. Grekov, K.M. Golant, S.A. Vasiliev, O.I. Medvedkov, and R.R. Khrapko. *Thermo-induced long-period fibre gratings.* in *IOCC-ECOC 97 - 11th International Conference on Integrated Optics and Optical Fibre Communications / 23rd European Conference on Optical Communications, Vol 2*: 53-56, 1997.

[9] D.D. Davis, T.K. Gaylord, E.N. Glytsis, S.G. Kosinski, S.C. Mettler, and A.M. Vengsarkar. *Long-period fibre grating fabrication with focused CO2 laser pulses.* Electronics Letters **34**(3): 302-303, 1998.

[10] B.J. Eggleton, P.S. Westbrook, R.S. Windeler, S. Spalter, and T.A. Strasser. *Grating resonances in air-silica microstructured optical fibers.* Optics Letters **24**(21): 1460-1462, 1999.

[11] V. Bhatia, D. Campbell, R.O. Claus, and A.M. Vengsarkar. *Simultaneous strain and temperature measurement with long-period gratings.* Optics Letters **22**(9): 648-650, 1997.

[12] V. Grubsky and J. Feinberg. *Long-period fiber gratings with variable coupling for real-time sensing applications.* Optics Letters **25**(4): 203-205, 2000.

[13] D.S. Starodubov, V. Grubsky, and J. Feinberg. *All-fiber bandpass filter with adjustable transmission using cladding-mode coupling.* IEEE Photonics Technology Letters **10**(11): 1590-1592, 1998.

[14] E.M. Dianov, D.S. Stardubov, S.A. Vasiliev, A.A. Frolov, and O.I. Medvedkov. *Refractive-index gratings written by near-ultraviolet radiation.* Optics Letters **22**(4): 221-223, 1997.

[15] B. Ortega, L. Dong, W. Liu, J. deSandro, L. Reekie, S. Tsypina, V. Bagratashvili, and R. Laming. *High-performance optical fiber polarizers based on long-period gratings in birefringent optical fibers.* IEEE Photonics Technology Letters **9**(10): 1370-1372, 1997.

[16] B. Guan, H. Tam, S. Ho, S. Liu, and X. Dong. *Growth of long-period gratings in H-2-loaded fiber after 193-nm UV inscription.* IEEE Photonics Technology Letters **12**(6): 642-644, 2000.

[17] C. Ye, S. James, and R. Tatam. *Simultaneous temperature and bend sensing with long-period fiber gratings.* Optics Letters **25**(14): 1007-1009, 2000.

[18] J. Blows and D.Y. Tang. *Gratings written with tripled output of Q-switched Nd: YAG laser.* Electronics Letters **36**(22): 1837-1839, 2000.

[19] A.I. Kalachev, D.N. Nikogosyan, and G. Brambilla. *Long-period fiber grating fabrication by high-intensity femtosecond pulses at 211 nm.* Journal of Lightwave Technology **23**(8): 2568-2578, 2005.

[20] A. Dragomir, D.N. Nikogosyan, A.A. Ruth, K.A. Zagorul'ko, and P.G. Kryukov. *Long-period fibre grating formation with 264 nm femtosecond radiation.* Electronics Letters **38**(6): 269-271, 2002.

[21] S.A. Slattery and D.N. Nikogosyan. *Long-period fiber grating inscription under high-intensity 352 nm femtosecond irradiation: Three-photon absorption and energy deposition in cladding.* Optics Communications **255**(1-3): 81-90, 2005.

[22] K.A. Zagorul'ko, P.G. Kryukov, Y.V. Larionov, A.A. Rybaltovskii, E.M. Dianov, N.S. Vorob'ev, A.V. Smirnov, M.Y. Shchelev, and A.M. Prokhorov. *Fabrication of a long-period grating in a fibre by second-harmonic radiation from a femtosecond Ti: sapphire laser.* Quantum Electronics **31**(11): 999-1002, 2001.

[23] P.G. Kryukov, Y.V. Larionov, A.A. Rybaltovskii, K.A. Zagorul'ko, A. Dragomir, D.N. Nikogosyan, and A.A. Ruth. *Long-period fibre grating fabrication with femtosecond pulse radiation at different wavelengths.* Microelectronic Engineering **69**(2-4): 248-255, 2003.

[24] X. Li, C. Yue, L. Xia, X. Chen, and S. Xie. *Novel technique for long period gratings fabrication using broad spectrum ultraviolet source.* Microwave and Optical Technology Letters **33**(5): 368-370, 2002.

[25] K. Chen, P. Herman, J. Zhang, and R. Tam. *Fabrication of strong long-period gratings in hydrogen-free fibers with 157-nm F-2-laser radiation.* Optics Letters **26**(11): 771-773, 2001.

[26] Y. Kondo, K. Nouchi, T. Mitsuyu, M. Watanabe, P. Kazansky, and K. Hirao. *Fabrication of long-period fiber gratings by focused irradiation of infrared femtosecond laser pulses.* Optics Letters **24**(10): 646-648, 1999.

[27] F. Hindle, E. Fertein, C. Przygodzki, F. Durr, L. Paccou, R. Bocquet, P. Niay, H. Limberger, and M. Douay. *Inscription of long-period gratings in pure silica and germano-silicate fiber cores by femtosecond laser irradiation.* IEEE Photonics Technology Letters **16**(8): 1861-1863, 2004.

[28] S.G. Kosinski and A.M. Vengsarkar. *Splice-based long-period fiber gratings*. in *Proceedings of 1998 Optical Fiber Communications Conference*: 278-279, 1998.

[29] B.H. Kim, Y. Park, T.J. Ahn, D.Y. Kim, B.H. Lee, Y. Chung, U.C. Paek, and W.T. Han. *Residual stress relaxation in the core of optical fiber by CO2 laser irradiation.* Optics Letters **26**(21): 1657-1659, 2001.

[30] C.S. Kim, Y. Han, B.H. Lee, W.T. Han, U.C. Paek, and Y. Chung. *Induction of the refractive index change in B-doped optical fibers through relaxation of the mechanical stress.* Optics Communications **185**(4-6): 337-342, 2000.

[31] Y. Rao, T. Zhu, Z. Ran, Y. Wang, J. Jiang, and A. Hu. *Novel long-period fiber gratings written by high-frequency CO2 laser pulses and applications in optical fiber communication.* Optics Communications **229**(1-6): 209-221, 2004.

[32] Y.J. Rao, Y.P. Wang, Z.L. Ran, and T. Zhu. *Novel fiber-optic sensors based on long-period fiber gratings written by high-frequency CO2 laser pulses.* Journal of Lightwave Technology **21**(5): 1320-1327, 2003.

[33] I. Hwang, S. Yun, and B. Kim. *Long-period fiber gratings based on periodic microbends.* Optics Letters **24**(18): 1263-1265, 1999.

[34] K. Morishita and Y. Miyake. *Fabrication and resonance wavelengths of long-period gratings written in a pure-silica photonic crystal fiber by the glass structure change.* Journal of Lightwave Technology **22**(2): 625-630, 2004.

[35] G. Rego, O. Okhotnikov, E. Dianov, and V. Sulimov. *High-temperature stability of long-period fiber gratings produced using an electric arc.* Journal of Lightwave Technology **19**(10): 1574-1579, 2001.

[36] G. Humbert and A. Malki. *Electric-arc-induced gratings in non-hydrogenated fibres: fabrication and high-temperature characterizations.* Journal of Optics A-Pure and Applied Optics **4**(2): 194-198, 2002.

[37] G. Rego, P.V.S. Marques, H.M. Salgado, and J.L. Santos. *Simultaneous measurement of temperature and strain based on arc-induced long-period fibre gratings.* Electronics Letters **41**(2): 60-62, 2005.

[38] G. Rego, R. Falate, J.L. Santos, H.M. Salgado, J.L. Fabris, S.L. Semjonov, and E.M. Dianov. *Arc-induced long-period gratings in aluminosilicate glass fibers.* Optics Letters **30**(16): 2065-2067, 2005.

[39] G. Rego, A.F. Fernandez, A. Gusarov, B. Brichard, F. Berghmans, J.L. Santos, and H.M. Salgado. *Effect of ionizing radiation on the properties of arc-induced long-period fiber gratings.* Applied Optics **44**(29): 6258-6263, 2005.

[40] G. Rego, P.V.S. Marques, J.L. Santos, and H.M. Salgado. *Arc-induced long-period gratings.* Fiber and Integrated Optics **24**(3-4): 245-259, 2005.

[41] G. Humbert, A. Malki, S. Fevrier, P. Roy, and D. Pagnoux. *Electric arc-induced long-period gratings in Ge-free air-silica microstructure fibres.* Electronics Letters **39**(4): 349-350, 2003.

[42] X. Shu, L. Zhang, and I. Bennion. *Sensitivity characteristics near the dispersion turning points of long-period fiber gratings in B/Ge codoped fiber.* Optics Letters **26**(22): 1755-1757, 2001.

[43] O.V. Ivanov. *Fabrication of long-period fiber gratings by twisting of a standard single-mode fiber.* Optics Letters **30**(24): 3290-3292, 2005.

[44] S. Oh, K. Lee, U. Paek, and Y. Chung. *Fabrication of helical long-period fiber gratings by use of a CO2 laser.* Optics Letters **29**(13): 1464-1466, 2004.

[45] V.I. Kopp, V.M. Churikov, J. Singer, N. Chao, D. Neugroschl, and A.Z. Genack. *Chiral fiber gratings.* Science **305**(5680): 74-75, 2004.

[46] C.Y. Lin and L.A. Wang. *Loss-tunable long period fibre grating made from etched corrugation structure.* Electronics Letters **35**(21): 1872-1873, 1999.

[47] M. Fujimaki, Y. Ohki, J.L. Brebner, and S. Roorda. *Fabrication of long-period optical fiber gratings by use of ion implantation.* Optics Letters **25**(2): 88-89, 2000.

[48] M. von Bibra, A. Roberts, and J. Canning. *Fabrication of long-period fiber gratings by use of focused ion-beam irradiation.* Optics Letters **26**(11): 765-767, 2001.

[49] A.F. Fernandez, B. Brichard, and F. Berghmans. *In situ measurement of refractive index changes induced by gamma radiation in germanosilicate fibers.* IEEE Photonics Technology Letters **15**(10): 1428-1430, 2003.

[50] H.S. Kim, S.H. Yun, I.K. Kwang, and B.Y. Kim. *All-fiber acousto-optic tunable notch filter with electronically controllable spectral profile.* Optics Letters **22**(19): 1476-1478, 1997.

[51] Y. Jeong, S. Baek, and B. Lee. *All-optical signal gating in cascaded long-period fiber gratings.* IEEE Photonics Technology Letters **12**(9): 1216-1218, 2000.

[52] C. Jauregui and J.M. Lopez-Higuera. *Virtual long-period gratings.* Optics Letters **30**(1): 14-16, 2005.

[53] S. Savin, M. Digonnet, G. Kino, and H. Shaw. *Tunable mechanically induced long-period fiber gratings.* Optics Letters **25**(10): 710-712, 2000.

[54] A. Martinez, I.Y. Khrushchev, and I. Bennion. *Thermal properties of fibre Bragg gratings inscribed point-by-point by infrared femtosecond laser.* Electronics Letters **41**(4): 176-178, 2005.

[55] S. Ramachandran, M. Das, Z. Wang, J. Fleming, and M. Yan. *High extinction, broadband polarisers using long-period fibre gratings in few-mode fibres.* Electronics Letters **38**(22): 1327-1328, 2002.

[56] K.J. Han, Y.W. Lee, J. Kwon, S. Roh, J. Jung, and B. Lee. *Simultaneous measurement of strain and temperature incorporating a long-period fiber grating inscribed on a polarization-maintaining fiber.* IEEE Photonics Technology Letters **16**(9): 2114-2116, 2004.

[57] X. Chen, K. Zhou, L. Zhang, and I. Bennion. *Optical chemsensors utilizing long-period fiber gratings UV-Inscribed in D-Fiber with enhanced sensitivity through cladding etching.* IEEE Photonics Technology Letters **16**(5): 1352-1354, 2004.

[58] S. Lee, R. Kumar, P. Kumar, P. Radhakrishnan, C. Vallabhan, and V. Nampoori. *Long period gratings in multimode optical fibers: application in chemical sensing.* Optics Communications **224**(4-6): 237-241, 2003.

[59] S.Z. Yin, S.H. Nam, Y. Yang, C. Zhan, and K.W. Chung. *Innovative fiber optic gratings: fabrications and applications*. in *International Symposium on Advances and Trends in Fiber Optics and Applications: Proceedings*: 49-57, 2004.

[60] T.J. Eom, S.J. Kim, T.Y. Kim, C.S. Park, and B.H. Lee. *Optical pulse multiplication and temporal coding using true time delay achieved by long-period fiber gratings in dispersion compensating fiber.* Optics Express **12**(26): 6410-6420, 2004.

[61] L. Dong, L. Reekie, and J. Cruz. *Long period gratings formed in depressed cladding fibres.* Electronics Letters **33**(22): 1897-1898, 1997.

[62] G. Humbert, A. Malki, S. Fevrier, P. Roy, J.L. Auguste, and J.M. Blondy. *Long period grating filters fabricated with electric arc in dual concentric core fibers.* Optics Communications **225**(1-3): 47-53, 2003.

[63] H.L. An, B. Ashton, and S. Fleming. *Long-period-grating-assisted optical add-drop filter based on mismatched twin-core photosensitive-cladding fiber.* Optics Letters **29**(4): 343-345, 2004.

[64] T. Allsop, D. Webb, and I. Bennion. *Investigations of the spectral sensitivity of long period gratings fabricated in three-layered optical fiber.* Journal of Lightwave Technology **21**(1): 264-268, 2003.

[65] A.A. Abramov, B.J. Eggleton, J.A. Rogers, R.P. Espindola, A. Hale, R.S. Windeler, and T.A. Strasser. *Electrically tunable efficient broad-band fiber filter.* IEEE Photonics Technology Letters **11**(4): 445-447, 1999.

[66] D.M. Costantini, C.A.P. Muller, S.A. Vasiliev, H.G. Limberger, and R.P. Salathe. *Tunable loss filter based on metal-coated long-period fiber grating.* IEEE Photonics Technology Letters **11**(11): 1458-1460, 1999.

[67] M. van Eijkelenborg, W. Padden, and J. Besley. *Mechanically induced long-period gratings in microstructured polymer fibre.* Optics Communications **236**(1-3): 75-78, 2004.

[68] G. Kakarantzas, T. Birks, and P. Russell. *Structural long-period gratings in photonic crystal fibers.* Optics Letters **27**(12): 1013-1015, 2002.

[69] V. Rastogi and K. Chiang. *Long-period gratings in planar optical waveguides.* Applied Optics **41**(30): 6351-6355, 2002.

[70] S.W. James and R.P. Tatam. *Optical fibre long-period grating sensors: Characteristics and application.* Measurement Science & Technology **14**(5): R49-R61, 2003.

[71] G. Rego, M. Melo, J.L. Santos, and H.M. Salgado. *Optical filters for fibre lasers and amplifiers*. in *London Communications Symposium 2002, Proceedings*: 49-52, 2002.

[72] A.M. Vengsarkar, J.R. Pedrazzani, J.B. Judkins, P.J. Lemaire, N.S. Bergano, and C.R. Davidson. *Long-period fiber-grating-based gain equalizers.* Optics Letters **21**(5): 336-338, 1996.

[73] P.F. Wysocki, J.B. Judkins, R.P. Espindola, M. Andrejco, and A.M. Vengsarkar. *Broad-band erbium-doped fiber amplifier flattened beyond 40 nm using long-period grating filter.* IEEE Photonics Technology Letters **9**(10): 1343-1345, 1997.

[74] I. Sohn and J. Song. *Gain flattened and improved double-pass two-stage EDFA using microbending long-period fiber gratings.* Optics Communications **236**(1-3): 141-144, 2004.

[75] M. Harumoto, M. Shigehara, and H. Suganuma. *Gain-flattening filter using long-period fiber gratings.* Journal of Lightwave Technology **20**(6): 1027-1033, 2002.

[76] H.J. Patrick, A.D. Kersey, W.K. Burns, and R.P. Moeller. *Erbium-doped superfluorescent fibre source with long period fibre grating wavelength stabilisation.* Electronics Letters **33**(24): 2061-2063, 1997.

[77] S. Ramachandran, M.F. Yan, E. Monberg, F.V. Dimarcello, P. Wisk, and S. Ghalmi. *Record bandwidth, spectrally flat coupling with microbend gratings in dispersion-tailored fibers.* IEEE Photonics Technology Letters **15**(11): 1561-1563, 2003.

[78] S. Veeriah, A.R. Faidz, Y.N. Phua, and V. Mishra. *Broadband spectrum based on mechanically induced cascaded long-period fibre gratings.* Microwave and Optical Technology Letters **44**(5): 463-465, 2005.

[79] C.Y. Lin and L.A. Wang. *A wavelength- and loss-tunable band-rejection filter based on corrugated long-period fiber grating.* IEEE Photonics Technology Letters **13**(4): 332-334, 2001.

[80] K.W. Chung and S.Z. Yin. *Analysis of a widely tunable long-period grating by use of an ultrathin cladding layer and higher-order cladding mode coupling.* Optics Letters **29**(8): 812-814, 2004.

[81] X.Y. Dong, X.F. Yang, P. Shum, and C.C. Chan. *Tunable WDM filter with 0.8-nm channel spacing using a pair of long-period fiber gratings.* IEEE Photonics Technology Letters **17**(4): 795-797, 2005.

[82] X. Gu. *Wavelength-division multiplexing isolation fiber filter and light source using cascaded long-period fiber gratings.* Optics Letters **23**(7): 509-510, 1998.

[83] K.S. Lee and T. Erdogan. *Transmissive tilted gratings for LP0.1-to-LP11 mode coupling.* IEEE Photonics Technology Letters **11**(10): 1286-1288, 1999.

[84] Y.W. Lee, J. Jung, and B. Lee. *Polarization-sensitive interference spectrum of long-period fiber grating pair separated by erbium-doped fiber.* IEEE Photonics Technology Letters **14**(9): 1312-1314, 2002.

[85] C.S. Kim, Y.G. Han, J.U. Kang, B. Choi, and J.S. Nelson. *Polarization-insensitive multi-wavelength switching based on polarization-selective long-period fiber gratings.* Optics Express **12**(24): 6082-6087, 2004.

[86] A.S. Kurkov, M. Douay, O. Duhem, B. Leleu, J.F. Henninot, J.F. Bayon, and L. Rivoallan. *Long-period fibre grating as a wavelength selective polarisation element.* Electronics Letters **33**(7): 616-617, 1997.

[87] B.L. Bachim, O.O. Ogunsola, and T.K. Gaylord. *Optical-fiber-to-waveguide coupling using carbon-dioxide-laser-induced long-period fiber gratings.* Optics Letters **30**(16): 2080-2082, 2005.

[88] M.J. Kim, T.J. Eom, U.C. Paek, and B.H. Lee. *Lens-free optical fiber connector having a long working distance assisted by matched long-period fiber gratings.* Journal of Lightwave Technology **23**(2): 588-596, 2005.

[89] T. Erdogan, D. Stegall, and A. Heaney. *Direct single-mode fiber to free space coupling assisted by a cladding mode*. in *Proceedings of 1999 Optical Fiber Communications Conference*: 171-173, 1999.

[90] V. Perlin and H. Winful. *Nonlinear pulse switching using long-period fiber gratings.* Journal of Lightwave Technology **18**(3): 329-333, 2000.

[91] J. Kutz, B. Eggleton, J. Stark, and R. Slusher. *Nonlinear pulse propagation in long-period fiber gratings: Theory and experiment.* IEEE Journal of Selected Topics in Quantum Electronics **3**(5): 1232-1245, 1997.

[92] Y. Kim, N. Kim, Y. Chung, U. Paek, and W. Han. *All-optical switching application based on optical nonlinearity of Yb3+ doped aluminosilicate glass fiber with a long-period fiber gratings pair.* Optics Express **12**(4): 651-656, 2004.

[93] K.S. Chiang, Y.Q. Liu, M.N. Ng, and S.P. Li. *Coupling between two parallel long-period fibre gratings.* Electronics Letters **36**(16): 1408-1409, 2000.

[94] J. Lauzon, A. Chandonnet, C. Xu, and W.P. Huang. *Grating-assisted fused fibre filter*. in *IOCC-ECOC 97 - 11th International Conference on Integrated Optics and Optical Fibre Communications / 23rd European Conference on Optical Communications, Vol 2*: 169-172, 1997.

[95] M. Kulishov and J. Azana. *Long-period fiber gratings as ultrafast optical differentiators.* Optics Letters **30**(20): 2700-2702, 2005.

[96] D. Stegall and T. Erdogan. *Dispersion control with use of long-period fiber gratings.* Journal of the Optical Society of America A-Optics Image Science and Vision **17**(2): 304-312, 2000.

[97] M. Das and K. Thyagarajan. *Dispersion compensation in transmission using uniform long period fiber gratings.* Optics Communications **190**(1-6): 159-163, 2001.

[98] Y. Han, C. Kim, J. Kang, U. Paek, and Y. Chung. *Multiwavelength Raman fiber-ring laser based on tunable cascaded long-period fiber gratings.* IEEE Photonics Technology Letters **15**(3): 383-385, 2003.

[99] C.D. Su and L.A. Wang. *Multiwavelength fiber sources based on double-pass superfluorescent fiber sources.* Journal of Lightwave Technology **18**(5): 708-714, 2000.

[100] R. Romero, O. Frazão, G. Rego, P.V.S. Marques, and H.M. Salgado. *Sampled Fibre Bragg Gratings Fabrication using an Electric Arc and their Applications*. in *Proceedings of 2002 Course on Photosensitivity in Optical Waveguides and Glasses*: paper 43/WA5, 2002.

[101] G. Humbert and A. Malki. *High performance bandpass filters based on electric arc-induced pi-shifted long-period fibre gratings.* Electronics Letters **39**(21): 1506-1507, 2003.

[102] L. Chen. *Phase-shifted long-period gratings by refractive index-shifting.* Optics Communications **200**(1-6): 187-191, 2001.

[103] S. Choi, T.J. Eom, Y. Jung, B.H. Lee, J.W. Lee, and K. Oh. *Broad-band tunable all-fiber bandpass filter based on hollow optical fiber and long-period grating pair.* IEEE Photonics Technology Letters **17**(1): 115-117, 2005.

[104] Y.G. Han, S.H. Kim, S.B. Lee, U.C. Paek, and Y. Chung. *Development of core mode blocker with H-2-loaded Ge-B codoped fibres.* Electronics Letters **39**(15): 1107-1108, 2003.

[105] T.E. Dimmick, D.A. Satorius, and G.L. Burdge. *All-fiber acousto-optic tunable bandpass filter*. in *Proceedings of 2001 Optical Fiber Communications Conference*: Paper WJ3, 2001.

[106] S. Khaliq, S.W. James, and R.P. Tatam. *Enhanced sensitivity fibre optic long period grating temperature sensor.* Measurement Science & Technology **13**(5): 792-795, 2002.

[107] X. Shu, T. Allsop, B. Gwandu, L. Zhang, and I. Bennion. *High-temperature sensitivity of long-period gratings in B-Ge codoped fiber.* IEEE Photonics Technology Letters **13**(8): 818-820, 2001.

[108] B.H. Lee, Y. Chung, W.T. Han, and U.C. Paek. *Temperature sensor based on self-interference of a single long-period fiber grating.* IEICE Transactions on Electronics **E83C**(3): 287-292, 2000.

[109] S. James, R. Tatam, A. Twin, R. Bateman, and P. Noonan. *Cryogenic temperature response of fibre optic long period gratings.* Measurement Science & Technology **14**(8): 1409-1411, 2003.

[110] Y. Han, C. Kim, U. Paek, and Y. Chung. *Performance enhancement of long period fiber gratings for strain and temperature sensing.* IEICE Transactions on Electronics **E83C**(3): 282-286, 2000.

[111] X.K. Zeng, Y.J. Rao, Y.P. Wang, Z.L. Ran, and T. Zhu. *Transverse load, static strain, temperature and vibration measurement using a cascaded FBG/EFPI/LPFG sensor system*. in *OFS 2002: 15th Optical Fiber Sensors Conference Technical Digest*: 199-202, 2002.

[112] Y. Liu, L. Zhang, and I. Bennion. *Fibre optic load sensors with high transverse strain sensitivity based on long-period gratings in B/Ge co-doped fibre.* Electronics Letters **35**(8): 661-663, 1999.

[113] X. Shu, K. Chisholm, I. Felmeri, L. Everall, K. Sugden, A. Gillooly, L. Zhang, and I. Bennion. *Novel optical load sensors based on mechanically induced sampled fiber Bragg gratings*. in *OFS 2003: 16th Optical Fiber Sensors Conference Technical Digest*: 654-657, 2003.

[114] H.J. Patrick, C.C. Chang, and S.T. Vohra. *Long period fibre gratings for structural bend sensing.* Electronics Letters **34**(18): 1773-1775, 1998.

[115] Y. Liu, L. Zhang, J. Williams, and I. Bennion. *Bend sensing by measuring the resonance splitting of long-period fiber gratings.* Optics Communications **193**(1-6): 69-72, 2001.

[116] D. Zhao, K. Zhou, X. Chen, L. Zhang, I. Bennion, G. Flockhart, W. MacPherson, J. Barton, and J. Jones. *Implementation of vectorial bend sensors using long-period gratings UV-inscribed in special shape fibres.* Measurement Science & Technology **15**(8): 1647-1650, 2004.

[117] G.D. VanWiggeren, T.K. Gaylord, D.D. Davis, E. Anemogiannis, B.D. Garrett, M.I. Braiwish, and E.N. Glytsis. *Axial rotation dependence of resonances in curved CO2-laser-induced long-period fibre gratings.* Electronics Letters **36**(16): 1354-1355, 2000.

[118] Y.P. Wang, J.P. Chen, and Y.J. Rao. *Torsion characteristics of long-period fiber gratings induced by high-frequency CO2 laser pulses.* Journal of the Optical Society of America B-Optical Physics **22**(6): 1167-1172, 2005.

[119] K.S. Chiang, Y.Q. Liu, M.N. Ng, and X.Y. Dong. *Analysis of etched long-period fibre grating and its response to external refractive index.* Electronics Letters **36**(11): 966-967, 2000.

[120] L.A. Wang, C.Y. Lin, and G.W. Chern. *A torsion sensor made of a corrugated long period fibre grating.* Measurement Science & Technology **12**(7): 793-799, 2001.

[121] H. Patrick, A. Kersey, and F. Bucholtz. *Analysis of the response of long period fiber gratings to external index of refraction.* Journal of Lightwave Technology **16**(9): 1606-1612, 1998.

[122] J.H. Chong, P. Shum, H. Haryono, A. Yohana, M.K. Rao, C. Lu, and Y.N. Zhu. *Measurements of refractive index sensitivity using long-period grating refractometer.* Optics Communications **229**(1-6): 65-69, 2004.

[123] B.H. Lee, Y. Liu, S.B. Lee, S.S. Choi, and J.N. Jang. *Displacements of the resonant peaks of a long-period fiber grating induced by a change of ambient refractive index.* Optics Letters **22**(23): 1769-1771, 1997.

[124] P.L. Swart. *Long-period grating Michelson refractometric sensor.* Measurement Science & Technology **15**(8): 1576-1580, 2004.

[125] X.W. Shu, X.M. Zhu, S. Jiang, W. Shi, and D.X. Huang. *High sensitivity of dual resonant peaks of long-period fibre grating to surrounding refractive index changes.* Electronics Letters **35**(18): 1580-1581, 1999.

[126] A.P. Zhang, L.Y. Shao, J.F. Ding, and S.L. He. *Sandwiched long-period gratings for simultaneous measurement of refractive index and temperature.* IEEE Photonics Technology Letters **17**(11): 2397-2399, 2005.

[127] G.M. Rego, J.L. Santos, and H.M. Salgado. *Refractive index measurement with long-period gratings arc-induced in pure-silica-core fibres.* Optics Communications **259**(2): 598-602, 2006.

[128] V. Bhatia. *Applications of long-period gratings to single and multi-parameter sensing.* Optics Express **4**(11): 457-466, 1999.

[129] X. Shu, L. Zhang, and I. Bennion. *Sensitivity characteristics of long-period fiber gratings.* Journal of Lightwave Technology **20**(2): 255-266, 2002.

[130] T. Allsop, D.J. Webb, and I. Bennion. *A comparison of the sensing characteristics of long period gratings written in three different types of fiber.* Optical Fiber Technology **9**(4): 210-223, 2003.

[131] X.W. Shu, X.M. Zhu, Q.L. Wang, S. Jiang, W. Shi, Z.J. Huang, and D.X. Huang. *Dual resonant peaks of LP015 cladding mode in long-period gratings.* Electronics Letters **35**(8): 649-651, 1999.

[132] T. Allsop, L. Zhang, D.J. Webb, and I. Bennion. *Discrimination between strain and temperature effects using first and second-order diffraction from a long-period grating.* Optics Communications **211**(1-6): 103-108, 2002.

[133] Y. Zhou, K. Gao, H. Rui, R. Qu, and Z. Fang. *Temperature and stress tuning characteristics of long-period gratings imprinted in Panda fiber.* IEEE Photonics Technology Letters **15**(12): 1728-1730, 2003.

[134] Y.G. Han, S.B. Lee, C.S. Kim, J.U. Kang, Y. Chung, and U.C. Paek. *Simultaneous measurement of temperature and strain using dual long-period fiber gratings with controlled temperature and strain sensitivities.* Optics Express **11**(5): 476-481, 2003.

[135] Y.G. Han, B.H. Lee, W.T. Han, U.C. Paek, and Y. Chung. *Fibre-optic sensing applications of a pair of long-period fibre gratings.* Measurement Science & Technology **12**(7): 778-781, 2001.

[136] H. Chi, X.M. Tao, D.X. Yang, and K.S. Chen. *Simultaneous measurement of axial strain, temperature, and transverse load by a superstructure fiber grating.* Optics Letters **26**(24): 1949-1951, 2001.

[137] O. Frazão, R. Romero, G. Rego, P.V.S. Marques, H.M. Salgado, and J.L. Santos. *Sampled fibre Bragg grating sensors for simultaneous strain and temperature measurement.* Electronics Letters **38**(14): 693-695, 2002.

[138] J.N. Jang, S.Y. Kim, S.W. Kim, and M.S. Kim. *Temperature insensitive long-period fibre gratings.* Electronics Letters **35**(24): 2134-2136, 1999.

[139] V. Bhatia, D.K. Campbell, D. Sherr, T.G. DAlberto, N.A. Zabaronick, G.A. TenEyck, K.A. Murphy, and R.O. Claus. *Temperature-insensitive and strain-insensitive long-period grating sensors for smart structures.* Optical Engineering **36**(7): 1872-1876, 1997.

[140] Y.P. Wang, Y.J. Rao, Z.L. Ran, T. Zhu, and X.K. Zeng. *Bend-insensitive long-period fiber grating sensors.* Optics and Lasers in Engineering **41**(1): 233-239, 2004.

[141] S.H. Nam, C. Zhan, J. Lee, C. Hahn, K. Reichard, P. Ruffin, K.L. Deng, and S.Z. Yin. *Bend-insensitive ultra short long-period gratings by the electric arc method and their applications to harsh environment sensing and communication.* Optics Express **13**(3): 731-737, 2005.

[142] O. Duhem, A. DaCosta, J.F. Henninot, and M. Douay. *Long period copper-coated grating as an electrically tunable wavelength-selective filter.* Electronics Letters **35**(12): 1014-1016, 1999.

[143] R. Falciai, A. Mignani, and A. Vannini. *Long period gratings as solution concentration sensors.* Sensors and Actuators B-Chemical **74**(1-3): 74-77, 2001.

[144] M.N. Ng, Z.H. Chen, and K.S. Chiang. *Temperature compensation of long-period fiber grating for refractive-index sensing with bending effect.* IEEE Photonics Technology Letters **14**(3): 361-362, 2002.

[145] T. Allsop, L. Zhang, and I. Bennion. *Detection of organic aromatic compounds in paraffin by a long-period fiber grating optical sensor with optimized sensitivity.* Optics Communications **191**(3-6): 181-190, 2001.

[146] R. Falate, R.C. Kamikawachi, M. Muller, H.J. Kalinowski, and J.L. Fabris. *Fiber optic sensors for hydrocarbon detection.* Sensors and Actuators B-Chemical **105**(2): 430-436, 2005.

[147] X.F. Chen, K.M. Zhou, L. Zhang, and I. Bennion. *High sensitivity biosensor based on dual-peak LPG sensitised by light cladding etching*. in *17th International Conference On Optical Fibre Sensors, Pts 1 And 2*: 383-386, 2005.

[148] S. Khaliq, S.W. James, and R.P. Tatam. *Fiber-optic liquid-level sensor using a long-period grating.* Optics Letters **26**(16): 1224-1226, 2001.

[149] J.P. Dankers, J.L. Lenhart, K.S. R., J.H. van Zanten, S.G. Advani, and R. Parnas. *Fibre optic flow and and cure sensing for liquid composite molding.* Optics Lasers Engineering **35**: 91-104, 2001.

[150] K.M. Tan, C.M. Tay, S.C. Tjin, C.C. Chan, and H. Rahardjo. *High relative humidity measurements using gelatin coated long-period grating sensors.* Sensors and Actuators B-Chemical **110**(2): 335-341, 2005.

[151] Z.Y. Wang, J.R. Heflin, R.H. Stolen, and S. Ramachandran. *Analysis of optical response of long period fiber gratings to nm-thick thin-film coatings.* Optics Express **13**(8): 2808-2813, 2005.

[152] S.W. James, I. Ishaq, G.J. Ashwell, and R.P. Tatam. *Cascaded long-period gratings with nanostructured coatings.* Optics Letters **30**(17): 2197-2199, 2005.

[153] I.D. Villar, I.R. Matias, and F.J. Arregui. *Long-period fiber gratings with overlay of variable refractive index.* IEEE Photonics Technology Letters **17**(9): 1893-1895, 2005.

[154] M.P. DeLisa, Z. Zhang, M. Shiloach, S. Pilevar, C.C. Davis, J.S. Sirkis, and W.E. Bentley. *Evanescent wave long period fiber Bragg grating as an immobilized antibody biosensor.* Analytical Chemistry **72**(13): 2895-2900, 2000.

3

Mechanisms of formation of arc-induced long-period fibre gratings

3.1 Introduction

The knowledge of the theoretical background related to long-period fibre gratings (LPFGs) as well as the underlying mechanisms responsible for the formation of gratings produced by arc-discharges, is of the most importance in order to predict and understand LPFGs behaviour whilst being submitted to external physical stimulus such as temperature, strain, loads, bending and gamma radiation. The theory of LPFGs can be found in several books [1-3], and in published literature [4, 5]. However, investigations concerned to the formation of arc-induced gratings are scarce [6, 7]. Therefore, this chapter is essentially dedicated to the last topic.

The chapter begins with a brief discussion of mode propagation in an optical fibre, considering a three layers approach, followed by the presentation of the fundamental equations related to coupling between the core mode and the cladding modes. Afterwards, the mechanisms of grating formation will be discussed and special relevance will be given to stress relaxation and to geometric deformations. For the former, experimental results from measurements performed at EPFL-Lausanne will be presented, and for the latter, computer simulations based on couple mode theory will be shown.

3.2 Theory of long-period fibre gratings

To understand what a LPFG is, it is first required the knowledge of propagation of modes in an optical fibre. Therefore, consider a particular optical fibre, as the one depicted in Figure 3.1, having a core radius r_1 and cladding radius r_2 and different refractive indices in each layer: n_1, n_2 and n_3. In general, this cylindrical waveguide support many modes of

propagation, that is, there are plenty of ways to guide the electromagnetic radiation. The radial

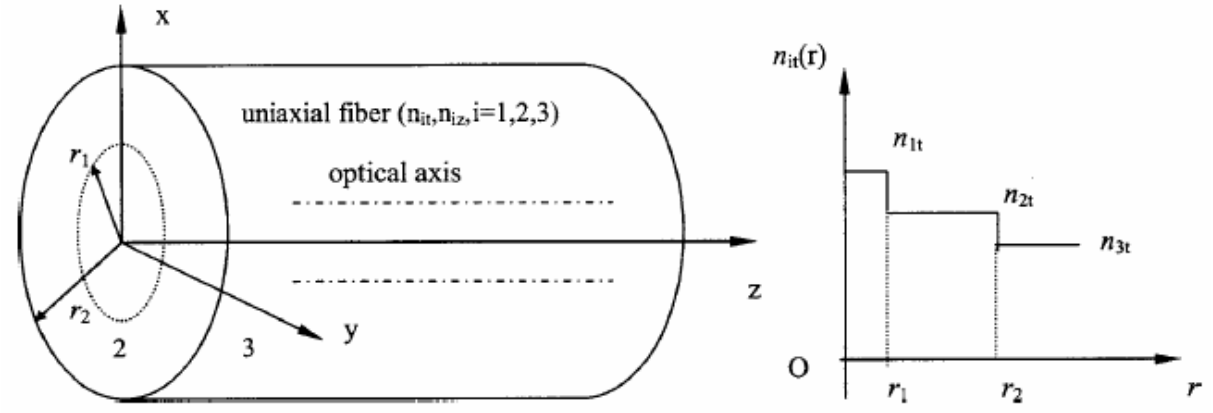

Figure 3.1 – Three-layered step-index uniaxial optical fibres and the transverse index profile. (Taken from [5]).

distribution of the energy carried by each mode is a characteristic of the mode. Depending on the core radius and also on the refractive index difference between the core and the cladding (Δn) only one mode may propagate (for wavelengths above cut-off). This is the case of singlemode optical fibres. For this mode, most of the energy is guided by the core, but a certain amount is also guided by the cladding and therefore, the core mode "sees" an effective refractive index that lies between the core and the cladding refractive indices. The other modes available in an optical fibre may be classified, according to the value of the third layer, as: cladding modes, radiation modes and leaky modes. The first occurs when the refractive index of the third layer is lower than that of the cladding, such as the case of a stripped fibre, being $n_3 = 1$ (air). In this case, several discrete cladding modes are guided by total internal reflection at the cladding-air interface. The effective refractive indices of those modes range between n_2 and n_3. For the case of $n_2 = n_3$, that is, an infinite cladding, total internal reflection is not possible and, therefore, light is lost through a continuum of radiation modes. When $n_2 < n_3$, light can propagate a certain distance due to hollow waveguide such as in the case of using passive/active fibre coatings, being these discrete modes called leaky-modes. In this work, the cladding modes are of main interest.

The field equations of the core and cladding modes are solutions of the wave equation that satisfy continuity conditions at the boundary. In general, the modes are TE, TM and hybrid HE/EH modes. If Δn is small, the weakly guide approximation can be used and the modes can be treated as linearly polarized, LP. Note that LP modes are a superposition of TE, TM and hybrid modes. For a singlemode fibre, the core mode is HE_{11} or LP_{01} and the field equation can be obtained considering two layers: core and cladding. For the cladding modes, a three layer geometry is required, even that Δn be small. As far as LPFGs are concerned, the

type of modes of interest depends on the symmetry of the perturbation that enables coupling from the core mode to the cladding modes. If the perturbation is axis symmetric the coupling is made to LP_{0j} (or HE_{1j}) cladding modes (j>1). On the other hand, if the perturbation is asymmetric coupling is made to LP_{1j} (or $HE_{2j} + TE_{0j} + TM_{0j}$) cladding modes (j>0).

As a final remark, note that usually the fibre is considered isotropic. However, when a fibre grating is stretched the transverse and axial components of the refractive index, in each layer, are different and, therefore, a uniaxial fibre approach may be required [5].

3.2.1 Coupling between the core mode and the cladding modes

LPFGs couple light from the core mode to cladding modes at wavelengths that satisfy the phase-matching condition [8]

$$\lambda^m = \left(n_{eff}^{co} - n_{eff}^{cl,m}\right)\Lambda \tag{3.1}$$

where λ^m is the resonance wavelength corresponding to coupling to the m^{th} cladding mode, Λ is the grating period, and n_{eff}^{co} and $n_{eff}^{cl,m}$ are respectively, the effective refractive indices of the core and of the cladding modes. Thus, the grating's transmission spectrum is characterised by a set of dips at those wavelengths. For each individual resonance, its transmission loss can be calculated by

$$T = 10.\log\left\{1 - \frac{\sin^2\left[k_g L\sqrt{1+\left(\frac{\delta}{k_g}\right)^2}\right]}{1+\left(\frac{\delta}{k_g}\right)^2}\right\} \tag{3.2}$$

where δ is the detuning parameter

$$\delta = \pi\left\{\frac{n_{eff}^{co} - n_{eff}^{cl,m}}{\lambda^m} - \frac{1}{\Lambda}\right\} \tag{3.3}$$

k_g is the grating coupling constant and L is the grating length. The coupling constant is proportional to the overlap integral of the core and cladding mode fields in the region altered

by the arc discharge (see eq. (3.9)), and it can be derived from the transverse coupling coefficient between the core and the m^{th} cladding mode which is expressed as [8, 9]

$$k_t(z) = \frac{\omega}{4}\int_0^{2\pi}\int_0^{r_{clad}} \Delta\varepsilon(r,\phi,z)\vec{E}_{co}(r,\phi).\vec{E}^{*}_{cl,m}(r,\phi)rdrd\phi \tag{3.4}$$

where $\vec{E}_{co}(r,\phi)$ and $\vec{E}^{*}_{cl,m}(r,\phi)$ are the transverse field components of the core and cladding modes (the symbol '*' means its complex conjugated); $\Delta\varepsilon$ is the permittivity change and for a small perturbation can be approximated by

$$\Delta\varepsilon(r,\phi,z) \simeq 2\varepsilon_0 n_0(r)\Delta n_{ind}(r,\phi,z) \tag{3.5}$$

where ε_0 is the vacuum permittivity, n_0 is the refractive index profile of the pristine fibre and Δn_{ind} is the refractive index change induced by the arc discharge. It was assumed that each mode carries the same power of 1 W. Note also that the integration needs to be performed over the entire cross section of the fibre since the arc discharge affects both the core and the cladding as can be confirmed experimentally through tomographic stress measurements (section 3.3.3), and also by the fact that for weak arc-induced LPFGs the shift of the resonance wavelengths during the grating's inscription is much smaller than in the case of UV-induced gratings (section 5.3.3). For the latter, only the photosensitive core is affected and, therefore, from the resonant condition a larger wavelength shift is expected.

Figure 3.2 (a) shows a typical spectrum of a grating obtained through computer simulations (Apollo Photonics v2.2a) considering a symmetric perturbation confined to the core such as the case of UV-induced gratings. The grating period was set to 540 μm and its length to 22 mm. Figure 3.2 (b) shows the spectrum of a grating arc-induced in the Corning SMF-28 fibre, with the same period and length. It is clear that an asymmetric perturbation results in a better fitting to the grating's spectrum. It should be stressed that in the case of arc-

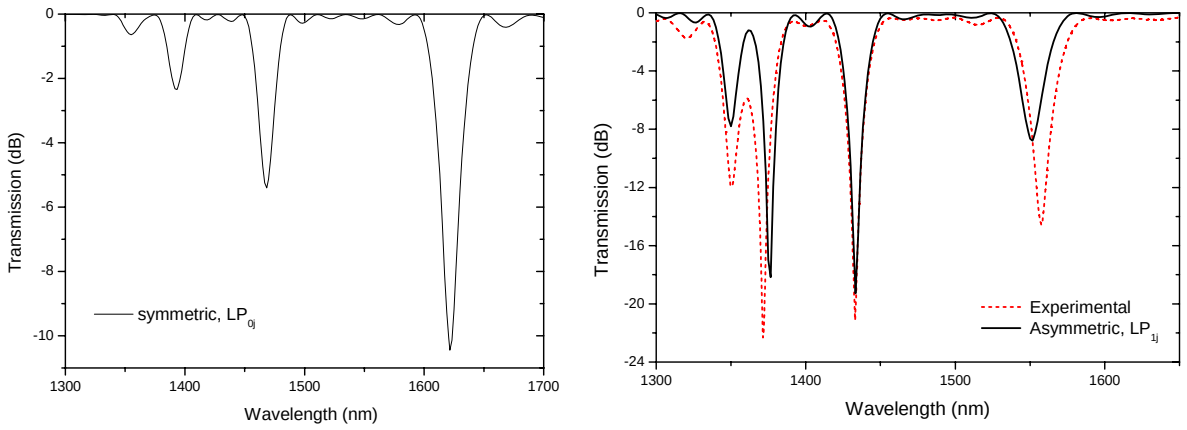

(a) (b)

Figure 3.2 – (a) Symmetric and (b) asymmetric perturbations.

induced gratings the perturbation occurs in the whole fibre's cross section and, therefore, simulations are harder to perform. Moreover, that perturbation may induce coupling among the cladding modes. Note also that when the spectrum exhibits two neighbour resonances multimode coupling [10] should be used instead of two mode coupling [4]. However, spectra of arc-induced gratings similar to the one presented in Figure 3.2 were also obtained. For instance, in section 5.3.1. (Figure 5.3) it can be observed the spectrum of a 400 μm LPFG induced in the aluminium doped fibre and Figure 3.3 also shows the spectrum of a grating written in the boron-germanium codoped fibre, from Fibercore.

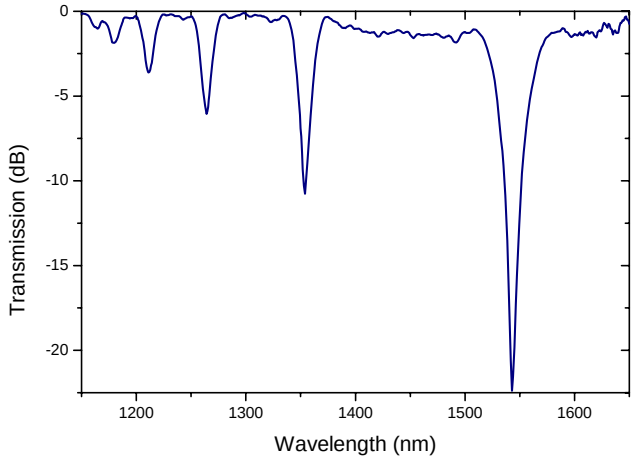

Figure 3.3 – Spectrum of a 415 μm LPFG induced in the B/Ge codoped fibre.

In order to assess the symmetry of the perturbation, the near field of several arc-induced gratings was measured. The procedure was as follows, the fibre was cleaved just after the grating and the near field of the radiation emerging from the fibre-end was detected by an infrared camera whilst the wavelength of a tunable laser (HQ4321A) was scanned around a particular grating resonance (positioned between 1520 and 1620 nm). Figure 3.4 (a)-(b) show the near field of two resonances positioned around 1550 nm that belongs to the gratings

shown respectively, in Figure 3.3 and Figure 3.2 (b). The intensity distribution presented in Figure 3.4 (a) indicates that coupling occurs to symmetric LP_{0j} cladding modes whilst its asymmetry in Figure 3.4 (b) indicates that the perturbation leads to coupling to LP_{1j} cladding modes. In general, the intensity distribution of the gratings under test was asymmetric inclusive for the 400 μm LPFG induced in the aluminium-doped fibre. Note that previous investigations on arc-induced gratings also pointed towards a contribution of asymmetric cladding modes to the near field pattern of the gratings [11, 12].

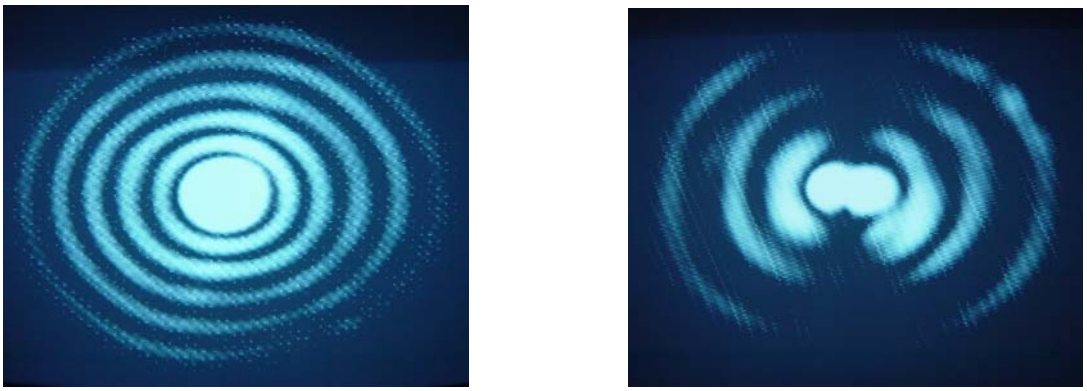

(a) (b)

Figure 3.4 – Intensity distribution in the near field for the (a) LP_{07} cladding mode of a 415 μm-LPFG written in the B/Ge fibre and (b) LP_{14} cladding mode of a 540 μm-LPFG written in the SMF28 fibre.

In conclusion, it was demonstrated that both type of perturbations can be induced by arc discharges and it is believed that the reasons for that rely on the alignment of the fibre between the electrodes during the gratings fabrication and/or the temperature gradient across the fibre due to an intrinsic asymmetry of the arc discharge.

3.3 The mechanisms of gratings formation

This is a topic of open research where several mechanisms have been proposed: diffusion of the core dopants, glass structure rearrangements as a result of densification or changes in the fictive temperature, elastic and viscoelastic stress relaxation and physical deformation of the fibre that includes both microbending and fibre tapering.

3.3.1 Dopants diffusion in silica glass

One of the first mechanisms proposed for the formation of arc-induced LPFGs was the diffusion of core dopants [13, 14]. The basis of these suggestions lays on former works

dedicated to the modification of the mode field diameter through thermal diffusion [15, 16]. For Ge-doped fibres, the desired modifications were achieved by keeping the fibres at temperatures above 1200 ºC for few hours (higher temperature requires lower times). However, during LPFGs fabrication the duration of the arc discharge is only a few seconds and, therefore, the diffusion coefficients of the dopants must be high in order to have a significant influence of diffusion on the grating formation. It is known that the diffusion coefficient of a single dopant depends among other factors, on temperature, on the presence of other codopants (such as the case of the increase of fluorine diffusion when codoped with phosphorus [17]), and may depend on its own concentration (as for phosphorus [18]). The fibres more often used in this thesis contain nitrogen or germanium. However, we have no knowledge of published results regarding the diffusion of nitrogen [13]. Consequently, the following discussion will be focused on Ge-doped silica glass fibres (standard singlemode fibres).

The Ge diffusion coefficient D can be estimated by using Arrhenius equation [16]

$$D = D_0 e^{-\frac{E}{RT}} \tag{3.6}$$

where D_0 is the pre-exponential term ($1.9\text{x}10^{-6}$ m^2/s), E is the activation energy ($2.9\text{x}10^5$ J/mol), T is the temperature (K) and R is the gas constant (8.314 $J.K^{-1}.mol^{-1}$). For a 1 *s* single arc discharge with an electric current of 9 mA, the fibre temperature was estimated to be 1320 ºC [19], and, therefore, a germanium diffusion coefficient of $5.9\text{x}10^{-16}$ m^2/s is obtained. In this calculation it was assumed a one-dimensional diffusion from a rectangular concentration distribution of the dopants, which is valid for diffusion lengths much smaller than the core radius. Under this assumption the diffusion length L can be written as

$$L = 2\sqrt{Dt} \tag{3.7}$$

where D is the diffusion coefficient and t the time. After substitution of D and t in Equation (3.7), a diffusion length of 49 nm is obtained, which is much smaller than the typical value of 4.3 μm for the fibre core radius. For a step index profile with a typical Δn of $4\text{x}10^{-3}$ gives a reduction in the local refractive index of $\sim 8\text{x}10^{-5}$. On the other hand, the increase of the core radius also increases the effective refractive index of the core mode by $\sim 5\text{x}10^{-5}$. Note that if a Gaussian profile would be assumed for the dopant concentration before and after the discharge [16], the effect on the refractive index would be even smaller. Therefore, for standard fibres submitted to a typical discharge of 9 mA for 1 s, the diffusion of germanium is

negligible for LPFGs formation. As a final remark, note that the same conclusion could also be drawn for nitrogen-doped fibres since no dopant diffusion could be observed after their annealing for 3 hours at 1500 °C [20]. Furthermore, if diffusion would occur during a 1 s discharge, it would be expected a significant correlation of core diameter with drawing temperature, which could not be observed (see section 3.3.3).

3.3.2 Changes in the glass structure

In this section it will be considered modifications of the glass structure that arises from densification or from changes in the fictive temperature of the fibre due to high cooling rates. Densification was the mechanism proposed to explain the changes observed in fibres having moderate and high germanium content in the core upon exposure to UV-laser radiation [21-23]. Borrelli *et al.* [24] demonstrated that densification has a strong dependence on composition and on wavelength of the UV-laser radiation. A similar effect was also found in fused silica samples submitted to femtosecond laser radiation [25]. Densification arises from modifications of ring structures in the silica network that, in turn, leads to changes in the Raman spectra [26, 27]. However, the origin of those modifications may be different for both laser exposures. Recently, Grubsky and Feinberg [28] have induced rewritable gratings in the core of boron-doped fibres by CO_2 laser radiation and they have suggested that gratings formation was due to reversible densification as a result of inelastic deformations.

The fictive temperature of a glass is the temperature at which the glass is formed after melting, that is, the glass structure at this temperature and at room temperature is the same [29]. It is known that the fictive temperature increases with the increase of the cooling rate. Different cooling rates occur during fibre drawing (depends on the drawing temperature and tension) and they also occur when the fibre is submitted to short time arc discharges (depends on the fabrication parameters: ~3000 ºC/s). Therefore, different cooling rates lead to fibres with different fictive temperatures which, in turn, results in fibres with different intrinsic properties such as viscosity, thermal expansion coefficient and refractive index [29, 30]. Thus, it was suggested that the high cooling rates involved during the short duration arc discharges could be responsible for the formation of arc-induced LPFGs [31, 32]. However, no change in the fictive temperature of a fibre submitted to arc discharges was found from Raman spectroscopy experiments [6]. Changes were observed in the Raman spectra but not in the bands associated with the fictive temperature. Yablon [33] explained this result through the flatteness of the temperature dependence of the refractive index in the typical range of fictive temperatures of optical fibres (Figure 3.5 (a)). Nevertheless, it is known that the annealing at high temperatures (1000 ºC) for long times (10 h) of fibres with high fictive temperatures results in changes of the glass structure and then in changes of its fictive temperature [34]. Furthermore, Kim and co-workers [35] demonstrated that the core and the

cladding have completely different fictive temperatures which, for typical cooling rates associated with the arc discharge, can be of 1150 ºC and 1620 ºC, respectively. Moreover, the temperature reached by the fibre during an arc discharge was estimated to be of about 1320 ºC [19]. Note also that the refractive index increases with the increase of the density (which is inversely proportional to the volume) for temperatures up to ~1500 ºC (Figure 3.5 (b)). Therefore, it is expected that at least in the core some change of the glass structure occurs, namely, an increase of the refractive index as a result of an increase in the fictive temperature. Further work is required to clarify this potential mechanism. In particular, the measurement of the fictive temperature in a sample treated with arc discharges with the same method as used by Kim *et al*. would allow a separation between the effect in core and cladding.

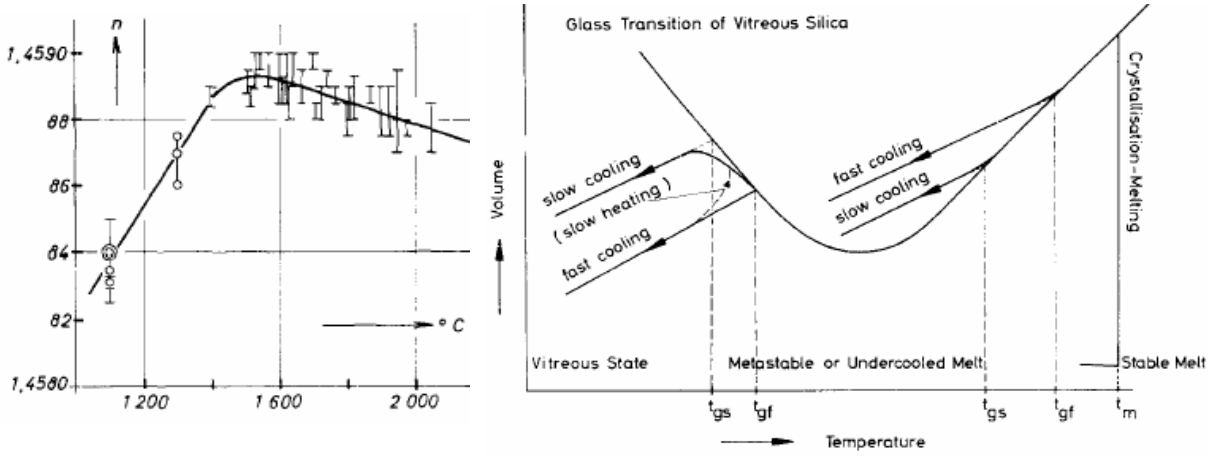

(a) (b)

Figure 3.5 – (a) Refractive index as a function of fictive temperature; (b) Volume versus temperature (Taken from [29]).

3.3.3 Stress relaxation

A standard singlemode fibre consists typically of a germanium-doped silica core and a pure-silica cladding. As a result of the doping, the properties of the core, in particular, its thermal expansion coefficient increases and its viscosity decreases when compared to the properties of the cladding. Therefore, during fibre drawing the higher viscosity material, in this case the cladding, cools more rapidly than the core and bears the brunt of the drawing tension, being thus under tensile stress. The melted core, in turn, is surrounded by the solid cladding and cannot expand being under compressive stress during cooling. Simultaneously, due to an higher thermal expansion coefficient, the core also exerts an hydrostatic pressure on the cladding. Hence, the final residual stress in the core is a result of two kinds of elastic stresses: thermal and draw induced. The former is associated with the different thermal expansion coefficients and are also present in the fibre preforms. The latter is induced by drawing and is associated with the different viscosities of core and cladding materials. Draw induced residual

stresses can be released during fibre annealing, that is, the fibre is heated to a high temperature (>1000 ºC) and is held for some time, followed by slow cooling to room temperature. Residual stresses are also released in a cleaved fibre-end. It has been proposed that the periodic stress relaxation caused by arc discharges or CO_2 laser radiation is an important mechanism of gratings formation [33, 36-38]. However, in a previous work [31] where gratings were written in pre-annealed fibres (stress free fibres) it was emphasised that stress relaxation was not the main mechanism responsible for arc-induced gratings formation. In order to clarify this apparent contradiction, stress measurements were, therefore, required. To evaluate the contribution of stress relaxation to grating formation, several LPFGs were fabricated by the electric arc technique in three nitrogen-doped fibres drawn with different drawing tensions. Gratings were also produced using increasing external pulling tensions. Afterwards, stress measurements were performed at EPFL-Lausanne.

The preform from which the nitrogen-doped fibres were drawn was manufactured by reduced-pressure plasma-chemical deposition [39]. The nitrogen-doped core layers incorporate 1 at% of nitrogen and are deposited in a pure silica supporting tube, which itself is embedded into several pure silica jacketing tubes. Drawing tensions of 65, 125, and 195 g, respectively, were used, corresponding to drawing temperatures of 1940, 1905, and 1880 °C at constant drawing speed. The difference in drawing tension results in different residual stress profiles due to a mismatch between core and cladding viscosity at the drawing temperature [40]. The core and cladding diameters of the three fibres were measured using a Photon Kinetics 2400 Fibre Geometry System and found to be 6.0 ± 0.2 μm and 126.0 ± 0.3 μm, respectively. Refractive near field measurements yield a core-cladding index difference of (1.10 ± 0.06) x 10^{-2} for all fibres under investigation. The photo-elastic contribution to the refractive index difference [41] was hence too small to be detected within the error of the refractive index measurement.

LPFGs inscription was performed as described in section 4.3.1. To evaluate the influence of this external load on the grating spectrum, three different weights (5.1, 22.8, and 36.3 g) have been used within the experiment. For all gratings, an electric arc was applied to the fibre using a current of 9 mA and a discharge time of 1 s. A period of 400 μm was chosen and 40 discharges were applied to the fibre, resulting in a total grating length of 16 mm. The LPFG transmission spectra have been measured using a white-light source and an optical spectrum analyser with a wavelength resolution of 1 nm.

To investigate the influence of fibre drawing tension on the grating spectra, LPFGs have been written in each of the three fibres using exactly the same arc discharge parameters. The external load applied to the fibre was set to 22.8 g. The three grating spectra obtained are shown in Figure 3.6. For each of the three fibres, five loss peaks in the transmission spectrum

can be identified. No significant dependence of peak loss or coupling strength on drawing tension could be observed within the reproducibility of the grating fabrication method. In contrast, the peak positions were found to differ significantly for the three fibres under investigation. However, no correlation was found between peak position and drawing tension.

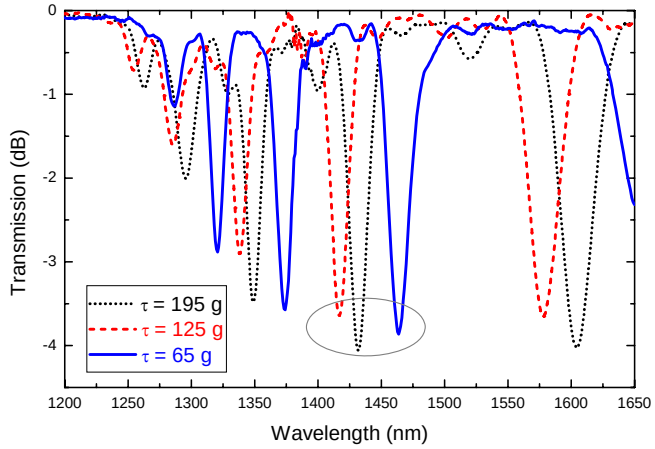

Figure 3.6 – Spectra of gratings inscribed in fibres drawn at different drawing tensions, using arc discharge. The external load was set to 22.8 g.

In addition, LPFGs have been inscribed using three different external loads. All gratings were written in the fibre drawn with the lowest drawing tension of 65 g. The corresponding grating spectra are shown in Figure 3.7. The peak positions of the gratings do not depend on external load, whereas the peak transmission losses increase with increasing external load. The rejection loss of the 5th resonance varies from 0.55 dB to 18.5 dB with external load of 5.1 g to 36.3 g. For the highest external load, a background loss of about -2 dB was found; in contrast, the background loss in the two other LPFGs does not exceed -0.25 dB.

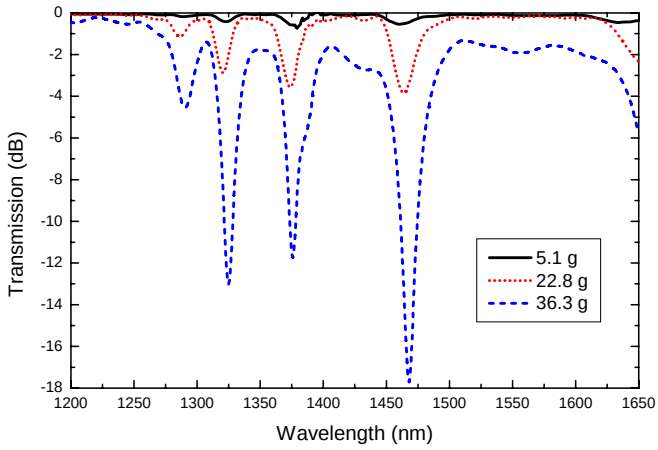

Figure 3.7 – LPFG spectra obtained for grating inscription with varying external load in the fibre drawn with the lowest drawing tension of 65 g.

To determine the two-dimensional stress profile of the fibres, the setup shown in Figure 3.8 was used. The axial stress induced phase retardation profile of the fibre is determined polarimetrically for 60 projection angles from 0° to 180°. Subsequently, the axial stress profile is calculated from the projection data by the inverse Radon transform [42]. The imaging system used consists of a 10x objective (NA=0.3) and a CCD camera (768x574 pixels). The sampled area in the object plane has a size of about 520x390 μm^2. In vertical direction, the area is divided into 7 rows of 82 pixels. To improve the signal to noise ratio, we average over the 82 pixels, which results in 7 sampling points with a resolution of about 55 μm along the fibre axis. The transverse spatial resolution is given by the diffraction-limit of the objective and is about 1.3 μm.

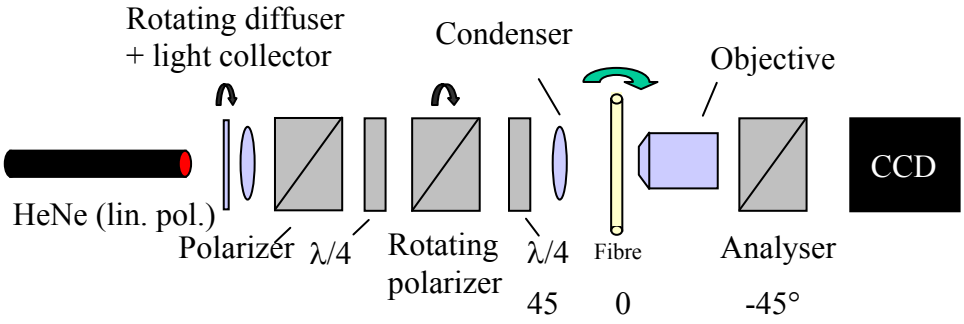

Figure 3.8 – Setup used for the measurement of the tomographic stress profiles (Taken from [42]).

To get direct information about stress changes due to arc discharge, tomographic stress measurements have been performed in the fibres before and after grating inscription. A typical stress profile obtained is given in Figure 3.9 for the fibre drawn with a tension of 125 g. Before the arc discharge, the stress profiles of all fibres were found to be symmetric.

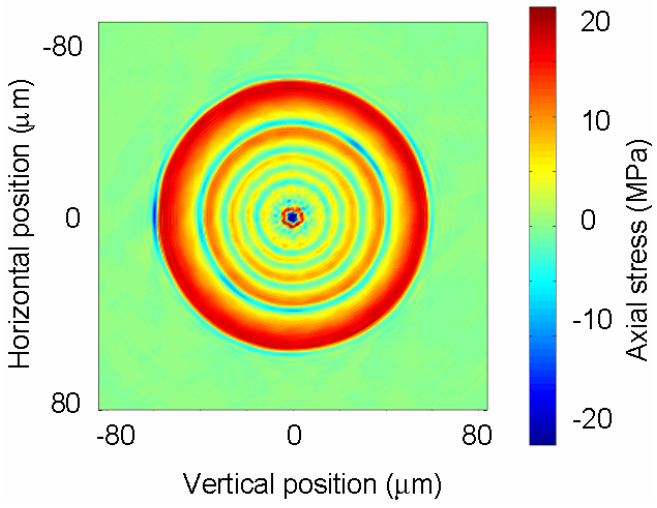

Figure 3.9 – Tomographic stress profile of the nitrogen-doped fibre drawn with a tension of 125 g.

One-dimensional stress profiles of the three pristine fibres are illustrated in Figure 3.10(a). The fibre cores are under compressive stress, whereas the surrounding silica tubes exhibit tensile stress. Figure 3.10(b) shows the core and outermost cladding tube stresses plotted as a function of drawing tension. As expected, a linear dependence of stress on drawing tension is found [40]. Extrapolation to zero drawing tension yields the stress values

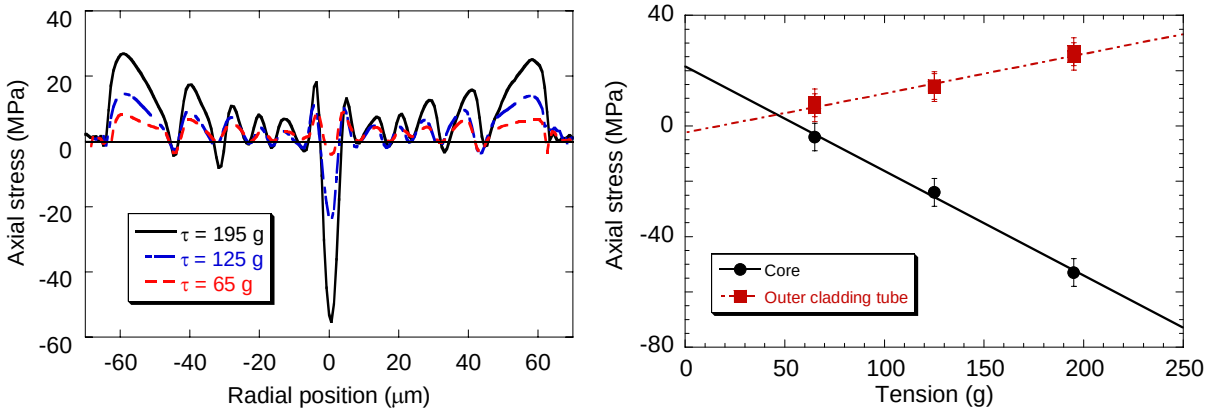

(a) (b)

Figure 3.10 – (a) Residual stress profiles of the three fibres drawn at different tensions and (b) Both core and cladding tube stresses change linearly with drawing tension.

of the preform, where only thermal stresses are present. If drawing induced stresses were annealed completely after arc discharge, the fibre stress profile would equal the preform stress profile with a tensile core stress of about 20 MPa and an almost vanishing stress value in the cladding. For the fibre drawn with the highest tension of 195 g, where the initially compressive core stress is almost -60 MPa, a stress modulation of up to 80 MPa could thus be achieved theoretically, corresponding to a potential index modulation of 5.2×10^{-4} [21], indeed sufficient for grating realization.

After the arc discharge, the stress profile changes considerably. In Figure 3.11, two-dimensional stress profiles of the fibres drawn with a tension of 195 g (above) and 65 g

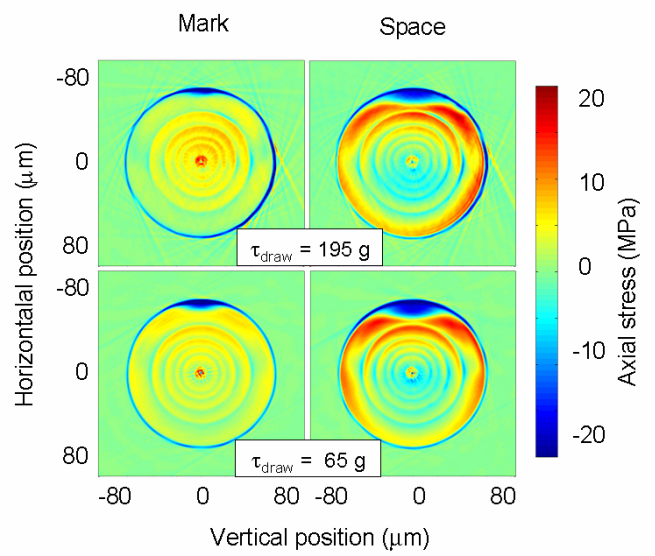

Figure 3.11 – Arc-induced two-dimensional stress profiles of the nitrogen-doped fibre for drawing tensions of 195 g (above) and 65 g (below). External load applied to both fibres was 22.8 g. The left and right columns show the profile at the position of arc discharge and in the middle of two discharges, respectively. Almost no dependence on the initial stress profile is found.

(below) after LPFG inscription are shown. For both fibres, the externally applied load during arc discharge was set to 22.8 g. The stress in the fibre exhibits mirror symmetry along the axis of arc discharge. The stress profiles do not depend on the initial stress profile, neither at the position of arc discharge ("mark"), nor in-between two adjacent arc discharge positions ("space"). The compressive core stress has been annealed to 15 MPa in the "mark" and 10 MPa in the "space" region, respectively. For both "mark" and "space", the fibre stress at the air-cladding interface has turned compressive.

In Figure 3.12, the modification of axial stress with external load applied to the fibre during discharge is shown for the fibre drawn with the highest tension. Again, we find stress modifications with mirror symmetry along the axis of arc discharge both in the "mark" (left column) and in the "space" (right column) region of the LPFG. Clearly, the quantity of residual stress in the cladding increases with external load for both regions. The residual stress in the "space" region almost doubles the stress in the "mark" region. However, the residual core stress is only slightly affected by the external load. For all loads, the residual core stress is approximately 15 MPa in the "mark" and about 10 MPa in the "space" region.

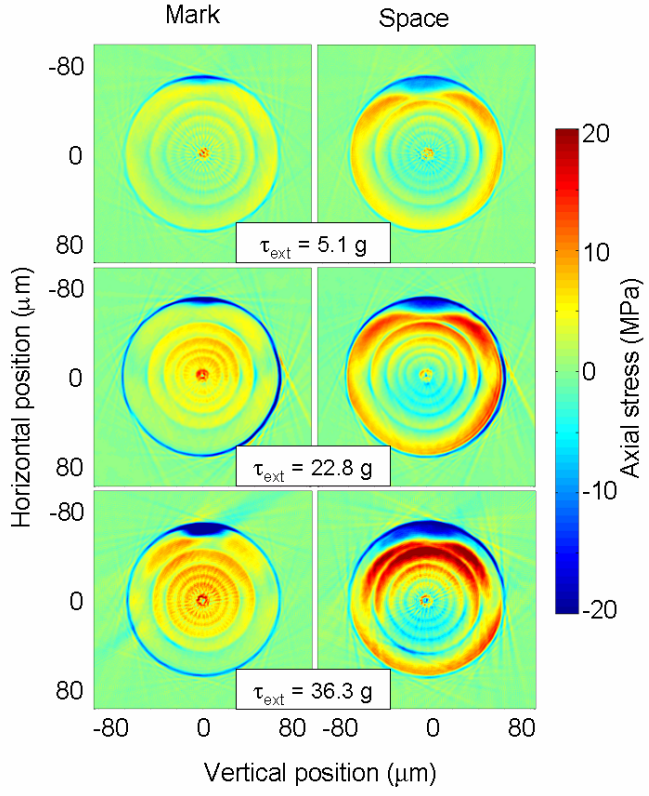

Figure 3.12 – Arc-induced two-dimensional stress profiles of nitrogen-doped fibre (τ_{draw}=195 g) as a function of external load applied during discharge (5.1 g above, 22.6 g middle, 36.3 g below). The higher the external load, the higher is the residual stress in the cladding.

From previous results it can be drawn the following conclusions: the grating's coupling strength does not depend on the initial stress but increases with the external load; the core stress modulation is too small to cause the observed coupling strength; the external load slows down stress relaxation. Furthermore, the length of the annealed region was estimated to be ~1 mm which is much larger than the grating period [7]. However, it is expected some contribution of stress relaxation to the coupling strength in situations where the annealed region is shorter than the grating period.

To show the general potential to induce stress changes in a pure-silica-core fibre with an electric arc, the stress profile of a splice made using a FITEL S148 fusion splicer, configured for standard singlemode fiber splicing, is illustrated in Figure 3.13 (a)-(b). The arc discharge clearly promotes stress relaxation, the core and the inner cladding become less compressive and the outer cladding less tensile.

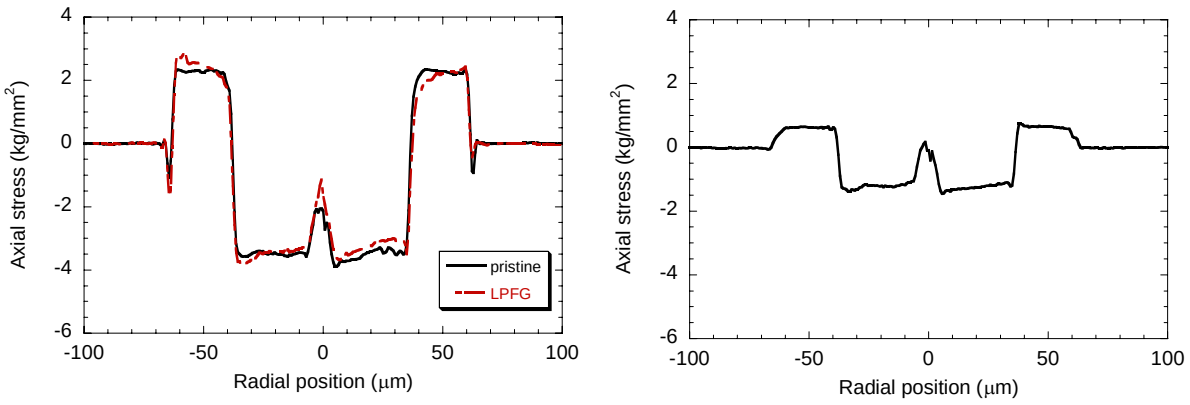

Figure 3.13 – (a) One-dimensional stress profiles of the pure-silica-core fibre inside and outside the LPFG. The two stress profiles are found to be almost identical; and (b) Stress profile of the pure-silica-core fiber after single arc discharge under conventional fusion conditions. Stress relaxation can clearly be observed.

Viscoelastic stress relaxation. Pre-annealing of the fibre

Recently, relaxation of inelastic stress was proposed as a possible mechanism for LPFGs formation [33]. Inelastic or viscoelastic stresses are frozen in the highest viscosity region of the fibre during its drawing, due to its time-dependent response to the applied tension. Frozen-in viscoelasticity is allowed to relax during annealing of the fibre for few seconds at temperatures close to the fictive temperature. Therefore, the effect of fibre pre-annealing on grating formation was analysed. The refractive index and residual stress profiles were measured before and after the heat treatment. In addition, two-dimensional stress profiles were recorded after LPFG inscription.

LPFGs were arc-induced in the nitrogen-doped fibre drawn with a tension of 195 g at a temperature of 1880 °C. Several samples of this fibre were annealed in a tubular oven at 1050 ºC for 30 min. To prevent the building of new stresses during the thermal treatment, the heating and cooling rates were kept at ~5 ºC/min. A small weight of 2.2 g was suspended at one end of each fibre samples to keep it straight. After cooling down to room temperature, LPFGs were written in the pre-annealed fibre samples. For gratings inscription, the fabrication parameters were set as follows: axial tension of 22.8 g, electric current of 9 mA, arc duration of 1 s and a grating period of 400 μm. The spectra of the gratings written in the pristine and pre-annealed fibres are presented in Figure 3.14. The coupling strength of the grating induced in the pre-annealed fibre is 3 to 4 times higher than that induced in the pristine one, despite the fact that the former has half the length of the latter. In addition, the spectrum of the former also moved towards lower wavelengths and the shift increases with the cladding modes order ranging from 30 (2^{nd}) to 65 nm (6^{th}).

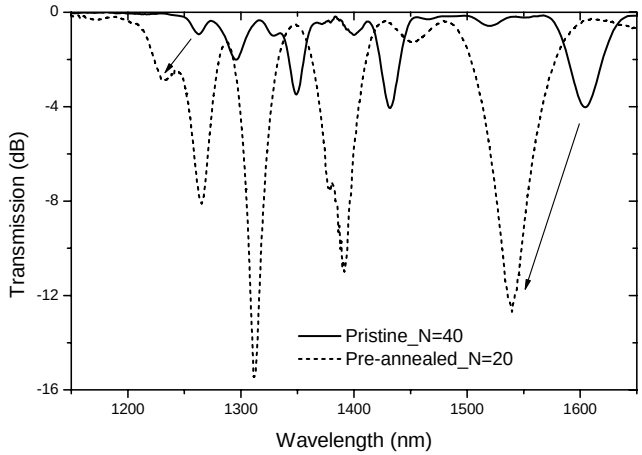

Figure 3.14 – Spectra of gratings written in the pristine and pre-annealed fibre. Note that the LPFG written in the pristine fibre is twice longer (40x400 μm =16 mm).

The fibre's refractive index profile (RIP) before and after pre-annealing was measured at room temperature (18 ºC) using a S14 Refractive Index Profiler from Photon Kinetics. For calibration, an oil with a refractive index of 1.47 (25 ºC and 632.8 nm) was used. The accuracy of the measurements was ~10^{-4}. For a fibre drawn from the same preform with a tension of 125 g, the refractive index was found to be significantly higher in the cladding (Figure 3.15). The thermal treatment induced an overall increase of the fibre refractive index in both fibres. In particular, almost the same value for the cladding refractive index is obtained. The cladding refractive index of the fibre drawn at 195 g can thus be increased by about 1.5x10^{-3} by annealing.

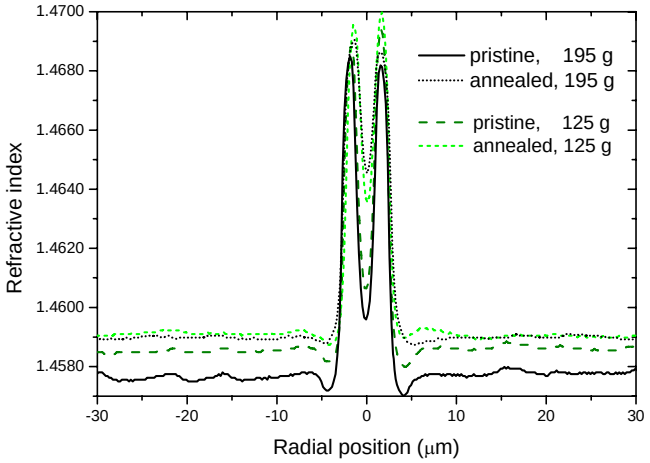

Figure 3.15 – Refractive index profiles of the fibres drawn with 125 g and 195 g, before and after annealing.

The stress profiles of the pristine and heat treated fibre samples were found to be azimuthally symmetric. Therefore, Figure 3.16 shows only the one-dimensional stress profiles. For the pristine fibre, the core is under compressive stress (-55 MPa), whereas the

surrounding silica tubes exhibit tensile stress up to a value of ~25 MPa. The annealing relaxes the drawing-induced stresses resulting from a mismatch in viscosity between core and cladding. The remaining tensile core stresses of about ~5 MPa result from the mismatch in thermal expansion coefficient between the core and the cladding.

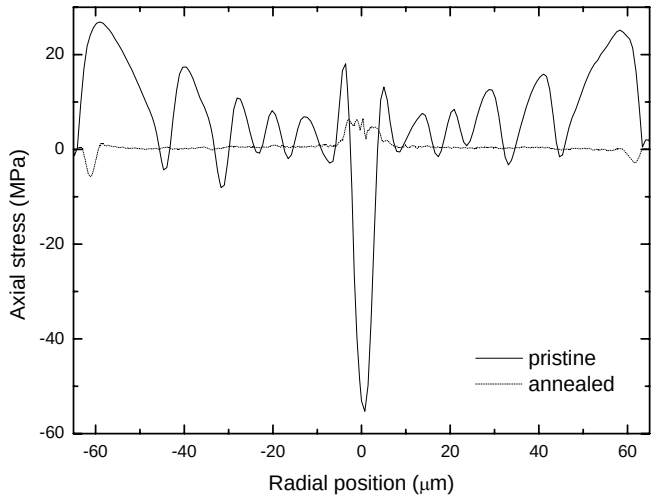

Figure 3.16 – One-dimensional stress profiles of the nitrogen doped fibre, before and after annealing.

Figure 3.17 shows the two-dimensional stress profiles for a grating induced in the pristine and pre-annealed fibre, respectively. The profiles were measured at two positions inside a grating period: midway between two discharges (space) and in the discharge region (mark). It can be clearly seen that changes in the stress profiles are more pronounced for the pre-annealed fibre. In the core region, strong asymmetric stresses up to 150 MPa were induced by the arc discharge. In contrast, the stress profile of the cladding only exhibits small asymmetries (±20 MPa). The increase in coupling strength shown in Figure 3.14 might thus be due to periodic stress-induced index changes in the fibre core.

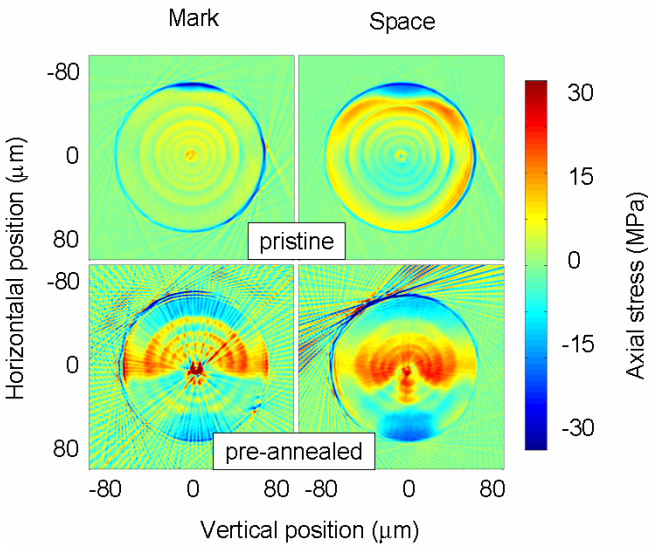

Figure 3.17 – Two-dimensional stress profiles measured inside two gratings induced in pristine and pre-annealed fibres. In the left column, the profile is shown directly at the position of arc discharge; the right column gives the profile just in the middle of two discharges. In order to keep a reasonable contrast in the cladding region, the scale was limited to ±30 MPa and, therefore, the colour of the core is saturated (150 MPa).

The cladding index changes related to stress changes (Figure 3.16) are, by photoelasticity, one order of magnitude smaller than the index changes actually observed (Figure 3.15). In contrast, the increase in cladding refractive index can be explained by the annealing of isotropic inelastic strains frozen into the fibre during its drawing process [33]. As the amount of inelastic strain increases with drawing tension, the annealing-induced index increase is higher for the fibre drawn with 195 g than for those with 125 g. The shift towards shorter wavelengths observed in Figure 3.14 might thus be originated by a decrease of the core-cladding index difference due to inelastic strain relaxation.

3.3.4 Geometric deformation

In section 3.3.3 it was shown that the grating's coupling strength increased with the increase of the external tension applied during the fabrication process. At the same time, it was observed that the fibre's cross section was reduced during the grating inscription, being that reduction larger for higher tensions applied. Applying typical arc discharge parameters (9 mA and 1 s), diameter reductions of ~5% and ~10% were measured for external tensions of respectively 22.8 g and 36.3 g. For a 5.1 g, the reduction is below 1%. Note that the fibre modulation depends on its composition. Softer fibres such as B/Ge codoped and sulphur-doped fibres exhibit larger modulations. Figure 3.18 shows a modulation of ~5% obtained during the inscription of a 540 µm-grating in the SMF28 fibre, from Corning. Therefore, the change of the fibre's cross section is a potential mechanism for grating's formation.

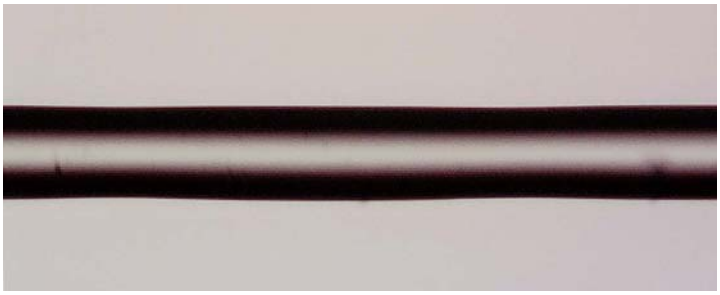

Figure 3.18 – Fibre modulation induced by arc discharges.

Two types of geometric deformation can occur in a fibre during an arc discharge: microbending [43] and tapering [12, 31, 44]. The former, occurs when the fibre is submitted intentionally to lateral strain, to an intrinsic asymmetry of the arc discharge or when the fibre is not well centred with the arc discharge whilst under axial tension. The latter occurs when the fibre well centred in between the electrodes, is submitted to axial strain caused by pulling weights of a few tens of grams. The extent of the change in the fibre cross-section depends not only on the pulling tension but also on the value of the electric current which establishes the temperature of the fibre. Figure 3.19 exemplifies the fabrication technique based on microbending. The fibre is fixed in two holders and then one of them is displaced laterally ~100 μm. Finally, an electric discharge is applied periodically. Microbending is a well known method to produce mechanical gratings and will be discussed in detail in Chapter 6.

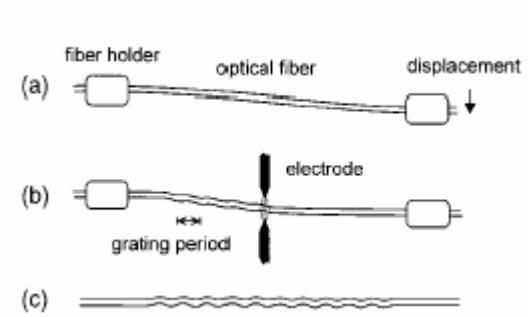

Figure 3.19 – Technique to arc-induce microbends in the fibre (Taken from [43]).

In what follows only fibre tapering will be analysed. In particular, the influence on the gratings spectra, that is, on the position of the resonant wavelengths and also on the coupling strength will be determined. Those calculations are based on the couple mode theory and assume that the core and the cladding have the same relative changes. For the simulations it was considered typical parameters of the SMF28 fibre: D_{core} = 8.6 μm, D_{clad} = 125.0 μm and $\Delta n = 5.1 \times 10^{-3}$, corresponding to ~3.46 mol% of germanium content. The dispersion relations

for the core (3.46 mol% of Ge) and cladding (pure SiO_2) materials were obtained using Sellmeier's equation [45]

$$n^2 - 1 = \sum_{i=1}^{3} \frac{A_i \lambda^2}{\lambda^2 - l_i^2} \tag{3.8}$$

in which n is the refractive index at the wavelength λ, and A_i and l_i are coefficients that depend on the germanium content. For the simulated grating, it was considered a sinusoidal perturbation of period 540 μm and a length of 22 mm. The position of the resonance wavelengths as a function of the core and cladding modulation, acting separately, is shown in Figure 3.20. As seen, whilst the reduction of the cladding diameter leads to an increase of the resonance wavelengths, the reduction of the core diameter leads to an opposite change. For the first symmetric cladding modes, the figure also shows that the latter is predominant when both changes occurs simultaneously. Note that a similar dependence on the fibre geometry was found for asymmetric cladding modes.

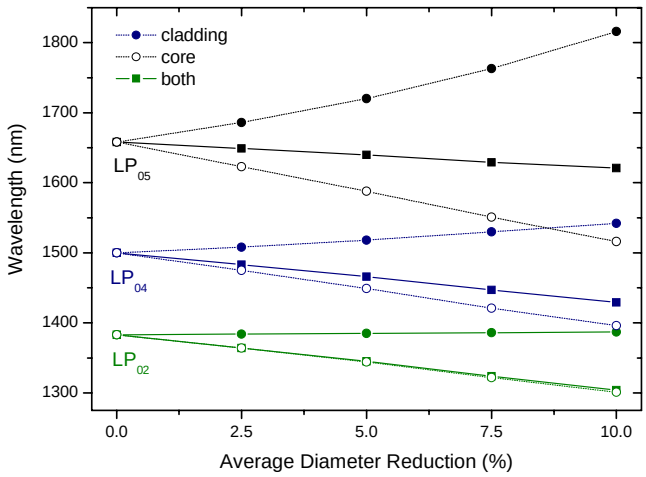

Figure 3.20 – Resonance wavelengths as a function of the geometric modulation (%): 0, 5, 10, 15 and 20.

To determine the influence of the fibre modulation on the coupling strength it was considered a Δn equal to the core-cladding difference in a length corresponding to the decrease of the core diameter (Figure 3.21). The change at the cladding-air interface was not taken into account since there the core mode is negligible. Moreover, the refractive index difference is too high to be considered a small perturbation. Since the coupling strength depends on the wavelength and as seen previously the change in the fibre geometry alters the position of the resonances, it was only taken into account the effect of the modulation and not the changes on the average core and cladding diameters.

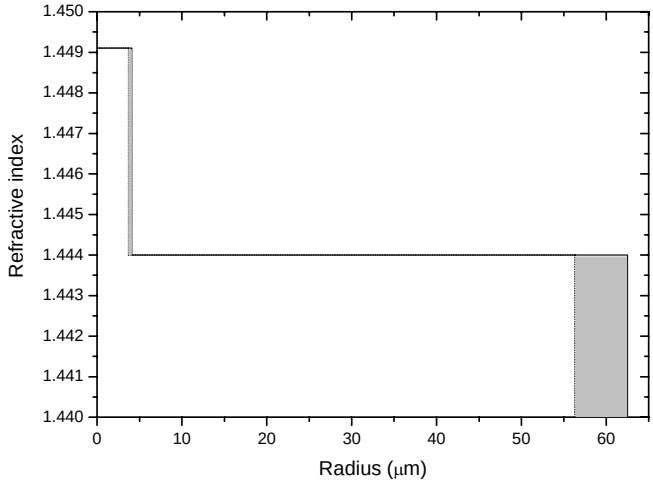

Figure 3.21 – Refractive index change due to the fibre modulation (the dark regions correspond respectively, to a reduction of the dimensions of the core and cladding of the fibre).

From Equations (3.4) and (3.5) the coupling constant can be expressed as [46]

$$k_g = C\frac{\pi \Delta n_{\mathrm{mod}} I}{\lambda_r} \tag{3.9}$$

where I is the overlap integral

$$I = \frac{\int_0^{2\pi}\int_{r_{co}-\Delta r}^{r_{co}} \vec{E}_{co}(r,\phi).\vec{E}^{*}_{cl,m}(r,\phi) r dr d\phi}{\sqrt{\int_0^{2\pi}\int_0^{\infty} \vec{E}_{co}(r,\phi).\vec{E}^{*}_{co}(r,\phi) r dr d\phi}\sqrt{\int_0^{2\pi}\int_0^{\infty} \vec{E}_{cl,m}(r,\phi).\vec{E}^{*}_{cl,m}(r,\phi) r dr d\phi}} \tag{3.10}$$

λ_{r} is the resonance wavelength, Δn_{mod} is the refractive index modulation ($\Delta n/2$) and C is a constant equal to the first coefficient in the Fourier transform of the grating pitch shape. For a sinusoidal profile it is equal to 1 and for a rectangular profile [46]

$$C = \frac{4}{\pi}\sin\frac{\pi d}{\Lambda} \tag{3.11}$$

where d is the length of the region affected by the arc. For this particular case, assuming a duty-cycle of 0.5, one gets $C = 4/\pi$. Figure 3.22 shows the coupling constant as a function of the core modulation for the first four cladding modes. As seen, it increases with the increase of the modulation being larger for the higher order cladding mode. Note, however, that for modulations of the order of 5%, the coupling constant associated with LP_{04} mode is about one order of magnitude less than required to achieve 100% coupling ($kL = \pi/2$). Furthermore, for

modulations of the order of 10% the requirement of having a small perturbation may not be fulfilled and therefore, the coupled-mode theory is not very accurate. In those cases, the transfer-matrix approach based on modal analysis [47, 48] may be a reliable alternative.

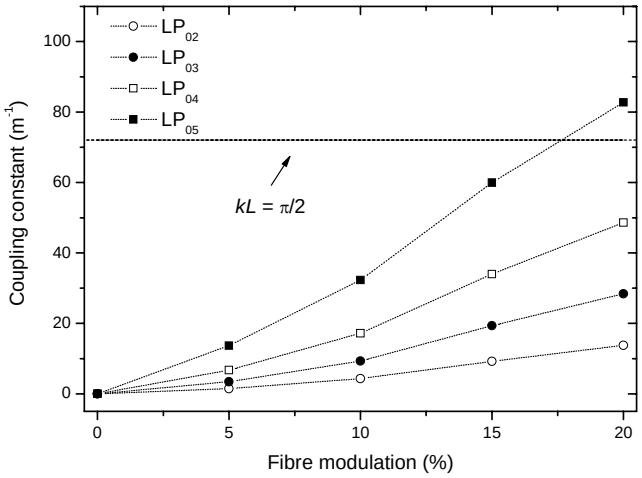

Figure 3.22 – Coupling constant as a function of the fibre's diameter modulation.

It should be stressed that this geometric change does not promote coupling to asymmetric cladding modes. However, if on top of the geometric modulation, an asymmetric perturbation of the refractive index was also induced in the same region, it would be expected the formation of a strong grating since in that case the overlap integral is 5 to 7 higher than for symmetric modes. In fact, that may be the reason for the strong coupling obtained for the grating written in the pre-annealed fibre, discussed in section 3.3.3, that shows a considerable "half-moon" stress change around the core region.

A closer look at Figure 3.18 enables one to conclude that, in fact, the periodic geometric modulation of the fibre is asymmetric. Furthermore, the fibre core is itself periodically shifted causing a microdeformation (Figure 3.23(b)) which, in turn, can promote coupling to asymmetric cladding modes as observed in previous spectra (Figure 3.2(b)). It should be noted that the position of the resonance wavelengths belonging to asymmetric cladding modes also shifts with the increase of the fibre modulation similarly as observed for the symmetric cladding modes (Figure 3.20). In order to estimate the influence of the microdeformation on the coupling constant we have assumed that the core shift induces a refractive index change as shown in Figure 3.24. Based on that and following a similar procedure, as for the symmetric case, we calculated the coupling constant as a function of increasing microdeformations (Figure 3.25). As seen, the estimated value of 0.35 μm for the core shift is sufficient to induce 100% coupling to asymmetric cladding modes.

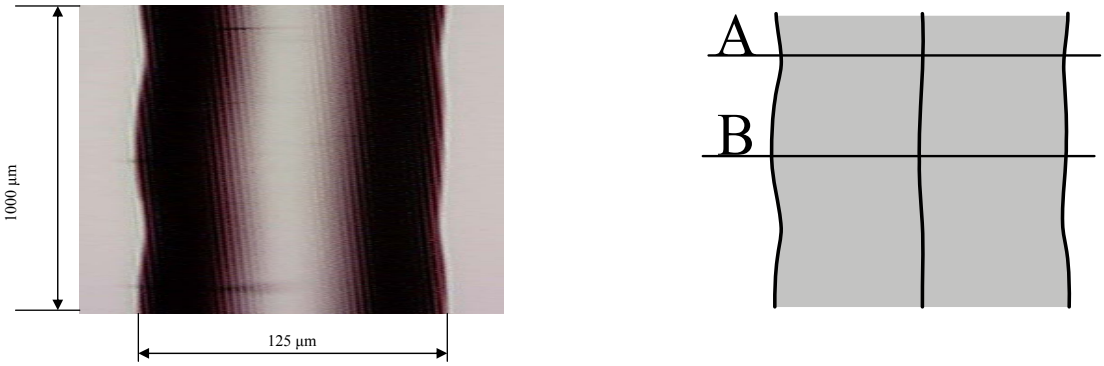

(a) (b)

Figure 3.23 – (a) Photograph of the fibre with its shape modified by arc discharges and (b) shift of the fibre central line (microdeformation).

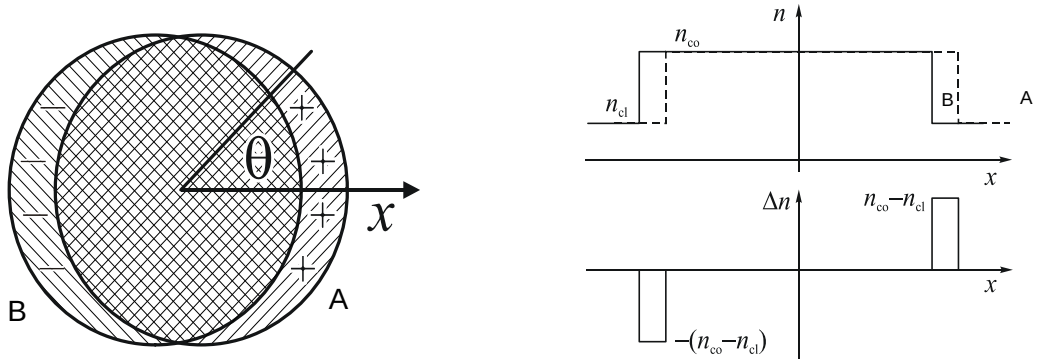

(a) (b)

Figure 3.24 – (a) Refractive index change due to the shift of the fibre core and (b) refractive index change along the *x* axis.

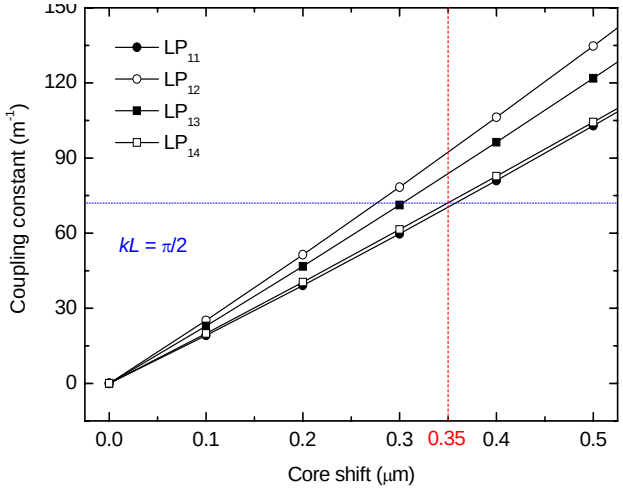

Figure 3.25 – Coupling constant as a function of the core shift.

3.4 Summary

In this chapter it was first presented the basic theory related to long-period fibre gratings. Afterwards, the different mechanisms proposed in the literature for the formation of arc-

induced gratings were discussed. Thus, in which concerns the eventual diffusion of the core dopants as a mechanism for gratings formation, it was concluded that for the typical dopants and arc discharge parameters involved in this work, this process is negligible. For an estimated fibre temperature of ~1400 ºC it is expected that changes in the glass structure may occur, namely in the core region for which the fictive temperature is lower. Elastic stress relaxation is a well known mechanism of gratings formation, but in the case of arc-induced gratings it will be effective only when the grating period is much larger than the arc dimensions. The viscoelastic stress relaxation can also contribute for gratings formation, as demonstrated in the annealing experiments where changes in the refractive index of the highest viscosity region as large as 10^{-3} were found. However, further studies are required to quantify the effect of a short duration arc discharge on viscoelastic stress release. Regarding the geometric modulation of the fibre, it was demonstrated that on its own is not sufficient to explain the observed enhancement on the gratings coupling strength, for increasing external loads. However, the estimated periodic shift of the fibre core due to the arc discharges, is big enough to induce coupling to asymmetric modes and, therefore, microdeformation is an effective mechanism for the formation of arc-induced gratings.

References

[1] C. Tsao, *Multilayered cylindrical waveguides*, in *Optical fibre waveguide analysis*. Oxford University Press: 243, 1992

[2] A.W. Snyder and J.D. Love, in *Optical waveguide theory*. Kluwer Academic Publishers, 2000

[3] A. Yariv, *Propagation of optical beams in fibers*, in *Optical Electronics*. Saunders College Publishing: 74, 1991

[4] T. Erdogan. *Cladding-mode resonances in short- and long-period fiber grating filters.* Journal of the Optical Society of America A-Optics Image Science and Vision **14**(8): 1760-1773, 1997.

[5] Z.J. Zhang and W.K. Shi. *Eigenvalue and field equations of three-layered uniaxial fibers and their applications to the characteristics of long-period fiber gratings with applied axial strain.* Journal of the Optical Society of America A-Optics Image Science and Vision **22**(11): 2516-2526, 2005.

[6] A. Malki, G. Humbert, Y. Ouerdane, A. Boukhenter, and A. Boudrioua. *Investigation of the writing mechanism of electric-arc-induced long-period fiber gratings.* Applied Optics **42**(19): 3776-3779, 2003.

[7] F. Durr, G. Rego, P.V.S. Marques, S.L. Semjonov, E. Dianov, H.G. Limberger, and R.P. Salathe. *Stress Profiling of Arc-Induced Long Period Fiber Gratings.* Journal of Lightwave Technology **23**(11): 3947-3953, 2005.

[8] A. Vengsarkar, P. Lemaire, J. Judkins, V. Bhatia, T. Erdogan, and J. Sipe. *Long-period fiber gratings as band-rejection filters.* Journal of Lightwave Technology **14**(1): 58-65, 1996.

[9] E. Anemogiannis, E. Glytsis, and T. Gaylord. *Transmission characteristics of long-period fiber gratings having arbitrary azimuthal/radial refractive index variations.* Journal of Lightwave Technology **21**(1): 218-227, 2003.

[10] Z. Liu and C. Yang. *Multi-mode coupling in long-period fibre gratings.* Chinese Physics Letters **21**(8): 1549-1552, 2004.

[11] M. Verhaegen, P. Orsini, D. Perron, X. Daxhelet, and S. Lacroix. *Long period gratings fabrication techniques*. in *Applications Of Photonic Technology 4 - Closing The Gap Between Theory, Development, And Application*: 156-161, 2000.

[12] M. Kim, D. Lee, B. Hong, and H. Chung. *Performance characteristics of long-period fiber-gratings made from periodic tapers induced by electric-arc discharge.* Journal of the Korean Physical Society **40**(2): 369-373, 2002.

[13] E.M. Dianov, V.I. Karpov, M.V. Grekov, K.M. Golant, S.A. Vasiliev, O.I. Medvedkov, and R.R. Khrapko. *Thermo-induced long-period fibre gratings*. in *IOCC-ECOC 97 - 11th International Conference on Integrated Optics and Optical Fibre Communications / 23rd European Conference on Optical Communications, Vol 2*: 53-56, 1997.

[14] S.G. Kosinski and A.M. Vengsarkar. *Splice-based long-period fiber gratings*. in *Proceedings of 1998 Optical Fiber Communications Conference*: 278-279, 1998.

[15] J.S. Harper, C.P. Botham, and S. Hornung. *Tapers in Single-Mode Optical Fiber by Controlled Core Diffusion.* Electronics Letters **24**(4): 245-246, 1988.

[16] K. Shiraishi, Y. Aizawa, and S. Kawakami. *Beam Expanding Fiber Using Thermal-Diffusion of the Dopant.* Journal of Lightwave Technology **8**(8): 1151-1161, 1990.

[17] J. Kirchhof, S. Unger, K.F. Klein, and B. Knappe. *Diffusion Behavior of Fluorine in Silica Glass.* Journal of Non-Crystalline Solids **181**(3): 266-273, 1995.

[18] J. Kirchhof, S. Unger, and J. Dellith. *Diffusion of phosphorus doped silica for active optical fibers.* Journal of Non-Crystalline Solids **345-46**: 234-238, 2004.

[19] G. Rego, L. Santos, B. Schroder, P. Marques, J. Santos, and H. Salgado. *In situ temperature measurement of an optical fiber submitted to electric arc discharges.* IEEE Photonics Technology Letters **16**(9): 2111-2113, 2004.

[20] V.I. Karpov, M.V. Grekov, E.M. Dianov, K.M. Golant, and R.R. Khrapko. *Ultra-thermostable long-period gratings written in nitrogen-doped silica fibers*. in *Proceedings of Reliability Photonics Materials and Structures Symposium*: 391-396, 1998.

[21] H.G. Limberger, P.Y. Fonjallaz, R.P. Salathe, and F. Cochet. *Compaction- and photoelastic-induced index changes in fiber Bragg gratings.* Applied Physics Letters **68**(22): 3069-3071, 1996.

[22] E.M. Dianov, V.G. Plotnichenko, V.V. Koltashev, Y.N. Pyrkov, N.H. Ky, H.G. Limberger, and R.P. Salathe. *UV-irradiation-induced structural transformation of germanosilicate glass fiber.* Optics Letters **22**(23): 1754-1756, 1997.

[23] M. Douay, W.X. Xie, T. Taunay, P. Bernage, P. Niay, P. Cordier, B. Poumellec, L. Dong, J.F. Bayon, H. Poignant, and E. Delevaque. *Densification involved in the UV-based photosensitivity of silica glasses and optical fibers.* Journal of Lightwave Technology **15**(8): 1329-1342, 1997.

[24] N.F. Borrelli, C.M. Smith, and D.C. Allan. *Excimer-laser-induced densification in binary silica glasses.* Optics Letters **24**(20): 1401-1403, 1999.

[25] J.W. Chan, T. Huser, S. Risbud, and D.M. Krol. *Structural changes in fused silica after exposure to focused femtosecond laser pulses.* Optics Letters **26**(21): 1726-1728, 2001.

[26] F.L. Galeener. *Planar Rings Invitreous Silica.* Journal of Non-Crystalline Solids **49**(1-3): 53-62, 1982.

[27] A. Pasquarello and R. Car. *Identification of Raman defect lines as signatures of ring structures in vitreous silica.* Physical Review Letters **80**(23): 5145-5147, 1998.

[28] V. Grubsky and J. Feinberg. *Rewritable densification gratings in boron-doped fibers.* Optics Letters **30**(11): 1279-1281, 2005.

[29] R. Bruckner. *Properties and Structures of Vitreous Silica. I.* Journal of Non-Crystalline Solids **5**: 123-175, 1970.

[30] R. Bruckner. *Properties and Structures of Vitreous Silica. II.* Journal of Non-Crystalline Solids **5**: 177-216, 1971.

[31] G. Rego, O. Okhotnikov, E. Dianov, and V. Sulimov. *High-temperature stability of long-period fiber gratings produced using an electric arc.* Journal of Lightwave Technology **19**(10): 1574-1579, 2001.

[32] K. Morishita and Y. Miyake. *Fabrication and resonance wavelengths of long-period gratings written in a pure-silica photonic crystal fiber by the glass structure change.* Journal of Lightwave Technology **22**(2): 625-630, 2004.

[33] A.D. Yablon. *Optical and mechanical effects of frozen-in stresses and strains in optical fibers.* IEEE Journal of Selected Topics in Quantum Electronics **10**(2): 300-311, 2004.

[34] D.M. Krol, K.B. Lyons, S.A. Brawer, and C.R. Kurkjian. *High-Temperature Light-Scattering and the Glass-Transition in Vitreous Silica.* Physical Review B **33**(6): 4196-4202, 1986.

[35] D.L. Kim, M. Tomozawa, S. Dubois, and G. Orcel. *Fictive temperature measurement of single-mode optical-fiber core and cladding.* Journal of Lightwave Technology **19**(8): 1155-1158, 2001.

[36] M. Akiyama, K. Nishide, K. Shima, A. Wada, and R. Yamauchi. *A novel long-period fiber grating using periodically released residual stress of pure-silica core fiber*. in *Proceedings of 1998 Optical Fiber Communications Conference*: 276-277, 1998.

[37] T. Enomoto, M. Shigehara, S. Ishikawa, T. Danzuka, and H. Kanamori. *Long-period fiber grating in a pure-silica core fiber written by residual stress relaxation.* in *Proceedings of 1998 Optical Fiber Communications Conference*: 277-278, 1998.

[38] B.H. Kim, Y. Park, T.J. Ahn, D.Y. Kim, B.H. Lee, Y. Chung, U.C. Paek, and W.T. Han. *Residual stress relaxation in the core of optical fiber by CO2 laser irradiation.* Optics Letters **26**(21): 1657-1659, 2001.

[39] E.M. Dianov, K.M. Golant, R.R. Khrapko, A.S. Kurkov, and A.L. Tomashuk. *Low-Hydrogen Silicon Oxynitride Optical Fibers Prepared by SPCVD.* Journal of Lightwave Technology **13**(7): 1471-1474, 1995.

[40] P.K. Bachmann, W. Hermann, H. Wehr, and D.U. Wiechert. *Stress in Optical Wave-Guides.2. Fibers.* Applied Optics **26**(7): 1175-1182, 1987.

[41] W. Hermann, M. Hutjens, and D.U. Wiechert. *Stress in Optical Wave-Guides.3. Stress-Induced Index Change.* Applied Optics **28**(11): 1980-1983, 1989.

[42] F. Durr. *Laser-induced stress changes in optical fibers*, in *PhD. Thesis*. École Polytechnique Fédérale de Lausanne. 61, 2005

[43] I. Hwang, S. Yun, and B. Kim. *Long-period fiber gratings based on periodic microbends.* Optics Letters **24**(18): 1263-1265, 1999.

[44] S. In, C. Chung, and H. Lee. *The resonance wavelength-tuning characteristic of the arc-induced LPFGs by diameter modulation*. in *OFS 2002: 15th Optical Fiber Sensors Conference Technical Digest*: 131-134, 2002.

[45] J.W. Fleming. *Dispersion in GeO_2-SiO_2 Glasses.* Applied Optics **23**(24): 4486-4493, 1984.

[46] S.A. Vasiliev and O.I. Medvedkov. *Long-period refractive index fiber gratings: properties, applications, and fabrication techniques*. in *Advances in Fiber Optics: Proceedings*: 212-223, 2000.

[47] G.W. Chern, L.A. Wang, and C.Y. Lin. *Transfer-matrix approach based on modal analysis for modeling corrugated long-period fiber gratings.* Applied Optics **40**(25): 4476-4486, 2001.

[48] G. Chern and L. Wang. *Transfer-matrix method based on perturbation expansion for periodic and quasi-periodic binary long-period gratings.* Journal of the Optical Society of America A-Optics Image Science and Vision **16**(11): 2675-2689, 1999.

4

The electric arc technique. Measurement of the fibre temperature whilst submitted to arc discharges

4.1 Introduction

Among the several techniques used to fabricate long-period fibre gratings, the electric arc technique is probably the one that offers more advantages. It is a simple and flexible point-by-point technique that does not require expensive laser systems. It enables the writing of LPFGs virtually in any kind of fibres, inclusive, non-photosensitive fibres and photonic crystal fibres, without the need for fibre hydrogenation and post-fabrication annealing. Furthermore, the fabricated gratings possess high thermal stability, enabling their use as high temperature sensors. It is therefore, worthwhile a deeper study of this fabrication technique.

The electric arc technique, as the CO_2 laser irradiation, promotes changes in optical fibres that rely on thermal effects and therefore, the measurement of the temperature reached by the fibre during an arc discharge is essential for the understanding of the mechanisms responsible for gratings formation and their related properties.

The chapter begins with an overview of the worldwide employment of this LPFGs fabrication technology. Afterwards, the procedure used in this work to fabricate LPFGs is described. A new infrastructure, under development, which aims to attain more flexibility and reproducibility in the fabrication process of the gratings, is also presented. Finally, two methods of estimating the fibre temperature whilst submitted to arc discharges are analysed.

4.2 Arc-induced long-period fibre gratings

The concept of long-period gratings (LPFGs) in which the light guided in the core is coupled to several cladding modes at specific resonant wavelengths, appeared in 1996 [1]. The formation of these former band rejection filters was due to a periodic modulation of the core refractive index induced by UV-radiation. LPFGs have been used in the past for coupling

between two guided modes. In the context of this work, the two step process used by Poole *et al.* in 1994 [2] is of particular interest. The method consisted in the periodic ablation of the fibre cladding using CO_2 laser radiation followed by periodic annealing using electric arc discharges. The same methodology was used in 1997 to produce band rejection filters [3]. It is interesting to note that almost simultaneously two different approaches, where only one of the former two steps was required, have been established [4, 5]. Dianov *et al.* (Russia) thermally induced LPFGs in nitrogen-doped fibres using arc-discharges and CO laser radiation, and they proposed nitrogen diffusion as the mechanism of formation of gratings. In 1998, Enomoto *et al.* (Japan) [6] wrote LPFGs in a pure-silica-core fibre due to stress relaxation. In USA, Kosinski and Vengsarkar [7] proposed different mechanisms, depending on the writing parameters, to arc-induce LPFGs in standard fibres. In 1999, Hwang *et al.* (Korea) [8] produced LPFGs through microbends. These gratings showed excellent optical performance and they withstood temperatures up to 800 ºC without degradation. In 2000, Verhaegen *et al.* (Canada) [9] analysed the fundamental mechanisms of gratings formation and they proposed as the most probable mechanism the change of stress distribution. In 2001, Palai *et al.* (India) [10] presented simulations on LPFGs written in the SMF28 and DSF fibres, from Corning, and they proposed Ge-diffusion as the mechanism of formation. In Portugal, Rego *et al.* [11] wrote high quality gratings in standard fibres and in nitrogen-doped and sulphur-doped fibres from FORC. It was demonstrated that a LPFG written in a standard fibre could stand temperatures up to ~1200 ºC, for several minutes. Furthermore, it was proposed that the arc-discharges could anneal/create stresses in the fibre and could also promote structural modifications in the glass. In 2002, Humbert and Malki (France) [12] and Morishita *et al.* (Japan) [13] also attributed the formation of the gratings to structural modifications due to the high heating/cooling rates. The formers also presented detailed results on stress relaxation in the 700-800 ºC temperature region. In Korea, Kim and co-workers [14] performed LPFGs by periodic tapering of the fibre. In the same year, Rego and co-workers have demonstrated the possibility to fabricate sampled fibre Bragg gratings (FBGs) through the writing of an UV-induced FBG on top of an arc-induced LPFG [15], and the possibility to apodise FBGs using arc discharges [16]. In 2003, Humbert *et al.* successfully wrote LPFGs in a Ge-free air-silica microstructure fibre [17] and in a dual concentric core fibre [18]. Malki *et al.* [19] performed Raman spectroscopy in LPFGs and concluded that a change of the glass structure took place despite no modification of the fictive temperature was measured. Thyagarajan *et al.* [20] presented a method to estimate LPFGs parameters such as the period and the duty-cycle. Rego *et al.* [21] investigated the properties of LPFGs written in a B/Ge doped fibre and they have also presented a study on the influence of uniform UV-exposure on arc-induced gratings. In 2004, Morishita *et al.* [22] fully characterised the process of LPFGs inscription in

a pure-silica PCF by the glass structure change. H. Dobb *et al.* (UK) [23] presented results of strain, temperature and bending sensitivities of a LPFG written in a PCF fibre. Humbert *et al*. [24] presented characterisations at high temperatures of LPFGs written in microstructured fibres. Yablon *et al.* [25] suggested that the relaxation of frozen-in viscoelasticity could be the main mechanism of arc-induced LPFGs. Rego *et al.* [26] estimated the temperature distribution in an optical fibre submitted to an electric arc discharge. In 2005, Rego *et al.* [27] have shown that the increase of the electric current leads to an increase of the strain sensitivity of arc-induced LPFGs. In USA, Nam *et al.* [28] fabricated ultra short LPFGs. Rego and co-workers (Portugal/Brazil/Russia) [29] have shown that LPFGs written in Al-doped and in Al/Er co-doped fibres exhibit linear temperature behaviour up to 700 ºC and they have also demonstrated that LPFGs inscribed in pure-silica-core fibres possess high resistance to γ-radiation (Portugal/Belgium) [30]. Morishita *et al.* [31] have shown that by heating the fibre at high temperatures it is possible to adjust the resonant wavelengths of arc-induced gratings. At last, Dürr *et al.* (Switzerland/Portugal/Russia) [32] have investigated the contribution of stress relaxation to the formation of gratings arc-induced in nitrogen doped fibres.

4.3 Fabrication technique

In this section a detailed description of LPFGs fabrication by the electric arc-discharge technique is given. The setup used during most of this work will be presented as well as the new infrastructure under development.

4.3.1 BICC fusion splicing machine

The fabrication process consists in placing an uncoated fibre between the electrodes of a fusion splicing machine (electrodes gap = 0.9-1.0 mm, electrodes apex angle = 20-40º). One end of the fibre is clamped in a fibre holder on top of a motorized translation stage (MTS) controlled with a precision of 0.1 μm. At the other end a weight is attached to keep the fibre under a constant axial tension (1-40 g). An arc discharge is then produced with an electric current of 8.5-10.0 mA during 0.5-2.0 s exposing a short portion of the length of fibre. Afterwards the fibre is moved by the grating period, typically 400-700 μm. The sequence arc discharge-fibre displacement (computer controlled) is repeated several times (15-100) until a required attenuation of the loss peak is obtained. During the fabrication process, the gratings spectra are monitored using an optical spectrum analyser, the illumination being provided by

a white light source. Figure 4.1 shows a photograph of the setup used to arc-induce the gratings.

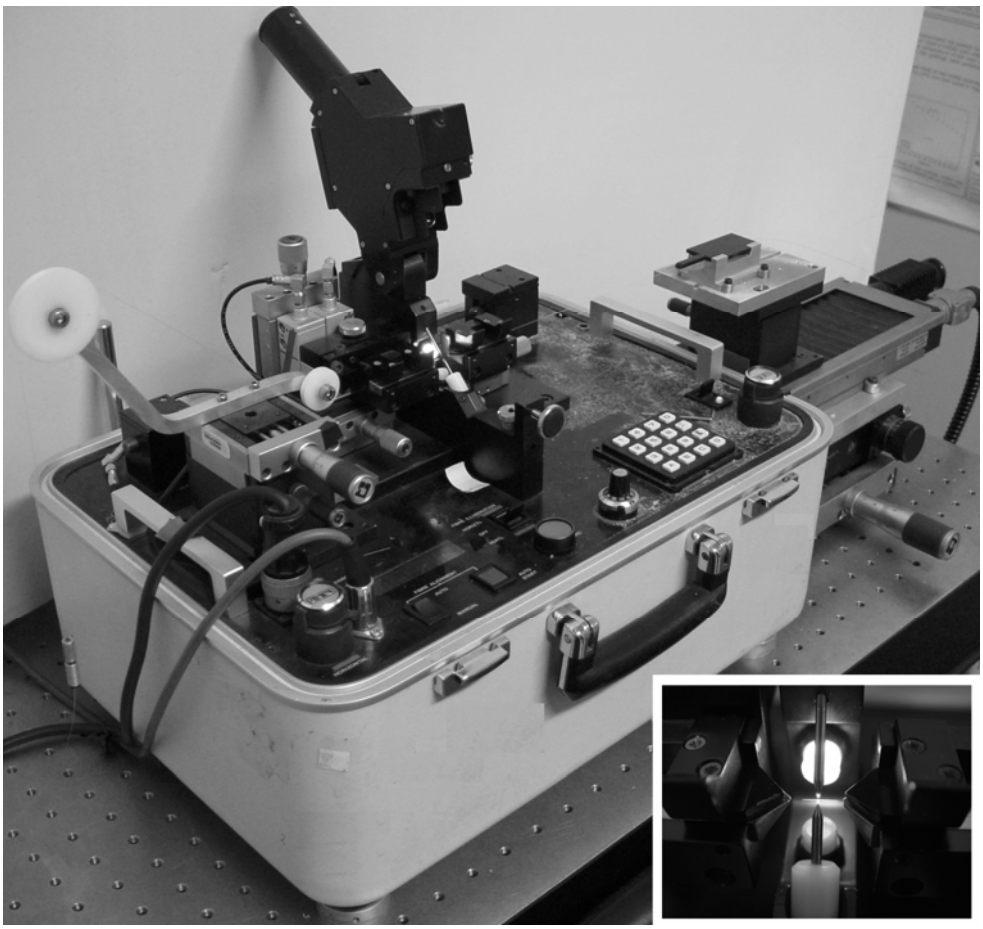

Figure 4.1 – Photograph of the experimental setup. Inset: Electrodes and v-grooves set.

To perform a full alignment of the setup, the platform with the set of pulleys enables movement in the plane perpendicular to the direction of the fibre displacement during the fabrication of the gratings. The platform with the motorized translation stage additionally allows for angular positioning. In this way, it is possible to place the fibre inside the v-grooves and guarantee that it remains there during gratings fabrication. Two microscopes are also used to monitor the fibre alignment. Another important issue, besides a proper alignment of the system, is its cleanness. To avoid contamination of the fibre, the v-grooves and the electrodes should be cleaned with alcohol and the fibre with acetone. Furthermore, before placing the fibre in between the electrodes, a few arc discharges should be performed to clean the electrodes from dust or SiO_2 particles. As far as the reproducibility of the technique is concerned, there are two other relevant factors. One, is the ambient conditions surrounding the electrodes region, in particular, air drafts and humidity. The other, is the electrodes state, since degradation occurs due to oxidation. The ideal situation to overcome these problems would be a controlled environment with an inert gas that could maintain good arc discharge

conditions. The actual situation is the protection of the arc discharge region with a kind of semi-open box and the replacement of the electrodes when required. The electrodes' polishing procedure is described in Appendix B.

4.3.2 The new setup

To overcome the limitations of the BICC fusion splicer setup a new facility was implemented. The BICC AFS3100 fusion splicer machine was adapted to allow computer control through LabView. However, since the machine requires a predefined sequence it is not flexible to changes of the fabrication parameters between discharges. Furthermore, the dimensions of the arc discharge which depends on the type of voltage applied and on the electrodes gap [33] limits the shortest period to about 200 μm.

Figure 4.2 shows a photograph of this new setup. It should be noted that several metal pieces had to be designed and fabricated in aluminium in order to allow the assembling of the infrastructure. The high voltage power supply was also produced at INESC-Porto Labs. The fibre alignment is performed with the help of two sets of v-grooves. The major difference, when compared to the previous setup is the existence of central grooves which help the fibre to remain in the same position relative to the electrodes. The electrodes are mounted on a x-y-z translation stage to position the fibre correctly in between them. The last step is executed with the help of a microscope enabling the view of the arc discharge. The whole fabrication process is controlled by a computer using LabView software which enables, in a straightforward way, the change of the electric current or the arc duration from one discharge to another. The power supply, however, brought about some problems that were not completely solved. It was observed that sometimes the current was too strong which would break the fibre, or to weak that the arc did not started. Other times the arc changed its path contouring the fibre during discharge. The major problem resides in the stabilization of the arc discharge provided by the high voltage power supply. Several attempts were made in order to fix that problem. The tests performed comprised the use of transformers with a DC or AC voltage output, the latter being rectified or not, changes of the output resistor, operation at different frequencies and duty cycles and the change of the input voltage. Furthermore, it was also used an initial peak voltage to start the arc followed by its decrease to a stabilized discharge, to prevent fusion of the fibre. It was observed that the arc discharge strongly depends on the type of output voltage, but in any case its cross section increases with the increase of the electrodes gap. Additional work is required to address the operation of the power supply. However, this is not the main objective of this work and so will not be discussed further.

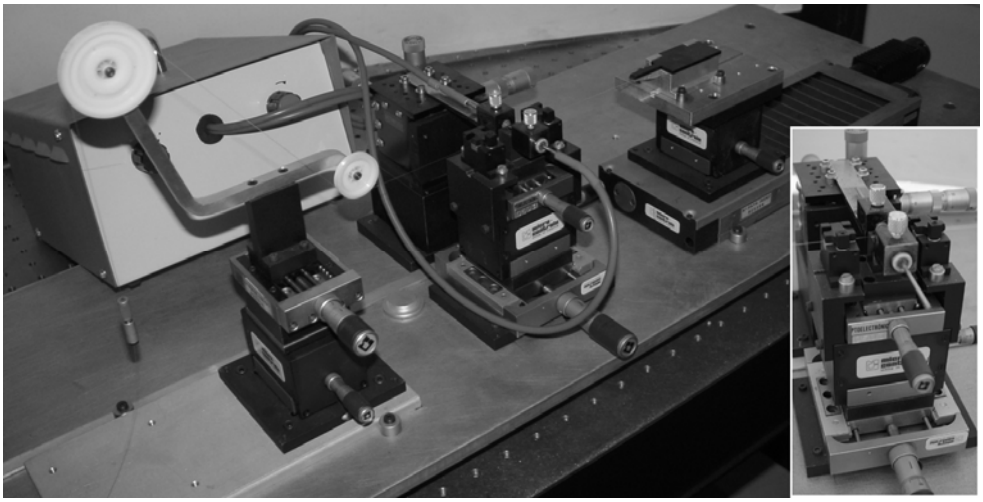

Figure 4.2 – Photograph of the experimental setup. Inset: Electrodes and v-grooves set.

4.4 Tubular oven

The tubular oven was customised to investigate the thermal behaviour of the gratings, enabling the reduction of the length of fibre coating to be removed whilst preventing any thermal gradient over a grating with a maximum length of 5 cm. However, as will be discussed in the next section, this oven was also used for calibration proposes during the measurement of the fibre temperature whilst submitted to an arc discharge.

The tubular oven has a length of 18 cm and a diameter of 2 cm. It contains two heaters (one in the centre and the other in both ends of the tube) which are controlled separately, by Eurotherm 2216 controllers, to keep the temperature constant in a region of about 5 cm. The temperature variation in that region was measured to be ±1 ºC at 800 ºC. The maximum working temperature is of ~1300 ºC (1350 ºC, for short periods). The oven can be computer controlled via LabView enabling all kind of heating cycles. Operation in the vertical position of the oven is also possible which might be important in avoiding unwanted elongation by external applied tensions usually used to prevent fibre bending. In this way, when submitted to high temperatures, the fibre is solely under its own weight.

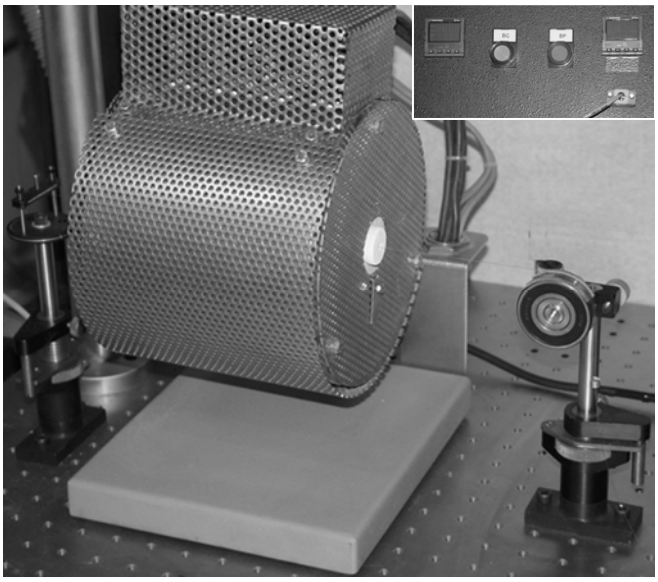

Figure 4.3 – Photograph of the tubular oven (fabricated by Termolab according to our requirements). Inset: Front panel of the oven's controller.

4.5 Measurement of the fibre temperature

In what concerns arc-induced gratings, the mechanisms responsible for their formation are still under investigation. In this context, the temperature reached by the fibre during the electric arc discharge is an important parameter to be considered. Moreover, the electric current of the arc discharges depends on the electrodes configuration and on their degradation, hence the temperature could be used instead to control adequately the fabrication conditions of these structures. In this section two methods will be described to determine the fibre temperature under the electric arc discharge. One is based on blackbody radiation and the other on the use of electrically insulated thermocouples.

4.5.1 Blackbody radiation

Conceptually, this method of assessing the fibre temperature during an arc discharge consists in the fitting of the blackbody expression to the radiation emitted by the fibre and detected using a Cronin spectrometer. The low intensity radiation emitted by the fibre section after being heated by an arc discharge of short duration (1 s), is guided through the same fibre towards the spectrometer where its spectral content is separated by a holographic grating being afterwards detected by an array of detectors. Note that each wavelength range is allocated simultaneously to a particular detector (there is no wavelength sweep). It should be stressed that an optical spectrum analyser (OSA) is not suitable for such kind of

measurements requiring high sensitivity and fast data acquisition. Moreover, a commercial spectrometer, such as, the USB 2000 from Ocean Optics with the appropriate grating could be used to perform these measurements but, instead we have used the Cronin spectrometer (a former prototype). Therefore, to estimate the fibre temperature several intermediate steps are required. First, the spectral response of the spectrometer has to be determined. Second, the method has to be tested by applying it to the measurement of well known predefined temperatures. Third, the fibre refractive index has to be determined since the radiation is generated inside a medium different from vacuum. Finally, the dependence of the fibre emissivity on temperature and wavelength, for the specified fitting range, has to be known.

The basis of this method is the Plank's blackbody radiation law [34]

$$I(\lambda,T)=\frac{c_1}{n^2\lambda^5}\frac{1}{e^{c_2/n\lambda T}-1} \tag{4.1}$$

where c_1 and c_2 are constants with values equal to $3.7415\text{x}10^{-16}$ W/m^2 and $1.4388\text{x}10^{-2}$ m.K, respectively. The other parameters have their common meaning.

Figure 4.4 shows the blackbody emission spectra in vacuum and in silica for two different temperatures. As it can be seen, the increase of the refractive index or temperature displaces the spectrum towards shorter wavelengths and increases its intensity.

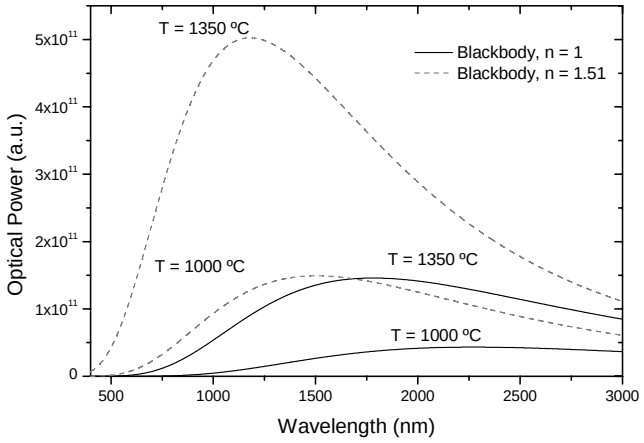

Figure 4.4 – Blackbody radiation for different temperatures and refractive indices.

Spectrometer spectral response

The Cronin spectrometer consists on a holographic diffraction grating and an array of detectors which enables detection over the 310-1100 nm wavelength range, with an optical resolution of 10 nm. A superluminescent laser diode with a peak wavelength at 846 nm and a bandwidth at full width half maximum (FWHM) of 29 nm was used to determine the wavelength accuracy (Figure 4.5(a)). The spectrometer broad spectral response (Figure

4.5(b)) was calibrated by comparing the spectra of a white light source registered by the Cronin spectrometer and by a calibrated OSA. It is interesting to note that the spectral response of the Cronin spectrometer is similar to the commercially available USB 2000 from Ocean Optics using grating #3.

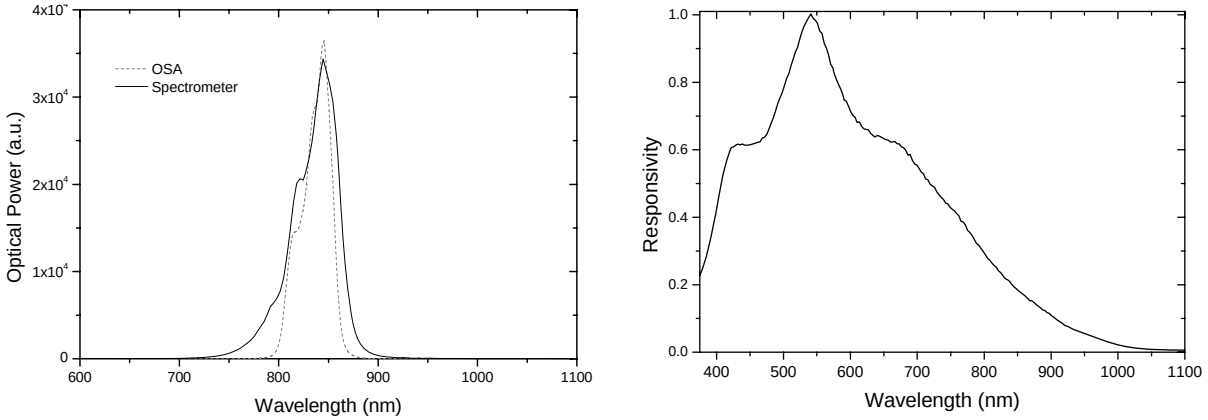

(a) (b)

Figure 4.5 – (a) Wavelength accuracy and (b) responsivity of the spectrometer.

Testing the method

Two pieces of multimode fibre (~2 m long) were used to collect the radiation from an oven at different temperatures above 1000 ºC. One piece was connected to the OSA and the other one to the computer controlled spectrometer (Figure 4.6). The recorded optical spectra were then fitted to the blackbody radiation expression in the 400-900 nm range. Note that in this case the value of n was set equal to 1 since the optical fibre was only used to guide the light. Figure 4.7(a) shows the emission spectra of the oven at temperatures above 1000 ºC, as measured by the OSA. The fitting of blackbody radiation expression to the emission spectrum corresponding to an oven temperature of 1350 ºC is also shown (c is an experimental constant resulting from fitting's optimization). The relative error in the determination of the oven temperature (T_{oven}) was lower than 2%, as shown in (Figure 4.7(b)) for two (#1 and #2) separate measurements performed by using the OSA (circles) and the spectrometer (squares).

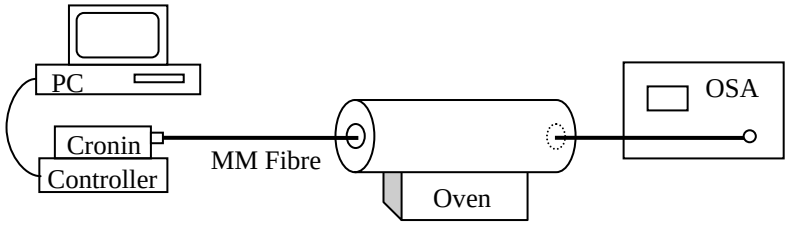

Figure 4.6 – Diagram of the set up used.

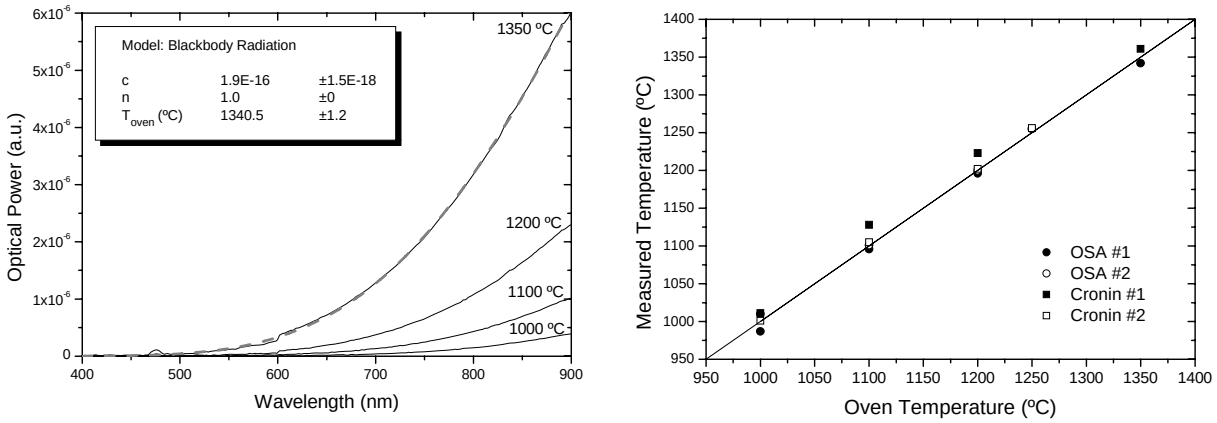

(a) (b)

Figure 4.7 – Fitting blackbody radiation expression to the oven emission spectra. (b) Measured temperature using Plank's law versus oven temperature.

Fibre refractive index

To determine the refractive index of the fibre, a short length was placed inside an oven with one end connected to the OSA and the other one to the spectrometer, allowing simultaneous detection by both devices. The temperature of the oven was increased slowly up to 1350 ºC. In this case, the radiation detected corresponds to the emission of the fibre while in thermal equilibrium with the oven. Fitting the blackbody radiation expression, in the 450-900 nm range, to the spectra of several independent experiments resulted in values of 1.48 ± 0.03 for the fibre refractive index. Taking into account that for pure silica the refractive index at room temperature is 1.456 (675 nm), that the core to cladding refractive index difference, Δn is 0.012 and assuming that the temperature dependence of the refractive index dn/dT is ~2.5×10^{-5} $^{\circ}C^{-1}$ [35], the refractive index calculated theoretically for a temperature difference of 1330 ºC is ~1.50. Note that the thermo-optic coefficient used is an average value for temperatures up to 1000 ºC. However, for higher temperatures, it is expected that this value falls due to a large increase of the silica thermal expansion coefficient [35, 36]. Therefore, the refractive index value obtained experimentally agrees well with the one expected for the considered temperature. Finally, note also that material dispersion for silica, obtained through Sellmeier's equation [37], has low influence on the temperature determination, the difference being within 10 ºC (Figure 4.8).

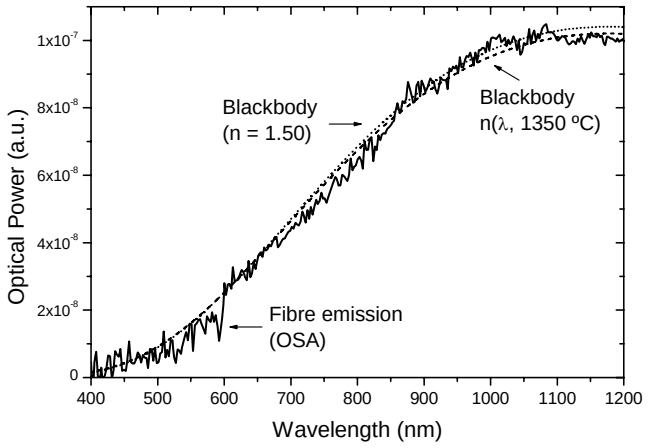

Figure 4.8 – Fibre emission.

Fibre emissivity

To determine the fibre emissivity, the dependence of the silica based glass on wavelength and on temperature has to be known. It is also required knowledge of the geometry of the cavity and its respective dimensions. As can be seen in Figure 4.4, for the temperatures under measurement the wavelength range of interest is between 0.4 and 3.0 μm. Note however that do to the spectral response of the spectrometer, fittings of the blackbody radiation expression to the experimental data are limited to about 0.9 μm. Unfortunately, there is a lack of data regarding the emissivity of silica in this spectral range since it corresponds to a region of high transparency. The absorption is mainly due to the tail of the ultraviolet absorption band and therefore, the respective absorption coefficient is relatively low, decreasing with increasing wavelength at room temperature. However, recent results indicate a possible inversion of that dependence at high temperatures. In fact, it was observed that the absorption coefficient at 1.06 μm is higher than at 0.5 μm [38]. Regarding the temperature dependence, for the same wavelength range, it is known that the absorption increases rapidly for temperatures above 1050 ºC [38]. These results were explained considering the formation of defect centres and due to electronic conduction.

Another important factor is the geometry of the cavity. For a cylindrical cavity it was shown [39] that its effective emissivity could be given by the following equation

$$\varepsilon_{eff} = \varepsilon \frac{1+4L/D}{1+\varepsilon(4L/D)} \tag{4.2}$$

where ε is the emissivity of silica, L is the length and D the diameter. For a fibre inside the oven in which the length (L = 180 mm) is much larger than its diameter (D = 52/125 μm), the effective emissivity is close to 1. This result makes the dependence of the silica emissivity on

wavelength and on temperature secondary issues and explains the good fitting obtained in Figure 4.8. A good agreement is obtained between the blackbody radiation and the experimental results.

The arc discharge

An arc discharge is a complex phenomenon during which a number of processes occur. In simple terms, it can be said that electrons are emitted by one electrode, the cathode, due to the high intensity electric field generated at the electrodes tip, and while in transit between the electrodes ionizes nitrogen and oxygen atoms, through impacts, creating a high temperature plasma comprising electrons and ions [40]. Figure 4.9(a) shows the arc emission spectra as recorded by the PR-714 Photo Research spectroradiometer and by the Cronin spectrometer. For the former, the radiation during the arc discharge was detected by the PR-714 placed ~2 m away from the splicing machine whilst focusing the discharge area. For the latter, the arc radiation was detected by a multimode fibre placed in the vicinity of the arc. Similar non-normalized spectra were obtained for both arrangements. Figure 4.9(b) shows the arc emission spectra in the presence of a light separated flow of nitrogen and oxygen. The sum of the spectra obtained individually for nitrogen and oxygen resembles the spectra obtained in Figure 4.9(a).

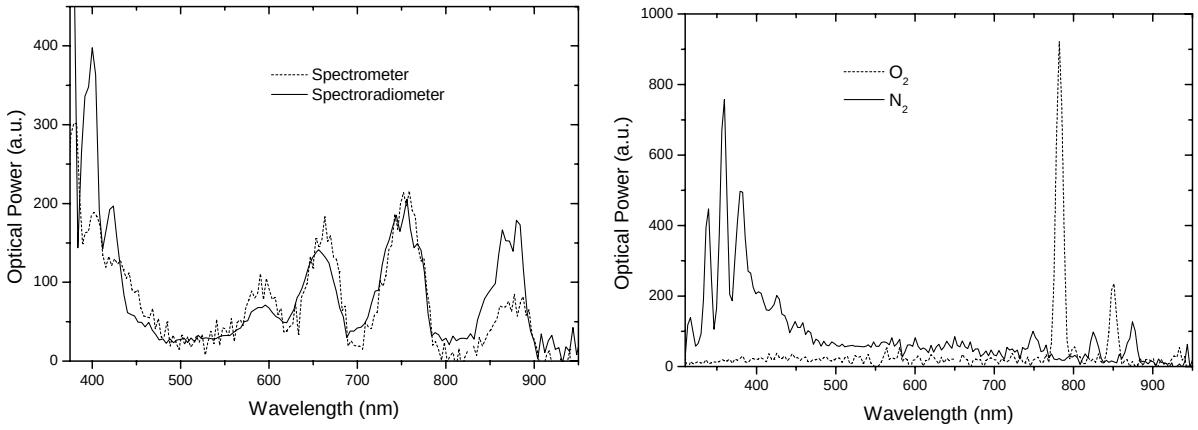

(a) (b)

Figure 4.9 – Arc emission spectra recorded by the (a) spectrometer/spectroradiometer in air and by the (b) spectrometer for separate flows of nitrogen and oxygen.

Fibre temperature

The experimental setup consists on the fusion splicing machine, to produce the arc discharges, a piece of multimode fibre to generate and guide the radiation and the Cronin spectrometer which is computer controlled, to detect the radiation (Figure 4.10). One end of a

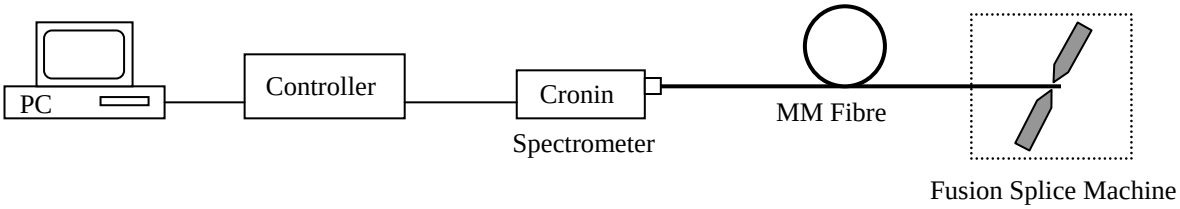

Figure 4.10 – Experimental Setup.

short piece of fibre (l < 0.5 m) was placed between the electrodes of a splicing machine (electrodes gap = 1 mm, tip angle ~ 40º) and the other end was connected to the spectrometer. An electric arc discharge (I = 9 mA, t = 3 s) was then produced on the fibre, close to its end, and the radiation was detected by the spectrometer during one second after thermal equilibrium. The process was repeated for increasing electric arc currents up to 13 mA. The registered spectra were corrected for the spectrometer response and fitted to the blackbody radiation expression over the 450-650 nm range, from which the fibre temperature (T_f) is obtained (Figure 4.11). In this estimation, the fibre refractive index was set equal to 1.48 and it was considered that the fibre emissivity was independent of the wavelength, being its value set equal to 1. Figure 4.11(b) shows the measured dependence of the fibre temperature with current. For an electric current of 9 mA an average temperature of 1365 was determined. Note that for higher currents, the temperature dependence of the refractive index was not taken into account and therefore it is possible that the slope of the linear fitting is higher than the value shown in Figure 4.11(b). The dispersion of the values measured for the low and high current limits is probably related with the low level of the signal detected and the deformation of the fibre, respectively. It should be highlighted that the region heated by the arc has a non-uniform temperature distribution, and consequently the fibre emission spectrum is the sum of all

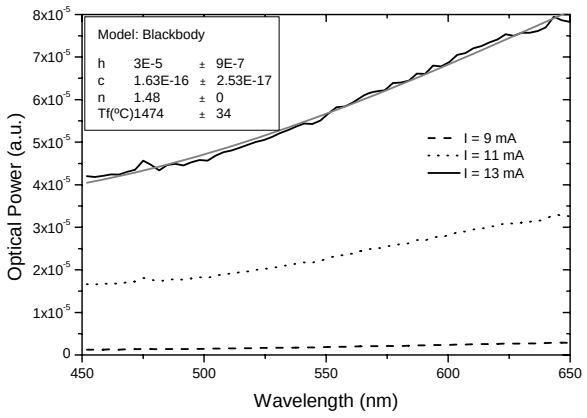

(a)

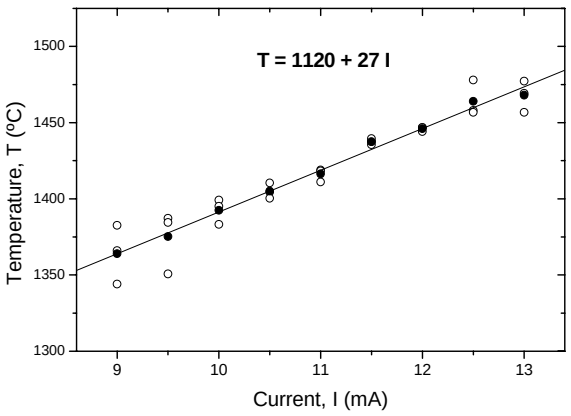

(b)

Figure 4.11 – (a) Fitting blackbody radiation expression to the fibre emission spectra detected by the spectrometer. (b) Fibre temperature versus arc discharge current.

contributions that results from dividing the heated region in smaller regions, each having a constant temperature. Therefore, the peak values of temperature obtained for each arc current are underestimated. Detailed studies on non-isothermal cavities can be found in [41]. To have a better understanding of this effect it was assumed a particular fibre temperature profile having a peak temperature of 1320 ºC [26] and consider the heated region divided in 9 smaller regions. Taking into account that the silica emissivity increases considerably with temperature, only regions above 1150 ºC contribute significantly to the overall spectrum. The silica emissivity, for a particular temperature, was estimated considering that it would be the same as the absorption in a length of 1 mm, at the same temperature. Moreover, to determine the effective fibre emissivity, the ratio L/D of the cavity was considered equal to 20 (1000/50). It arose from the calculations that the emissivity at 1320 ºC was 3 and 8 times higher than the ones at respectively, 1230 ºC and 1150 ºC. Figure 4.12 shows the blackbody emission spectrum of each region with temperatures above 1150 ºC and the overall spectrum. Fitting these curves to the blackbody radiation expression resulted in a temperature of 1280 ºC. Therefore, taking into account the uncertainty in the refractive index (± 40 ºC) and the temperature distribution (~40 ºC), the estimated peak value of the fibre temperature, correspondent to an arc discharge of 9 mA, is 1400 ± 50 ºC.

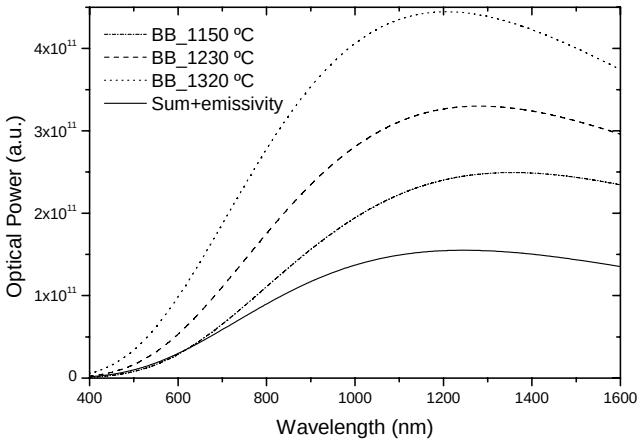

Figure 4.12 – Effect of having a non-uniform fibre temperature.

In conclusion, a method was presented based on the blackbody radiation for the determination of the temperature of a small piece of fibre exposed to an electric arc discharge. The radiation emitted by the fibre was first detected using a Cronin spectrometer and then its spectrum was fitted to the blackbody radiation expression. An average temperature of about 1365 ºC was obtained for the region exposed to an electric current of 9 mA. However, a peak temperature of 1400 ± 50 ºC was estimated assuming a realistic temperature profile. It should

be stressed that these calculations are strongly influenced by the thermal behaviour and the wavelength dependence of two physical parameters of the fibre, namely its refractive index and emissivity.

4.5.2 Electrically insulated thermocouples

Another approach to determine the temperature of an optical fibre during an electric arc discharge was carried out using electrically insulated thermocouples. In this approach, the basic requirements were to guarantee that the arc discharge remained unperturbed and that the temperature sensor had dimensions comparable to those of an optical fibre. That was achieved by fabricating a thermocouple inside a silica capillary with an outer diameter similar to that of a standard optical fibre. In this way, the electrical isolation of the thermocouple is also guaranteed. Note, however, that since the thermocouple has a thermal conductivity different from that of silica glass the temperature reached by an optical fibre during an arc discharge is necessarily different from that of this measuring system. Therefore, the following methodology was used. First, the temperature distribution in the thermocouple was measured and then the temperature profile for an optical fibre was estimated through a simplified heat transfer model simulated by a finite element method using a commercial partial differentiation solver.

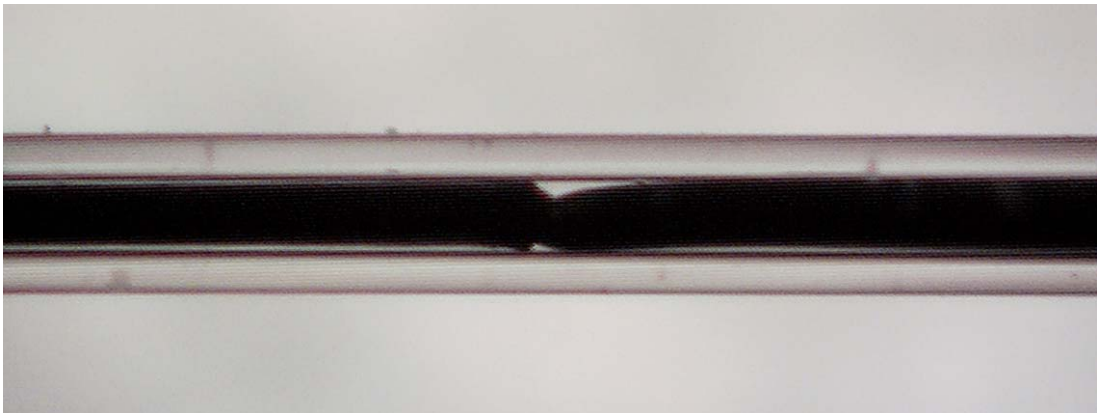

Figure 4.13 – 50/50 thermocouple fabricated by applying arc discharges.

In order to accomplish the initial goal, several steps were performed. The first step consisted on the assembling of electrically shielded type S thermocouples (platinum wire and platinum-10% rhodium alloy provided by Goodfellow) using wires with diameters of 25 μm and 50 μm in four distinct configurations: 25/25, 50/50, 25/50 and 50/25. To assemble the type S thermocouples *in situ*, a cleaved silica capillary (D_{in}/D_{out} = 56 μm/125 μm) was fixed on the reference v-groove of the BICC fusion splicing machine. A straight platinum wire was placed on the other v-groove, with x-y-z position control. Actuating on the micrometer

controller, the wire was introduced about 20 mm inside the capillary. Afterwards, the whole process was repeated for the Pt-10%Rh alloy until physical contact of the wires occurred inside the capillary. After centring the region to be fused with the electrodes of the splicing machine (the gap between electrodes is 1.0 mm and the electrode apex angle is 40º), an electric arc discharge (I > 15 mA) was applied whilst pushing the wires against each other. Figure 4.14 shows one of the 50/50 thermocouple assembled by this technique.

Experimental setup

Following the thermocouple assembly, the electric current was reduced to 9 mA and arc discharges of 3 s duration were applied in different axial positions of the wires. The voltage in the thermocouples was measured using an Agilent 34401A multimeter, controlled by a simple LabView program (Figure 4.14). For each position, the equilibrium voltage was registered and it was converted to temperature using the reference function for type S thermocouples based on the ITS-90 [42]. The process dynamics, for the 50 μm thermocouple, during the heating and cooling down is shown in Figure 4.15. It can be seen that the system reaches the thermal stationary equilibrium in less than 1 s. This holds for all thermocouples used independently of the axial position and of the electric current values (I < 15 mA).

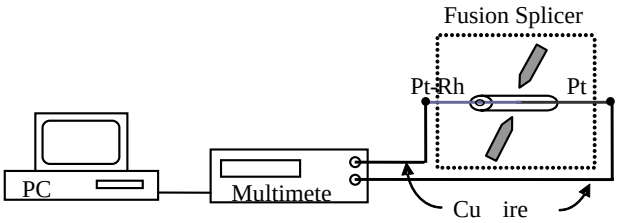

Figure 4.14 – Experimental setup used to measure the voltage on the thermocouples during the electric arc discharges.

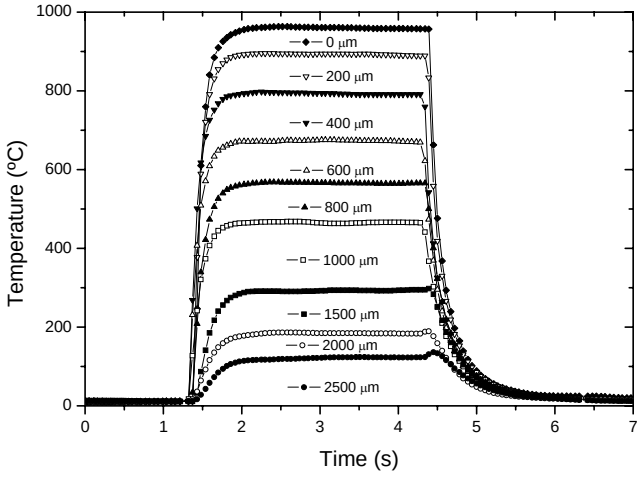

Figure 4.15 – Time evolution of the temperature in the 50 μm-thermocouple for discharges produced at several axial positions on the Pt-10%Rh wire.

The time constants for the three thermocouples were obtained by fitting the curves corresponding to the time dependence of the temperature at the thermocouple junction (Figure 4.16). By extrapolation of the data for the case of having no thermocouple (zero diameter) the time constant for the silica capillary was estimated to be 72 ± 2 ms (Figure 4.16(b)). Afterwards, by taking the ratio of the cross sections for the fibre and the capillary, a value of 90 ms was obtained for the time constant of the optical fibre. Therefore, the fibre reaches thermal equilibrium (the time required to achieve 99% of the stationary temperature) in about 415 ms.

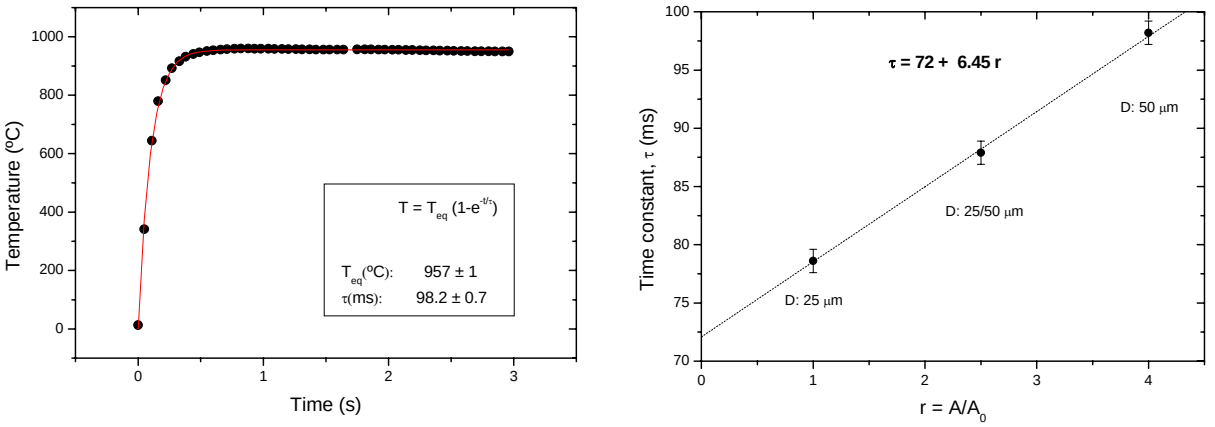

(a) (b)

Figure 4.16 – (a) Time constant for the 50 μm thermocouple obtained by fitting the temperature evolution at the thermocouple junction depicted in the previous figure. (b) Time constants for the three thermocouples.

Figure 4.17 shows the temperature distribution in the 25 μm and 50 μm thermocouples, obtained by applying arc discharges in steps of tenths to hundreds of micrometers for about 5 mm on both sides of the thermocouple junction. A region of about 150 μm to 200 μm around the thermocouple junction presents an almost constant temperature, which may correspond to the dimensions of the central zone of the arc-discharges (inset Figure 4.17).

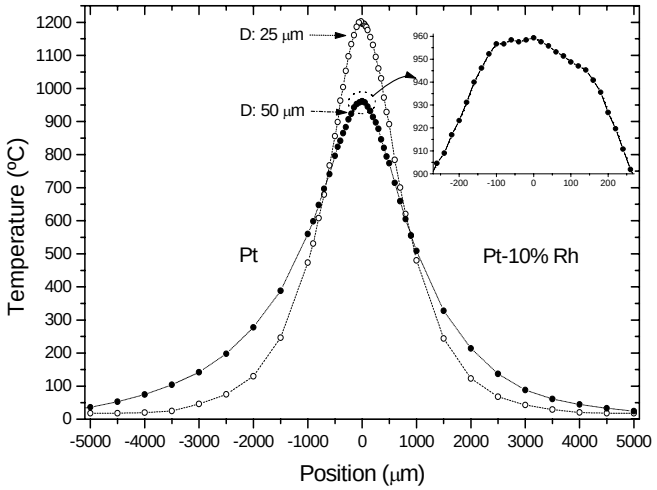

Figure 4.17 – Temperature distribution in the 25 μm and 50 μm-type S thermocouples. Inset: Temperature distribution around the junction of the 50 μm-type S thermocouple.

To assess the thermocouples performance, they were placed inside the tubular oven and its temperature was increased from 800 ºC to 1200 ºC, in steps of 100 ºC. For each step, the thermocouples temperature was registered after reaching thermal equilibrium. Temperature measurements were compared with a calibrated type-R thermocouple. The overall accuracy of the measured values was estimated to be better than 5 ºC.

Estimation of the capillary temperature

The peak temperature of the capillary was obtained assuming that as the energy dissipated through the wires approaches zero, the thermocouple temperature would approach the capillary temperature without thermocouple. The energy dissipated through the wires, per unit of time P_d was calculated using the standard heat transfer expression for conduction

$$P_d = -k_{Pt}\left(\frac{\pi}{4}D_T^2\right)\left(\frac{\Delta T}{L}\right)_{Pt} \tag{4.3}$$

in which k, D_t and $\Delta T/L$ represent, respectively, the thermal conductivity of the thermocouple wire, its diameter and the temperature gradients in the vicinity of the thermocouple junction. The temperature dependence of the thermal conductivity for platinum was taken from the literature, whereas for the alloy it was estimated based on data from a recent paper in which several platinum alloys were examined at high temperatures. Although at room temperature, the thermal conductivity of platinum is almost twice that for the alloy, at high temperatures both have similar values due to the higher temperature coefficient of the thermal conductivity for the platinum alloy. In fact, it was observed experimentally from data concerning the power dissipation in thermocouples composed of wires with different diameters, that the difference

between the thermal conductivities of platinum and the alloy decreases from about 45% at room temperature to 15% at 1000 ºC [43] (see Table I). The result of this analysis is shown in Figure 4.18 where the peak temperature measured by three thermocouples with different diameters is plotted as a function of the power dissipated in the thermocouples. The error bars in the x-axis accounts for the uncertainty in the thermocouples diameter (±1 μm) and on the thermal conductivity of the alloy (10%), whereas the error bars in the y-axis accounts for the uncertainty in the thermocouple positioning between the electrodes which, in turn, affects the temperature measurement (±10 ºC). The linear fitting applied to the experimental data points towards a capillary temperature of approximately 1430 ºC with an overall uncertainty of ±50 ºC.

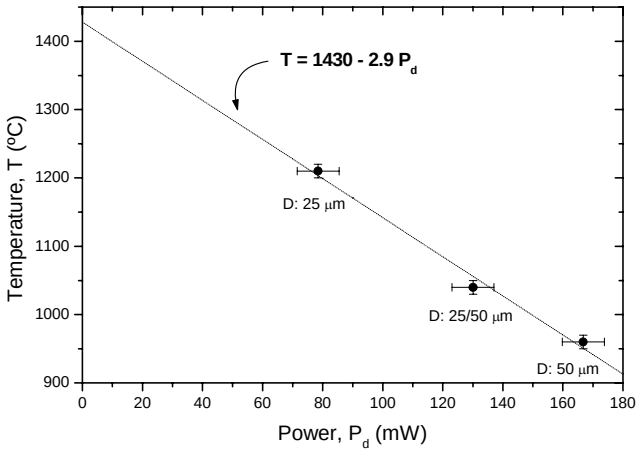

Figure 4.18 – Peak temperature versus power dissipated through the thermocouples.

Estimation of the fibre temperature through simulations

To determine the temperature profile in the fibre several steps are required. First, the experimental temperature profiles in the thermocouples are fitted to the simulation results by tuning the thermal power delivered by the arc, the dimensions of the point source used and the separation between the point source and the silica capillary. Second, the thermocouples are removed from the previous system and for the same power, the temperature profile in the capillary is derived. This allows a comparison between the peak temperature of the capillary and the value estimated graphically (Figure 4.18). Finally, a similar calculation is performed for the case of having an optical fibre instead of the capillary. Note that for each set of thermocouples, independent simulations were realized using a simplified heat transfer model of the assembly based on a finite element analysis. Radial heat transfer was simulated by a finite element method using a commercial partial differentiation solver (Flex PDE 2.13 from PDE Solutions Inc.), assuming a two dimensional steady state conduction model, which holds for the period after thermal stationary equilibrium is reached. The boundary conditions applied to the dash box shown in Figure 4.19 are as follows: heat is transferred to the system

through a narrow arc discharge, the internal radiative heat transfer within the silica capillary is neglected but radiative heat transfer is considered at the capillary surface, along with a convection contribution; by symmetry there is no heat transfer along the axis of the thermocouple and the boundary is at room temperature (300 K). Figure 4.19 summarises the types of heat transfer involved in the simulations. Table I gives the expressions for the temperature dependence of the physical parameters used in the simulations. The dimensions of the point source and its distance to the silica capillary were set equal to 5 μm and 412.5 μm (electrodes' gap equal to 950 μm), respectively.

Table I. Temperature dependence of the physical parameters used in the simulations.

Designation	Expression	Range
Thermal conductivity of air [44]	$k = 3.84x10^{-3} + 7.66x10^{-5}T - 1.54x10^{-8}T^2$	
Convection heat transfer coefficient of air [44]	$h(56) = 310.197 + 2.392x10^{-1}T - 1.906x10^{-5}T^2$	T > 1200 K
idem (external surface) [44]	$h(125) = 55.910 + 3.249x10^{-1}T - 1.164x10^{-4}T^2$	T < 1100 K
Thermal conductivity of Pt [43]	$k = 77.8 + 2.15x10^{-2}(T - 300)$	
Thermal conductivity of Pt/Rh [43]	$k = 43.5 + 4.3x10^{-2}(T - 300)$	
Specific heat of Pt [45]	$C_p = 125.15 + 2.655x10^{-2}T$ $\overline{C_p} = \begin{cases} 1.3x10^5 + (T-1173)[C_p(T)+156.3]/2 \\ T - 293 \end{cases}$	T > 1200 K
Density of Pt	$\rho = \frac{21450}{1+3a}$ $a = 9.122x10^{-4}(T-293) + 7.467x10^{-8}(T-293)^2 + 4.258x10^{-11}(T-293)^3$ $\overline{\rho} = \begin{cases} 1.864x10^7 + (T-1173)[\rho(T)+20892.4]/2 \\ T - 293 \end{cases}$	
Specific heat of SiO_2 [45]	$C_p = \frac{T - 2x10^5}{23.1992 + T} + 1.7x10^{-3}(T + 8x10^5)$ $\overline{C_p} = \begin{cases} 5.666x10^5 + (T-900)[C_p(T)+1153]/2 \\ T - 300 \end{cases}$	
Density of SiO_2 [46]	$\rho = \begin{cases} 2222.5 - 9.10x10^{-3}T \\ 2426.0 - 1.57x10^{-1}T \end{cases}$ $\overline{\rho} = \begin{cases} \frac{2.171x10^6 + (T-1273)[\rho(T)+2210.9]/2}{T-293} \\ \frac{2.392x10^6 + (T-1373)[\rho(T)+2210]/2}{T-293} \end{cases}$	$T \le 1400K$ $T > 1400K$ $T \le 1400K$ $T > 1400K$
Thermal conductivity of SiO_2 [44, 45]	$k = \begin{cases} -48.661 + 1.349x10^{-1}T - 1.208x10^{-4}T^2 + 3.75x10^{-8}T^3 \\ 7.8x10^{-1} - 5.4x10^{-2}e^{\frac{T+379}{354}} + 1.65x10^{-1}e^{\frac{T+379}{405}} \end{cases}$	$T \ge 1000K$ $T < 1000K$
Emissivity of SiO_2 [47]	$\varepsilon = 0.056 + 1.90e^{-\frac{T}{552}}$	T > 900 K

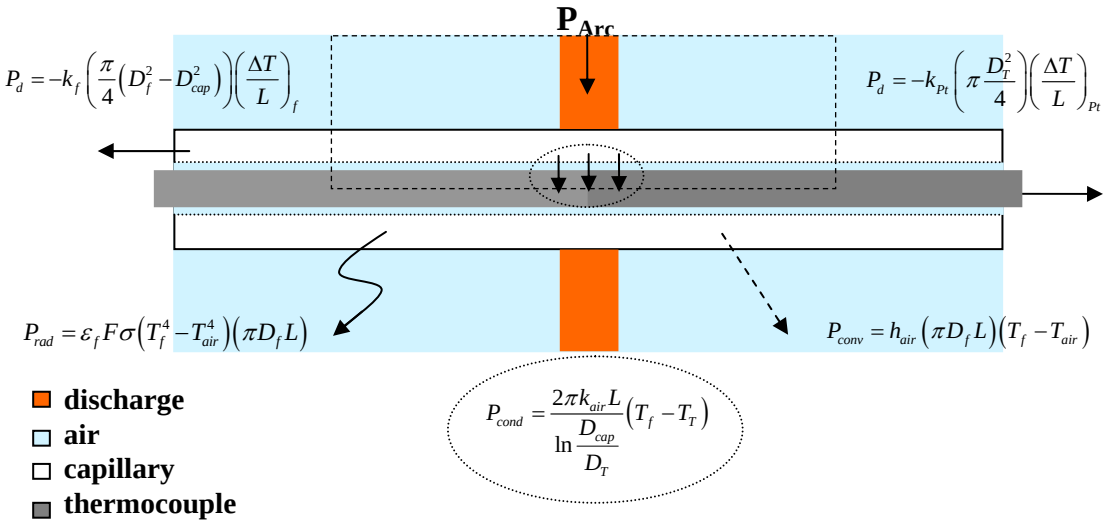

Figure 4.19 – Heat transfer equations for the system consisting of a silica capillary, with a thermocouple inside, submitted to an arc discharge through air.

The results obtained from simulations for the 50 μm thermocouple are shown in Figure 4.20 to Figure 4.23, corresponding to the various steps taken to obtain the temperature profile for the fibre. Figure 4.20 shows the temperature distribution of the whole system consisting of thermocouple and capillary; Figure 4.21 shows the result of fitting the simulations to the data of the temperature profile of the 50 μm thermocouple and the temperature profile of the silica capillary with the thermocouple inserted; finally Figure 4.22 and Figure 4.23 plots the temperature distribution and profile of the system without thermocouple and of the fibre.

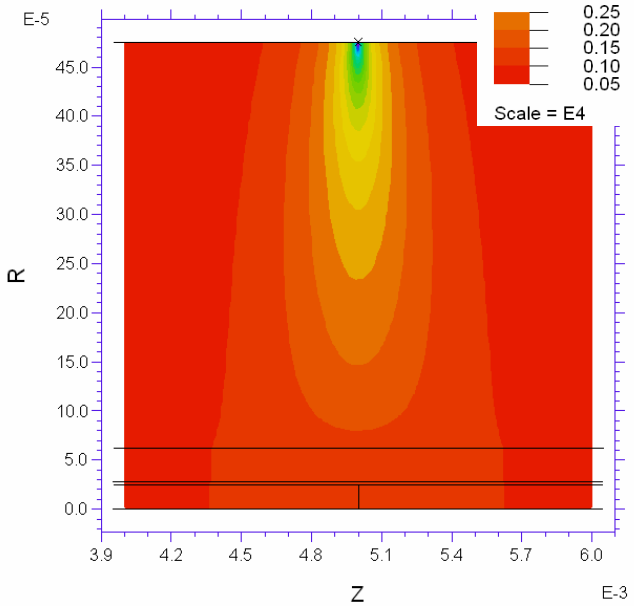

Figure 4.20 – Temperature distribution (in Kelvin) in the system consisting of thermocouple and capillary: R is the radius from the thermocouple axis up to the point source (475 μm) and Z is the distance from the thermocouple junction (5±1 mm).

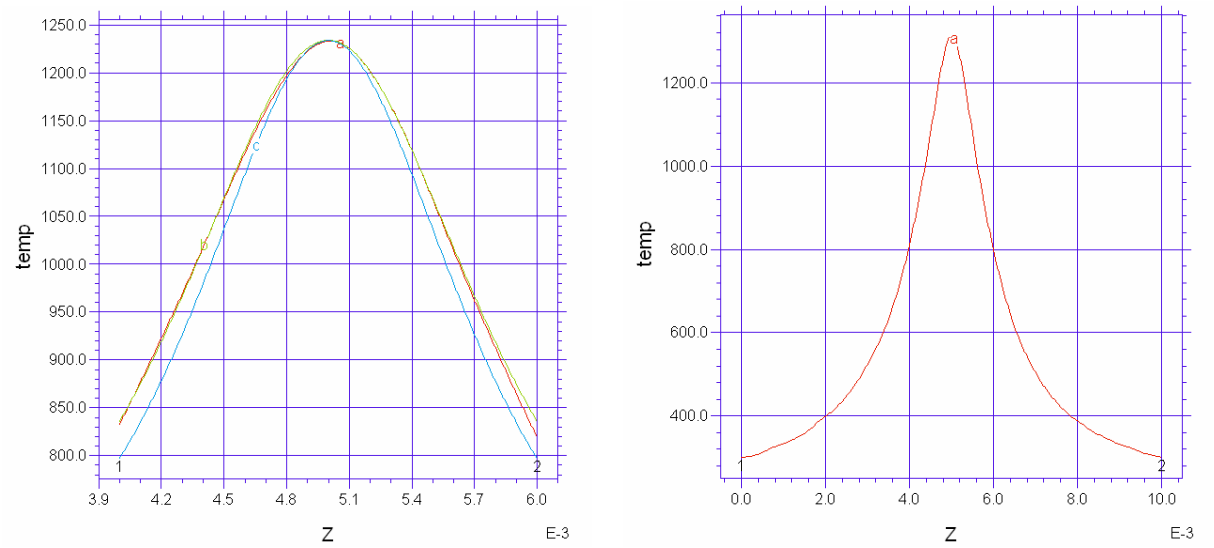

(a) (b)

Figure 4.21 – (a) Fitting of the simulation results (in red) to the experimental data for the 50 μm thermocouple temperature profile (in blue and green for Pt and Pt/Rh wires, respectively); and (b) simulation result corresponding to the temperature profile (in Kelvin) of the silica capillary with the 50 μm thermocouple inserted (T_{peak} = 1045 ºC).

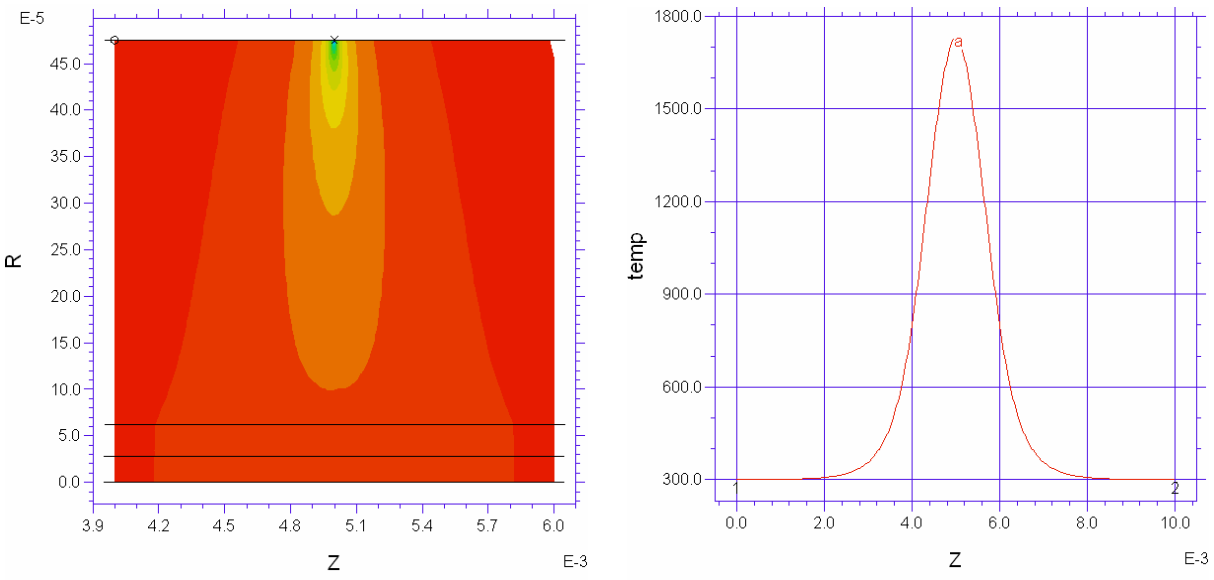

(a) (b)

Figure 4.22 – Simulation results corresponding to (a) temperature distribution in the system without thermocouple; and (b) temperature profile (in Kelvin) in the silica capillary (T_{peak} = 1445 ºC).

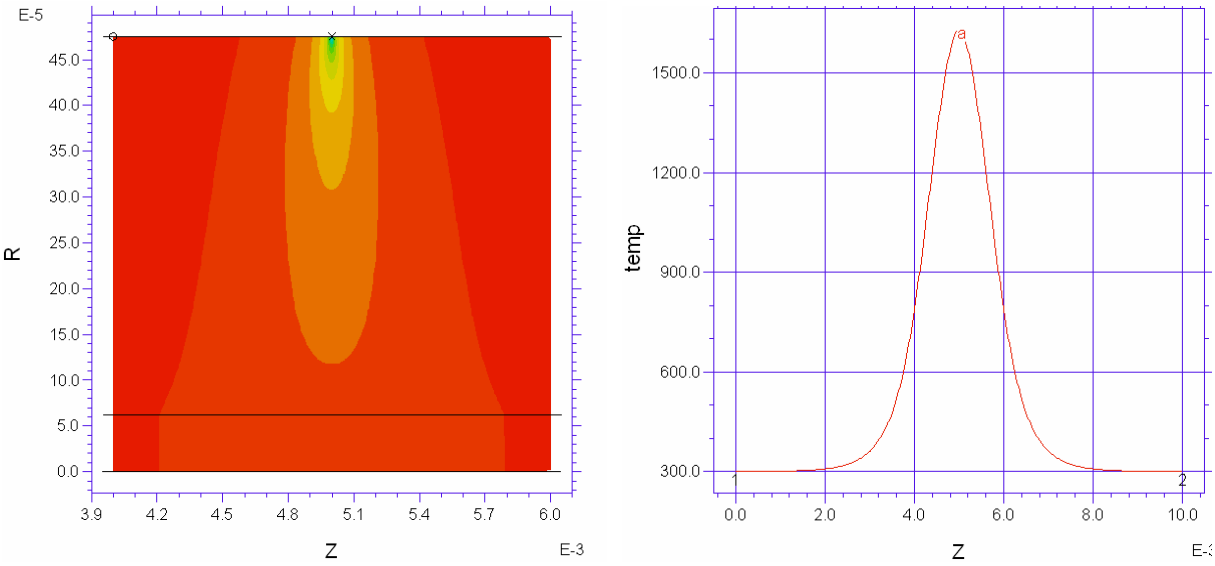

(a) (b)

Figure 4.23 – (a) Simulation results corresponding to (a) temperature distribution of the optical fibre; and (b) temperature profile (in Kelvin) in the optical fibre (T_{peak} = 1350 ºC).

Figure 4.24 summarises the most important results of the simulations and shows in particular the estimated temperature profiles in the capillary and in a fibre. The correspondent capillary peak temperature is of about 1445 ºC, in good agreement with the value obtained from Figure 4.18. The peak value of the fibre temperature of approximately 1350 ºC is also in good agreement with the estimated value determined in section 4.5.1. The temperature value reported by Mohanna [48], for a discharge of 9 mA, is about 200 ºC higher. However, the comparison cannot be easily done since crucial data, such as the electrodes gap, was not given.

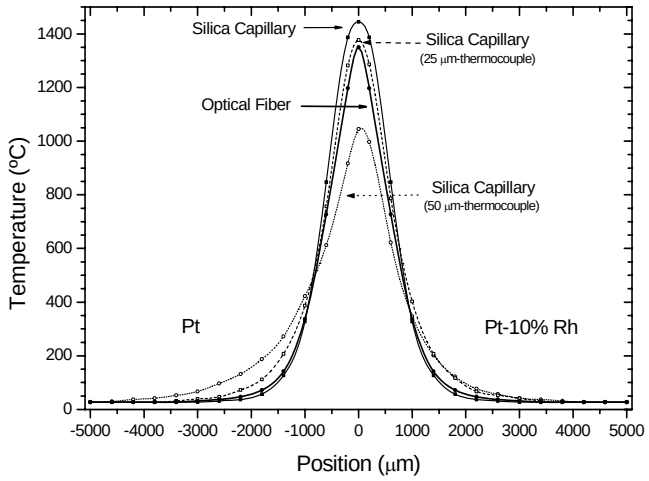

Figure 4.24 – Temperature profiles in the capillary (with and without thermocouples inside) and in the fibre computed by finite element analysis

Peak temperature versus electric current

The dependence of the peak temperature on the electric current was also investigated. Arc discharges with electric currents between 9 mA and 15 mA were applied to the thermocouples junction. As shown in Figure 4.25, a linear dependence between the peak temperature and the electric current of the arc discharge was found for all thermocouples. Considering the temperature value of 1350 ºC obtained for an electric current of 9 mA and a slope of 60 ºC/mA (this underestimated value corresponds to the slope of the 25 μm thermocouple, however regarding the dependence of the slopes on the thermocouples diameters shown in Figure 4.25, it should be, nevertheless, close to the real value), a fibre temperature close to 2000 ºC would be expected for an electric current of 20 mA. This temperature value matches the one obtained using a micro-radiation thermometer [49].

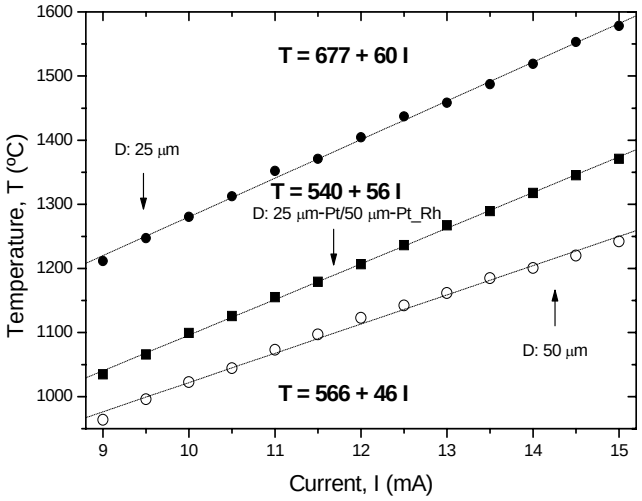

Figure 4.25 – Peak temperature versus electric current for the various thermocouples used.

In conclusion, a technique based on electrically insulated thermocouples for the measurement of the temperature of an optical fibre whilst being heated through electric arc discharges was presented. The thermocouples were assembled *in situ* by applying high current arc discharges (15 to 18 mA, 1 s) to the wires in physical contact, placed previously inside a silica capillary. Arc discharges with lower currents (9 to 15 mA) applied at different axial positions produced a temperature profile in the wires. For a current of 9 mA, a capillary temperature of 1430 ± 50 ºC was obtained by extrapolation of the experimental data for near-zero diameter thermocouples. The temperature profiles in the capillary and in the optical fibre were determined by solving the classical heat transfer equations making use of the data obtained for the thermocouples with different diameters. The respective peak temperatures calculated for the fibre (capillary) was of about 1350 ºC (1445 ºC). The fibre temperature values agree well with those obtained using other techniques [49, 50]. This method allows the

measurement of an important parameter, the fibre temperature under electrical arc discharges that concerns not only the control of the LPFGs fabrication process, but also the mechanisms responsible for their formation.

4.6 Temperature microsensor electrically insulated

The originality of the latter method led to the submission of a patent that will be described briefly in this section. The temperature microsensor is presented in two distinct configurations. The former is shown in Figure 4.26(a) and corresponds to the thermocouple described in section 4.5.2. The second enables the thermocouple fabrication prior to its introduction into a silica structure with two or more holes, as for instance, a Twin-Hole-Fibre (Figure 4.26(b)). The end containing the thermocouple junction is afterwards sealed by applying heat. The presented configurations, after calibration of the thermocouples and treatment of the data related to heat transfer in the system allows, among other applications, the temperature measurement in low size systems or in situations where a high temperature gradient exists, as in the temperature measurement of samples submitted to electric arc discharges or laser radiation. These microsensors can also play an important role in the adjustment of the arc parameters of fusion splicing machines.

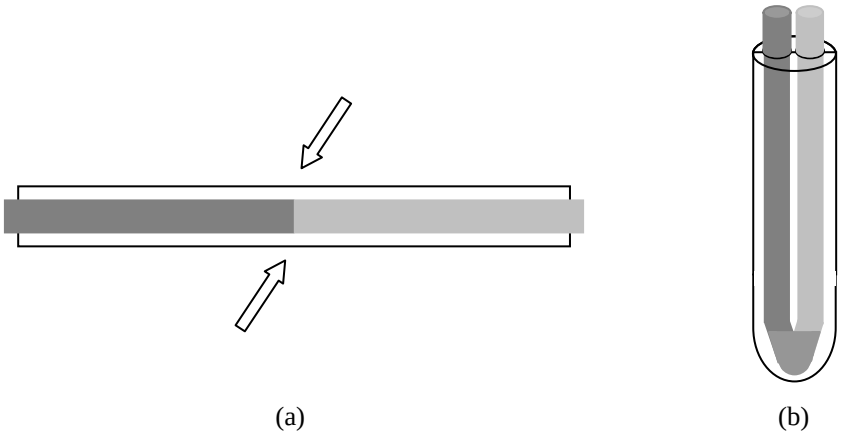

Figure 4.26 – Temperature microsensor in (a) a silica capillary (b) Twin-Hole-Fibre.

4.7 Summary

In this chapter the technique by which LPFGs are induced through arc discharge in optical fibres was described. A setup under development was also presented. This new infrastructure will further increase flexibility in the LPFGs fabrication process. The tubular oven used in this work for LPFGs characterisation was also described. Afterwards, two methods to estimate the temperature reached by the fibre during LPFGs fabrication were thoroughly examined. The first is based on the blackbody radiation and the second on electrically insulated thermocouples assembled in situ by arc discharges. Finally, the latter method gave rise to a patent submission that was also briefly discussed (Appendix D, in Portuguese).

References

[1] A. Vengsarkar, P. Lemaire, J. Judkins, V. Bhatia, T. Erdogan, and J. Sipe. *Long-period fiber gratings as band-rejection filters.* Journal of Lightwave Technology **14**(1): 58-65, 1996.

[2] C.D. Poole, H.M. Presby, and J.P. Meester. *2-Mode Fiber Spatial-Mode Converter Using Periodic Core Deformation.* Electronics Letters **30**(17): 1437-1438, 1994.

[3] C. Narayanan, H.M. Presby, and A.M. Vengsarkar. *Band-rejection fibre filter using periodic core deformation.* Electronics Letters **33**(4): 280-281, 1997.

[4] S.G. Kosinski, G.A. Ten Eyck, and A.M. Vengsarkar. *Method for making long-period fiber gratings*, in *European Patent EP0840146*. 1998-05-06, 1998

[5] E.M. Dianov, V.I. Karpov, M.V. Grekov, K.M. Golant, S.A. Vasiliev, O.I. Medvedkov, and R.R. Khrapko. *Thermo-induced long-period fibre gratings*. in *IOCC-ECOC 97 - 11th International Conference on Integrated Optics and Optical Fibre Communications / 23rd European Conference on Optical Communications, Vol 2*: 53-56, 1997.

[6] T. Enomoto, M. Shigehara, S. Ishikawa, T. Danzuka, and H. Kanamori. *Long-period fiber grating in a pure-silica core fiber written by residual stress relaxation.* in *Proceedings of 1998 Optical Fiber Communications Conference*: 277-278, 1998.

[7] S.G. Kosinski and A.M. Vengsarkar. *Splice-based long-period fiber gratings*. in *Proceedings of 1998 Optical Fiber Communications Conference*: 278-279, 1998.

[8] I. Hwang, S. Yun, and B. Kim. *Long-period fiber gratings based on periodic microbends.* Optics Letters **24**(18): 1263-1265, 1999.

[9] M. Verhaegen, P. Orsini, D. Perron, X. Daxhelet, and S. Lacroix. *Long period gratings fabrication techniques*. in *Applications Of Photonic Technology 4 - Closing The Gap Between Theory, Development, And Application*: 156-161, 2000.

[10] P. Palai, M. Satyanarayan, M. Das, K. Thyagarajan, and B. Pal. *Characterization and simulation of long period gratings fabricated using electric discharge.* Optics Communications **193**(1-6): 181-185, 2001.

[11] G. Rego, O. Okhotnikov, E. Dianov, and V. Sulimov. *High-temperature stability of long-period fiber gratings produced using an electric arc.* Journal of Lightwave Technology **19**(10): 1574-1579, 2001.

[12] G. Humbert and A. Malki. *Characterizations at very high temperature of electric arc-induced long-period fiber gratings.* Optics Communications **208**(4-6): 329-335, 2002.

[13] K. Morishita, S.F. Yuan, and Y. Miyake. *Refractive-index changes and long-period fiber gratings made by rapid solidification*. in *Proceedings of 2002 IEEE/LEOS Workshop on Fibre And Optical Passive Components*: 98-103, 2002.

[14] M. Kim, D. Lee, B. Hong, and H. Chung. *Performance characteristics of long-period fiber-gratings made from periodic tapers induced by electric-arc discharge.* Journal of the Korean Physical Society **40**(2): 369-373, 2002.

[15] O. Frazão, R. Romero, G. Rego, P.V.S. Marques, H.M. Salgado, and J.L. Santos. *Sampled fibre Bragg grating sensors for simultaneous strain and temperature measurement.* Electronics Letters **38**(14): 693-695, 2002.

[16] G. Rego, R. Romero, O. Frazão, P.V.S. Marques, and H.M. Salgado. *Apodisation of uniform Fibre Bragg Gratings using electric arc discharges*. in *Proceedings of 2002 IEEE/LEOS Workshop on Fibre and Optical Passive Components*: 13-16, 2002.

[17] G. Humbert, A. Malki, S. Fevrier, P. Roy, and D. Pagnoux. *Electric arc-induced long-period gratings in Ge-free air-silica microstructure fibres.* Electronics Letters **39**(4): 349-350, 2003.

[18] G. Humbert, A. Malki, S. Fevrier, P. Roy, J.L. Auguste, and J.M. Blondy. *Long period grating filters fabricated with electric arc in dual concentric core fibers.* Optics Communications **225**(1-3): 47-53, 2003.

[19] A. Malki, G. Humbert, Y. Ouerdane, A. Boukhenter, and A. Boudrioua. *Investigation of the writing mechanism of electric-arc-induced long-period fiber gratings.* Applied Optics **42**(19): 3776-3779, 2003.

[20] K. Thyagarajan, M. Das, and M.N. Satyanarayan. *A simple and direct method to estimate long period grating parameters.* Optics Communications **218**(1-3): 67-72, 2003.

[21] G. Rego, J.L. Santos, P.V.S. Marques, and H.M. Salgado. *Study of the properties of arc-induced long-period gratings and Bragg Gratings in B/Ge doped fibers*. in *Proceedings of the Bragg Gratings, Photosensitivity and Poling in Glass Waveguides Conference*: 121-123, 2003.

[22] K. Morishita and Y. Miyake. *Fabrication and resonance wavelengths of long-period gratings written in a pure-silica photonic crystal fiber by the glass structure change.* Journal of Lightwave Technology **22**(2): 625-630, 2004.

[23] H. Dobb, K. Kalli, and D.J. Webb. *Temperature-insensitive long period grating sensors in photonic crystal fibre.* Electronics Letters **40**(11): 657-658, 2004.

[24] G. Humbert and A. Malki. *Characterizations at high temperatures of long-period gratings written in germanium-free air-silica microstructure fiber.* Optics Letters **29**(1): 38-40, 2004.

[25] A.D. Yablon, M.F. Yan, P. Wisk, F.V. DiMarcello, J.W. Fleming, W.A. Reed, E.M. Monberg, D.J. DiGiovanni, J. Jasapara, and M.E. Lines. *Refractive index perturbations in optical fibers resulting from frozen-in viscoelasticity.* Applied Physics Letters **84**(1): 19-21, 2004.

[26] G. Rego, L. Santos, B. Schroder, P. Marques, J. Santos, and H. Salgado. *In situ temperature measurement of an optical fiber submitted to electric arc discharges.* IEEE Photonics Technology Letters **16**(9): 2111-2113, 2004.

[27] G. Rego, P.V.S. Marques, H.M. Salgado, and J.L. Santos. *Simultaneous measurement of temperature and strain based on arc-induced long-period fibre gratings.* Electronics Letters **41**(2): 60-62, 2005.

[28] S.H. Nam, C. Zhan, J. Lee, C. Hahn, K. Reichard, P. Ruffin, K.L. Deng, and S.Z. Yin. *Bend-insensitive ultra short long-period gratings by the electric arc method and their applications to harsh environment sensing and communication.* Optics Express **13**(3): 731-737, 2005.

[29] G. Rego, R. Falate, J.L. Santos, H.M. Salgado, J.L. Fabris, S.L. Semjonov, and E.M. Dianov. *Arc-induced long-period gratings in aluminosilicate glass fibers.* Optics Letters **30**(16): 2065-2067, 2005.

[30] G. Rego, A.F. Fernandez, A. Gusarov, B. Brichard, F. Berghmans, J.L. Santos, and H.M. Salgado. *Effect of ionizing radiation on the properties of arc-induced long-period fiber gratings.* Applied Optics **44**(29): 6258-6263, 2005.

[31] K. Morishita and A. Kaino. *Adjusting resonance wavelengths of long-period fiber gratings by the glass-structure change.* Applied Optics **44**(24): 5018-5023, 2005.

[32] F. Durr, G. Rego, P.V.S. Marques, S.L. Semjonov, E. Dianov, H.G. Limberger, and R.P. Salathe. *Stress Profiling of Arc-Induced Long Period Fiber Gratings.* Journal of Lightwave Technology **23**(11): 3947-3953, 2005.

[33] Y. Kato, S. Seikai, N. Shibata, S. Tachigami, Y. Toda, and O. Watanabe. *Arc-Fusion Splicing of Single-Mode Fibers.2. A Practical Splice Machine.* Applied Optics **21**(11): 1916-1921, 1982.

[34] E.F. Zalewski, *Radiometry and Photometry*, in *Handbook of Optical Materials*. Mc Graw-Hill: Chap. 24 & 25, 1995

[35] R. Bruckner. *Properties and Structures of Vitreous Silica. I.* Journal of Non-Crystalline Solids **5**: 123-175, 1970.

[36] J.W. Fleming. *Sub Glass Transition Relaxation in Optical Fibers*. in *Proceedings of 2004 Optical Fiber Communications Conference*: TuB2, 2004.

[37] M.J. Adams, *Circular waveguides and step-index fibres*, in *An Introduction to Optical Waveguides*. John Wiley & Sons: 243, 1981

[38] Y. Shuto, S. Yanagi, S. Asakawa, M. Kobayashi, and R. Nagase. *Evaluation of high-temperature absorption coefficients of optical fibers.* IEEE Photonics Technology Letters **16**(4): 1008-1010, 2004.

[39] W. Zhihai, C. Jiahua, Z. Hanyi, and Z. Bingkun. *A sensitive high-speed and high-temperature optical fiber sensor.* Journal of Tsinghua University **28**(s3): 31-8, 1986.

[40] J.D. Cobine, in *Gaseous Conductors*. Mc Graw-Hill: 290, 1941

[41] V.I. Sapritsky and A.V. Prokhorov. *Spectral Effective Emissivities of Nonisothermal Cavities Calculated by the Monte-Carlo Method.* Applied Optics **34**(25): 5645-5652, 1995.

[42] G.W. Burns, M.G. Scroges, G.F. Strouse, M.L. Croarkin, and W.F. Guthrie, *Temperature-electromotive force reference functions and tables for the letter designated thermocouple types based on the ITS-90*, in *NIST Monograph*: 175, 1993

[43] Y. Terada. *Thermal Conductivities of Platinum Alloys at High Temperatures.* Platinum Metal Review **49**(1): 21-26, 2005.

[44] A.J.C. Grellier. *Characterisation of optical fibre tapering using a CO_2 laser*. Kent University, Canterbury, U. K., 2000

[45] Y.S. Touloukian and C.Y. Ho, *Thermophysical Properties of Matter: The TPRC Data Series*, in *Thermophysical Properties of Matter: The TPRC Data Series*. Purdue University, 1970

[46] H. Scholze, in *Glass: Nature, Structure and Properties*. Springer-Verlag: 208, 1991

[47] D. Tschumperlé and M. Nicolardot. *Fiber Cooling Modelisation During Draw Using CFD*. in *ASME CFD Symposium, Proceedings*: E13, 2001.

[48] Y. Mohanna. *Electric arc temperature estimation of a fibre splicer.* IEE Proc.-Optoelectronics **142**: 313-315, 1995.

[49] I. Hatakeyama and H. Tsuchiya. *Fusion Splices for Single-Mode Optical Fibers.* IEEE Journal of Quantum Electronics **14**(8): 614-619, 1978.

[50] G. Rego, P.V.S. Marques, H.M. Salgado, and J.L. Santos. *Measurement of the temperature of an optical fiber submitted to an electric arc discharge*. in *Second European Workshop On Optical Fibre Sensors: Proceedings*: 374-377, 2004.

5

Properties of arc-induced gratings

5.1 Introduction

In the last chapter it was described the technique to arc-induce long-period fibre gratings. In this one, our attention will be centred on the properties of the produced gratings since there lays the basis for their applications which will be discussed in Chapter 8.

The chapter begins with a study on the effects of the fabrication parameters on the gratings spectra. Afterwards, the thermal behaviour of the produced gratings is analysed, followed by an investigation of LPFGs response to changes of physical quantities, such as temperature and strain. The polarization dependent loss of arc-induced gratings which is an important issue to optical communications is also discussed. Experimental results on the interactions between arc-induced gratings and UV-radiation are also given. Finally, the effect of ionising radiation on the properties of arc-induced gratings is presented.

5.2 Gratings properties

Gratings produced using the electric arc technique possess several important and unique properties that position them as the best candidates for some applications when compared to the performance of gratings produced by other techniques. Arc-induced gratings have very high temperature stability, even when they are written in standard germanium doped fibres [1]. This property may be shared with other gratings whose formation is based on thermal effects such as the ones fabricated by CO_2 or CO laser radiation [2, 3]. Therefore, in opposition to UV-induced gratings, these thermal gratings can be used as high temperature sensors. Another important aspect is that the temperature dependence of the resonant wavelengths belonging to gratings written in Ge-doped fibres is non-linear, whilst for gratings inscribed in Ge-free fibres that dependence is more likely to be linear. In fact, gratings arc-induced in Al-doped and Al/Er-doped fibres have shown a remarkable linear dependence up

to 700 ºC [4]. This property might be useful not only in the sensing domain but also in optical communications. Note also that these fibres are not photosensitive and, therefore, techniques other than UV laser radiation are required for gratings inscription.

A unique feature of the electric arc technique is the possibility to tune the gratings sensitivity, for instance to temperature and strain by changing the fabrication parameters [5]. This enables the fabrication of compact sensor heads to the simultaneous measurement of physical parameters, being also possible to make the sensor insensitive to a particular parameter [6].

Arc induced gratings are also very promising to perform sensing in ionising radiation environments [7]. It should be stressed that to take advantage of the intrinsic properties of pure-silica-core fibres also requires a step towards fabrication techniques such as the electric arc. Therefore, it is worthwhile to have a close look on the general properties of these gratings.

5.3 Influence of the fabrication parameters

In this section it is presented the contribution of the different fabrication parameters to the gratings inscription. Thus, it will be analysed the influence of the type of fibre, the gratings period and length, the arc discharge parameters (electric current and duration), the pulling tension and also the heat treatment of the fibre.

5.3.1 Type of fibre

About two tenths of fibres have been used in this work. Gratings were written in different types of singlemode fibres: standard Ge-doped fibres such as Sumitomo (1.5 mol%), Corning SMF28 (3.0 mol%), Siecor (6.0 mol%), a dispersion-shifted fibre from Corning (12 mol%), the HI980 also from Corning and the B/Ge codoped fibre PS1500 from Fibercore were used. LPFGs were also arc-induced in several Ge-free silica based fibres, such as, the pure-silica-core fibres described in section 5.5.2. Other fibres, with unusual composition, produced by SPCVD technology at FORC-GPI in Moscow were also used. One fibre ($\Delta n \leq 0.006$ and $\lambda_{cut\text{-}off}$~1.0 μm) contains sulphur (0.4 wt%) and chlorine (2 wt%) as main dopants. This fibre has a loss of 0.4 dB/km at both wavelengths of 1.3 and 1.55 μm. A second fibre contains nitrogen (Δn=0.01, D_{core}=4.0 μm and $\lambda_{cut\text{-}off}$~0.9 μm). Figure 5.1 shows the spectra of two gratings written in these two fibres. Gratings were also inscribed in other three nitrogen doped fibres

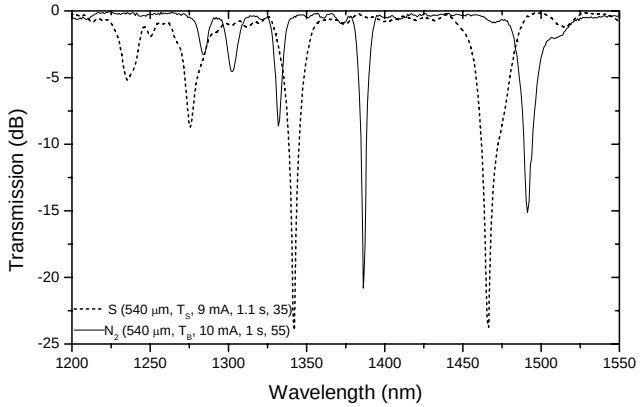

Figure 5.1 – Spectra of two gratings written in the sulphur and nitrogen doped fibres.

drawn with different drawing tensions. They have been used to investigate the mechanisms of gratings formation as described in Chapter 3. In a fourth one, it has been written the grating with the shortest period (see section 5.3.4). It can be concluded that the electric arc technique enables the writing of LPFGs in any kind of fibre independently of its composition. It should be stressed that no relation was found between a particular dopant concentration and the grating strength.

Recently, we have written LPFGs in aluminosilicate fibres and it was shown that the resonant wavelengths of these gratings shift linearly with temperature. These results are very promising for fibre lasers and amplifiers and also for temperature sensing. Therefore, special attention will be given to those Ge-free silica based fibres produced by MCVD technology at FORC-GPI, in Moscow. One fibre, Al (D_{core} = 4.3 μm, $D_{clad.}$ = 125.8 μm and $\lambda_{cut\text{-}off}$ = 0.92 μm) has its core doped with alumina oxide, whilst the other, Al/Er (D_{core} = 4.6 μm, $D_{clad.}$ = 125.9 μm and $\lambda_{cut\text{-}off}$ = 0.99 μm) contains alumina oxide and erbium in the core. The absorption spectrum of the Al/Er fibre was measured by the cut-back method [8] showing two peaks centred at 0.98 μm and 1.53 μm with absorption coefficients of ~12 dB/m and ~16 dB/m, respectively. As a result of such high absorption, for the gratings inscription in this fibre it was required the concatenation of short pieces of Al/Er fibre in between a standard fibre. The refractive index profiles of both fibres, which were measured using a S14 Refractive Index Profiler from Photon Kinetics (room temperature = 22 ºC, refractive index of the calibration oil = 1.47@25 ºC & 632.8 nm), are presented in Figure 5.2. As it can be seen, for Al^{3+} doped and Er^{3+}/Al^{3+} co-doped fibres the difference between the refractive indices of the core and cladding is equal to 1.71×10^{-2} and 1.88×10^{-2}, respectively.

For the inscription of the LPFGs the fabrication parameters were set as follows: an axial tension of 22.8 g, an electric current of 9 mA, an arc duration of 1 s and a grating period of 400 μm. The choice of the period was determined by the appearance of grating resonances in the 1.52-1.57 μm wavelength range. The spectra of the gratings written in the Al and Al/Er

fibres are presented in Figure 5.3. The resonances belonging to the grating written in the Al fibre are, as expected, positioned at shorter wavelengths ($\Delta\lambda \sim 100$ nm), since that fibre has smaller core diameter and Δn as shown in Figure 5.2.

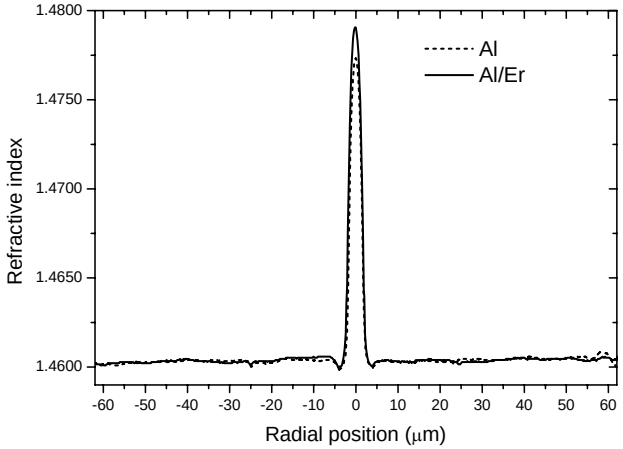

Figure 5.2 – Refractive index profiles of the aluminosilicate fibres.

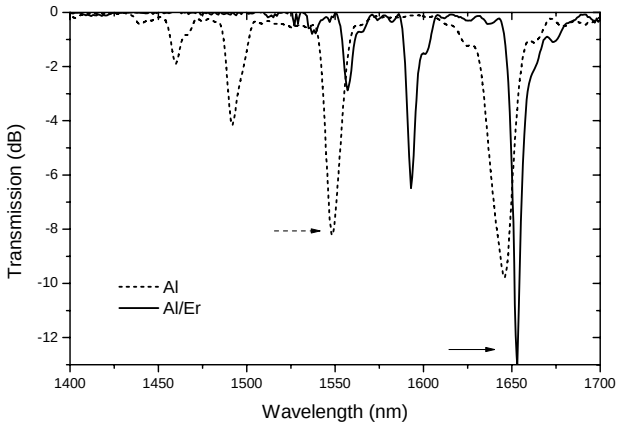

Figure 5.3 – Transmission spectra of two 400 μm LPFGs arc-induced in both fibres (arrows indicate coupling to cladding modes of the same order).

5.3.2 Resonant wavelengths versus grating period

Several gratings with periods ranging from 400 to 680 μm were written in the SMF28 fibre from Corning, a standard singlemode fibre with a core diameter of 8.6 μm which contains 3.46 mol% of GeO_2. Figure 5.4 shows the dependence of the lowest resonant wavelengths on the grating period. As expected from the resonant condition, the position of the resonant peaks shifts towards longer wavelengths as the grating period increases. This figure also shows the result of fitting the experimental data to symmetric and asymmetric perturbations. The simulations were performed using the Apollo Photonics v2.2a software program and enables one to conclude that for arc-induced gratings the core mode is coupled to LP_{1j} cladding modes (j>1).

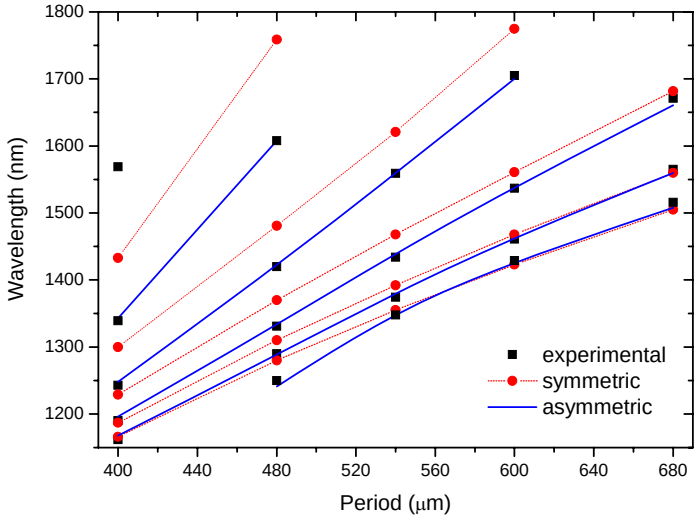

Figure 5.4 – Resonant wavelength versus period for the lowest cladding modes. The experimental data was fitted considering both types of perturbations: symmetric and asymmetric.

5.3.3 Grating length

The evolution of the strength and resonance wavelength, of a particular cladding mode resonance, was monitored during grating fabrication and results are shown in Figure 5.5(a)-(b). The first puts in evidence the occurrence of back-coupling after the 17th arc discharge whilst the second shows that the first order cladding mode resonance shifts considerably toward longer wavelengths when a high external tension is used during grating fabrication. Figure 5.6 shows the growth of two gratings written with different pulling tensions. The resonance wavelengths of the higher order resonances shifts only moderately (Figure 5.6b). It can also be seen that the gratings bandwidth decreases with the increase of their length.

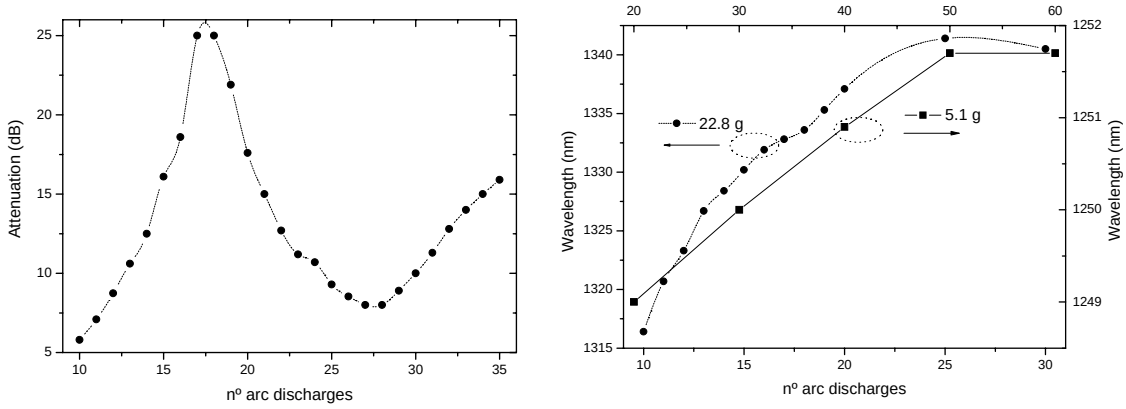

(a) (b)

Figure 5.5 – Evolution of the (a) transmission loss and (b) resonant wavelength.

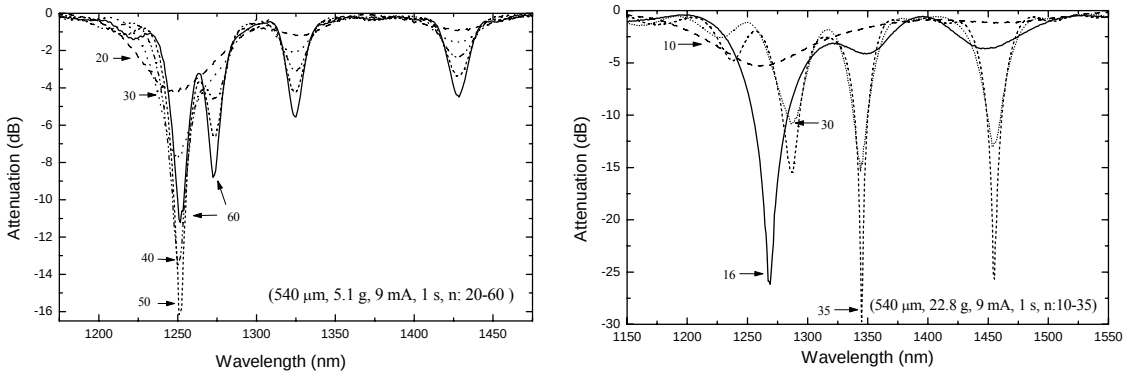

(a) (b)

Figure 5.6 – Evolution of two LPFGs written using an external tension of (a) 5.1 g and (b) 22.8 g.

5.3.4 Electric current, arc duration and external tension

The influence of the writing parameters on the spectra of the LPGs induced in the SMF28 fibre was also investigated. As it can be seen in Figure 5.7, the increase of the external tension displaces the spectrum towards longer wavelengths and increases the grating coupling strength. It was also observed that the fabrication conditions employed lead to a periodic tapering of the fibre. Although a decrease of the cladding diameter contributes to an upper shift, as occurs during fibre etching [9], the dominant effect is nevertheless, the decrease of the core that reduces the guided mode effective refractive index leading to a downshift of the resonances [10] (see also section 3.3.4). However, the displacement of the grating resonances show a different behaviour, which is believed to be related to the inhibition of stress relaxation due to the applied external tension [11, 12]. The mechanism that leads to an increase on the coupling strength is enhanced by fibre tapering. The increase of the electric current or the arc duration also reduces the core diameter and therefore increases the coupling strength; nevertheless, both parameters lead to a down shift of the spectrum. This can be due to enhancement of stress relaxation, mainly caused by an increase of the arc current which is

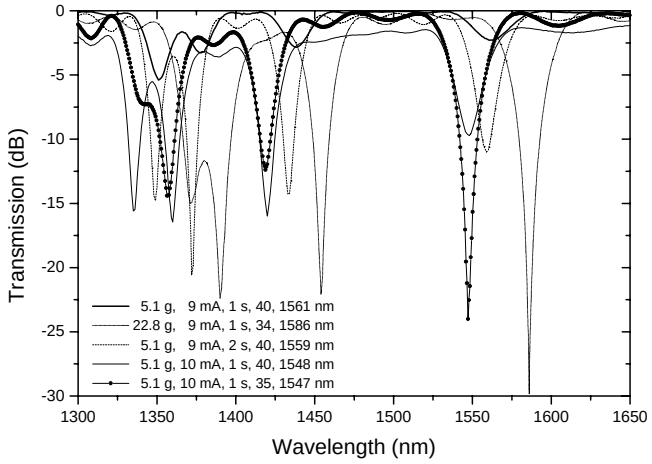

Figure 5.7 – Influence of the writing parameters on the LPFGs spectra.

directly related to the fibre temperature. Note that in a B/Ge doped fibre, the increase of the electric current also produces a downshift of the resonant wavelengths [13] and therefore the shift cannot be explained by diffusion. Figure 5.7 also puts in evidence one major problem of the electric arc technique, that is, some lack of reproducibility. Although the resonant wavelengths are fairly stable, the strength of the loss-peaks may vary a lot, for gratings written under the same conditions. The reasons for that behaviour may be of two types: intrinsic to the mechanism of gratings formation or intrinsic to the fabrication process. The first is related to the asymmetric changes induced by the arc discharge that may differ from discharge to discharge which may have a significant influence on the coupling strength. The second are the changes on the relative position between the fibre and the electrodes, electrodes degradation and their repositioning on replacement, dust on the fibres or on the electrodes and changes on the ambient conditions (e.g., humidity). Moreover, the use of high external tension might amplify the problem. Therefore, to have reproducibility a precise alignment of the fibre is required, as well as electrodes holders enabling accurate repositioning and a clean controlled environment.

Another drawback of the technique is the limit imposed on the shortest period that can be produced. A minimum period of 240 μm has been used to write gratings in a nitrogen-doped fibre (Δn = 0.04, D_{core} = 2.0 μm and $\lambda_{cut\text{-}off} \sim$ 0.9 μm), from FORC. Similar periods have been used to produce a filter at 1.06 μm in a Corning DSF fibre (12 mol% of GeO_2, MFD = 10.5 ± 1.0 μm at 1.55 μm and $\lambda_{cut\text{-}off}$ = 1.26 μm) [14]. This limitation is mainly due to the dimensions of the arc discharge, which increases with the increasing of the electrodes gap [15]. For an electric current of 9 mA and 1 s duration (electrodes parameters: gap = 1.0 mm, apex angle = 40 º), an arc discharge waist of 150-200 μm was estimated [16]. However, the fibre length where a refractive index change takes place depends on the temperature profile established on the fibre during the arc discharge and on the prevailing mechanism responsible for that change. Recently, Thyagarajan *et al.* [17] estimated an affected region of about 312 μm for LPGs induced in the SMF28 fibre using the TRITEC Fase II fibre splicer (electrodes gap ~ 1.0 mm), although set for a presumable higher electric current [18]. In this case, the index modulation was attributed to core dopants diffusion.

5.3.5 Effect of pre-annealing

As discussed in section 3.3.3, gratings with the same length written in pre-annealed nitrogen-doped fibres have higher coupling strengths than the ones induced in pristine fibres. The position of the resonances are also located at shorter wavelengths. Similar results were obtained for gratings written in the SMF28 fibre pre-annealed at different temperatures

(Figure 5.8). However, the annealing at 1100 ºC leads to a large increase in the background loss of the produced gratings.

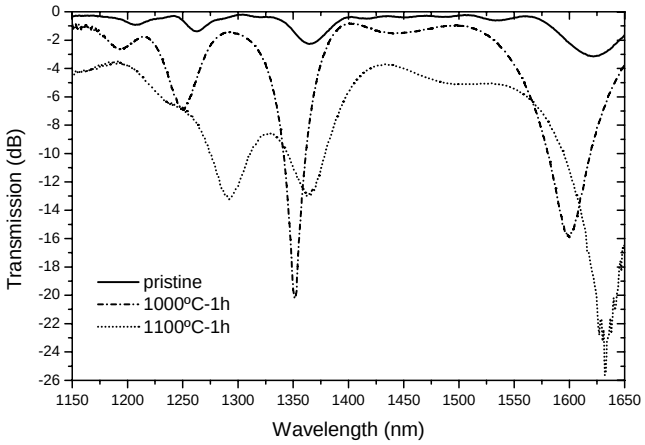

Figure 5.8 – Temperature dependence of several LPGs written in different types of fibres.

5.4 Thermal behaviour

5.4.1 Heating up to high temperatures

To investigate th thermal behaviour of the gratings they were placed, under a pulling tension of 5.1 g to prevent bending, inside the tubular oven described in section 4.4. The oven temperature was then increased from room temperature up to 1200 ºC in steps of 50 ºC to 100 ºC, being the gratings spectra recorded after a dwell time of 15 min. The main results related to the temperature dependence of the resonant wavelengths are summarised in Figure 5.9 to

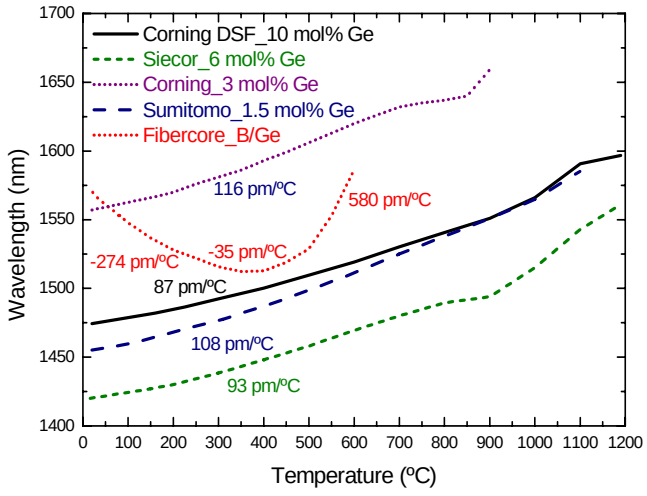

Figure 5.9 – Temperature dependence of several LPFGs written in Ge-doped fibres.

Figure 5.12. In general, as the temperature increases the resonant peaks move towards longer wavelengths (Figure 5.9). However, LPFGs written in B/Ge doped fibres do not follow that behaviour due to the presence of boron that alters the temperature dependence of the refractive index (exhibiting different thermo-optic coefficients). Another interesting feature is the fact that, for some fibres, the temperature sensitivity decreases at temperatures between 700 ºC and 1000 ºC, the exact temperature range being dependent on the fibre type. This phenomenon related to relaxation of intrinsic stresses can be better visualized in the case of the sulphur-doped fibre (Figure 5.10). Moreover, for the pure-silica-core fibre and for the Fibercore B/Ge-doped fibre, stress relaxations were found at temperatures as low as 300 ºC [13]. Relaxations at about 400 ºC were also recently found in elongation experiments with several types of fibres drawn with different drawing tensions [19].

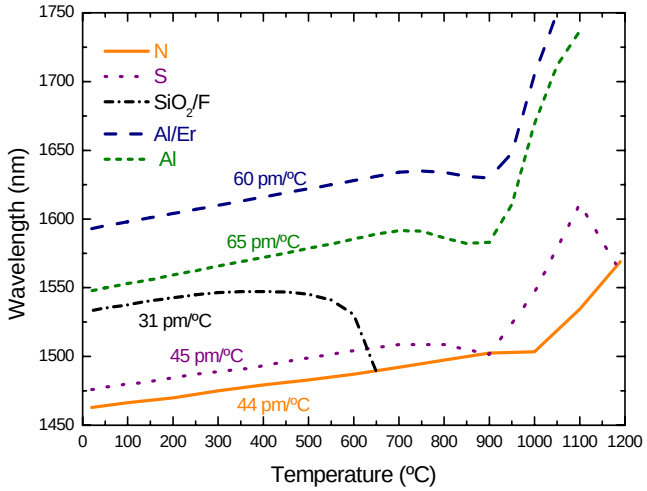

Figure 5.10 – Temperature dependence of several LPFGs written in Ge-free fibres.

Another important conclusion that can be drawn from comparison between these two figures is that the resonant wavelengths of gratings written in germanium doped fibres shifts non-linearly with temperature whilst germanium free fibres exhibits a linear dependence. This can be better observed in Figure 5.11, where clearly the temperature sensitivity coefficients for the gratings written in the aluminosilicate fibres are constant up to 700 ºC. On the other hand, the resonant wavelengths of gratings induced in the Corning fibres show a quadratic dependence on temperature. The linear dependence obtained for germanium free fibres are of great interest for optical fibre sensors.

Table 1 summarises the typical results obtained for several resonances belonging to gratings written in fibres having different dopants and geometries.

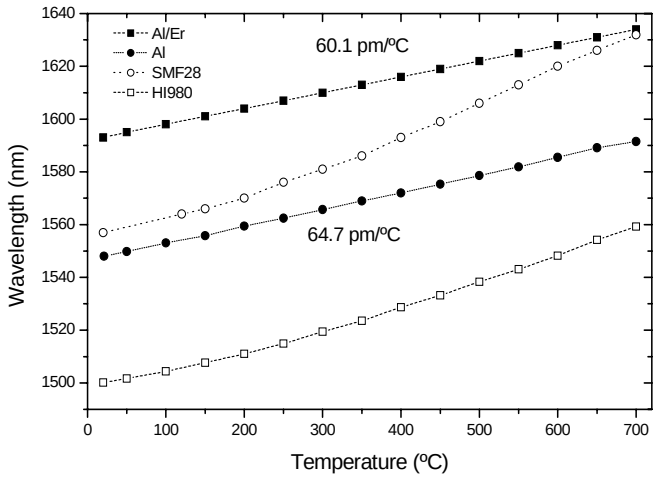

Figure 5.11 – Quadratic and linear temperature dependence shown by gratings written respectively, in germanium doped and in aluminosilicate fibres.

Table 1. Thermal behaviour of gratings written in different fibres

Fibre	mol% Ge Technique	Dcore/μm	Λ/μm	Mode order	Thermal sensitivity/pmºC^{-1}
Sumitomo	1.5_VAD	8.3	540	4	58.1 + 0.125T
SMF-28	3_?	8.6	540	4	72.3 + 0.12T
Siecor	6_OVD	8.3	540	4	76.7 + 0.11T
HI-980	?_OVD	~4?	540	5	56.2 + 0.09T
Corning_DSF	12_VAD	5.1	540	3	39.4 + 0.13T
Al	MCVD?	4.25	400	4	64.7 T≤700
Al/Er	MCVD?	4.55	400	4	60.1 T≤700
S	SPCVD	?	540	4	50 T≤700
Oxford_SiO_2/F	?	9	730	2	47.1 T≤300
ACREO_SiO_2/F	?	?	730	3	40.1 T≤300
N'94	SPCVD	2	240	6	45 T≤900
N'96	SPCVD	4.5	540	5	43 T≤900
N1905	SPCVD	6.2	400	4	67 T≤400
N1940	SPCVD	5.8	400	4	51.9 T≤400

It is well known that the temperature sensitivity increases with the order of the cladding modes and also with the temperature itself (Figure 5.12). The fibre type and the writing parameters also affect the temperature sensitivity values. The latter can lead to changes of ±5%, for temperatures up to 120 ºC.

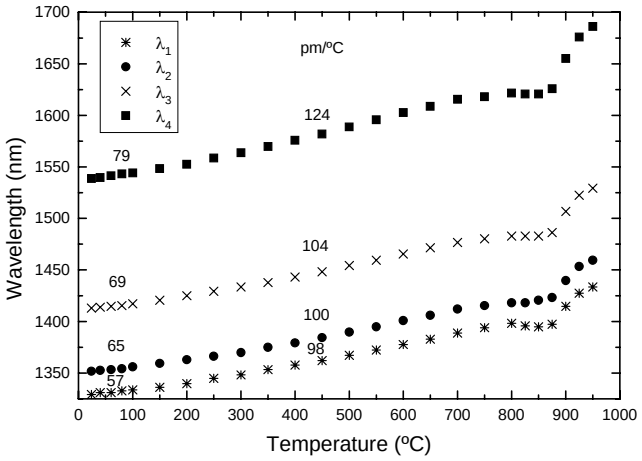

Figure 5.12 – Thermal behaviour of four resonances belonging to a 540 μm LPFG written in the Siecor fibre.

Figure 5.13(a) shows the transmission spectra of a grating at room temperature and at 1190 ºC. This LPFG written in the Corning DSF fibre withstood 30 min at such a high temperature, with only minor changes. This is a remarkable result, regarding the fact that gratings written in the B/Ge-doped fibre are destroyed at temperatures below 900 ºC or when compared to the behaviour of UV-induced gratings. Moreover, the subsequent degradation has been related to the deformation of the fibre caused by the applied external tension (5.1 g) while the fibre was heated to a temperature in the limit of the softening range (Figure 5.13 (b)). In fact, it was later measured an elongation rate of ~6 mm/min for a 180 mm long SMF-28 fibre at 1300 ºC under a tension of only 1.1 g.

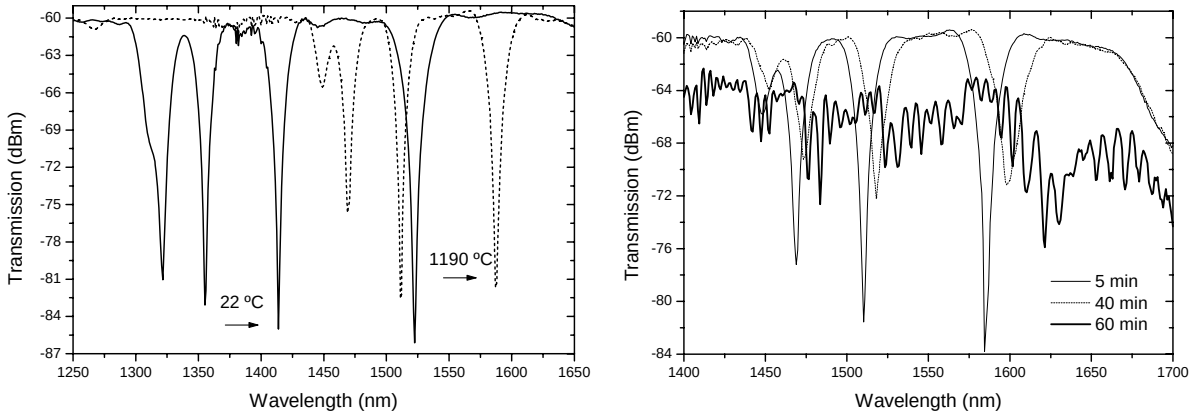

(a) (b)

Figure 5.13 – (a) High temperature stability of a 430 μm LPG written in the Corning DSF fibre; and (b) the afterwards degradation due to elongation of the fibre.

5.4.2 Heating cycles

One grating, LPFG #1 (5.1 g, 9 mA, 1 s, 40), was submitted to four heating cycles from room temperature up to 900 ºC (Figure 5.14). It was observed that the stress was released after the first annealing and that during the third annealing the fibre was in a thermodynamic equilibrium (similar curves were obtained for the 3rd and 4th heating cycles). Figure 5.14 also shows the result of heating a second grating, LPFG #2 (5.1 g, 9 mA, 1 s, 40), up to 700 ºC followed by a dwell time of 15 h. During this period the spectrum moved towards lower wavelengths, due to stress relaxation, the shift being 18 nm for the third resonance. Note that the shift is larger (25 nm) for higher order cladding modes (4th). It should be also noted that these shifts may depend on the fabrication parameters since for a grating (1.1 g, 12 mA, 0.5 s, 40) annealed during 17h, the shift measured was of -55 nm. After cooling down slowly to room temperature, the grating was submitted to an annealing temperature of 800 ºC for 6h. This time the spectrum moved 55 nm to longer wavelengths. This may reflect a rearrangement of the glass structure towards a new thermodynamic equilibrium as a consequence of the interplay between stress relaxation and the fibre thermal expansion coefficients and viscosities, which are also time and temperature dependent.

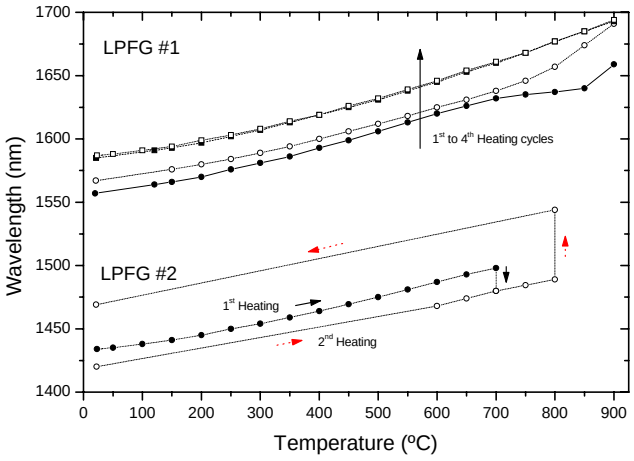

Figure 5.14 – Thermal behaviour of an LPFG submitted to several heating cycles.

5.4.3 Time dependence at temperatures near the strain and annealing points

Stress relaxation at temperatures in the range 700 ºC – 800 ºC was first observed in [1]. Latter, Humbert *et al.* [20] gave detailed information regarding this effect. Figure 5.15 shows the movement of two resonant wavelengths belonging to a LPFG, written in the Corning SMF28 fibre, kept at 800 ºC, for 6 h. Initially, the grating spectrum moves toward lower wavelengths, being the shift larger for the higher order resonance (4th). After about 90 min, the spectrum starts moving towards longer wavelengths until an equilibrium position is reached. It is interesting to note that the overall shift obtained for the annealing of LPFG #2 at

both 700 ºC and 800 ºC and for the grating shown in Figure 5.15 is the same ~55 nm. The shift presented in [20] for the same resonance of a similar grating is much shorter and, therefore, the difference may be attributed to distinct values of the electric currents used. Note also that the annealing at 900 ºC leads to a shift towards longer wavelengths, that is, stress relaxation occurs during the increase of temperature (Figure 5.14).

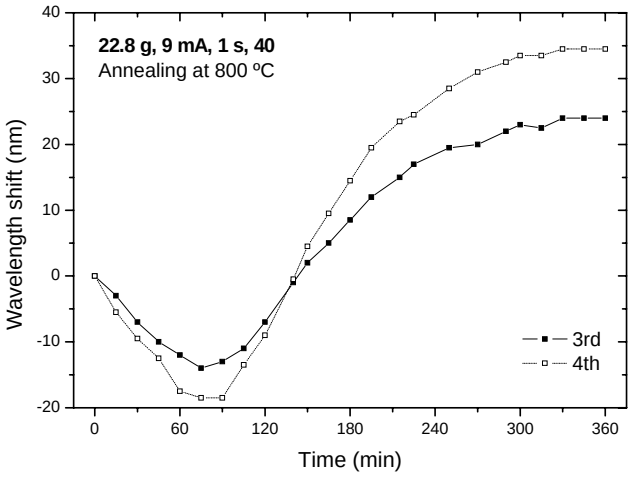

Figure 5.15 – Time dependence of the resonant wavelength at 800 ºC.

The thermal annealing of several gratings written in different types of fibre was also performed at 1000 ºC during 24 h. As shown in Figure 5.16 whilst the gratings written in the germanium doped fibres move towards longer wavelengths, for gratings inscribed in germanium free fibres (a pure-silica-core fibre and a nitrogen doped fibre) the shift is much larger and precisely in the opposite direction. There is no clear understanding of the reasons

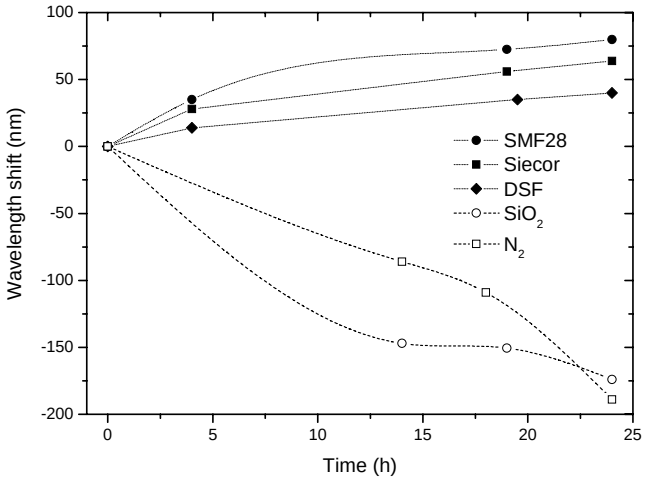

Figure 5.16 – Time dependence of the resonant wavelength at 1000 ºC.

for this behaviour. The standard fibres appears to approach an equilibrium situation, after a process of stress relaxation and thermal expansion, whilst for the other fibres diffusion and

chemical processes might be involved leading to a degradation of the pristine fibre. As shown in Figure 5.17, gratings annealed at 1000 ºC for 1 day exhibits some degree of degradation. A similar study was conducted by Morishita *et al.* [21] in the Corning SMF28 fibre. The shifts obtained are larger which might be due to the higher arc currents used in their work.

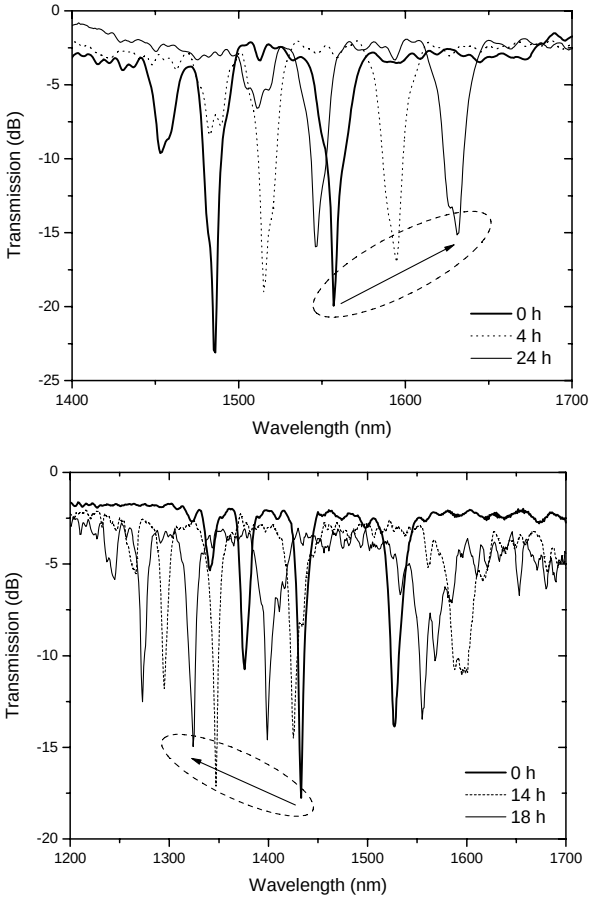

(a) (b)

Figure 5.17 – Evolution of the spectra of two gratings written in the (a) SMF28 fibre; and in a (b) nitrogen doped fibre during annealing at 1000 ºC.

It should be stressed that annealing at higher temperatures for a couple of hours wash out the grating (1100 ºC) [21] followed by a degradation of the fibre itself (1200 ºC) [1].

5.5 LPFGs sensitivity to external parameters

When gratings are subjected to changes of physical parameters such as temperature, strain, bending, torsion, load or refractive index their transmission spectra is altered accordingly. This property is useful in the sensing domain, since by monitoring the displacement of the

gratings resonant wavelengths it is possible to measure the change of one or more physical parameters. The effect of bending and torsion on arc-induced LPFGs has been used for implementing fibre optic intensity sensors [22, 23]. Nevertheless, a detailed characterization of the performance of these gratings under bending, torsion and loading is required. In this section, the response of arc-induced gratings to temperature, strain and external refractive index is discussed.

5.5.1 Temperature and strain

It is known that LPFGs fabrication techniques, such as the electric arc or CO_2 laser irradiation, can change the geometry and/or promote azimuthal asymmetries in the refractive index profile of the optical fibres [1, 11, 24]. Therefore, by varying the typical fabrication parameters of such techniques some control of the sensitivity characteristics of LPFGs is obtained, due to their dependence on the fibre structure [25, 26]. In this section, it is presented a study on the influence of the fabrication parameters on the sensitivity of the gratings for changes in the applied strain and temperature.

Figure 5.18 summarises the obtained results, corresponding to the 4^{th} resonance of the 540 μm LPFGs. The strain sensitivity can be changed considerably from +0.11 to -0.36 pm/με, when the electric current increases from 9 to 12 mA. In Figure 5.18, the points joined have similar attenuation losses and were obtained for three different electric arc currents, therefore showing the effect of this parameter on the gratings sensitivity to strain. This figure also suggests a possible dependence, under certain experimental conditions, of the strain sensitivity on the attenuation of the loss-peaks. For example, for a current of 10 mA and peaks with an attenuation ranging from 6 to 24 dB, there is a change in sensitivity from -0.14 to -0.86 pm/με. On the other hand, the temperature sensitivity can be changed from 68 to 60 pm/ºC (for temperatures up to 110 ºC), when the electric current increases from 9 to 11 mA (Figure 5.19(a)). It is also noticed that the pulling tension considerably changes the temperature sensitivity. Moreover, the quadratic dependence of the resonant wavelengths on temperature becomes more pronounced with the increase of the electric current (Figure 5.19(b)).

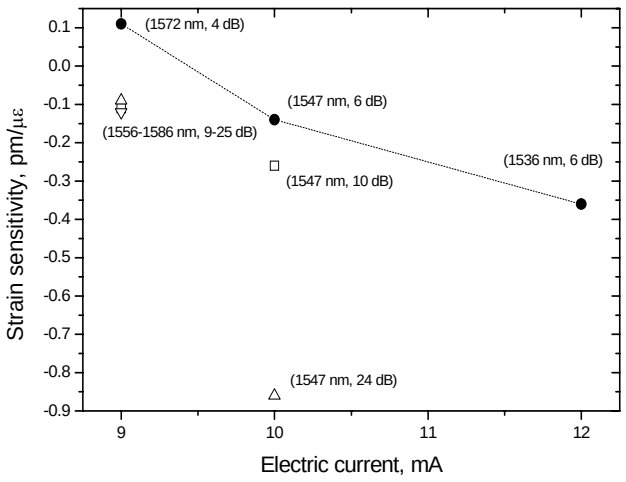

Figure 5.18 – Strain sensitivity of 540 μm-LPFGs as a function of the electric current (in brackets: resonant wavelengths and attenuation of the loss-peaks).

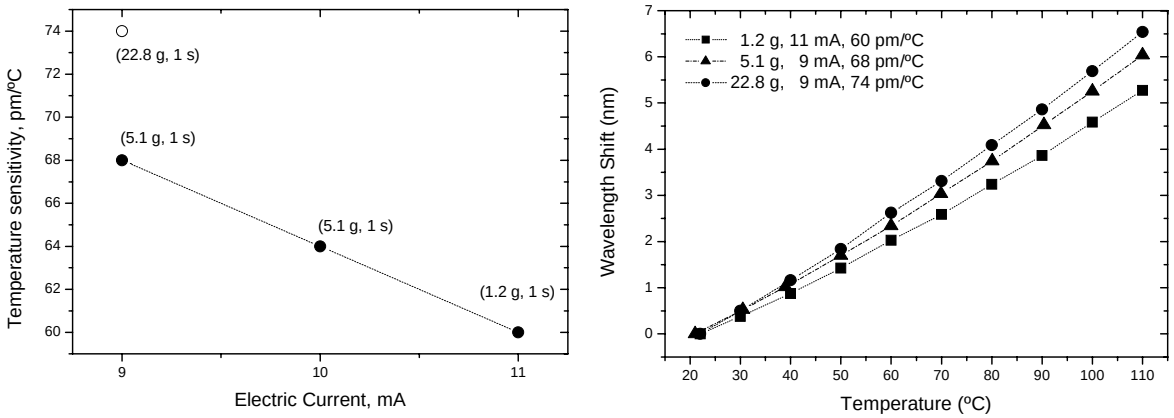

(a) (b)

Figure 5.19 – (a) Temperature sensitivity of 540 μm-LPFGs as a function of the electric current; (b) shift of the resonant wavelength with temperature for gratings produced under different fabrication parameters.

It is worthwhile to attempt on the influence of the grating period on the temperature and strain sensitivities. As it was discussed in section 5.4, for a particular period, the temperature sensitivity increases with the order of the cladding modes and for a particular resonance, it increases with the grating period (Figure 5.20). This figure also suggests a linear dependence of the temperature sensitivity on the resonant wavelength, which might be possible according to the expressions presented by Shu *et al.* [25] and taking into account that we are dealing with the first cladding modes for a limited range of grating periods. Further work is, nevertheless, necessary to clarify this issue. Regarding the strain sensitivity and for a particular grating period, it was first observed for UV-induced gratings that the algebraic value of the strain sensitivity increases with the order of the cladding modes [26]. Recently, a theoretical discussion on this subject was also presented [27]. For a particular resonance, the

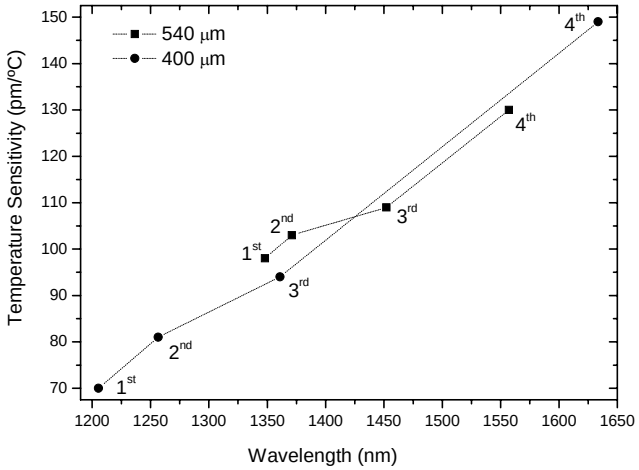

Figure 5.20 – Dependence of the temperature sensitivity on the order of the cladding modes resonances for 400 μm and 540 μm-LPFGs.

strain sensitivity (the algebraic value) decreases with the increase of the grating period as shown in Figure 5.21.

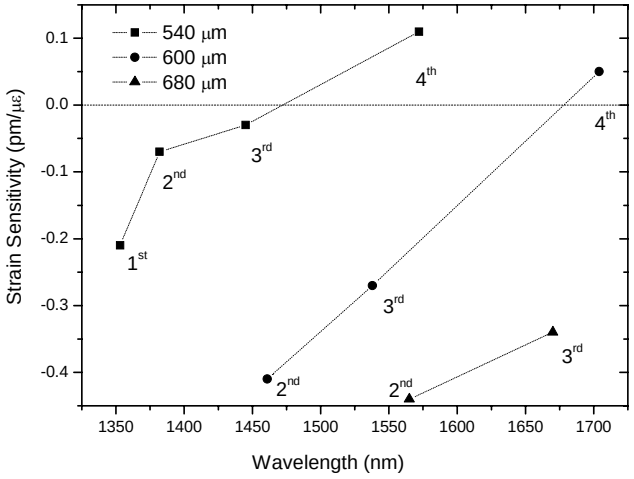

Figure 5.21 –Dependence of the strain sensitivity on the order of the cladding modes resonances for three gratings having different periods.

The above results enable one to conclude that the several resonances of a single grating exhibit different sensitivity to strain and temperature. That fact was used by Bhatia [28] to develop a sensor able to discriminate both physical parameters, being the drawback of the proposed scheme the requirement of having two light sources. Other approaches, based on the fact that by changing the fabrication parameters of the electric arc technique it is possible not only to tune the position of the resonances but also to tune their sensitivity to strain and temperature, will be presented in Chapter 8. It should be emphasised that these properties of the electric arc technique have not been demonstrated, so far, by any other LPFGs fabrication technique.

5.5.2 Refractive index of the surrounding medium

In this section we present results of the sensitivity of LPFGs arc-induced in pure-silica-core fibres to changes of the ambient refractive index, namely, when gratings in air are immersed in water.

LPFGs were arc-induced in a standard singlemode Ge-doped fibre (Corning SMF28: D_{core} = 8.6 μm, $D_{clad.}$ = 125 μm and $\lambda_{cut\text{-}off}$ = 1.27 μm) and in two pure-silica-core fibres with a fluorine-doped silica cladding. Concerning the Ge-free fibres, one is from Oxford Electronics, SMPS 1300-125 P (D_{core} = 9 μm, $D_{clad.}$ = 125 μm and *N.A.* = 0.11) and the other is from ACREO (*MFD* = 12.9 μm, $D_{clad.}$ = 150 μm and $\lambda_{cut\text{-}off}$ = 1.36 μm). The refractive index profiles of the Oxford and Corning fibres were measured using the S14 Refractive Index Profiler, from Photon Kinetics and are presented in Figure 5.22. As shown, the Oxford fibre has an inner cladding, doped with fluorine to depress the refractive index, and an outer silica cladding which has a refractive index slightly higher than that of the core. This might be attributed to fluorine diffusion from the inner cladding to the core during the fibre drawing [29].

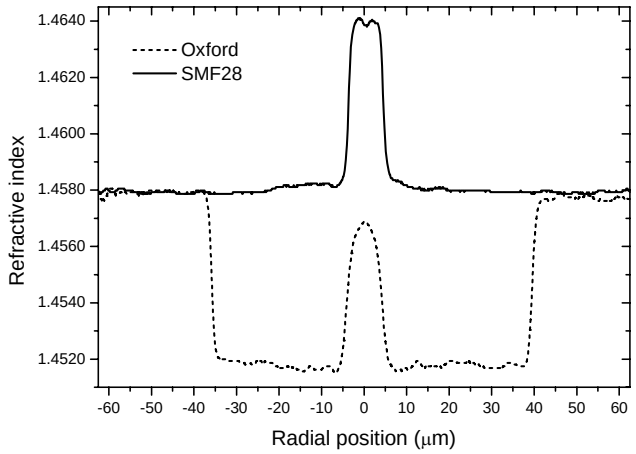

Figure 5.22 – Refractive index profiles of the 125 μm cladding diameter fibres.

Grating periods of Λ = 730 μm and 540 μm, were chosen respectively for the pure-silica-core fibres and for the Corning SMF28 fibre such that a resonance band appeared around 1.55 μm. Figure 5.23 shows the transmission spectra of three gratings produced in those fibres, being the fabrication parameters written in the captions.

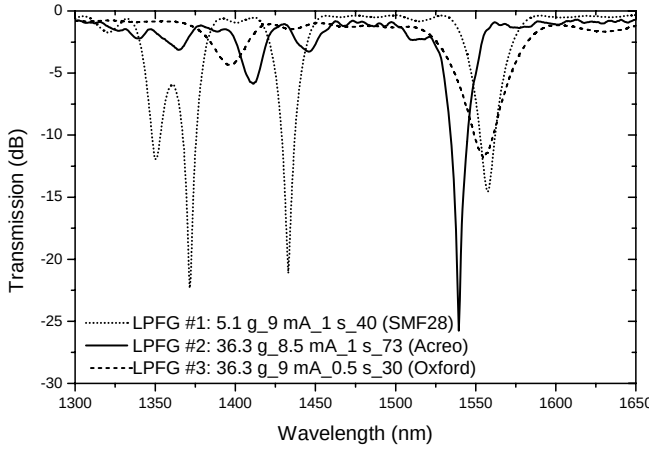

Figure 5.23 – Transmission spectra of the gratings under investigation.

The spectra of two gratings written in two different fibres, on air and immersed in water, are shown in Figure 5.24. As it can be seen, as the refractive index of the external medium increases the spectrum moves towards shorter wavelengths. This can be understood through an increase of the effective refractive index of the cladding, which according to the resonance condition leads to lower resonant wavelengths. The shift is longer for the pure-silica-core fibre than for the standard fibre. That, is a result of doping the cladding with fluorine which lowers its refractive index and therefore reduces the refractive index difference between the cladding and its surroundings increasing the grating sensitivity [30]. The high insertion loss for the pure-silica-core fibre is due to mode-field mismatch.

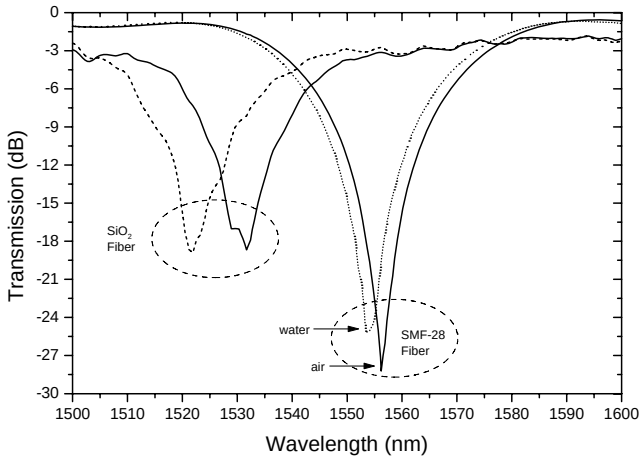

Figure 5.24 – LPFGs spectra in air and in water for two different fibres.

Table I summarises the wavelength displacements obtained for the three gratings. It is interesting to note that when going from air to water the highest sensitivity was obtained for the SiO_2 fibre with the largest cladding diameter. Further results will be presented in Chapter 8 in the context of a refractive index sensor.

TABLE 1. Resonant wavelength shift upon changing the surrounding medium from air to water.

	Δλ/nm
Medium / Fibre	Air-water 1-1.3325
SiO_2-125 μm	5.21
SiO_2-150 μm	8.96
SMF28-125 μm	2.34

5.6 Polarization dependent loss measurements

The equalization of the gain spectra of erbium doped fibre amplifiers (EDFAs) is one of the most important applications of long-period fibre gratings (LPFGs) in optical communications. In such application, the performance of the optical filter is directly related to its polarization properties. Several studies concerned with the polarization dependent loss (PDL) of gratings produced by UV and CO_2 laser radiation have been published [24, 31-33]. However, PDL measurements on arc-induced gratings are only briefly described in [34, 35]. Moreover, the presented results were obtained by considering solely two orthogonal polarizations and, therefore, they correspond somehow to an approximation. Note that for optical components exhibiting both PDL and polarization mode dispersion (PMD), the two principal states of polarization corresponding to maximum and minimum power values are not orthogonal [36]. In this section we discuss the polarization dependent loss of arc-induced gratings under different fabrication parameters.

The PDL properties of the produced gratings were investigated using the setup shown in Figure 5.25. The light from the Photonetics EDFA, was polarized linearly by using a fibre polarizer. The polarization state of the input light is afterwards scanned by the polarization controller, an Agilent 11896A, before going through the LPFG and be detected by the OSA.

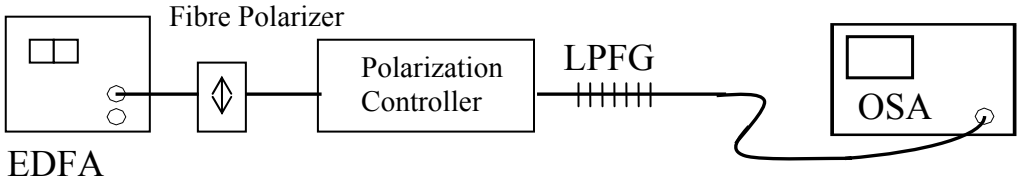

Figure 5.25 – Experimental setup for PDL measurement.

The PDL values were measured by searching at a particular wavelength in the vicinity of the resonant wavelength, for the maximum and minimum transmitted power. Afterwards, the spectrum of the grating corresponding to the fast and slow axis was registered and the PDL determined by the absolute difference of those spectra. On a second iteration, the whole process was repeated at the wavelength where the maximum PDL value occurred. Therefore, although the wavelength dependence of the PDL may comport some error the maximum value of the PDL is fairly accurate. The two extreme PDL_{max} values obtained for the produced gratings are shown in Figure 5.26(a)-(b). A maximum value of 8.5 dB was obtained for a grating written using an arc discharge of 9 mA during 2 s whilst applying a tension of 5.1 g to the fibre. The minimum PDL_{max} value was of 0.45 dB and was obtained for a grating written using an arc discharge of 12 mA during 0.5 s whilst applying a tension of 1.1 g to the fibre. Note that a similar PDL value was also obtained for a grating produced by using an arc-discharge of 10 mA for 1 s and the same pulling tension of 1.1 g. Figure 5.26(b) also shows that two gratings with similar wavelength separation (~1 nm) may exhibit completely different PDL values. Therefore, an important conclusion can be drawn, that is, the PDL values depend not only on the wavelength separation, but also on the gratings strength and bandwidth.

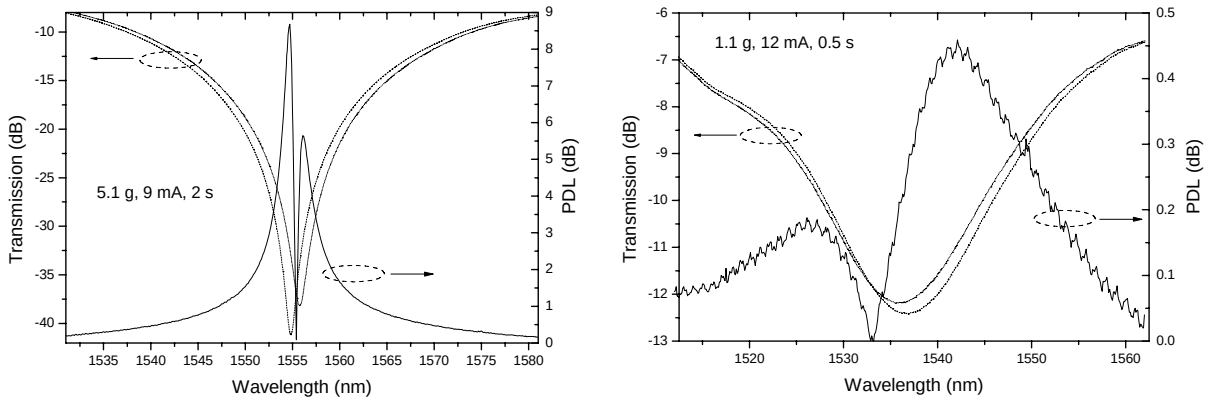

(a) (b)

Figure 5.26 – Two gratings showing the (a) maximum and (b) minimum PDL values obtained.

Figure 5.27 shows the PDL_{max} versus the transmission loss for gratings arc-induced in the SMF28 fibre. Note that for the same number of arc discharges employed, gratings written with an external tension of 5.1 g show different transmission loss values. The issues related to the reproducibility of the electric arc technique are discussed in section 5.3.4. In any case, it can be concluded that as the transmission loss increases the maximum PDL value also

increases and that for the same transmission loss, the use of a higher tension leads to lower PDL values.

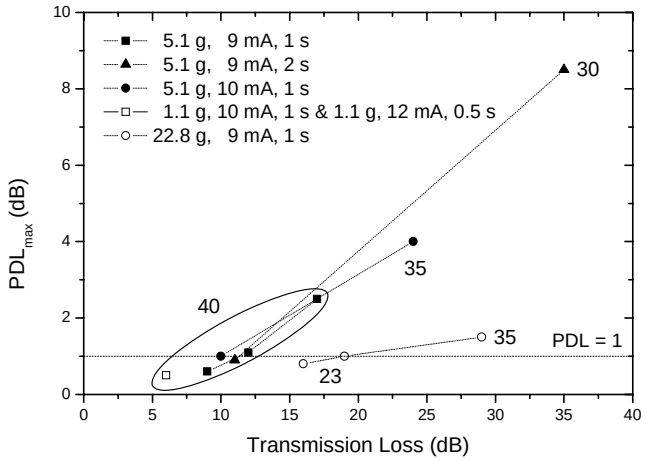

Figure 5.27 – PDL values as a function of the transmission loss for several gratings written in the Corning SMF28 fibre.

To validate the previous results, the PDL of a new set of gratings written in another standard singlemode fibre, from Siecor (6 mol% Ge), was measured by the polarization scanning method [33]. The instruments used were a computer controlled polarization analyzer (HP8509B) and an external tunable laser (HP8167A). For each wavelength, all polarization states in the Poincaré sphere were virtually generated in order to find the minimum and maximum power transmitted through the grating. Figure 5.28(a) shows the transmission spectrum of one grating for the fast and slow axis as determined by the polarization scanning method. The absolute difference of these two curves gives the correspondent PDL values. It was experimentally verified that, for each wavelength, the two principal states of polarization, that corresponds to a maximum and to a minimum, are not orthogonal which confirms that LPFGs possess both PDL and differential group delay (DGD). The PMD is in general determined as an average of the DGD, but in the presence of PDL their relationship is not trivial [36]. The DGD was software calculated from the wavelength dependence of the Jones matrix eigenvalues and an estimation of its spectral dependence is shown in Figure 5.28(b). These results had to be performed in steps of 1 nm due to a limitation of the equipment used. The maximum PDL values obtained for several gratings arc induced in the Siecor fibre using different pulling tensions are shown in Figure 5.29. In general, these values are slightly higher than the ones presented previously, nevertheless, this figure allows for the same conclusions as the ones drawn from Figure 5.27.

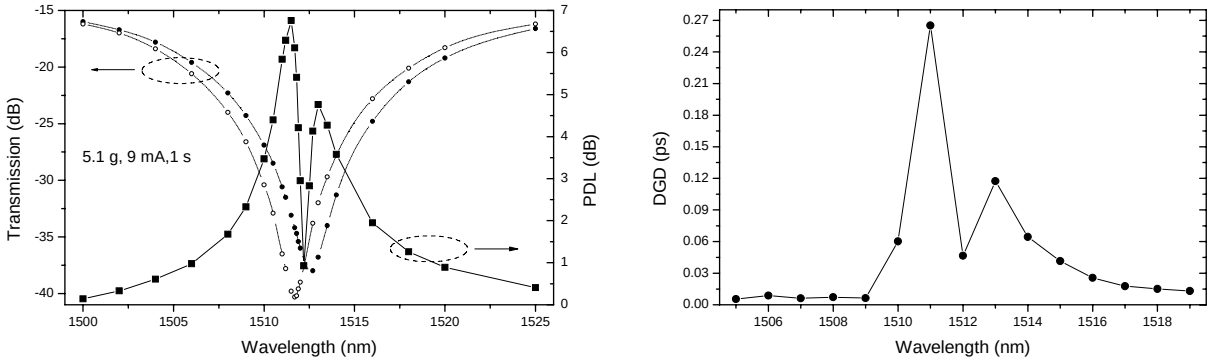

(a) (b)

Figure 5.28 – (a) Transmission spectrum of the grating for two polarizations and the correspondent spectral PDL as obtained in the Poincaré sphere. (b) Spectral DGD of the grating.

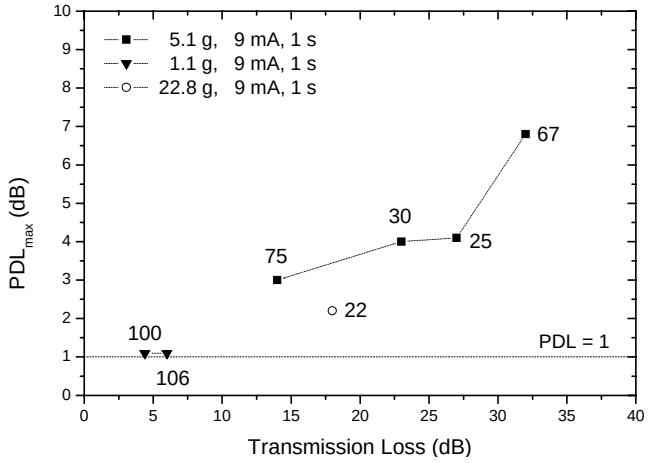

Figure 5.29 – PDL values as a function of the transmission loss for several gratings written in the Siecor fibre.

Next, we will compare the PDL values obtained experimentally with results published in the literature, for gratings produced using different techniques. Figure 5.30 summarises that comparison. In the following discussion of the results, data will appear in the form (Transmission Loss, PDL_{max}). As can be seen, the PDL value (11, 4.5) obtained by Kim *et al.* [35] for an arc-induced grating (open circle) is higher than the ones presented in this work. An even higher value is expected for gratings induced by microbending through arc discharges [34] since it is known that, in general, microbending leads to gratings with large PDL values. In fact, a value as large as 18 dB was achieved for a mechanically induced grating [37] (not shown in Figure 5.30). Also a large value for PDL (16, 8) was obtained by Zhu *et al.* [33], however, in this case, it is not known the technique used to produce the grating (open inverted triangle). The PDL value (16, 3) exhibited by a grating produced by high intensity femtosecond 352 nm pulses [32] fits well the experimental results obtained for gratings fabricated with a pulling tension of 5.1 g (open square). It is interesting to note that gratings induced by CO_2 laser pulses show PDL values between 1 and 2 dB (filled triangle) for a large

range of transmission loss values: (5, 1.9) [38]; (10, 1.2) [31]; (14, 1.2) [24]; (24, 1.7) [39]. The PDL of the weaker grating is higher than the one obtained for arc-induced gratings produced using a 1.1 g. The PDL of the 10 dB grating is comparable to gratings produced with 5.1 g, whilst for gratings with greater coupling strengths the PDL compares to the 22.8 g-LPFGs. The PDL of UV-induced gratings (244-248 nm) ranges from about zero to 1.5 dB: (5, 1.4) [40]; (10, 0.2) [31]; (20, 1.5) [41]. These values (filled square) compares to the ones obtained for arc-induced gratings in case of low (1.1 g) and high transmission loss (22.8 g). For the intermediate transmission loss, the PDL value is remarkably lower than other obtained for gratings produced by other techniques.

In the case of UV-induced gratings, PDL results from birefringence induced in the fibre core due to one-side exposure. The PDL values are intrinsically low and can be further reduced by a double-side UV exposure [42] or by heating the fibre during gratings inscription [40]. The latter can be achieved by using a heating coil or by a proper choice of the pulses repetition rate. The thermal heat generated will enhance the fibre photosensitivity and will lead to a decrease of the induced birefringence. Single-side exposure and birefringence also induced in the fibre cladding are the reasons pointed by the authors [32] to explain the higher PDL value obtained for a grating induced by femtosecond laser pulses when compared to gratings produced by UV and CO_2 laser radiation. As discussed in [31], gratings produced by CO_2 laser radiation promotes changes in both the core and the cladding and therefore the PDL values of those gratings are, in principle, higher than for UV gratings. Oh *et al.* [40] proposed two methods to reduce the gratings PDL: a double side exposure or rotation of the fibre during exposure to the CO_2 laser radiation. As far as arc-induced gratings are concerned, it was recently demonstrated that arc discharges promotes asymmetric stress relaxation in the cladding of optical fibres [24] and therefore, according to [31], arc-induced gratings falls in the same category as the ones produced by CO_2 laser pulses. Indeed, both techniques enable the fabrication of gratings showing similar PDL values, considering that the larger pulling tension is used to produce strong arc-induced gratings. It is known that the increase of the pulling tension leads to a reduction of the fibre cross section which, in turn, enhances the coupling strength and decreases the number of periods required to achieve a particular transmission loss (section 5.3.4). Simultaneously, it is believed that this geometric effect might contribute to obtain a more homogeneous distribution of birefringence. Finally, it should be stressed that independently of the technique used to fabricate the gratings, their PDL values can be substantially reduced by using a Sagnac loop interferometer [43].

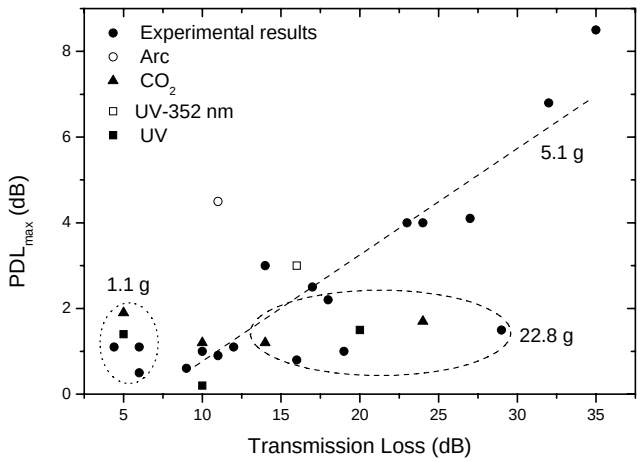

Figure 5.30 – Comparison of PDL values for gratings produced using different techniques.

5.7 Exposure of LPFGs to UV radiation

Fibre optics superstructures such as sampled fibre Bragg gratings which are able to perform simultaneous measurements of physical parameters are of great interest [44]. This superstructure consists on writing a Bragg grating on top of a LPFG (see Chapter 7). To take full advantage of the properties of both gratings, the knowledge of the evolution of their spectra is required. This evolution depends on their relative physics position and, also, on the relative position of their resonant wavelengths, the latter being affected by the well known process used to enhance the fibre photosensitivity, that is, hydrogen loading.

5.7.1 Effect of hydrogen out-diffusion

Prior to the writing of Bragg gratings, or to the exposure of LPFGs to uniform UV radiation, the fibres are hydrogenated. However, out-fibre diffusion of hydrogen occurs after removing the fibre from the high-pressure chamber. This in turn affects the position and the strength of the resonance peaks of the LPFG and, therefore, a study of the impact of hydrogen out-diffusion is important.

Two arc-induced LPFGs were hydrogenated for two weeks at room temperature and at a pressure of 120 bar. Afterwards, one was placed inside a tubular oven at 50 ºC and the other was kept at room temperature. Their transmission spectra were periodically monitored. Figure 5.31(a) shows the evolution of the resonant wavelengths as hydrogen out-diffuses from the fibre. The general behaviour for all modes is their movement to higher wavelengths followed by a decrease till reaching their initial values. This movement is, primary, due to out-diffusion from the cladding which causes a decrease of the effective index of the cladding modes and, therefore, an increase in Δn. Afterwards occurs predominantly the diffusion from the core which causes a decrease in n_{co} and, consequently, of Δn. As expected the hydrogen out-

diffusion affects mostly the cladding modes of higher order since they are closely located to the air-cladding interface where the diffusion rate is higher. A similar behaviour also occurs when the fibre is kept at room temperature (Figure 5.31(b)). The main difference is clearly shown in Figure 5.32(a), i. e., the whole process is slower at room temperature in accordance to the higher diffusion rate of the hydrogen at 50 ºC.

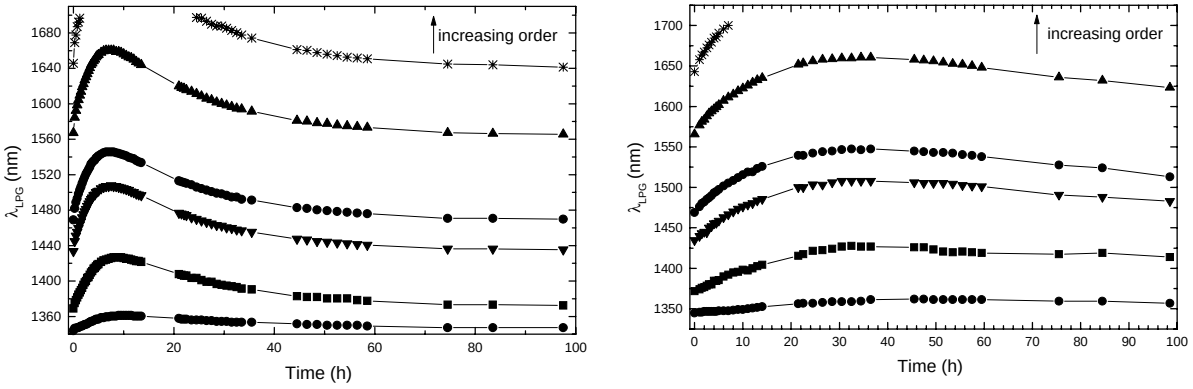

(a) (b)

Figure 5.31 – H_2 out-diffusion at (a) 50 ºC and (b) at room temperature.

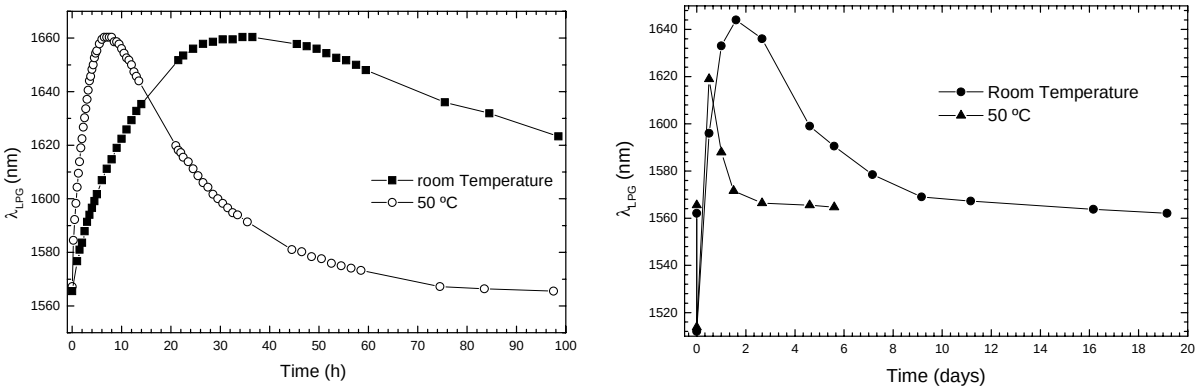

(a) (b)

Figure 5.32 – (a) Evolution of the 5th mode at both temperatures. (b) H_2 out-diffusion in fibres hydrogenated for one week.

As a normal procedure the fibres are hydrogen loaded for one week prior to the writing of the Bragg gratings. Therefore we have also studied the influence of the hydrogen on the LPFGs after hydrogenation for one week. The most important aspect is that after removing the fibre from the high pressure chamber the whole spectrum moved to lower wavelengths, which is a clear indication that the fibre was not saturated with hydrogen (Figure 5.32(b)). This result agrees well with calculations presented in [45] for the in-fibre hydrogen diffusion. After all the hydrogen had out-diffused from the fibre the spectra of the gratings are fully recovered.

5.7.2 Uniform UV exposure

LPFGs were written in the Fibercore-PS1500 B/Ge co-doped fibre through electric arc discharges. Grating periods in the range 400-425 μm were chosen in order to exhibit a resonant peak (its position shifts ~2.7 nm/μm) in the third telecommunication window. The other fabrication parameters (external mechanical tension, electric current and time) were in the range of 0-5.1 g, 8.5-9 mA and 0.5-1 s, respectively. It was found that the increase of the writing time and tension leads to a displacement of the spectrum towards longer wavelengths, while a current increase has the opposite effect. The pre-annealing of the fibre at 700 ºC for 1 h also leads to a down-shift of the resonant wavelengths. Using the highest values of the respective ranges we measured a change of the pristine fibre's cross section of 3% while for other fibres this change is negligible [1].

Arc-induced LPFGs were exposed to uniform UV-radiation. The LPFG#1 (5.1 g, 8.5 mA, 0.5 s, 415 μm, n=60) was exposed with a fluence per pulse of ~0.6 J/cm^2. Figure 5.33 shows the spectrum evolution as a function of the total fluence. For comparison, a second LPFG#2 (5.1 g, 9 mA, 1 s, 562 μm, n=30) written in a standard Ge-doped fibre (6 mol%) was also exposed to uniform UV-radiation (~0.55 J/cm^2) after being hydrogenated for 10 days at room temperature and at 100 bar (Figure 5.34). It can be seen that as the fluence increases the spectra moves toward longer wavelengths and the attenuation of the loss-peaks decreases. The former behaviour is due, as expected, to the increase of the refractive index in the core during the UV-exposure. The latter is a result of the decrease of the refractive index modulation in the core, which may suggest that the arc-discharges also increase the core refractive index. The figures also show that despite the remarkable reduction of the transmission loss (especially for the Ge-doped fibre) it was impossible to erase completely the gratings. This is attributed to two factors: on one hand, there is a UV-induced grating with the same periodicity of the arc-induced one that is growing in the spectral vicinity of the former and, on the other hand, as was previously discussed, for the writing parameters used in the inscription of the LPFG in the B/Ge doped fibre the arc-discharges have only slightly changed the fibre photosensitivity and, therefore, the reduction of the index modulation was not so effective during the UV-exposure.

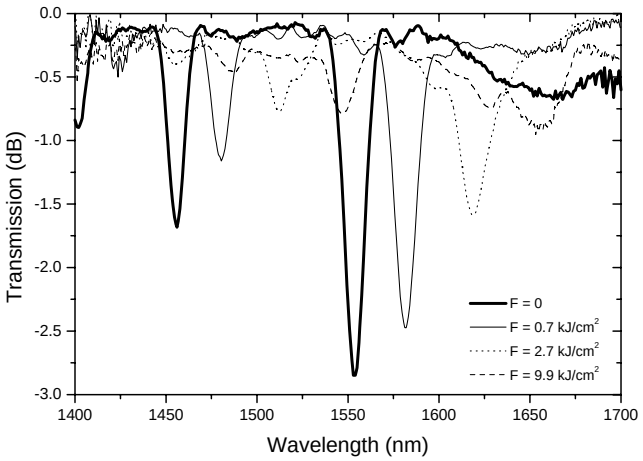

Figure 5.33 – Evolution of the spectrum of the LPFG#1 written in the B/Ge doped fibre during uniform UV-exposure.

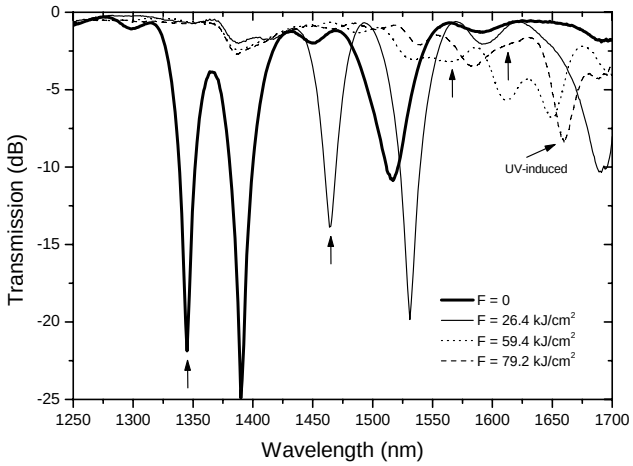

Figure 5.34 – Evolution of the spectrum of the LPFG#2 written in the Ge-doped fibre during uniform UV-exposure.

5.7.3 Thermal recover

In order to find out if it is possible to recover the arc-induced gratings after the UV-exposure, both gratings were placed inside a tubular oven. After annealing the LPFG#1 at 300 ºC for 90 min, only small changes in the spectrum occurred. Consequently, the temperature was raised to 400 ºC, during which an increase of the attenuation of the loss-peaks was clearly noticed. After 1 h at this temperature the grating was cooled down to room temperature and its spectrum was almost fully recovered. However, it appeared displaced ~40 nm towards longer wavelengths. Afterwards the grating was submitted to a second annealing at the same temperature for 13 h. After cooling down, the spectrum was completely recovered, although displaced ~46 nm with respect to the original spectrum (Figure 5.35). The LPFG#2 was first annealed at 120 ºC for 15 h for hydrogen out-fibre diffusion and then annealed during 1 h at

400 ºC up to 700 ºC in steps of 100 ºC. As seen in Figure 5.36 only at 600 ºC a clear recover started to take place. After cooling down from 700 ºC the spectrum was fully recovered,

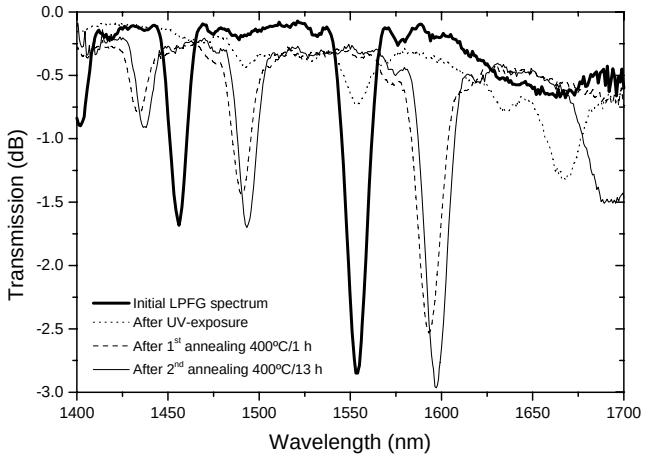

Figure 5.35 – LPFG#1 spectra after thermal annealing at 400 ºC.

however a displacement of 119 nm towards longer wavelengths was found. This change may be attributed to a reaction of the hydrogen with the germanium doped silica matrix during the first annealing performed above 100 ºC [46].

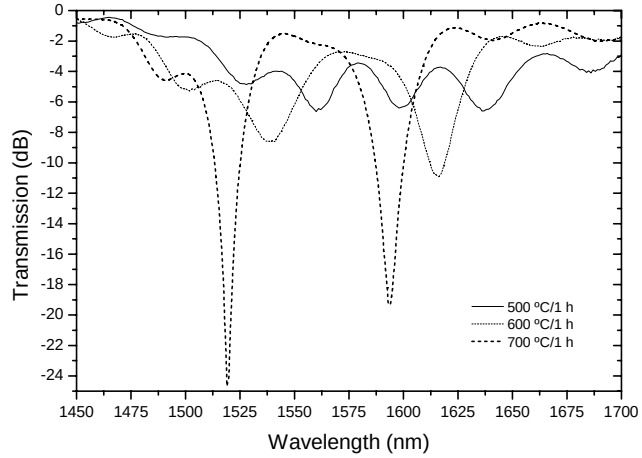

Figure 5.36 – LPFG#2 spectra at different annealing temperatures.

In conclusion, it was demonstrated that for certain writing conditions it is possible to erase (> 20 dB of extinction ratio) arc-induced gratings through uniform UV-exposure, thus providing a practical method to investigate the mechanisms of electric arc-induced refractive index changes. It was also demonstrated the possibility to recover the spectrum of the gratings through temperature annealing, although it appears displaced towards longer wavelengths. Permanent thermally induced refractive index changes were found.

5.8 Effect of ionising radiation on the properties of arc-induced gratings

The well-known properties of optical fibre sensors make them very attractive for the application in the nuclear industry where they can perform, among others, structural integrity and temperature monitoring [47]. The implementation of such sensors is compromised by their sensitivity to radiation. It is, therefore, of interest to study the effect of radiation on LPFGs written in pure-silica-core fibres, which are usually expected to be more radiation-resistant as compared with germanium-doped fibres [48, 49]. Writing techniques based on CO_2 lasers [50], OH-flooding with subsequent Excimer ArF-irradiation [51], femtosecond laser pulses exposure [52] or arc-discharges [53, 54] were found to be suitable for the fabrication of gratings in pure-silica-core fibres.

In this section the radiation tolerance of long-period fibre gratings written in pure-silica core fibres using the arc-discharge technique is evaluated. The LPFGs spectra during γ-irradiation are measured *in situ* and the influence of radiation on the temperature and strain sensitivity coefficients is also addressed.

5.8.1 Gratings fabrication and characterisation

LPFGs were arc-induced in the two pure-silica-core fibres describe in section 5.5.2. In order to obtain a grating resonance around 1.55 μm the grating should have a specific period. It was experimentally found that a period of 730 μm allows for the desired dip position. We have also investigated the dependence of the writing parameters on the grating characteristics. Figure 5.37 shows the spectra of the LPFGs induced in the Oxford fibre at a number of fabrication conditions. As it can be seen the optimum writing parameters that lead to resonances with dip loss-peaks and low background losses are an arc current of 9 mA during 0.5 s, combined with the use of a pulling tension of 36.3 g. For the ACREO fibre the same writing parameters also allowed for the inscription of good optical quality gratings, exhibiting a resonance near 1.55 μm.

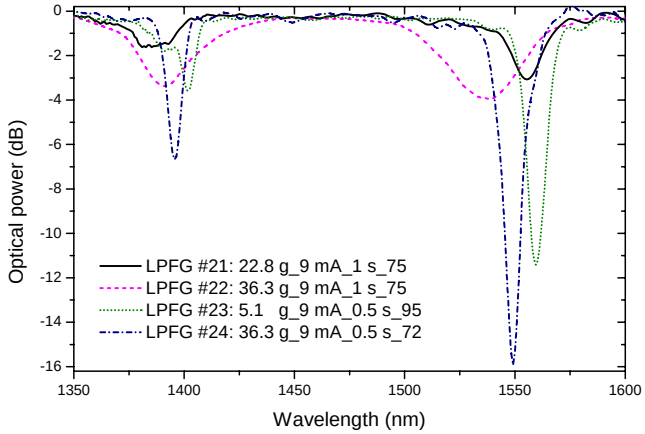

Figure 5.37 – Transmission spectra of four gratings written in the Oxford fibre using different parameters.

The thermal behaviour of gratings written in both fibres was investigated. Two gratings were placed, under a pulling tension of 5.1 g (to prevent gratings bending), inside a tubular oven having a length of 18 cm and a diameter of 2 cm. The temperature of the oven was increased from room temperature up to 1000 ºC in steps of 50 ºC. At each step the gratings spectra were recorded after a dwell time of 30 min. Figure 5.38(a)-(b) show the thermal behaviour of the 1.55 μm gratings resonances. The shift is non-monotonous on the temperature. For temperatures below 250 ºC the shift is well approximated with a linear dependence. For temperatures above ~350 ºC a shift towards shorter wavelengths is observed. In the case of the grating written in the ACREO fibre, a shift towards longer wavelengths was afterwards registered for temperatures above 700 ºC [1]. This shift was accompanied by a strong decrease in the attenuation dip being the grating almost completely erased for temperatures above 800 ºC. The non-monotonous behaviour presented may be related to temperature activation-dependent stress relaxation [55]. It may be noted that in standard Ge-doped fibres stress relaxation starts at temperatures above 700 ºC (section 5.4.1). However, depending on the fibre dopants and on the drawing tension, stress relaxations below 400 ºC were already observed [13, 19]. Note also that at such temperatures is not expected that fluorine diffusion occurs [56]. The thermal behaviour of the gratings spectra for temperatures above ~400 ºC, indicates that these fibres may not be suited for applications at high temperatures.

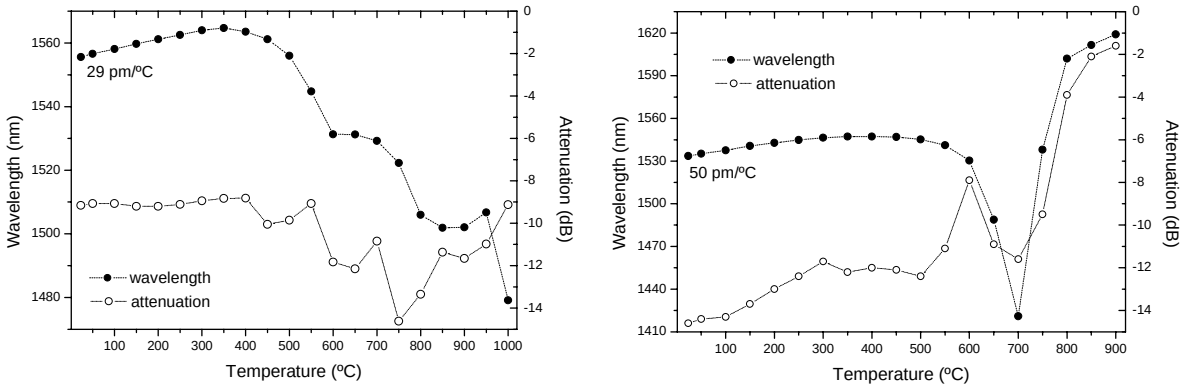

(a) (b)

Figure 5.38 – Temperature dependence of the resonant wavelength and respective attenuation for (a) LPFG #7 written in Oxford fibre and (b) LPFG #2 written in ACREO fibre.

The temperature sensitivity coefficients of the gratings written in Oxford and ACREO fibres are 28.9 ± 0.2 and 49.9 ± 0.3 pm/ºC, respectively, for the temperature range from 20 to 100 ºC. In previous publications [50, 53] similar values (29 and 37 pm/ºC) were found for the temperature sensitivity of gratings induced in pure-silica-core fibres. For comparison, the temperature sensitivity coefficients for gratings written in standard Ge-doped fibres are typically 70 pm/ºC, considering the same temperature range. Since at room temperature the contribution of the thermo-optic coefficients of the core and cladding materials are more important than the fibre thermal expansion coefficient, these results may reflect the fact that the thermo-optic coefficient of F-doped silica is closer to that of pure silica than the Ge-doped silica one.

5.8.2 Gratings irradiation

Eight LPFGs (#1, #3, #6 and #7 written in Oxford fibre and #2, #4, #5 and #8 written in ACREO fibre) were evaluated under ^{60}Co irradiation in the RITA irradiation facility (SCK-CEN, Belgium) [57]. For the present experiment the gamma dose rate was about 1 kGy/h [H_2O] with a total gamma dose of about 560 kGy. The temperature in the irradiation rig was kept constant at 37.4 ± 0.1 °C.

The LPFGs were inserted into protective stainless steel capillary tubes. The fibre was fixed at the two ends of the capillary by putting a droplet of melted wax, which solidified when cooled. The transmission spectrum of the gratings was measured using broadband LEDs from BW-Tek, an OSA and two SM optical switches (OS) (Figure 5.39). The emission of the optical sources was continuously monitored via an internal reference fibre. The use of a temperature-stabilized FBG as an external wavelength reference allowed a wavelength measurement stability better than 20 pm throughout the experiment.

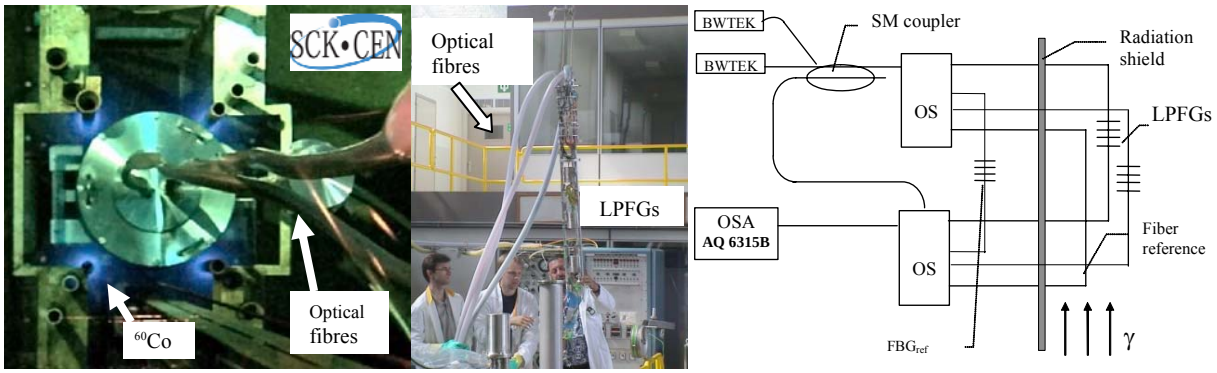

Figure 5.39 – Experimental setup used for LPFGs irradiation.

Figure 5.40 shows the evolution of the LPFG #1 spectra during γ-radiation. A monotonous amplitude change of the main transmission dip with an increase of the dose is observed. A similar result was observed for some gratings, while others showed irregular behaviour. However, when the LPFGs where characterised off-line approximately one month after irradiation, for all gratings the experimental spectra showed almost no difference with those taken before irradiation. The spectra of two gratings written in both fibres before and after irradiation are presented in Figure 5.41. After irradiation, the gratings were stored at normal laboratory conditions and it appears unrealistic that radiation-induced changes would be annealed completely. We believe, therefore, that the observed response is not a direct radiation effect on the grating itself but on its packaging. Arc-induced gratings are very sensitive to bending, especially when a high pulling tension is applied during their inscription, since that produces an intrinsic fibre bending in the grating region, as also occurs during fibre

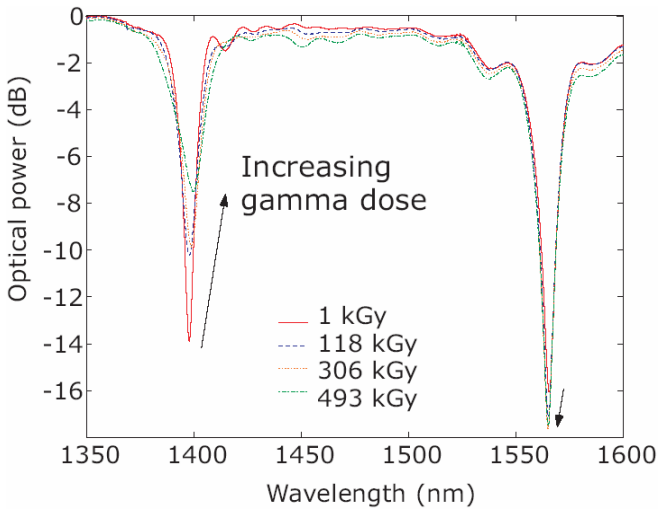

Figure 5.40 – *In-situ* measurement of the evolution of the LPFG #1 spectrum during the irradiation.

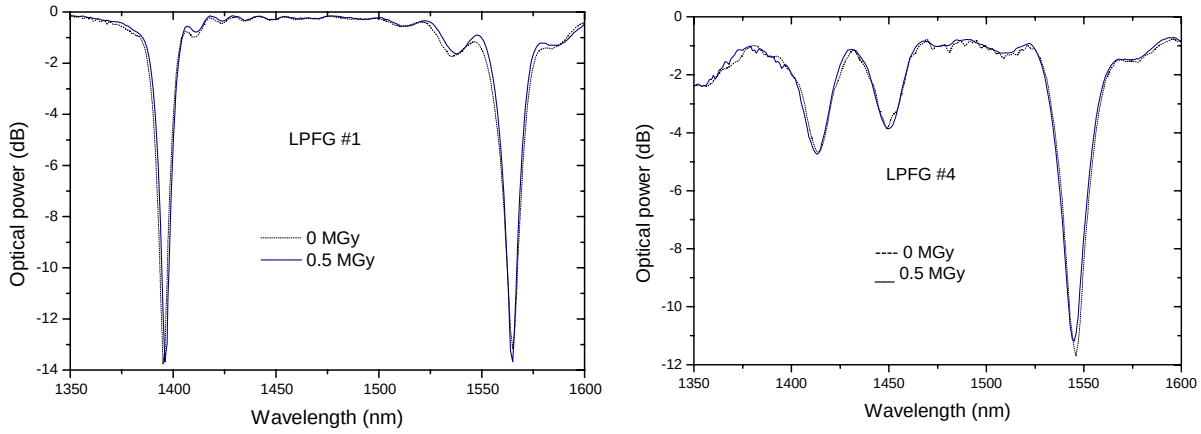

Figure 5.41 – Effect of γ-radiation on (a) LPFG #1 and (b) LPFG #4.

drawing. Taking into account that the fibre, under a pulling tension of 36.3 g, reaches a temperature of about 1320 ºC during an arc discharge [16], the gratings fabrication process can be considered a kind of fibre redrawing [58]. Furthermore, the asymmetry of the arc-discharge might also induce a temperature gradient across the fibre leading to a reinforcement of the fibre bending. Note that to avoid post-fabrication fibre bending inside the protective capillary, the fibres were put under a slight tension using wax for fixation. A radiation-induced modification of the wax could result in a change of the tension which might explain the observed behaviour. To verify this suggestion, we have investigated the effect of bending on the gratings spectra. It was found that peak amplitude changes almost identical to those observed under radiation could be reproduced when going from a straight position of the fibre to a loosely one inside a 0.6 mm metallic tube (Figure 5.42). In a future work, special attention should be paid to the strain applied to the LPFGs during the in-situ measurements to minimize the bending effects.

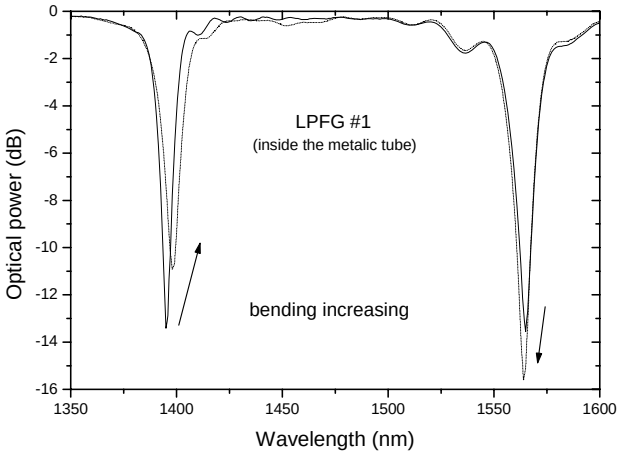

Figure 5.42 – Effect of bending on LPFG #1.

5.8.3 Gratings temperature and strain sensitivity

Ionising radiation can potentially influence not only the resonance position and amplitude but also its sensitivity to strain and temperature. In order to determine the temperature dependence of the transmission dip position for the LPFGs written in the Oxford fibre, gratings were placed inside the tubular oven with a 5.1 g weight attached to the fibre. The temperature of the oven was, afterwards, increased from room temperature up to 100 °C, in steps of 10 °C. At each step and after temperature stabilization, the transmission spectra of the gratings were recorded using the noise spectrum of an erbium doped fibre amplifier (EDFA) from Photonetics, and an OSA set to a 0.1 nm resolution.

Figure 5.43 shows the temperature dependence of the resonant wavelength of the gratings written in Oxford fibre, for two non-irradiated gratings, LPFG #17 and LPFG #24, and for two gratings, LPFG #6 and LPFG #7, submitted to a total radiation dose of 0.5 MGy. All gratings, fabricated under the same conditions, exhibit a temperature sensitivity of 28.9 ± 0.2 pm/ºC. These results may indicate that gamma irradiation does not affect the temperature sensitivity of the arc-induced LPFGs. Similar results were obtained for LPFG #1. For this grating, results of the temperature sensitivity measurements before and after irradiation are given in Figure 5.44(a). The temperature sensitivity remained unchanged after the irradiation experiment. Note that the temperature sensitivity value of 17.7 ± 0.2 pm/ºC obtained for this grating is lower than the value of 28.9 ± 0.2 pm/ºC observed for other gratings. The difference may be attributed to the fact that the configuration of the electrodes used in its fabrication was

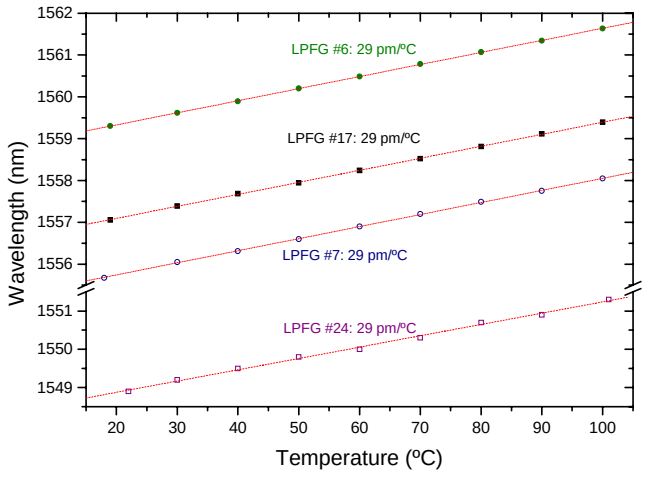

Figure 5.43 – Temperature sensitivities of two non-irradiated gratings (LPFG #17 & #24) and two irradiated gratings (LPFG #6 & #7), written in the Oxford fibre.

different from the previous one and that is analogous to a change in the electric current of the arc discharge. A change of the current may have a significant influence on the temperature sensitivity. In fact, it is known that modifications of the writing parameters lead to changes in

the temperature and strain sensitivities of arc-induced gratings in the SMF-28 fibre (section 5.5.1).

To measure the grating sensitivity to strain, the fibre was fixed at two points separated by 250 mm, one of them being on a micrometer positioner. The LPFG was then pulled in steps of 0.05 mm with the total displacement being up to 0.5 mm. The shift of the resonance position was measured using the EDFA with the OSA set to a 0.1 nm resolution. The values obtained for the strain sensitivity of the gratings written in the Oxford fibre ranged from -0.60 to -1.45 pm/με. Figure 5.44(b) shows the strain measurement results for LPFG #1 before and after irradiation. No significant difference was obtained for the strain sensitivity measured before and after the irradiation. Therefore, it might be concluded that γ-radiation doses up to

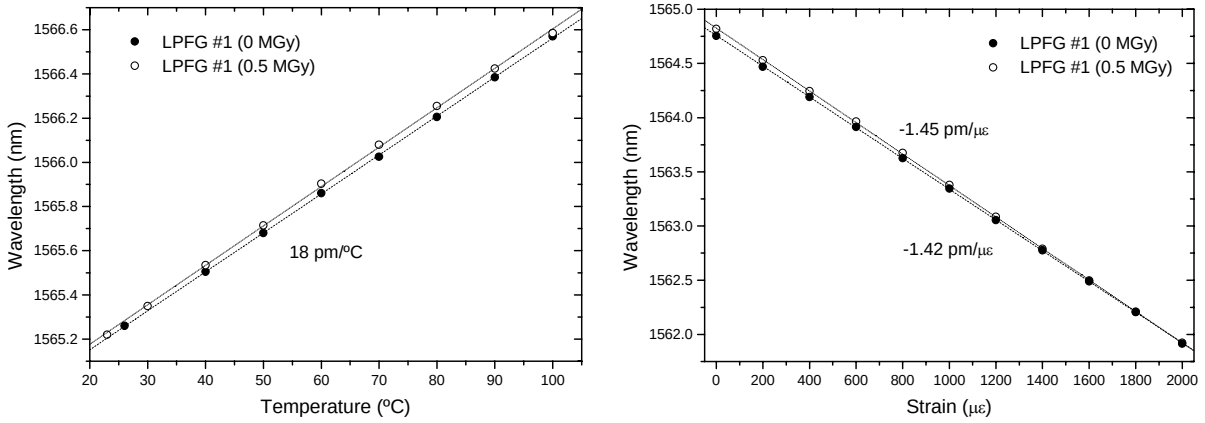

(a) (b)

Figure 5.44 –Temperature (a) and strain (b) sensitivity of LPFG #1, before and after irradiation.

0.5 MGy have negligible effect on the temperature and strain sensitivities of the gratings written in the Oxford fibre, which indicates a general characteristic of pure-silica-core fibres.

In conclusion, the writing parameters, which allow fabrication of fibre gratings with strong loss-peaks and low background losses using electric arc discharges, were experimentally determined for Oxford and ACREO pure-silica-core fibres. The influence of gamma radiation on the properties of gratings fabricated with this technique was investigated. The experiment showed that after radiation doses in excess of 0.5 MGy transmission spectra of the gratings written in both fibres remained almost unchanged. The temperature and strain sensitivities of LPFGs written in the Oxford fibre are also not affected by gamma radiation. Thus, these results suggest that LPFGs written in pure-silica-core fibres are suited for applications in ionised radiation environments.

5.9 Summary

In this chapter it was analysed the contribution of the fabrication parameters to the grating formation. Afterwards, the thermal behaviour of the produced gratings was discussed. The sensitivity of LPFGs to changes of temperature and strain was also presented. A comparison of the values of the polarization dependent loss of arc, CO_2 and UV induced gratings is also given. The exposure of arc-induced gratings to UV-radiation was investigated. At last, it was studied the effect of ionising radiation on the properties of arc-induced gratings.

In a near future a full characterization on the effect of bending, torsion and loading on the spectra of arc-induced gratings will be performed. There are other issues that for their importance for the development of new devices requires further studies. Namely, the behaviour of gratings at very high temperatures, the ability to tune the strain and temperature sensitivity coefficients of arc-induced gratings by changing the fabrication parameters and their polarization dependent loss.

References

[1] G. Rego, O. Okhotnikov, E. Dianov, and V. Sulimov. *High-temperature stability of long-period fiber gratings produced using an electric arc.* Journal of Lightwave Technology **19**(10): 1574-1579, 2001.

[2] E.M. Dianov, V.I. Karpov, M.V. Grekov, K.M. Golant, S.A. Vasiliev, O.I. Medvedkov, and R.R. Khrapko. *Thermo-induced long-period fibre gratings*. in *IOCC-ECOC 97 - 11th International Conference on Integrated Optics and Optical Fibre Communications / 23rd European Conference on Optical Communications, Vol 2*: 53-56, 1997.

[3] D.D. Davis, T.K. Gaylord, E.N. Glytsis, and S.C. Mettler. *Very-high-temperature stable CO2-laser-induced long-period fibre gratings.* Electronics Letters **35**(9): 740-742, 1999.

[4] G. Rego, R. Falate, J.L. Santos, H.M. Salgado, J.L. Fabris, S.L. Semjonov, and E.M. Dianov. *Arc-induced long-period gratings in aluminosilicate glass fibers.* Optics Letters **30**(16): 2065-2067, 2005.

[5] G. Rego, P.V.S. Marques, H.M. Salgado, and J.L. Santos. *Simultaneous measurement of temperature and strain based on arc-induced long-period fibre gratings.* Electronics Letters **41**(2): 60-62, 2005.

[6] G. Rego, R. Falate, H.J. Kalinowski, J.L. Fabris, P.V.S. Marques, H.M. Salgado, and J.L. Santos. *Simultaneous temperature and strain measurement based on arc-induced long-period fiber gratings*. in *17th International Conference On Optical Fibre Sensors, Pts 1 And 2*: 679-682, 2005.

[7] G. Rego, A.F. Fernandez, A. Gusarov, B. Brichard, F. Berghmans, J.L. Santos, and H.M. Salgado. *Effect of ionizing radiation on the properties of arc-induced long-period fiber gratings.* Applied Optics **44**(29): 6258-6263, 2005.

[8] E. Desurvire, in *Erbium-doped fiber amplifiers: principles and applications*. John Wiley & Sons, New York: 207-255, 1994

[9] S.A. Vasiliev, E.M. Dianov, D. Varelas, H.G. Limberger, and R.P. Salathe. *Postfabrication resonance peak positioning of long-period cladding-mode-coupled gratings.* Optics Letters **21**(22): 1830-1832, 1996.

[10] S. In, C. Chung, and H. Lee. *The resonance wavelength-tuning characteristic of the arc-induced LPFGs by diameter modulation*. in *OFS 2002: 15th Optical Fiber Sensors Conference Technical Digest*: 131-134, 2002.

[11] F. Durr, G. Rego, P.V.S. Marques, S.L. Semjonov, E. Dianov, H.G. Limberger, and R.P. Salathe. *Stress Profiling of Arc-Induced Long Period Fiber Gratings.* Journal of Lightwave Technology **23**(11): 3947-3953, 2005.

[12] A.D. Yablon, M.F. Yan, P. Wisk, F.V. DiMarcello, J.W. Fleming, W.A. Reed, E.M. Monberg, D.J. DiGiovanni, J. Jasapara, and M.E. Lines. *Refractive index perturbations in optical fibers resulting from frozen-in viscoelasticity.* Applied Physics Letters **84**(1): 19-21, 2004.

[13] G. Rego, J.L. Santos, P.V.S. Marques, and H.M. Salgado. *Study of the properties of arc-induced long-period gratings and Bragg Gratings in B/Ge doped fibers*. in *Proceedings of the Bragg Gratings, Photosensitivity and Poling in Glass Waveguides Conference*: 121-123, 2003.

[14] G. Rego, M. Melo, J.L. Santos, and H.M. Salgado. *Optical filters for fibre lasers and amplifiers*. in *London Communications Symposium 2002, Proceedings*: 49-52, 2002.

[15] Y. Kato, S. Seikai, N. Shibata, S. Tachigami, Y. Toda, and O. Watanabe. *Arc-Fusion Splicing of Single-Mode Fibers.2. A Practical Splice Machine.* Applied Optics **21**(11): 1916-1921, 1982.

[16] G. Rego, L. Santos, B. Schroder, P. Marques, J. Santos, and H. Salgado. *In situ temperature measurement of an optical fiber submitted to electric arc discharges.* IEEE Photonics Technology Letters **16**(9): 2111-2113, 2004.

[17] K. Thyagarajan, M. Das, and M.N. Satyanarayan. *A simple and direct method to estimate long period grating parameters.* Optics Communications **218**(1-3): 67-72, 2003.

[18] P. Palai, M. Satyanarayan, M. Das, K. Thyagarajan, and B. Pal. *Characterization and simulation of long period gratings fabricated using electric discharge.* Optics Communications **193**(1-6): 181-185, 2001.

[19] J.W. Fleming. *Sub Glass Transition Relaxation in Optical Fibers*. in *Proceedings of 2004 Optical Fiber Communications Conference*: TuB2, 2004.

[20] G. Humbert and A. Malki. *Annealing time dependence at very high temperature of electric arc-induced long-period fibre gratings.* Electronics Letters **38**(10): 449-450, 2002.

[21] K. Morishita and A. Kaino. *Adjusting resonance wavelengths of long-period fiber gratings by the glass-structure change.* Applied Optics **44**(24): 5018-5023, 2005.

[22] J.M. Baptista, S.F. Santos, G. Rego, O. Frazao, and J.L. Santos. *Measurement of Angular Rotation using a Long Period Fiber Grating in a Self-Referenced Fiber Optic Intensity Sensor*. in *2005 IEEE LEOS Annual Meeting Conference Proceedings, Vols 1 And 2*: 806-807, 2005.

[23] J.M. Baptista, S.F. Santos, G. Rego, O. Frazao, and J.L. Santos. *Micro-displacement or bending measurement using a long-period fibre grating in a self-referenced fibre optic intensity sensor.* Optics Communications **260**(1): 8-11, 2006.

[24] H.S. Ryu, Y. Park, S.T. Oh, Y.J. Chung, and D.Y. Kim. *Effect of asymmetric stress relaxation on the polarization-dependent transmission characteristics of a CO2 laser-written long-period fiber grating.* Optics Letters **28**(3): 155-157, 2003.

[25] X. Shu, L. Zhang, and I. Bennion. *Sensitivity characteristics of long-period fiber gratings.* Journal of Lightwave Technology **20**(2): 255-266, 2002.

[26] V. Bhatia. *Applications of long-period gratings to single and multi-parameter sensing.* Optics Express **4**(11): 457-466, 1999.

[27] O.V. Ivanov. *Coupling of hybrid modes in strained and heated fibers.* Optics Communications **239**(4-6): 311-321, 2004.

[28] V. Bhatia, D. Campbell, R.O. Claus, and A.M. Vengsarkar. *Simultaneous strain and temperature measurement with long-period gratings.* Optics Letters **22**(9): 648-650, 1997.

[29] K. Lyytikainen, S.T. Huntington, A.L.G. Carter, P. McNamara, S. Fleming, J. Abramczyk, I. Kaplin, and G. Schotz. *Dopant diffusion during optical fibre drawing.* Optics Express **12**(6): 972-977, 2004.

[30] H. Patrick, A. Kersey, and F. Bucholtz. *Analysis of the response of long period fiber gratings to external index of refraction.* Journal of Lightwave Technology **16**(9): 1606-1612, 1998.

[31] B. Bachim and T. Gaylord. *Polarization-dependent loss and birefringence in long-period fiber gratings.* Applied Optics **42**(34): 6816-6823, 2003.

[32] C. Caucheteur, A. Fotiadi, P. Megret, S.A. Slattery, and D.N. Nikogosyan. *Polarization properties of long-period gratings prepared by high-intensity femtosecond 352-nm pulses.* IEEE Photonics Technology Letters **17**(11): 2346-2348, 2005.

[33] Y.H. Zhu, E. Simova, P. Berini, and C.P. Grover. *A comparison of wavelength dependent polarization dependent loss measurements in fiber gratings.* IEEE Transactions on Instrumentation and Measurement **49**(6): 1231-1239, 2000.

[34] I. Hwang, S. Yun, and B. Kim. *Long-period fiber gratings based on periodic microbends.* Optics Letters **24**(18): 1263-1265, 1999.

[35] M. Kim, D. Lee, B. Hong, and H. Chung. *Performance characteristics of long-period fiber-gratings made from periodic tapers induced by electric-arc discharge.* Journal of the Korean Physical Society **40**(2): 369-373, 2002.

[36] B. Huttner, C. Geiser, and N. Gisin. *Polarization-induced distortions in optical fiber networks with polarization-mode dispersion and polarization-dependent losses.* IEEE Journal of Selected Topics in Quantum Electronics **6**(2): 317-329, 2000.

[37] G. Rego, M. Morais, J.L. Santos, and H.M. Salgado. *PDL and DGD measurements of mechanically induced long-period fiber gratings*. in *London Communications Symposium 2003, Proceedings*: 77-80, 2003.

[38] S.T. Oh, W.T. Han, U.C. Paek, and Y. Chung. *Azimuthally symmetric longperiod fiber gratings fabricated with CO2 laser.* Microwave and Optical Technology Letters **41**(3): 188-190, 2004.

[39] D.D. Davis, T.K. Gaylord, E.N. Glytsis, and S.C. Mettler. *CO2 laser-induced long-period fibre gratings: spectral characteristics, cladding modes and polarisation independence.* Electronics Letters **34**(14): 1416-1417, 1998.

[40] S. Oh, W. Han, U. Paek, and Y. Chung. *Reduction of birefringence and polarization-dependent loss of long-period fiber gratings fabricated with a KrF excimer laser.* Optics Express **11**(23): 3087-3092, 2003.

[41] B. Lee, J. Cheong, and U. Paek. *Spectral polarization-dependent loss of cascaded long-period fiber gratings.* Optics Letters **27**(13): 1096-1098, 2002.

[42] A.M. Vengsarkar, Q. Zhong, D. Inniss, W.A. Reed, P.J. Lemaire, and S.G. Kosinski. *Birefringence Reduction in Side-Written Photoinduced Fiber Devices by a Dual-Exposure Method.* Optics Letters **19**(16): 1260-1262, 1994.

[43] C.S. Kim, B. Choi, J.S. Nelson, Q. Li, P.Z. Dashti, and H.P. Lee. *Compensation of polarization-dependent loss in transmission fiber gratings by use of a Sagnac loop interferometer.* Optics Letters **30**(1): 20-22, 2005.

[44] O. Frazão, R. Romero, G. Rego, P.V.S. Marques, H.M. Salgado, and J.L. Santos. *Sampled fibre Bragg grating sensors for simultaneous strain and temperature measurement.* Electronics Letters **38**(14): 693-695, 2002.

[45] F. Bakhti, J. Larrey, P. Sansonetti, and B. Poumellec. *Impact of hydrogen in-fiber and out-fiber diffusion on central wavelength of UV-written long period grating.* in *Proceedings of the Bragg Gratings, Photosensitivity and Poling in Glass Waveguides Conference*: 55-57, 1997.

[46] R.M. Atkins and P.J. Lemaire. *Effects of Elevated-Temperature Hydrogen Exposure on Short-Wavelength Optical Losses and Defect Concentrations in Germanosilicate Optical Fibers.* Journal of Applied Physics **72**(2): 344-348, 1992.

[47] A. Gusarov, Y. Defosse, O. Deparis, M. Blondel, A.F. Fernandez, F. Berghmans, and M. Decréton. *Effect of ionizing radiation on the properties of fiber Bragg gratings written in Ge-doped fiber*. in *Proceedings of the Bragg Gratings, Photosensitivity and Poling in Glass Waveguides Conference*: paper BThC30-1, 2001.

[48] T. Kakuta, K. Sakasai, T. Shikama, M. Narui, and T. Sagawa. *Absorption and fluorescence phenomena of optical fibers under heavy neutron irradiation.* Journal of Nuclear Materials **263**: 1893-1896, 1998.

[49] P. Niay, P. Bernage, M. Douay, E. Fertein, F. Lahoreau, J.F. Bayon, T. Georges, M. Monerie, P. Ferdinand, S. Rougeault, and P. Cetier. *Behavior of Bragg Gratings, Written in Germanosilicate Fibers, against Gamma-Ray Exposure at Low-Dose Rate.* IEEE Photonics Technology Letters **6**(11): 1350-1352, 1994.

[50] T. Enomoto, M. Shigehara, S. Ishikawa, T. Danzuka, and H. Kanamori. *Long-period fiber grating in a pure-silica core fiber written by residual stress relaxation*. in *Proceedings of 1998 Optical Fiber Communications Conference*: 277-278, 1998.

[51] J. Albert, M. Fokine, and W. Margullis. *Grating formation in pure silica-core fibers*. in *Proceedings of the Bragg Gratings, Photosensitivity and Poling in Glass Waveguides Conference*: paper BThC9-1, 2001.

[52] F. Hindle, E. Fertein, C. Przygodzki, F. Durr, L. Paccou, R. Bocquet, P. Niay, H. Limberger, and M. Douay. *Inscription of long-period gratings in pure silica and germano-silicate fiber cores by femtosecond laser irradiation.* IEEE Photonics Technology Letters **16**(8): 1861-1863, 2004.

[53] M. Akiyama, K. Nishide, K. Shima, A. Wada, and R. Yamauchi. *A novel long-period fiber grating using periodically released residual stress of pure-silica core fiber*. in *Proceedings of 1998 Optical Fiber Communications Conference*: 276-277, 1998.

[54] A.F. Fernandez, G. Rego, A. Gusarov, B. Brichard, J.L. Santos, H.M. Salgado, and F. Berghmans. *Evaluation of long-period fiber grating temperature sensors in nuclear environments*. in *Second European Workshop On Optical Fibre Sensors: Proceedings*: 88-91, 2004.

[55] K. Saito and A.J. Ikushima. *Effects of fluorine on structure, structural relaxation, and absorption edge in silica glass.* Journal of Applied Physics **91**(8): 4886-4890, 2002.

[56] J. Kirchhof, S. Unger, K.F. Klein, and B. Knappe. *Diffusion Behavior of Fluorine in Silica Glass.* Journal of Non-Crystalline Solids **181**(3): 266-273, 1995.

[57] A.F. Fernandez, H. Ooms, B. Brichard, M. Coeck, S. Coenen, F. Berghmans, and M. Decreton. *SCK-CEN irradiation facilities for radiation tolerance assessment*. in *IEEE Radiation Effects Data Workshop*: 171-176, 2002.

[58] A.D. Yablon, M.F. Yan, D.J. DiGiovanni, M.E. Lines, S.L. Jones, D.N. Ridgway, G.A. Sandels, I.A. White, P. Wisk, F.V. DiMarcello, E.M. Monberg, and J. Jasapara. *Frozen-in viscoelasticity for novel beam expanders and high-power connectors.* Journal of Lightwave Technology **22**(1): 16-23, 2004.

6

Mechanically induced long-period fibre gratings

6.1 Introduction

In Chapter 4 a technique was presented to produce permanent gratings by applying arc discharges to the optical fibre. However, since LPFGs possess periods of the order of hundreds of micrometers they can also be induced mechanically through periodic microbending. In this chapter a new technique is described to fabricate gratings by winding a string around a fibre/grooved tube set. This method, as the arc discharge technique, can potentially be applied to any kind of fibre and is also simple, flexible and low-cost. Another important advantage over other techniques is the fact that these gratings can be produced without removing the fibre coating and therefore the fibre keeps its mechanical integrity. The main characteristic of the produced gratings is their reversibility, that is, after removing the perturbation the gratings also vanish. Mechanically induced long-period fibre gratings (MLPFGs) are very sensitive to external pressures enabling a good control over their transmission characteristics. Therefore, it is not surprising that the main published application of these gratings is the gain flattening of EDFAs.

This technology is also very useful in research labs since it provides a simple and fast way to produce an optical filter. Furthermore, it can be used to estimate, for a particular fibre, the resonant wavelengths of a permanent grating produced by other techniques. Since microbending is also a potential mechanism concerning the formation of arc-induced gratings it seems important to compare the gratings spectra produced by both techniques.

The chapter begins with a brief overview of the MLPFGs technology. A new fabrication technique is then described followed by the analysis of a set of fabrication parameters that allows control over the gratings transmission spectra. The response of these gratings to applied strain, temperature and loads is also discussed. Afterwards, the polarization dependent loss and the differential group delay of the produced gratings under load are investigated and a birefringence compensation method is presented. Finally, two examples of the employment of these gratings are given for both application fields. In optical communications, the equalization of an EDFA gain spectrum and in optical fibre sensors, an interrogation scheme

comprising a fibre Bragg grating (FBG) and a MLPFG with dynamic loss control by applying loads to it are discussed.

6.2 Microbending long-period fibre gratings

The same technology that was employed 25 years ago in the fabrication of microbend sensors [1], that consisted in squeezing a multimode fibre between a set of grooved plates, are nowadays being used to mechanically induce long-period fibre gratings in singlemode fibres. These gratings, in turn, find application in optical communications and fibre sensors.

Several techniques were published in the literature to produce mechanical gratings but they share the same aim, that is, to induce periodic stress and/or microbending in a singlemode fibre. Some examples of these techniques are shown in Figure 6.1. Despite their distinct appearance, they possess in fact great similarities as far as the effects induced in the fibre are concerned. Indeed, it seems reasonable to admit that both mechanisms for the fabrication of MLPFGs act simultaneously leading to the formation of the grating, only the relative contribution of each may depend on the fabrication technique. The basic fabrication configurations consist in a fibre laying on a flat surface that is periodically pressed by a coiled wire [2-4], a grooved plate [5] (shown in Figure 6.1(a)) or a periodic array of copper wires [6] or graphite rods [7, 8]. In a modified version, the fibre is pressed against two out-of-phase arrays of graphite rods [9] (shown in Figure 6.1(b)). Alternatively, a wire can be wound around the fibre [10] or around the fibre/grooved tube set [11], shown in Figure 6.1(c) and Figure 6.1(d), respectively. As a final note regarding the fabrication techniques, it was also demonstrated that by gluing a fibre onto a corrugated metal or silica substrate, microbending can be thermally induced due to the different thermal expansion coefficients of both materials [12, 13].

The configurations presented in [2-7] enable wavelength tunability through adjustment of the angle between the fibre and the mechanical grooves and control of the transmission loss by applying loads to the gratings. The configurations relying on the winding of the wire allows a good control of the transmission loss by changing the number of turns. Further control can also be achieved in the latter configuration by applying loads. Regarding the wavelength tunability, these techniques are not so flexible. However, some ways to obtain it will be presented in section 6.5.2 with respect to the technique of Figure 6.1(d) that is discussed in this chapter.

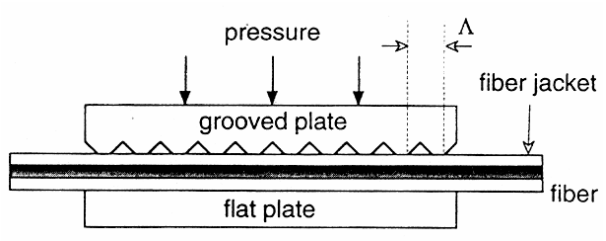

(a)

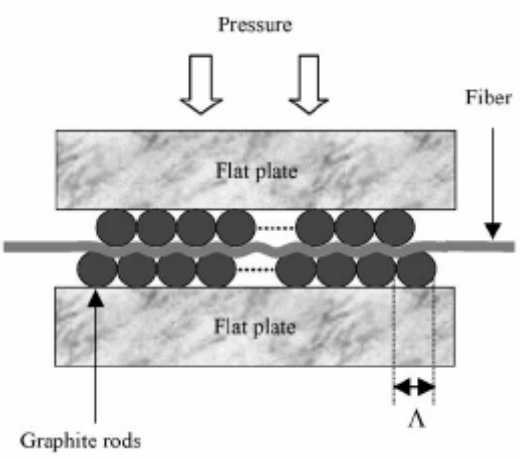

(b)

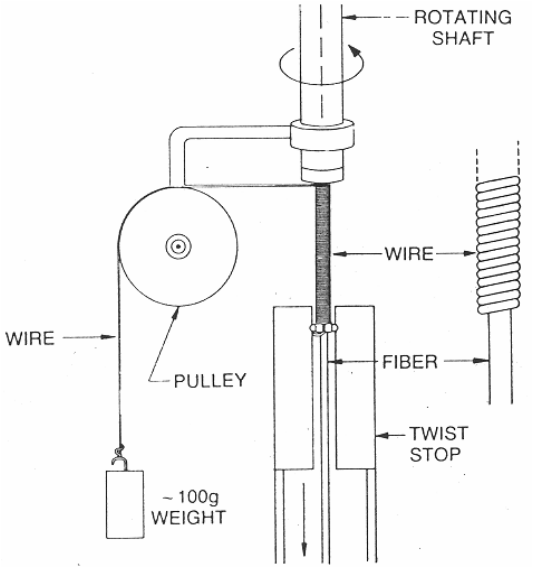

(c)

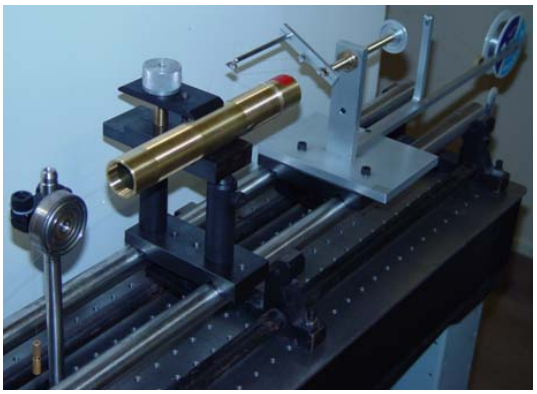

(d)

Figure 6.1 – Fabrication techniques: (a) Grooved Plate. (Taken from [5]). (b) Two out-of phase arrays of graphite rods. (Taken from [9]). (c) Wire wound around the fibre. (Taken from [10]). (d) Nylon string wound around a fibre/ grooved tube set.

The MLPFGs characteristics enables their use as optical communication devices, such as fibre mode couplers [14, 15], variable optical attenuators [16, 17], bandpass filters [3], narrowband filters for WDM systems [7], band-rejection filter in a multiwavelength all-fibre ring laser [18] or as EDFAs gain flatteners [9, 19-22]. They can also be used as fibre polarizers since they are intrinsically birefringent [5, 23, 24]. On the other hand, they can become polarization insensitive by twisting the fibre before writing the grating [25, 26]. MLPFGs can also be used separately or with other structures in optical sensing of physical parameters like torsion [27], pressure [6, 11, 28], temperature and strain [29, 30]. Furthermore, by changing their strength, MLPFGs can be employed in the interrogation of other fibre gratings, such as an FBG [31]. Moreover, mechanical gratings have been

performed in photonic crystal fibres [32-35] and in microstructured polymer fibres [36] opening their range of application.

6.3 Fabrication technique

In this section the fabrication technique based on the winding of a wire around a fibre/grooved tube set used to mechanically induce the fibre gratings is described. As will be discussed in the next section there is a set of fabrication parameters that determines the spectra of the gratings and therefore requires the specification of a reference configuration and of the correspondent typical grating spectrum. Afterwards, modifications of the reference configuration will be performed in order to analyse the mechanisms of gratings formation.

6.3.1 Description of the technique

The fabrication process is illustrated in Figure 6.2 and consists of four steps. First, a fibre is positioned on top of a 35 mm-diameter brass tube, with a 60 mm long grooved region, and is fixed on one end of the tube. On the other end, the fibre is placed over a pulley and is kept under tension by means of a suspended clamped weight (W1). On a second step, a nylon string that goes through a system of pulleys to reduce friction during winding and is fixed on the same end of the tube. Weights (W2) are then hung on a movable pulley nearby the nylon string supply drum. Finally, after lowering the weight towards the ground, the drum is fixed and the screw is turned. This process winds the nylon string around the tube pressing the fibre against the v-grooves (see inset in Figure 6.2). The evolution of the gratings spectra is

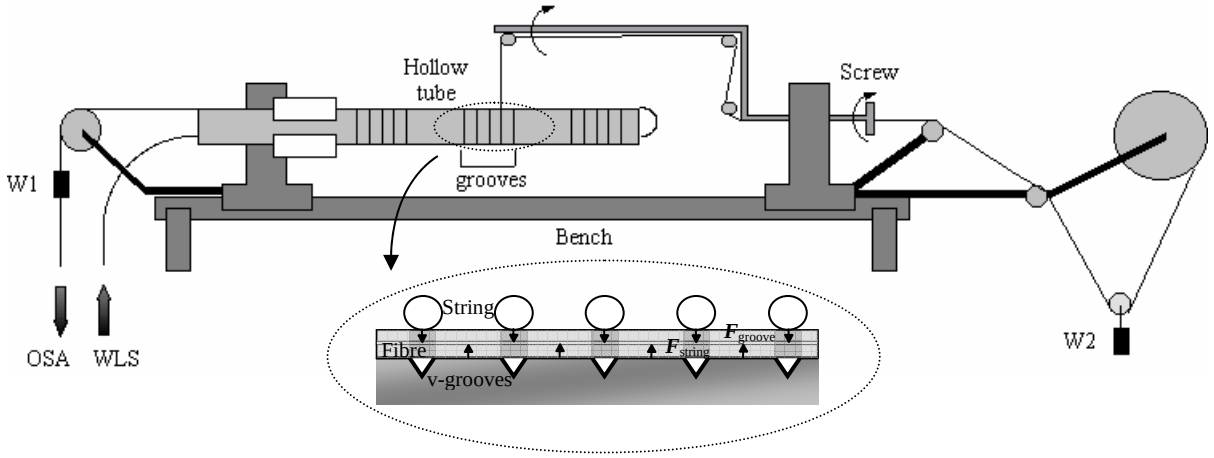

Figure 6.2 – Experimental setup. Inset: Arrangement of the nylon string/fibre/v-grooves set.

monitored using a white light source (WLS) and an optical spectrum analyser (OSA), set to a resolution of 1 nm.

6.3.2 Reference configuration

In what follows and unless specified otherwise, the reference configuration consists on the coated fibre SMF-28 #2, under a slight tension caused by a suspended weight of 5.1 g. The v-grooves have a period of 600 μm and are 150 μm deep. A typical grating is obtained after 70 turns of a 250 μm-nylon string kept under tension by means of a 41.8 g weight. Note that the tension applied to the fibre helps to maintain it perpendicular to the grooves direction. If this situation is not ensured, an increase on the background loss can be registered accompanied by a slight decrease of the transmission loss of the resonant bands. Figure 6.3 shows a typical spectrum of a grating performed under the reference conditions. The important aspects that can be extracted from this figure are that the background loss is negligible, the existence of a resonant wavelength in the third telecommunication window and with a considerable transmission loss. As will be discussed in the next sections this loss can be further increased by a judicious choice of the fabrication parameters.

Next the mechanisms of MLPFGs formation will be investigated.

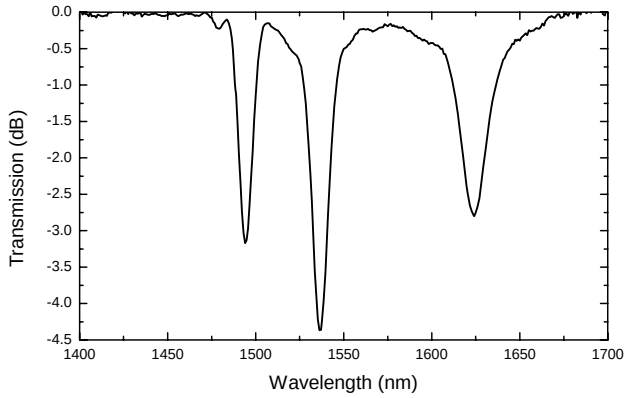

Figure 6.3 – Typical grating spectrum.

6.3.3 Other fabrication configurations and mechanisms of gratings formation

MLPFGs formation has been attributed to refractive index modulation through the photoelastic effect owing to periodic applied pressure or to microdeformations [2, 14]. Note however that associated with microbending changes of the refractive index also occurs due to the photoelastic effect since bending itself also induce material compression and stretching [37]. Regarding this technique and in order to separate possible contributions from both mechanisms (pressure and bending) several modifications of our particular setup arrangement were made. In a first experiment, aluminium paper was placed over the tube before putting

the fibre. As a result, no grating appeared during the winding of the nylon string. The same result was obtained when the fibre directly placed over the grooved tube was submitted to loads up to 1 kg. However, it was found that if the nylon string was wound around the tube prior to place the fibre and afterwards the same weight of 1 kg was applied, a weak grating appeared with a transmission loss of about one half of the obtained for a grating induced with the reference arrangement. Moreover, if instead of applying the weight, another length of nylon string was wound around the fibre/nylon string/grooved tube set, that would result in a two times increase of the transmission loss when compared to the reference grating (see Figure 6.4). Note that this configuration also leads to a shift of the spectrum towards longer wavelengths which can be attributed to an increase of the effective period as a result of the fibre bending. The above results mean that the pressure caused by the nylon string and by the v-grooves does not play a fundamental role in their growth. Therefore, it may be concluded that grating formation is mainly related with periodic microbending.

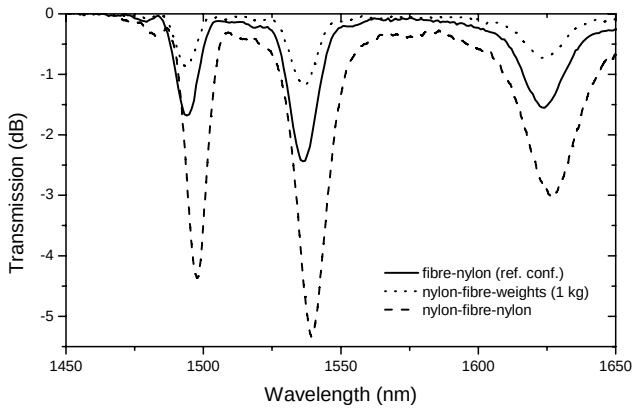

Figure 6.4 – Gratings spectra for different configurations.

6.4 Fabrication parameters

As for other fabrication techniques, the fibre type (in this case, the coating is also important), the period and the number of perturbations (here, called the number of turns of the nylon string) affect the final grating spectrum. There are, however, other parameters intrinsic to this particular technique, the type of wire/string, its diameter, the tension (weight) and the geometry of the v-grooves. Therefore, in order to determine their relative influence, comparisons will be made against the reference configuration.

In this section the influence of the fabrication parameters on the transmission loss and on the bandwidth of the resonant bands belonging to the performed gratings is analysed. It is

anticipated that for a specific fibre the resonant wavelengths are exclusively determined by the grating period (section 6.5).

6.4.1 Number of turns of the nylon string

The evolution of a grating as the number of turns of the nylon string is increased from 20 to 80 in steps of 10 is shown in Figure 6.5. The grating grows almost linearly with the number of turns, whilst its resonant wavelengths remain unchangeable. The growth rate of the second mode is about 0.08 dB/turn, while for the other two modes it is approximately 0.06 dB/turn. As a result of the slow and constant growth of the grating it is possible to achieve a good control over the transmission loss. Note also that as for other types of gratings the bandwidth decreases with the increase of the length of the grating. As mentioned previously, gratings produced using this technique are reversible, that is, after unwind the initial transmission of the fibre is recovered.

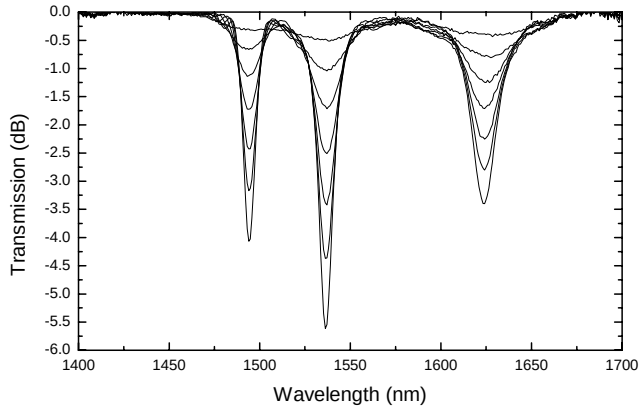

Figure 6.5 – Growth of a grating as a function of the number of turns *n* (increases from 20 to 80 in steps of 10).

6.4.2 Tension on the nylon string

The effect of increasing the tension on the nylon string, is the reinforcement of the fibre microbends and consequently the strength of the resonant bands also increase (see Figure 6.6(a)). As seen in Figure 6.6(b), for weights greater than 41.8 g the non-linear behaviour of the grating growth becomes more pronounced. As a result, a four times increase of the tension leads to nine times increase of the transmission loss of the second resonance. The grating bandwidth also increases with the increase of the applied tension.

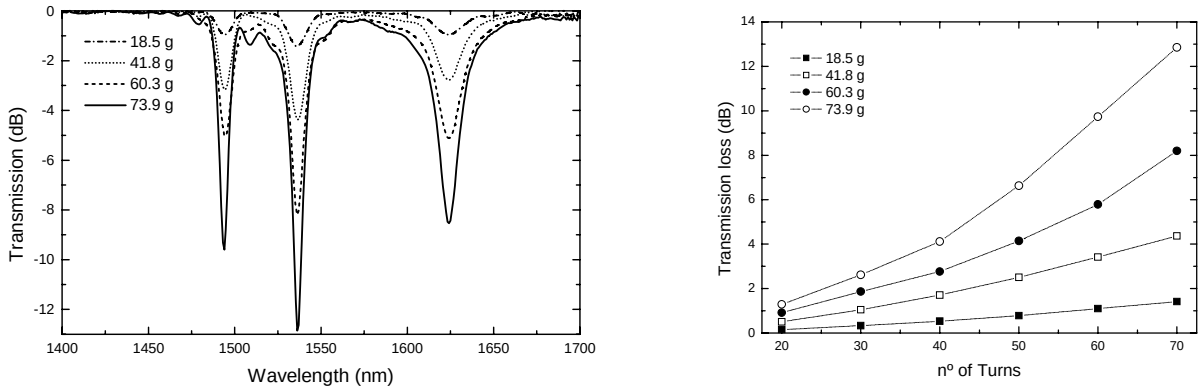

(a) (b)

Figure 6.6 – Effect of increasing the string tension on (a) gratings spectra (b) transmission loss.

6.4.3 Diameter of the string

The effect of the diameter of the nylon string is shown in Figure 6.7. Nylon strings with diameters of 180 μm or 250 μm have a similar effect on the grating growth. However, when a diameter of 350 μm was used, the transmission loss almost duplicated. This is attributed to an increase in friction due to the small size of the v-groove of the pulleys compared with the string diameter which has a similar effect to an increase of the tension. An increase of the bandwidth is also observed.

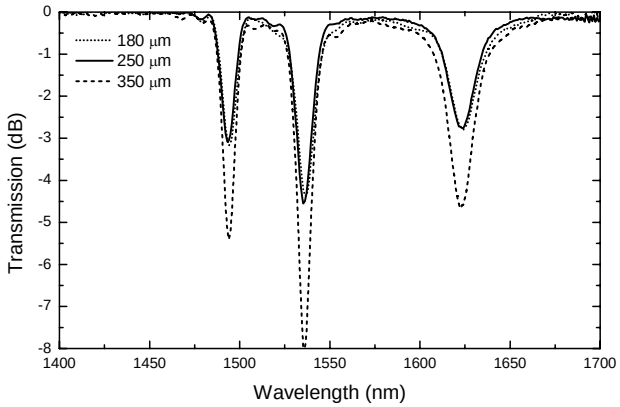

Figure 6.7 Influence of the diameter of the nylon string

6.4.4 V-groove depth

The parameters of the v-grooves used in this study are summarised in Table I. (see also Figure 6.8).

Table I. – Geometrical parameters of the v-grooves and of the nylon strings.

d_{string}/μm	d_{depth}/μm	d_{open_v}/μm	d_{thread}/μm
180	100	116	484
250	150	173	427
350	270	312	258
	380	439	161

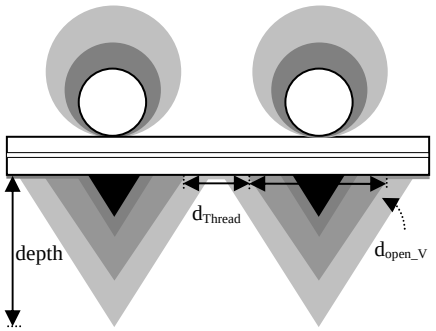

Figure 6.8 – Diagram of the arrangement of the string/ uncoated fibre/v-grooves with different dimensions.

Figure 6.9 shows that deeper v-grooves correspond to higher strength of the loss-peaks. The growth rate of the second mode is about four times higher for the v-grooves with a 380 μm-depth than for the ones with a 100 μm-depth. Notice that this change in the depth of the v-grooves corresponds to a decrease of three times in the thread width and therefore it leads to an increase of fibre bending. The grating bandwidth remains unchanged.

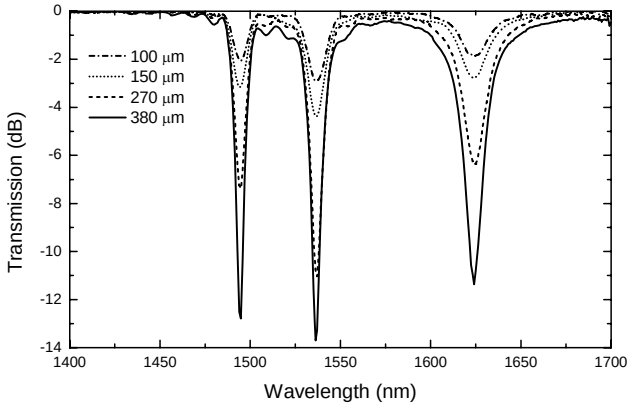

Figure 6.9 – Influence of the depth of the v-grooves.

6.4.5 Nylon string versus copper wire

To compare the effect of having strings with different mechanical properties, the nylon strings were replaced by copper wires with similar diameters. Figure 6.10 shows that copper wires are more efficient in inducing fibre microbending. This result was already expected due to the higher rigidity of copper. However, the background loss increases considerably. The grating bandwidth also increases. Note that the reproducibility of the technique is worst for copper wires probably as a result of friction mechanisms.

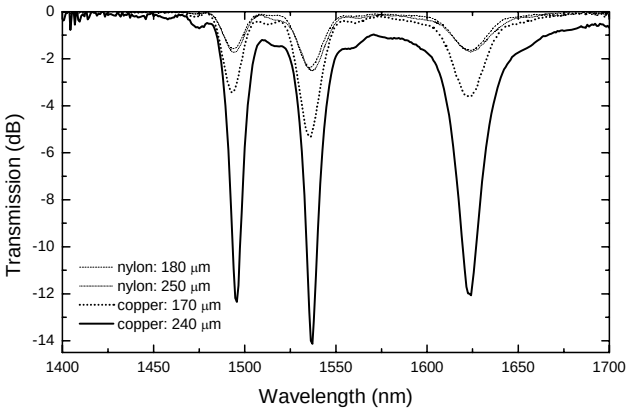

Figure 6.10 – Influence of the strings type: nylon versus copper.

6.4.6 Fibre coating

The properties of the coating material also determine the growth rate of the gratings. It was impossible to perform gratings in a soft silica-rubber fibre coating even using the best parameters discussed above. Alternatively, the growth rate of the gratings produced in a recoated fibre is much higher (85%) than for the original jacket. If a grating is performed in the same physical region of the fibre as a previous one a slight increase in the transmission loss is obtained. Repeating the process four to five times leads to an increase of about 30% of the transmission loss towards saturation. Although slight periodic depressions in the coating were observed, the mechanical strength of the fibre is maintained.

Figure 6.11(a)-(b) shows that removing the coating of the fibre prior to perform the grating leads to higher growth rates. The background loss is comparable or even lower than the typical values obtained for coated fibres (< 0.2 dB). The mechanical strength of the fibre is still high, as is confirmed by the fact that no fibre breakage occurred after performing hundreds of gratings. Figure 6.11(a) also shows a slight shift of the spectrum towards shorter wavelengths accompanied by a decrease of the gratings bandwidth.

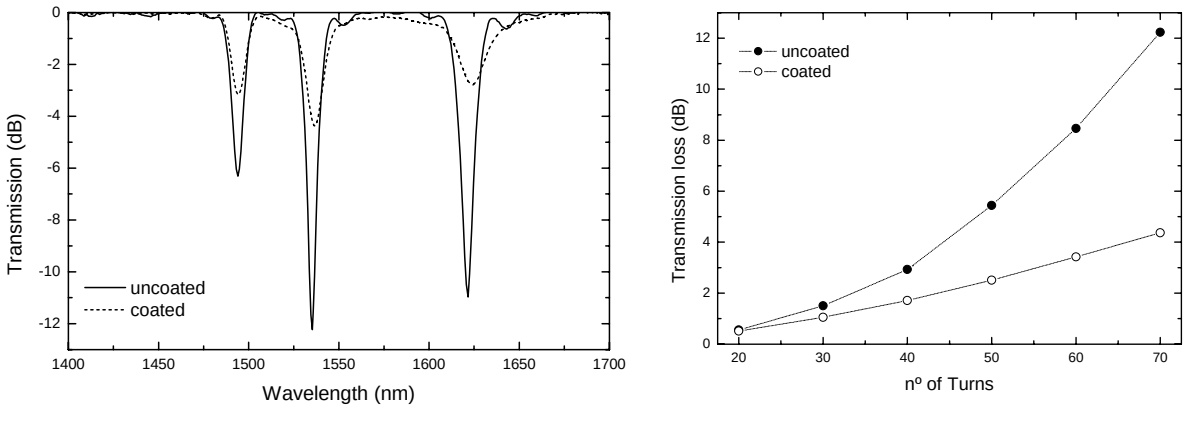

(a) (b)

Figure 6.11 Effect of removing the fibre coating on the (a) gratings spectra (b) transmission loss.

6.4.7 Relaxation

During reliability studies, it was found that relaxation/adjustment of the string/fibre/grooves set causes either growth or decrease of the transmission loss towards stabilisation, depending on the configuration used. For all configurations the transmission loss decreased in time, except when using the nylon string and the coated fibre, but even in this case it depends on the coating material. As an example, the transmission loss of a grating performed in the fibre SMF-28 #2, after its recoating, also decreases during the stabilisation process. As seen in Figure 6.12, the stabilisation time ranges from less than 1 h up to 5 h, depending on the configuration. During this process changes of 27% in the initial value of the transmission loss were measured. The magnitude of the change increases with the number of turns. For the coated fibre, an increase of the room temperature leads to longer stabilisation times and also to larger changes in the gratings strength. The opposite is true for the uncoated fibre.

In a recent work [31] only minor changes were detected on the strength of a MLPFG submitted to loads up to 774.7 g during 5 h. In this case, the fibre was stretched prior to the grating fabrication through the winding of the nylon string under a tension of 73.9 g. Therefore, these two parameters, the tension on the fibre and the tension on the nylon string are important in determining the gratings stability.

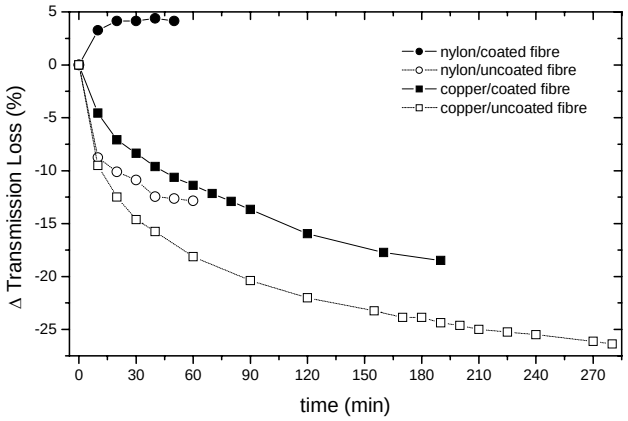

Figure 6.12 Time evolution of the gratings at room temperature (~21 ºC)

6.4.8 Discussion of the results

From the results obtained it can be concluded that fabrication parameters such as higher tensions, deeper grooves and larger string diameters contribute to stronger MLPFGs. The use of copper instead of nylon and the decrease of the fibre cross section also increase the transmission loss of the resonant bands. Moreover, the most effective factors are the tension, the copper wires and the uncoated fibre. As will be discussed in the next section, the reduction of the cladding diameter also increases the growth rate of the grating. In that case, the mechanical integrity can also be preserved by recoating the fibre after the etching process.

The bandwidth (FWHM) of these gratings is typically in the range of 10 nm to 30 nm. As for other types of gratings the bandwidth decreases during the fabrication process. In general, the same factors that leads to an increase of the transmission loss also contributes to the increase of the bandwidth, being particularly large when using a 240 μm-diameter copper wire, a high tension, or a fibre without coating combined with deep v-grooves.

This technique of producing MLPFGs offers high repeatability being the difference in the strength of two gratings written in the same conditions below 1%. However, there are several factors that can strongly affect this result. Abnormal friction in the pulleys or small deviations in the relative position of the fibre/grooves/string/pulley assembly can lead to changes of about 20%. Temperature related effects might also contribute to some discrepancies. Therefore, to obtain a practical device some feedback mechanism which correlates, for instance, the transmission loss and the applied loads, might be needed to overcome the relaxation phenomenon.

6.5 Resonance wavelengths

In order to produce a useful filter for optical communications or sensing fields a good control is required over the position of the resonance wavelengths and of the transmission loss of the resonant bands. In the last section it was demonstrated that this technique of MLPFGs fabrication enables a good control over the transmission loss. In this section the means to accurately positioning and tune the resonant wavelengths will be presented.

6.5.1 Resonance wavelengths versus grating period

Gratings were induced in three singlemode fibres, two Ge-doped silica based fibres from Corning, named SMF-28 #1 and SMF-28 #2, and an aluminosilicate fibre from FORC, named Al. For all fibres, the diameter of the core, cladding and coating as well as the cut-off wavelength was measured. The results of those measurements are given in table II.

Table II. - Parameters of the fibres

Fibre	D_{core}/μm	$D_{cladding}$/μm	$D_{coating}$/μm	$\lambda_{cut\text{-}off}$/μm
SMF-28 #1	8.6	125.1	200	1.27
SMF-28 #2	8.6	125.1	200	1.31
Al	4.3	125.9	230	1.27

The dependence of the resonance wavelengths position on the grating period according to the resonance condition, for each fibre, is shown in Figure 6.13. For these gratings it has been experimentally verified that the position of the resonance wavelengths is mainly defined by the period of the v-grooves. Important information can be extracted from Figure 6.13 regarding the required fibre and grating period for a particular application. Furthermore, it is seen that despite only four grating periods were used, ranging from 400 μm to 700 μm, several resonance wavelengths that fall in the third telecommunication window were obtained. Thus, this technique offers a straightforward way to produce filters in an important wavelength range regarding potential applications in both fields.

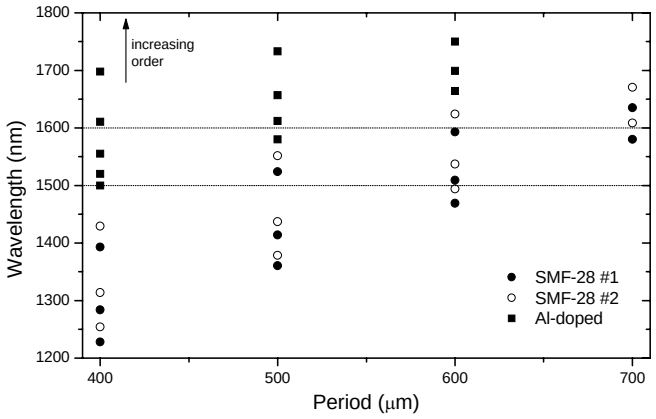

Figure 6.13 – Wavelength versus period for three fibres.

6.5.2 Positioning of the resonances

If technical limitations concerning the period of the v-grooves are assumed or if high precision on the positioning of the peaks is required, the tunability of the resonance wavelengths of a grating, in a particular fibre, can be achieved using a post- or pre-grating fabrication method. The former consists in changing the strain ($\Delta\lambda < 3$ nm) or the temperature (0.05 nm/ºC) of the grating. In the latter, the tuning can be achieved by changing the angle between the fibre and the v-grooves. However, this change leads to small reproducible tunability (~5 nm) due to the curvature of the cylindrical tube that origins a less effective coupling and distorts the spectrum of the grating. Despite the fact that straightforward modifications such as the increasing of the diameter of the tube or putting the fibre in directional grooves could result in some improvement, we are aware of the intrinsic limitations of this configuration with regard to wavelength tunability.

A well-known process of repositioning the resonance wavelengths of the LPFGs is through the etching of the fibre cladding [38]. Therefore, gratings were performed in fibre SMF-28 #2 after its cladding diameter has been etched by a 40% solution of HF at an etching rate of ~2 μm/min. If required, the etching rate can be reduced by further dilution or by using

a buffer solution [39, 40]. Figure 6.14(a) shows the spectra of the gratings obtained for different cladding diameters. As previously reported [38-40] the reduction of the cladding of the fibre leads to a stronger coupling, that is, less turns of the nylon string are needed to achieve the maximum strength of the loss-peaks. A shift of the resonant loss-peaks towards longer wavelengths also occurs. Furthermore, this shift increases with the order of the cladding modes and for the second resonance is of about 19 nm, 64 nm and above 200 nm for, respectively, 10 min, 20 min and 30 min of etching time (see Figure 6.14(b)). The fibre mechanical integrity can be preserved, to some extent, by recoating it after the etching process.

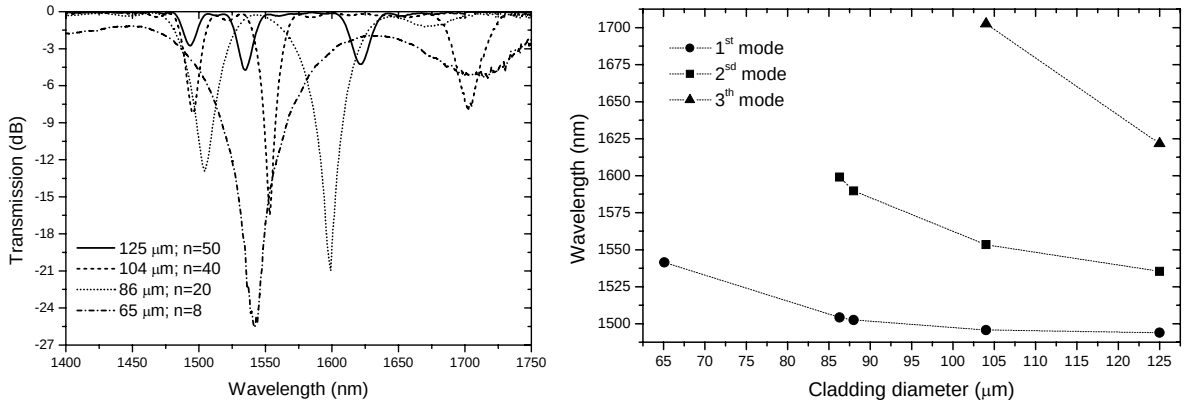

(a) (b)

Figure 6.14 – (a) Gratings spectra for different cladding diameters (b) Wavelength versus cladding diameter.

Another approach to change the position of the resonances is the pre-annealing of the fibre before performing the grating. The results of pre-annealing the fibre are shown in Figure 6.15. A shift of 16 nm was obtained after submitting the SMF-28 #1 fibre to a temperature of 1050 ºC during 1 hour. Since there is a temperature gradient along the 18 cm of the oven, depending on the region where the nylon is wound the resonances appears at different wavelengths. However, for this annealing conditions, the fibre becomes brittle afterwards. As discussed in the previous chapter, annealing the fibre at temperatures in the range of 700 to 800 ºC, can lead to similar tunabilities without severe degradation of the fibre structure. Therefore, a mechanical grating was also induced in a fibre pre-annealed at 800 ºC during 1 hour. In this case, a shift of 15 nm towards shorter wavelengths, for the third cladding mode resonance, was observed (see Figure 6.15).

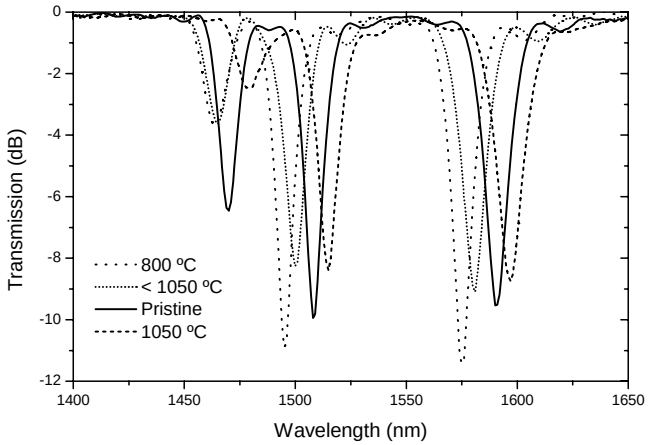

Figure 6.15 – Effect of fibre pre-annealing.

Recently [41], it was demonstrated that twisting the fibre prior to perform the grating leads to large wavelengths shift. The tunability increases with the twist rate and can be greater than 100 nm. This large value results from the fact that a coated fibre bears larger torsions when compared to the uncoated fibres used during the writing of gratings by other techniques. On the other hand, these writing techniques also weakness the fibres which reduce even more the maximum value allowed for the twist rate. Figure 6.16 shows that by twisting the fibre SMF-28 #2 at a rate of only ±3 rad/cm results in a 10 nm shift towards shorter wavelengths. Therefore, fibre twisting in the fabrication of MLPFGs is a flexible and straightforward way to achieve tuning of the gratings.

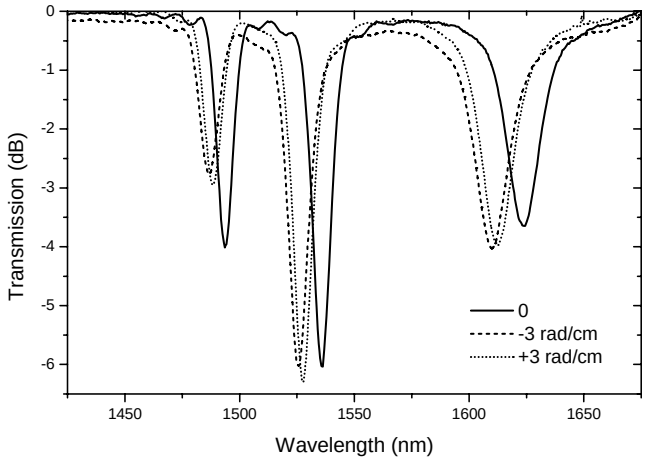

Figure 6.16 – Effect of twisting the fibre.

6.5.3 MLPFGs versus LPFGs

The technique for mechanically induce gratings is very helpful in research labs for providing in a simple and fast way useful optical filters. It also helps to estimate roughly the grating period to be used by other fabrication techniques such as the electric arc when resonances at a

particular wavelength range are required. Figure 6.17 shows the spectra of gratings induced mechanically and by arc discharges in the SMF-28 #1 and Al fibres using the same period of 400 μm. As it can be seen, for both fibres the spectra of the gratings induced mechanically are similar to the ones produced by arc discharges. However, the resonant wavelengths of the former are positioned at longer wavelengths. The displacement depends on the fibre and on the order of the cladding modes. For the Al fibre, the displacement reaches about 60 nm.

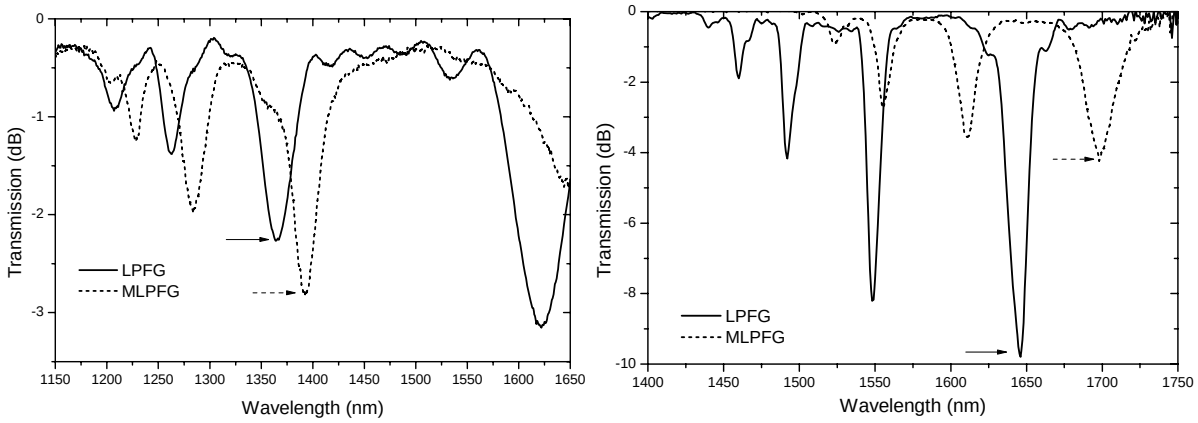

Figure 6.17 – Spectra of 400 μm gratings induced mechanically and by arc discharges in (a) SMF-28 #1 and (b) Al fibres.

Figure 6.18 shows the resonant positions as a function of the grating period for gratings induced in the SMF-28 #1 fibre. The resonances correspond to coupling from the core mode to asymmetric cladding modes (LP_{1j}), as verified through computer simulations. For the same

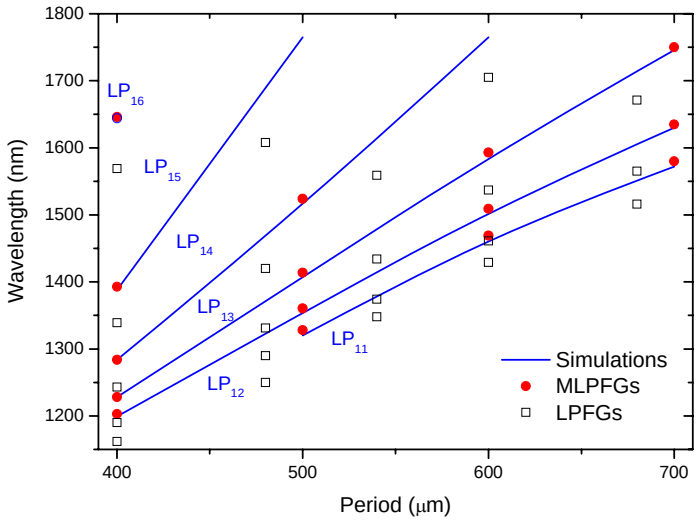

Figure 6.18 – Resonant wavelengths, corresponding to coupling to asymmetric cladding modes, as a function of the grating period.

period, the resonant wavelengths of arc-induced gratings are shorter than those of MLPFGs. The difference obtained comparing both fabrication techniques might be due to stress relaxation/viscoelasticity promoted by the arc discharges [42]. As shown in Chapter 4, the fibre reaches a temperature of about 1320 ºC during the discharge and, therefore, it partially anneals the intrinsic stresses of the fibre [43].

6.6 Gratings response to strain, temperature and pressure

Regardless of the specific applications of MLPFGs and despite the intrinsic limitations of this fabrication technique, an investigation of their sensitivity to physical parameters such as strain, temperature and pressure is required.

In the following measurements the reference configuration is considered, as described in section 6.3.2. The gratings spectra were recorded using an erbium broadband source and an OSA with a resolution set to 0.1 nm.

6.6.1 Strain and temperature sensitivities

When tension is applied to the fibre after the grating fabrication, its spectrum moves towards shorter wavelengths, the strain sensitivity of the second resonance being approximately - 0.62 pm/με (see Figure 6.19(a)).

In order to investigate the temperature behaviour of these gratings, a heater was placed inside the hollow tube and centred with the grooved region. Gratings produced with both types of strings were heated from 21 ºC up to 30 ºC. The temperature sensitivity obtained for the nylon string and copper wire was respectively, 0.05 nm/ºC and 0.07 nm/ºC. For the same temperature range, the optical power loss of the second resonance changed 0.4 dB/ºC and 0.08 dB/ºC for the nylon and copper, respectively. Figure 6.19(b) shows that the resonant wavelengths shift linearly with temperature whilst the transmission loss increases quadratically.

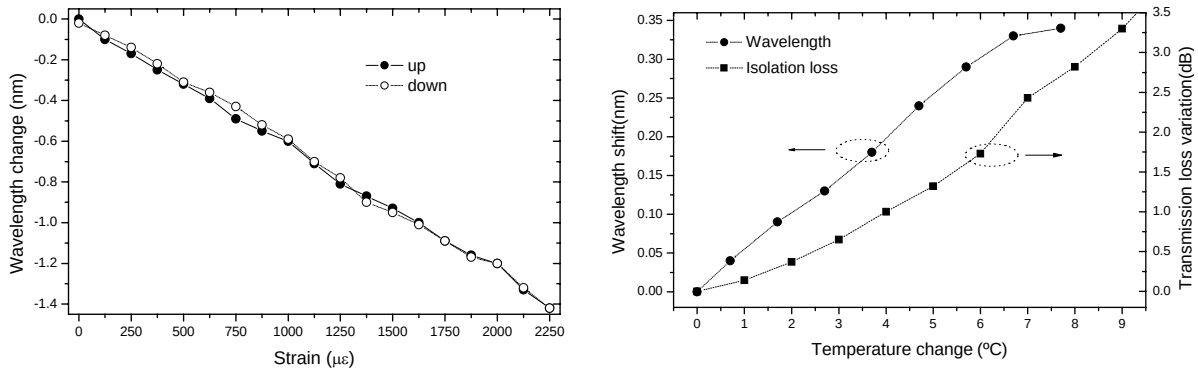

(a) (b)

Figure 6.19 – (a) Strain sensitivity. (b) Wavelength and transmission loss dependence on temperature.

6.6.2 Sensitivity to loads

Gratings produced in fibre SMF-28 #2, with and without coating, using both types of strings were also submitted to loads. A flat surface was put on top of the wound string and was loaded with distributed weights up to ~700 g. Figure 6.20(a) shows the transmission spectrum of a grating as a function of the external loads applied to it. The effect of loading a MLPFG performed in an uncoated fibre is shown in Figure 6.20(b). As it can be seen for weights above 378 g back-coupling occurs, that is, the energy is now coupled to the core mode. These MLPFGs have shown sensitivities to loads as high as 20 dB/kg.

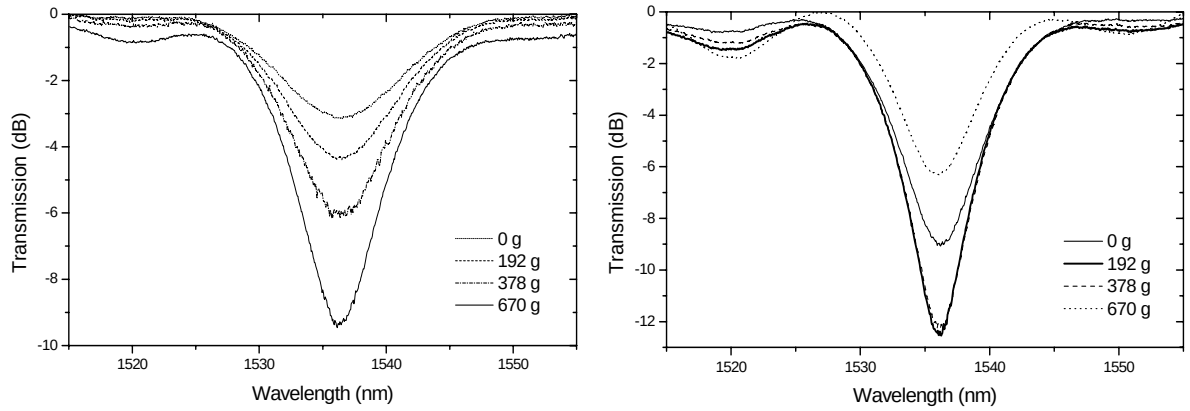

(a) (b)

Figure 6.20 – Grating spectra as a function of applied loads to a (a) coated fibre (b) uncoated fibre.

In another experiment, the optical power loss of the three resonances was monitored during the complete cycle of loading and unloading. Figure 6.21 shows a typical example of the response of these gratings to applied external pressure where nylon string and coated fibre were used. For all configurations there is some hysteresis although limited to 2% for loads up to 200 g. As expected the results are worst for loads up to 700 g, the maximum deviation

being obtained for nylon strings and copper wires of ~6% and ~12%, respectively. Nevertheless, it is possible to change the transmission loss by more than 10 dB keeping the hysteresis limited to 2%. Therefore MLPFGs, can find application as pressure gauges.

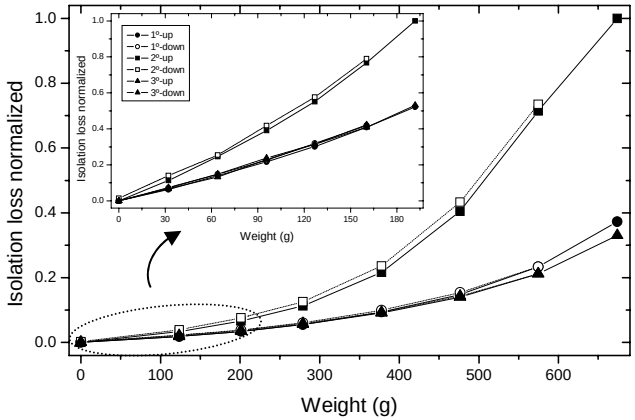

Figure 6.21 Response of the gratings to external applied pressure.

6.7 Gratings polarization-dependent loss and differential group delay

It is known that MLPFGs are intrinsically polarisation sensitive and exhibit polarization mode dispersion (PMD) due to linear birefringence caused by external pressures [5]. However, these properties may depend on a particular fabrication technique.

In this section, the study of the polarisation-dependent loss (PDL) properties of the produced gratings will be presented. PDL as high as 20 dB was obtained and therefore these gratings can be used as wavelength selective fibre polarizers. Another, important application of MLPFGs is the equalization of the EDFAs gain spectra. However, in this case PDL is a drawback and therefore a simple birefringence compensation scheme is also analysed.

6.7.1 Gratings PDL

Whilst the gratings are being performed, geometric and stress-induced birefringence is introduced to some extent. Moreover, it arises from the phase-matching condition (Eq. 3.1) that birefringence leads to a split of the resonance bands for two orthogonal polarizations (see Figure 6.22). On the other hand, the existence of PDL gives rise to differential group delay (DGD) through the differential attenuation of the electric fields of two orthogonal polarizations. Therefore, the MLPFGs possess both PDL and DGD.

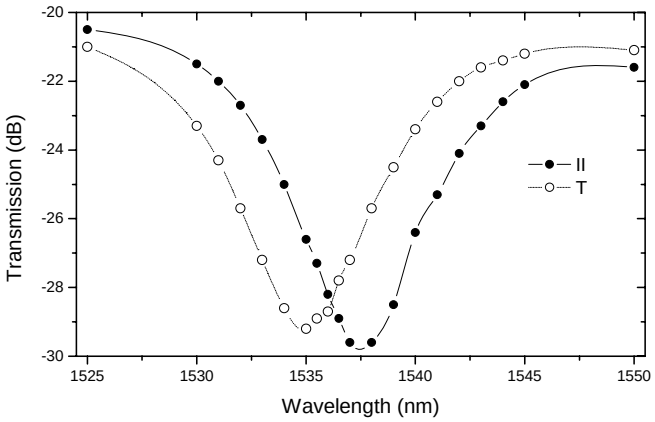

Figure 6.22 Grating spectrum for two orthogonal polarizations.

The gratings PDL was determined using the polarization-scanning method [44], that is, for each wavelength all polarization states in the Poincaré sphere were virtually generated in order to find the minimum and maximum power transmitted through the grating. The DGD was software calculated from the wavelength dependence of the Jones matrix eigenvalues. The instruments used were a computer controlled polarization analyser (HP8509B) and an external tunable laser (HP8167A). Figure 6.23 and Figure 6.24 show the spectral dependence of the PDL and DGD of two gratings produced in the fibre with and without coating for different values of the external applied pressure. It can be seen that the spectral PDL and DGD have similar behaviour and both follow the change of the transmission loss independently of the weights increase (see Figure 6.23 and Figure 6.24 and recall back-coupling in Figure 6.20(b)). Thus, it might be concluded that DGD is more a result of the existence of PDL then “pure” birefringence.

It was experimentally verified that, for each wavelength, the two principal states of polarization, that correspond to a maximum and to a minimum are not orthogonal which confirms that MLPFGs possess both PDL and DGD. The PMD is in general determined as an average of the DGD, but in the presence of PDL their relationship is non trivial [45].

Notice that for a specific transmission loss required, lower PDL and DGD values are obtained if one removes the fibre coating or increases the tension on the nylon string instead of increasing the loads. The configuration which consists in the wind of the nylon string before performing the grating also leads to lower PDL and DGD values.

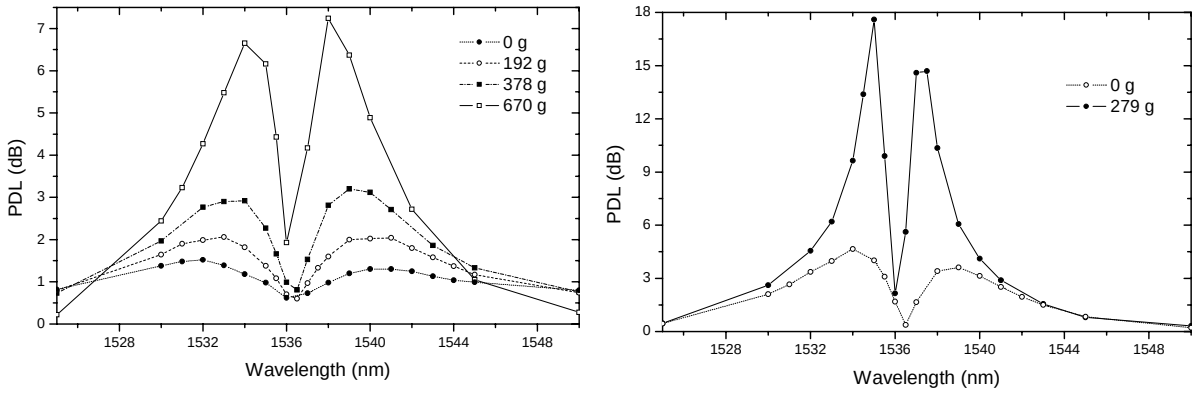

(a) (b)

Figure 6.23 – Spectral PDL of the grating as a function of applied loads. (a) coated fibre (b) uncoated fibre.

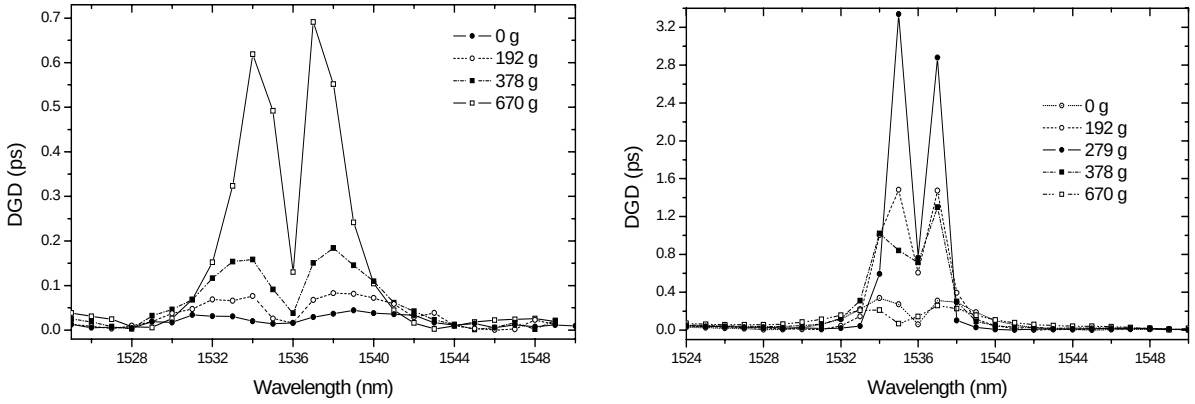

(a) (b)

Figure 6.24 – Spectral DGD of the grating as a function of applied loads (a) coated fibre (b) uncoated fibre.

6.7.2 Birefringence compensation

In order to investigate the possibility to compensate the birefringence of the MLPFGs, two similar gratings were simultaneously performed fixing the fibre on the top and on the bottom of the grooved tube prior to the wind around of the nylon string. The fibre coating was removed on purpose to obtain DGD values well above the random noise. Figure 6.24a shows the transmission spectra of the top, the bottom and of both gratings. The gratings DGD is also shown in Figure 6.25(a). Afterwards, a half wave plate was inserted in between the gratings, to rotate the polarization, and the maximum value of the DGD was measured as a function of the rotation angle (see Figure 6.25(b)). As seen, although it was not possible to fully compensate the birefringence, maybe due to non-identical gratings, a considerable reduction was obtained. Another approach based on the twist of the fibre was published in the literature [25]. Recently, it was also proposed to use fibre design to control the PDL of MLPFGs [46].

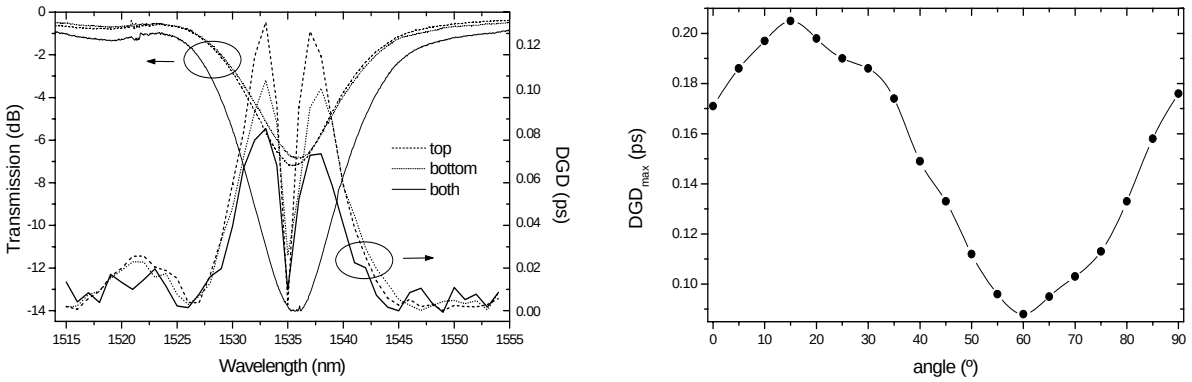

(a) (b)

Figure 6.25 – (a) Gratings transmission spectra and the correspondent DGD. (b) Maximum value of DGD as a function of the rotation angle.

6.8 MLPFGs applications

In this section two applications of the MLPFGs are described. In optical communications, the equalization of an EDFA gain curve is achieved and in optical fibre sensors, a dynamic filter for the interrogation of FBGs is demonstrated.

6.8.1 EDFAs gain flattening

The equalization of an EDFA gain curve was accomplished in three steps (see Figure 6.26). First, the fibre was twisted at a rate of ~2 rad/cm in order to obtain a resonant wavelength at 1531 nm. Afterwards, the grating was performed using the reference configuration except for the use of the 73.9 g weight instead of 41.8 g. Finally, loads up to 410 g were applied to the MLPFG such that the desired transmission loss was obtained. Figure 6.27 shows the gain curve of the EDFA before and after the equalization, as recorded by the OSA set to a resolution of 0.5nm. The difference in the spectral gain was reduced from 9 dB to 2 dB. Further improvements can be achieved by a better choice of the fabrication parameters or through the concatenation of several gratings.

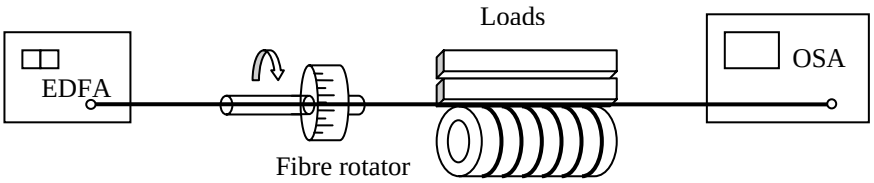

Figure 6.26 – Setup used for the equalization of the EDFA gain curve.

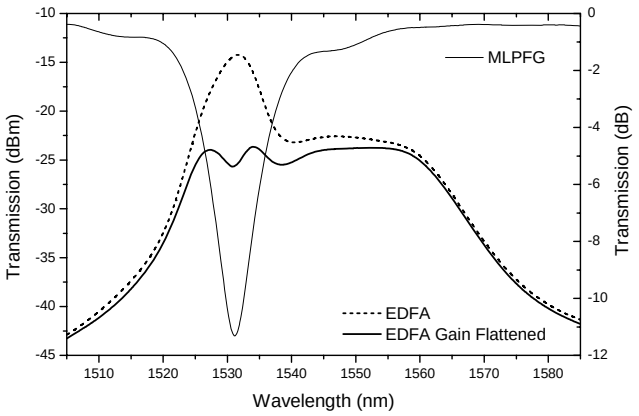

Figure 6.27 – EDFA emission spectrum with a gain flattening optical filter.

6.8.2 Interrogation of a FBG

Another application of these gratings is in sensing schemes to interrogate FBGs where the dynamic range of the physical parameters under measurement can vary considerably. Figure 6.28 shows how MLPFGs can fulfil that requirement. First, the resonant wavelength of a FBG is judiciously chosen such that it is located in the slope of the MLPFG attenuation bands. As shown in section 6.5.2 strain and torsion can be applied to the fibre to position the resonant wavelengths of the MLPFG bands. Then, depending on the sensitivity required to measure some physical parameters, loads are applied to the MLPFG such that a desirable slope of the attenuation band is attained (see Figure 6.29).

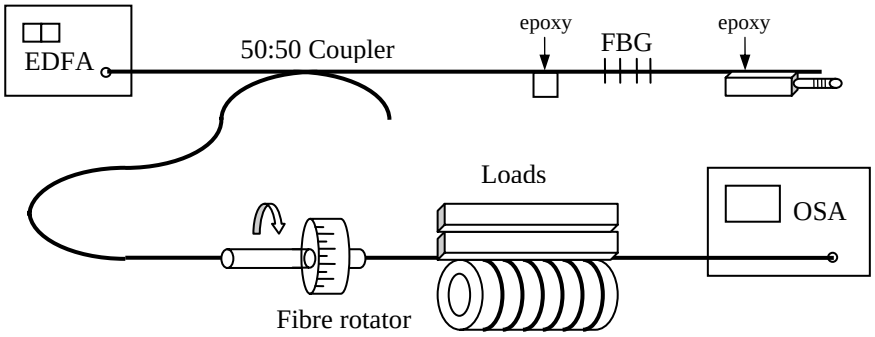

Figure 6.28 – Setup used for the interrogation of the FBG.

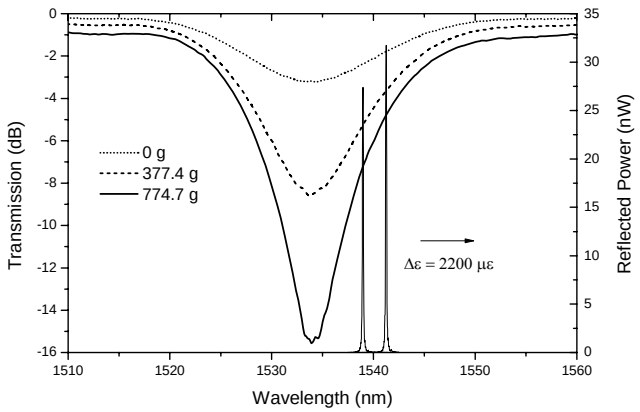

Figure 6.29 FBG interrogation scheme comprising a MLPFG with dynamic control.

For each particular strength of the MLPFG the FBG was submitted to strain up to 2200 με, in steps of 200 με. At each step, the peak wavelength and the reflected power was recorded by the OSA, set to a resolution of 50 pm. Figure 6.30 summarises the achieved results. The FBG strain sensitivity is of 1.14 pm/με (see Figure 6.30a). The detected power can vary from 2.23 nW/με to 3.2 nW/με when changing the MLPFG strength by applying loads up to 774.7 g (see Figure 6.30b).

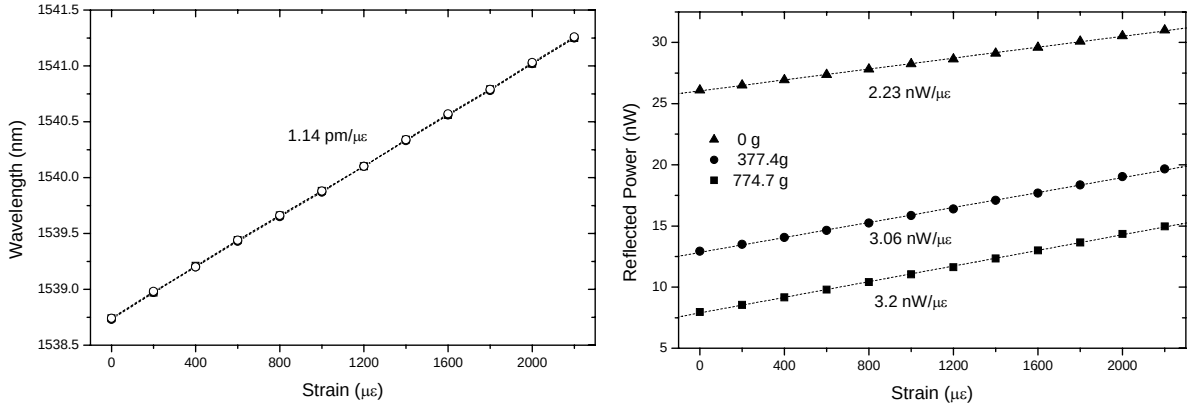

(a) (b)

Figure 6.30 (a) Wavelength and (b) reflected power of the FBG as a function of the applied strain. The FBG is interrogated by a MLPFG whose strength is changed through loads.

6.9 Summary

A simple, flexible and low-cost technique to mechanically induce LPFGs was described. This technique based on periodic microbending has also high reproducibility as far as some intrinsic aspects are well controlled. The produced MLPFGs have low insertion loss (< 0.2

dB), bandwidths ranging from 10 to 30 nm and the transmission loss can be higher than 20 dB. The major advantage of this technique is that it provides a good control over the strength of the resonant bands. Through a proper choice of the fabrication parameters and by changing the number of turns of the string it is possible to control the transmission loss with a precision better than 0.1 dB. Further control can be accomplished by applying external loads. A large tunability of the resonant wavelengths can be achieved through the etching of the fibre cladding before perform the grating. Pre-annealing of the fibre and the fibre twisting are also means to be considered.

As a result of the high sensitivity to loads (20 dB/kg) and the ease of implementation with other structures, these gratings can be used for multi-parameter sensing. MLPFGs performed under certain conditions may exhibit PDL values as high as 18 dB, for particular wavelengths. However, for moderate values of transmission loss a proper choice of the fabrication parameters and/or method, which avoids the use of loads, results in lower PDL values. Therefore, taking also into account that a considerable reduction of the DGD is obtained when a birefringence compensation method is implemented, MLPFGs can act as gain equalizers.

In a future work special attention should be paid to a better understanding of the relaxation effects. Making use of the several advantages of the technique other practical applications should be pursued.

References

[1] J.W. Berthold. *Historical Review of Microbend Fiberoptic Sensors.* Journal of Lightwave Technology **13**(7): 1193-1199, 1995.

[2] C.B. Probst, A. Bjarklev, and S.B. Andreasen. *Experimental-Verification of Microbending Theory Using Mode-Coupling to Discrete Cladding Modes.* Journal of Lightwave Technology **7**(1): 55-61, 1989.

[3] K. Chen, Q. Sheng, and X. Dong. *Band-rejection and bandpass filters based on mechanically induced long-period fiber gratings.* Microwave and Optical Technology Letters **42**(1): 15-17, 2004.

[4] T. Yokouchi, Y. Suzaki, K. Nakagawa, M. Yamauchi, M. Kimura, Y. Mizutani, S. Kimura, and S. Ejima. *Thermal tuning of mechanically induced long-period fiber grating.* Applied Optics **44**(24): 5024-5028, 2004.

[5] S. Savin, M. Digonnet, G. Kino, and H. Shaw. *Tunable mechanically induced long-period fiber gratings.* Optics Letters **25**(10): 710-712, 2000.

[6] M. Yokota, H. Oka, and T. Yoshino. *Mechanically induced long period fiber grating and its application for distributed sensing*. in *OFS 2002: 15th Optical Fiber Sensors Conference Technical Digest*: 135-138, 2002.

[7] H. Kwon, N. Lee, and J. Song. *Narrowband LPFG filter based on a pair of fiber deformers*. in *Conference on Lasers and Electro-Optics 2001, Proceedings*: 262-263, 2001.

[8] W. Xin-Wei, Z. Zhen-Yu, Z. Huai-Xuan, and S. Qiu-Qin. *Spectral characteristics of Mechanically Induced Long-Period Fibre Gratings by New Double-Layer Grating Templates.* Chinese Physics Letters **22**(8): 1951-1954, 2005.

[9] I. Sohn and J. Song. *Gain flattened and improved double-pass two-stage EDFA using microbending long-period fiber gratings.* Optics Communications **236**(1-3): 141-144, 2004.

[10] C.D. Poole, C.D. Townsend, and K.T. Nelson. *Helical-Grating 2-Mode Fiber Spatial-Mode Coupler.* Journal of Lightwave Technology **9**(5): 598-604, 1991.

[11] G. Rego, J. Fernandes, J. Santos, H. Salgado, and P. Marques. *New technique to mechanically induce long-period fibre gratings.* Optics Communications **220**(1-3): 111-118, 2003.

[12] C. Lin, Q. Li, A. Au, Y. Jiang, E. Wu, and H. Lee. *Strain-induced thermally tuned long-period fiber gratings fabricated on a periodically corrugated substrate.* Journal of Lightwave Technology **22**(7): 1818-1827, 2004.

[13] E.B. Wu, R.C. Yang, K.C. San, C.H. Lin, F. Alhassen, and H.P. Lee. *A highly efficient thermally controlled loss-tunable long-period fiber grating on corrugated metal substrate.* IEEE Photonics Technology Letters **17**(3): 612-614, 2005.

[14] R.C. Youngquist, J.L. Brooks, and H.J. Shaw. *Birefringent-Fiber Polarization Coupler.* Optics Letters **8**(12): 656-658, 1983.

[15] R.C. Youngquist, J.L. Brooks, and H.J. Shaw. *2-Mode Fiber Modal Coupler.* Optics Letters **9**(5): 177-179, 1984.

[16] S. Veeriah, A.R. Faidz, Y.N. Phua, and V. Mishra. *Broadband spectrum based on mechanically induced cascaded long-period fibre gratings.* Microwave and Optical Technology Letters **44**(5): 463-465, 2005.

[17] S. Ramachandran, M.F. Yan, E. Monberg, F.V. Dimarcello, P. Wisk, and S. Ghalmi. *Record bandwidth, spectrally flat coupling with microbend gratings in dispersion-tailored fibers.* IEEE Photonics Technology Letters **15**(11): 1561-1563, 2003.

[18] K.R. Sohn and K. Taek. *Multiwavelength all-fiber ring laser using side-polished fiber comb filter and mechanically formed long-period fiber gratings.* IEEE Photonics Technology Letters **17**(2): 309-311, 2005.

[19] I.B. Sohn, J.G. Baek, N.K. Lee, H.W. Kwon, and J.W. Song. *Gain flattened and improved EDFA using microbending long-period fibre gratings.* Electronics Letters **38**(22): 1324-1325, 2002.

[20] M. Tachibana, R.I. Laming, P.R. Morkel, and D.N. Payne. *Erbium-Doped Fiber Amplifier with Flattened Gain Spectrum.* IEEE Photonics Technology Letters **3**(2): 118-120, 1991.

[21] J. Cho and K. Lee. *PDL-compensated mechanically induced long-period grating for EDFA gain flattening.* Fiber and Integrated Optics **23**(6): 447-451, 2004.

[22] K.R. Sohn and K.T. Kim. *Thermo-optically tunable band-rejection filters using mechanically formed long-period fiber gratings.* Optics Letters **30**(20): 2688-2690, 2005.

[23] C.H. Lin, Q. Li, and H.P. Lee. *Periodic microbending-induced core-to-cladding mode coupling in polarization-maintaining fibers.* Optics Letters **28**(12): 998-1000, 2003.

[24] G. Rego, M. Morais, J.L. Santos, and H.M. Salgado. *PDL and DGD measurements of mechanically induced long-period fiber gratings*. in *London Communications Symposium 2003, Proceedings*: 77-80, 2003.

[25] J. Cho and K. Lee. *A birefringence compensation method for mechanically induced long-period fiber gratings.* Optics Communications **213**(4-6): 281-284, 2002.

[26] J.W. Ham, J.H. Lee, J.Y. Cho, H.S. Jang, and K.S. Lee. *A birefringence compensation method for mechanically induced long-period fiber gratings in optical communication and sensing systems*. in *OFS 2002: 15th Optical Fiber Sensors Conference Technical Digest*: 565-568, 2002.

[27] J.Y. Cho, J.H. Lim, and K.S. Lee. *Optical fiber twist sensor with two orthogonally oriented mechanically induced long-period grating sections.* IEEE Photonics Technology Letters **17**(2): 453-455, 2005.

[28] X. Shu, K. Chisholm, I. Felmeri, L. Everall, K. Sugden, A. Gillooly, L. Zhang, and I. Bennion. *Novel optical load sensors based on mechanically induced sampled fiber Bragg gratings*. in *OFS 2003: 16th Optical Fiber Sensors Conference Technical Digest*: 654-657, 2003.

[29] J.L. Arce-Diego, J. Gonzalez-Garcia, D. Pereda-Cubian, and D.A. Gonzalez-Fernandez. *Optical fiber transducer based on LPFG and microbends for multi-parameter sensing*. in *LEOS 2001: 14th Annual Meeting of the IEEE Lasers & Electro-Optics Society, Vols 1 And 2, Proceedings*: 782-783, 2001.

[30] J.L. Arce-Diego, J.P. Campo, and D.P. Cubian. *Optical fibre transducer based on SPFG and microbends for multi-parameter sensing*. in *Proceedings of 2002 IEEE/LEOS Workshop on Fibre and Optical Passive Components*: 176-181, 2002.

[31] G. Rego, H. Salgado, and J. Santos. *Interrogation of a Fiber Bragg Grating using a Mechanically Induced Long-Period Fiber Grating.* IEEE Sensors Journal (to be published), 2006.

[32] M. van Eijkelenborg, W. Padden, and J. Besley. *Mechanically induced long-period gratings in microstructured polymer fibre.* Optics Communications **236**(1-3): 75-78, 2004.

[33] J. Lim, H. Jang, K. Lee, J. Kim, and B. Lee. *Mach-Zehnder interferometer formed in a photonic crystal fiber based on a pair of long-period fiber gratings.* Optics Letters **29**(4): 346-348, 2004.

[34] J.H. Lim, K.S. Lee, J.C. Kim, and B.H. Lee. *Tunable fiber gratings fabricated in photonic crystal fiber by use of mechanical pressure.* Optics Letters **29**(4): 331-333, 2004.

[35] J. Kim, G.J. Kong, U.C. Paek, K.S. Lee, and B.H. Lee. *Demonstration of an ultra-wide wavelength tunable band rejection filter implemented with photonic crystal fiber*. IEICE Transactions on Electronics **E88C**(5): 920-924, 2005.

[36] M.D. Nielsen, G. Vienne, J.R. Folkenberg, and A. Bjarklev. *Investigation of microdeformation-induced attenuation spectra in a photonic crystal fiber*. Optics Letters **28**(4): 236-238, 2003.

[37] A. Bjarklev and S.B. Andreasen. *Microbending Characterization of Optical Fibers from Artificially Induced Deformation.* Electronics Letters **25**(6): 417-419, 1989.

[38] S.A. Vasiliev, E.M. Dianov, D. Varelas, H.G. Limberger, and R.P. Salathe. *Postfabrication resonance peak positioning of long-period cladding-mode-coupled gratings.* Optics Letters **21**(22): 1830-1832, 1996.

[39] K. Zhou, H. Liu, and X. Hu. *Tuning the resonant wavelength of long period fiber gratings by etching the fiber's cladding.* Optics Communications **197**(4-6): 295-299, 2001.

[40] S.C. Kim, Y.C. Jeong, S.W. Kim, J.J. Kwon, N.K. Park, and B.H. Lee. *Control of the characteristics of a long-period grating by cladding etching.* Applied Optics **39**(13): 2038-2042, 2000.

[41] O.V. Ivanov. *Wavelength shift and split microbend long-period of cladding mode resonances in fiber gratings under torsion.* Optics Communications **232**(1-6): 159-166, 2004.

[42] A.D. Yablon. *Optical and mechanical effects of frozen-in stresses and strains in optical fibers.* IEEE Journal of Selected Topics in Quantum Electronics **10**(2): 300-311, 2004.

[43] F. Durr, G. Rego, P.V.S. Marques, S.L. Semjonov, E. Dianov, H.G. Limberger, and R.P. Salathe. *Stress Profiling of Arc-Induced Long Period Fiber Gratings.* Journal of Lightwave Technology **23**(11): 3947-3953, 2005.

[44] Y.H. Zhu, E. Simova, P. Berini, and C.P. Grover. *A comparison of wavelength dependent polarization dependent loss measurements in fiber gratings.* IEEE Transactions on Instrumentation and Measurement **49**(6): 1231-1239, 2000.

[45] B. Huttner, C. Geiser, and N. Gisin. *Polarization-induced distortions in optical fiber networks with polarization-mode dispersion and polarization-dependent losses.* IEEE Journal of Selected Topics in Quantum Electronics **6**(2): 317-329, 2000.

[46] S.E. Golowich and S. Ramachandran. *Impact of fiber design on polarization dependence in microbend gratings.* Optics Express **13**(18): 6870-6877, 2005.

7

Fabrication of devices through arc-discharges

7.1 Introduction

The electric arc technique has a wide range of application being particularly useful in the fabrication of fibre optic devices. Besides fibre optics, its huge potentiality is well patented in Chapter 4, where electrically insulated platinum-platinum/rhodium thermocouples were fabricated by applying arc discharges. Although this work is dedicated to arc-induced gratings it is worthwhile discussing other devices that can be produced by this versatile technique.

In this chapter the fabrication of more complex fibre optic components based on fibre Bragg gratings (FBGs) and long-period fibre gratings (LPFGs) is described, namely, bandpass filters and sampled FBGs (SFBGs). The apodisation of FBGs through arc discharges is also demonstrated.

7.2 Applications of the electric arc technique

As far as fibre optics technology is concerned, arc discharges were first applied to fibre fusion splicing [1, 2]. Afterwards, several other fibre optics components appeared. The simplest example is a fibre taper, which can be produced in a straightforward way by applying a time controllable arc discharge whilst the fibre is kept under a constant tension. The loss evolution can be followed by an optical spectrum analyser (or an optical power meter). The length of the taper region can be controlled by displacing the fibre during the arc discharge [3]. If the previous process is further continued a fibre probe may be achieved, that is, the fibre is stretched till rupture, the dimensions of the fibre tip being of the order of 100 nm [4]. Optical fibre probes can be used for atomic force microscopy. Fibre couplers and wavelength division multiplexers are two other examples of important devices that have been fabricated by this technique [5, 6]. Based on core dopants diffusion the fabrication of modefield expanders [7, 8] was also demonstrated. As discussed in Chapter 3 the same mechanism was also proposed

for the formation of LPFGs [9, 10]. So far in this work, only single arc-induced gratings were treated, however more complex structures can be fabricated.

The typical loss band of a LPFG can be converted into a bandpass by inserting a phase shift in the middle of the grating during its fabrication. This can be accomplished by applying one or more arc discharges in the middle of a LPFG. Figure 7.1(a) shows a π-shift grating obtained after submitting a LPFG, induced in the Sumitomo fibre by using the setup described in Appendix A.5, to 5 extra arc-discharges applied to its centre. Exposing a short section in the middle of a grating to UV-radiation also leads to a similar result (Figure 7.1(b)). In this case, a grating with a length of 24 mm was initially arc-induced in the B/Ge co-doped fibre, from Fibrecore, and afterwards a region with a length of 1 mm was exposed during 30 min to a fluence per pulse of ~0.7 J/cm^2 and at a repetition rate of 20 Hz. The drawback associated to the use of UV radiation instead of arc discharges is that the former decays with temperature, and therefore those gratings cannot be used at high temperatures (they are erasable above 400 ºC). A different approach to reach the same goal was demonstrated in arc-induced gratings by Humbert *et al.* [11]. There, a phase shift in the middle of the grating is produced by changing the grating pitch by half a period. Figure 7.2 shows the initial and final spectra of a phase-shift grating arc-induced in the Corning SMF-28 fibre using the following fabrication parameters: weight of 5.1 g, a period of 540 μm, an electric current of 9.5 mA, an arc duration of 1 s and 35 discharges were produced on each side of the phase shift region (displacement of 118 μm) [12].

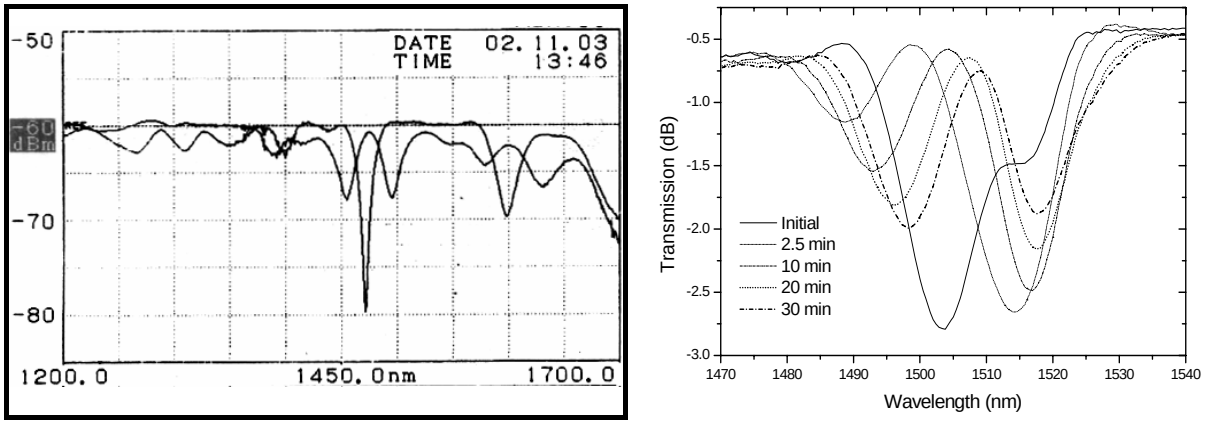

(a) (b)

Figure 7.1 – (a) π-shift produced after 5 arc discharges in the middle of the grating; (b) Evolution of the phase-shifted LPFG during the UV-exposure.

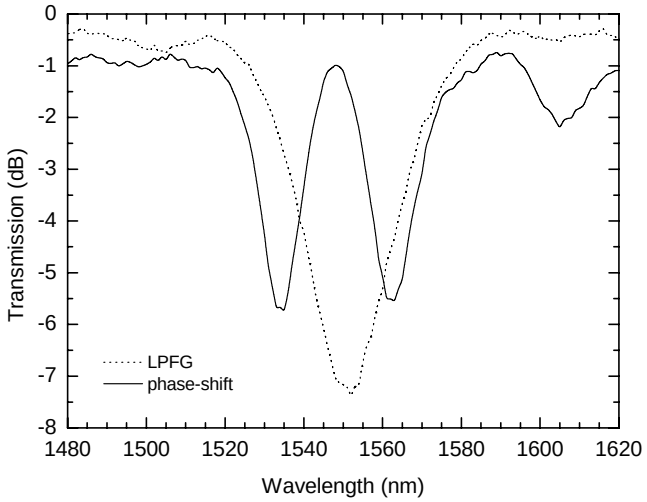

Figure 7.2 – Grating transmission spectra before and after the phase-shift.

The concatenation of two identical LPFGs leads to a well known Mach-Zehnder interferometer (Figure 7.3). This figure shows the transmission spectrum of two LPFGs arc-induced in the B/Ge co-doped fibre (5.1 g, 9 mA, 0.5 s, 425 μm, 60 discharges), each having a transmission loss of 3 dB at 1.55 μm. One half of the light is coupled from the fundamental mode to the cladding mode and the other half goes through the core. These two paths can be seen as arms of an interferometer, since the light that is guided by the cladding is coupled back by the second grating it interferes with the light guided by the core. However, as will be discussed in section 7.5, if a core mode blocker is created in between the two gratings a bandpass filter is generated.

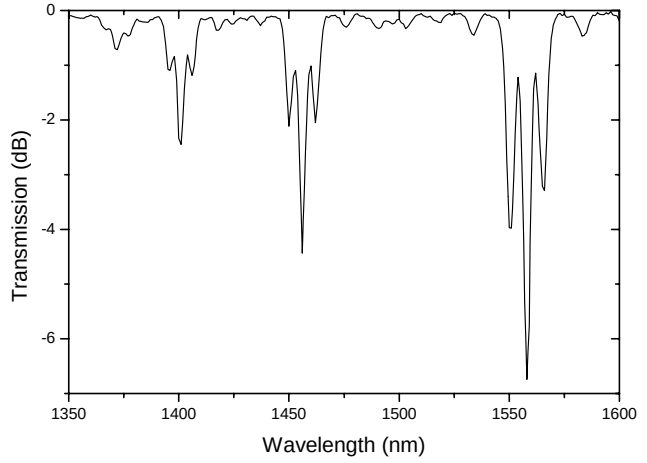

Figure 7.3 – Transmission spectrum of two concatenated LPFGs (Mach-Zehnder) separated by ~25 mm.

Arc discharges can also be used to produce Fabry-Perot (F-P) filters by applying them in the middle of a UV-induced FBG. A 10 mm-long Bragg grating under tension, caused by a weight of 5.1 g, was submitted to electric arc discharges of 8.5 mA during 0.5 s each. Figure

7.4 shows the original reflection spectrum of the grating and the afterwards evolution of the F-P filter. It is interesting to note that after 5 consecutive discharges in the same physical place the initial F-P spectrum was recovered, i.e., the F-P spectra correspondent to the first and sixth discharges are equal. This is probably due to a phase change of 2π caused by an elongation of the B/Ge co-doped fibre during the arc discharges, since the periodicity of this process remained constant even after 50 arc discharges and, therefore, could not be explained by thermal annealing of the fibre photosensitivity due to the discharges.

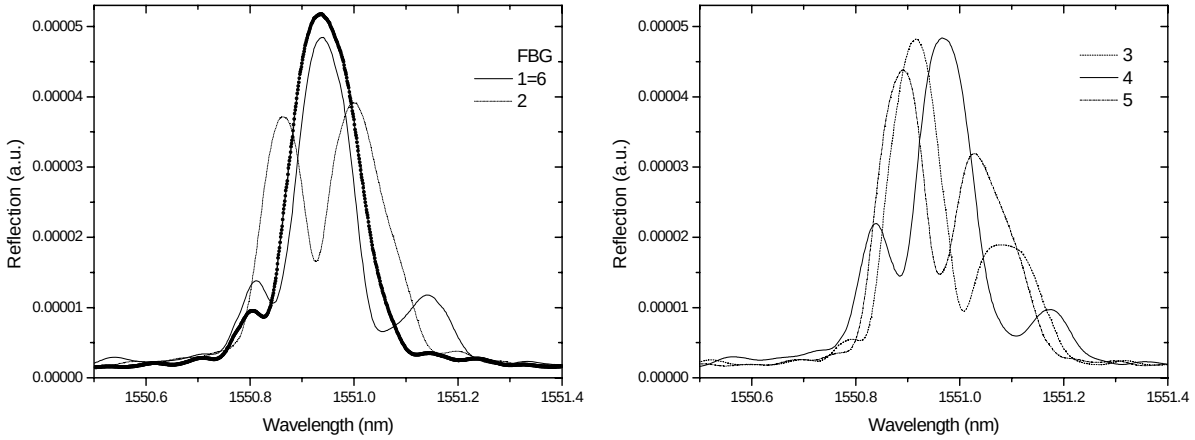

Figure 7.4 – Fabry-Perot spectrum regarding the number of arc-discharges: (a) 0-2 and 1≡6; (b) 3-5.

Finally, the electric arc technique also allows to apodise FBGs [13] and to fabricate SFBGs [14]. For their relevance these two topics and the fabrication of bandpass filters will be described in the following sections.

7.3 Apodisation of fibre Bragg gratings

The well known spectral response of uniform fibre Bragg gratings (FBGs) is not desirable in some optical communications applications due to the presence of side-lobes which are caused by the step produced in the effective refractive index. The apodisation of a FBG gives not only a reduction of the side lobes but also changes its dispersion characteristics. Several methods have been used to apodise FBGs, namely, a phase mask with variable diffraction efficiency [15], automatic pure apodisation through a phase mask [16], stretching the fibre [17] and UV-pulse interferometry [18]. In this section the symmetric apodisation of a FBG using electric arc discharges is presented.

To demonstrate the apodisation method, a uniform 5 mm long FBG centred at $\lambda_B = 1555$ nm and with a bandwidth (FWHM) of 0.3 nm was photoimprinted using a diffractive phase mask illuminated with a KrF excimer laser operating at 248 nm. The length of the FBG was chosen in order to be possible to measure the side-lobes in the optical spectrum analyser (OSA) at its maximum resolution of 0.08 nm.

Figure 7.5 shows a close view of the FBG apodisation set-up. The fibre, placed in a motorized translation stage with a resolution of 0.1 μm, was longitudinally moved along its axis in such way that the grating was moved towards the heating zone in steps of 200 μm. On each step an electric arc discharge was produced with a current less than 9 mA during 0.5 s. After the grating have sensed the heat from the arc discharge for the first time, the steps were decreased to 50 μm and the time duration, t, was increased exponentially from 0.5 s to 2.5 s (according to the empirical relation: $t = 0.5\ e^{5\ i/(k-1)}$, where $i = 1$ until $I = 35$ with $k = 100$ to control the increasing of the time) as the grating was approaching the arc discharge region; 35 electric arc discharges on each side of the grating were needed to achieve the apodised grating shown in Figure 7.6. The fibre movement and the arc discharges were synchronised by a personal computer. The whole process was monitored in real time using a broadband optical source and an OSA in order to obtain the best reflection spectrum for the apodisation profile.

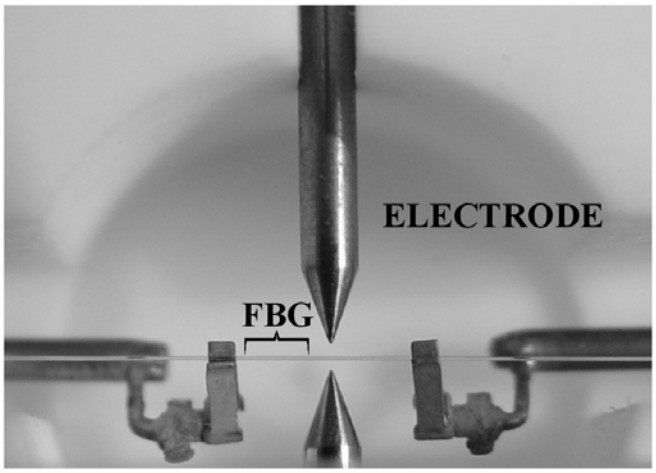

Figure 7.5 –Photograph showing in detail the main part of the apodisation setup (Appendix A.4).

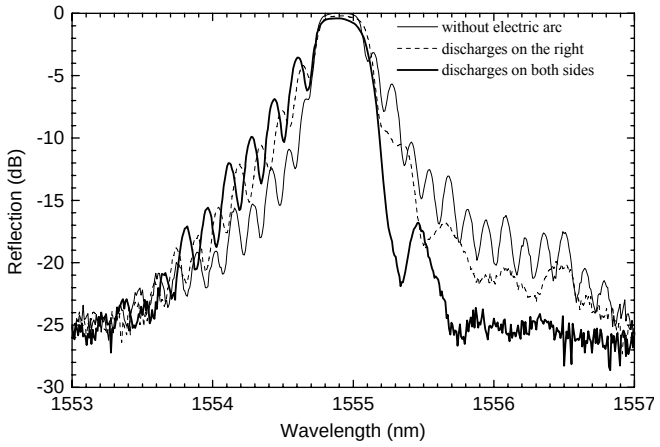

Figure 7.6 – Reflection spectra versus wavelength. Initial FBG (solid line), FBG with 35 discharges on the right (dash line) and FBG with 35 discharges on both sides (bold solid line).

The reflection spectrum of the grating after the apodisation process (Figure 7.6) shows that the longer wavelength side-lobes were reduced due to the smoothing of the refractive index modulation profile, as caused by the high temperature annealing during the arc discharges. The shorter wavelength resonances became more evident as a result of the effective refractive index change that produces cavity effects at those wavelengths [19, 20]. The spectrum also shows a slight decrease of the peak reflectivity as expected since the refractive index modulation step profile was partially erased.

These results enable one to conclude that a non-uniform effective index longitudinal distribution was obtained after the apodisation process instead of the uniform FBG. Better results are expected if a preconditioning photosensitivity response and effective index profile are accomplished by exposing the fibre to the electric arc before the grating photoinscription in the same region.

7.4 Sampled fibre Bragg gratings

A sampled fibre Bragg grating (SFBG) is a contradirectional coupling grating whose effective refractive index amplitude and/or phase is modulated through a long periodic structure. The special reflection characteristics of SFBGs make them very useful and attractive devices for optical communications and fibre sensors. Several methods have been proposed to produce SFBGs: translating an ultraviolet writing beam along a fibre/phase mask assembly while its intensity is periodically varied [21], writing a periodic sinc modulation of the refractive index profile plane by plane [22] and using a long period index modulation based on photoelastic

effect [23]. In this section the fabrication of a superstructure grating by writing a FBG with a 248 nm UV source over an arc-induced LPFG is demonstrated.

The fabrication of the SFBG comprises two different stages. In the first a LPFG (22.8 g, < 10 mA, 1 s, 400 μm, 66 discharges) is written in a Corning dispersion-shifted fibre using the setup described in Appendix A.4. Prior to the writing of the Bragg grating the LPFG was kept under high-pressure hydrogen atmosphere in order to enhance its photosensitivity due to hydrogen diffusion into the glass matrix. In the second stage a 10 mm long FBG was written over the LPFG using a uniform diffractive phase mask illuminated with a KrF laser operating at 248 nm to give rise to the SFBG.

The superstructure is originated by a periodic modulation of the effective refractive index amplitude caused by the multiplication of two signals of different spatial frequencies (a rapidly varying component with period Λ and a slowly varying envelope with a period M). The spatial frequency content of this superstructure can be approximated by a comb of delta functions centred at the Bragg frequency [21]. In terms of reflection spectrum there will be reflection peaks separated in wavelength by $\Delta\lambda = \lambda_B^2/(2\, n_{eff}\, M)$. Separations in the range of 1.5 to 3.5 nm were obtained for periods M ranging from 250 to 600 μm. Figure 7.7(a)-(b) show respectively, the reflection spectrum of a LPFG with 521 μm period and the experimentally determined variation of $\Delta\lambda$ with the period M of the LPFG, being clear a good agreement with the values derived from the theoretical equation.

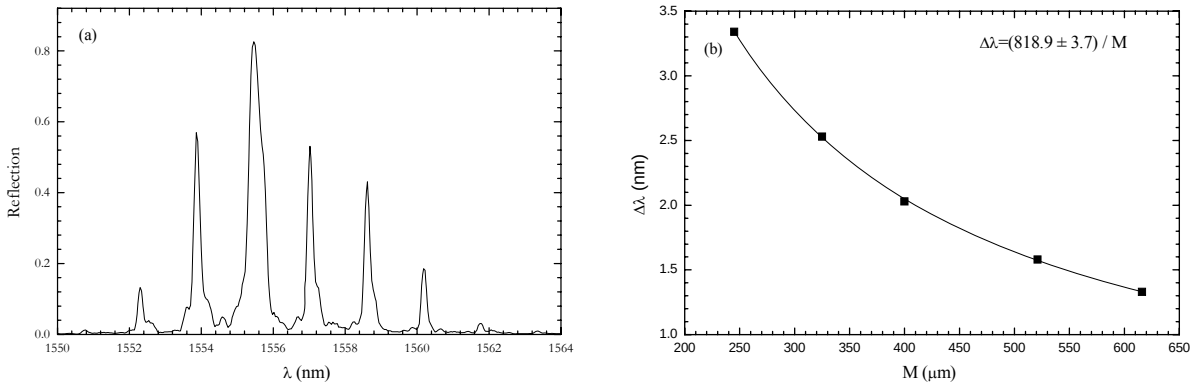

(a) (b)

Figure 7.7 – (a) Reflection spectrum of a sampled FBG; (b) Variation of Δλ with the LPFG period (M).

Further work is needed to understand the reasons for the formation of the SFBGs. Preliminary results indicate that LPFGs fabricated by the setup described in Appendix A.4 allow a better growth of the sampled FBGs when compared to the ones fabricated by the BICC fusion splicer. The reason may be related to the fact that in the former the lateral

dimension of the arc is smaller and the discharge has an higher energy density. Therefore, a larger region is available for the grating to grow and the annealing might be more effective. It is also not clear if fibre tapering also contributes to the formation of the sampled structure.

Another question that arises is the following: if the region heated by the arc is not completely annealed, it is expected that each of the several reflection peaks may consist in two peaks as Figure 7.7(a) in fact suggests. That can be explained by the different averaged refractive indices exhibited by the pristine and heated regions which may enable the simultaneous inscription of two SFBGs. To investigate this possibility, a SFBG was produced by writing a FBG over a LPFG arc-induced in the Sumitomo fibre using the setup described in Appendix A.4. Afterwards, a single reflection peak from the SFBG was swept by a wavelength tunable laser, in steps of 1 pm, the radiation being detected by an optical power meter. However, as shown in Figure 7.8 each reflection peak seems to be a single one. The reason for the different results may be related with the fibres composition, since the former has its core doped with 12 mol% of germanium whilst the latter contains only 1.5 mol%. Therefore, this study was not conclusive regarding the effect of the electric arc discharges on the fibre's photosensitivity.

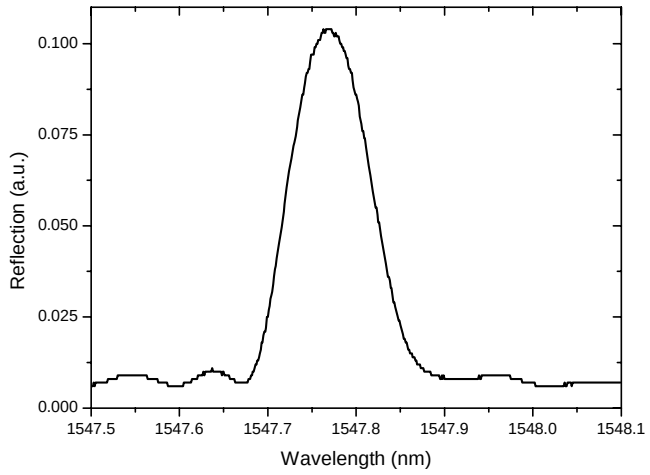

Figure 7.8 – Single reflection peak from a SFBG.

SFBGs enable the implementation of multiwavelength fibre laser sources [14] and, in the sensing domain they can be used for simultaneous measurement of temperature and strain as will be discussed in the next chapter.

7.5 Core mode blockers

A bandpass filter based on long-period fibre gratings was first proposed by Starodubov *et al.* [24]. The key element for the fabrication of such filters is the core mode blocker (CMB), that is, in between the two identical concatenated LPFGs the core of the fibre is destroyed such that light is no longer guided by the fundamental mode. Therefore, light that is rejected by the first grating is afterwards coupled back by the second one, the transmission spectrum of the bandpass filter being similar to the inverted spectrum of the individual gratings. In this section the means to create the core mode blocker will be discussed.

A CMB can be obtained by exposing a hydrogenated Ge-doped fibre to intense near-UV light (300-305 nm), the core being destroyed by a local thermal effect [24] or by exposing a hydrogenated B/Ge co-doped fibre to an electric arc discharge [25]. Core damage can also be achieved by the fibre fuse effect [26, 27] initiated by an argon ion laser [28].

A different approach to have the fundamental mode blocked and that can be applied to any kind of fibre, is by inserting a short section of a silica capillary in between the two LPFGs [29]. To keep the insertion loss low the capillary diameter should be close to the core diameter of the fibre. Prior to have knowledge of this work, we have also obtained core mode blockers by using a silica capillary with a diameter of 25 μm (the same that was used for measuring the fibre temperature in Chapter 4).

Figure 7.9(a) shows the spectra of two arc-induced gratings having a transmission loss of approximately 3 dB at ~1.55 μm. A core mode blocker was then produced in between the gratings by splicing a short section, less than 0.5 mm, of the silica capillary. The spectrum of the resultant bandpass filter is shown in Figure 7.9(b). As expected the insertion loss is very high, nevertheless, the obtained isolation, above 30 dB, is an interesting result.

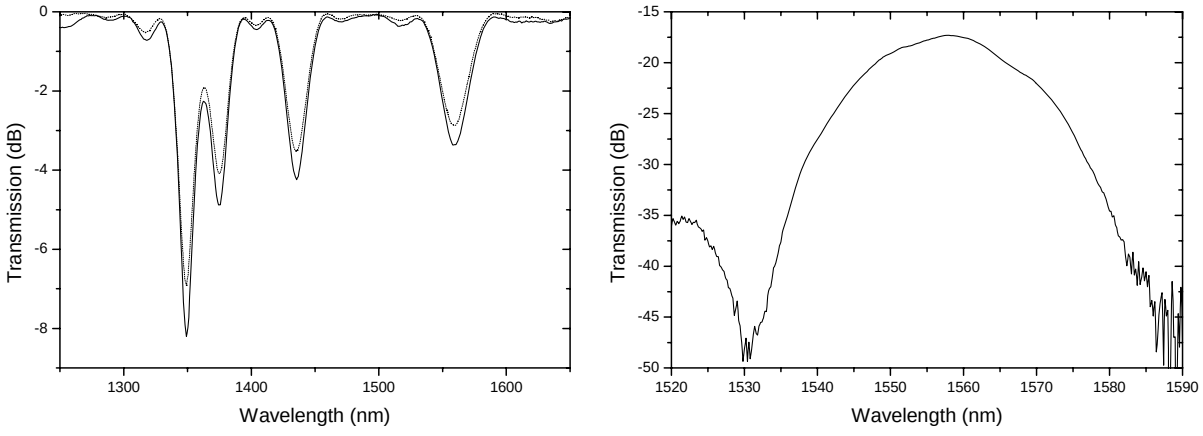

(a) (b)

Figure 7.9 – (a) LPFGs transmission spectra; (b) Bandpass filter.

Through the capillary technique several core mode blockers were produced using the Fitel fusion splicer being the parameters of the discharge set to values well below the ones used for splicing standard fibres. Figure 7.10(a) shows a photograph of a typical CMB

fabricated. Note that several arc discharges were applied in the same physical place to reduce the dimensions of the capillary in the splice region. The performance of the CMB as bandpass filters was evaluated through mechanically induced long-period fibre gratings (MLPFGs). A MLPFG was produced by the technique described in the previous chapter, in a fibre containing a CMB. The grating is located near the CMB and its transmission spectrum is shown in Figure 7.10(b). Afterwards, a second MLPFG was fabricated after the CMB. The evolution of the transmission spectrum of the bandpass filter as a function of the number of turns of the nylon string is shown in Figure 7.11(a). The lowest insertion loss and the highest isolation were obtained after 33 turns, however the side-lobes in the transmission

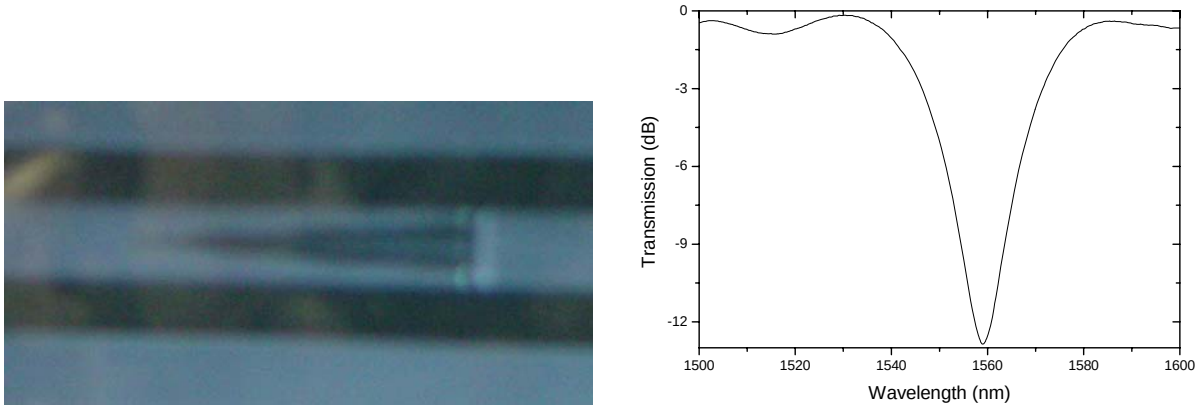

(a) (b)

Figure 7.10 – (a) Typical photograph of the region containing the capillary after the splices; (b) MLPFG transmission spectrum.

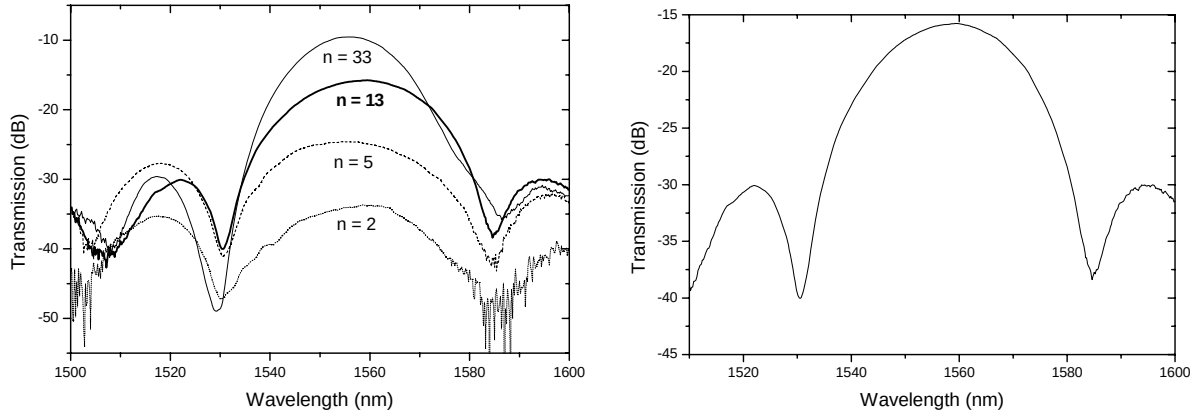

(a) (b)

Figure 7.11 – (a) Evolution of the transmission spectrum of the bandpass filter for different number of turns; (b) Transmission spectrum of the bandpass filter for 13 turns of the nylon string during the fabrication of the second grating.

spectrum are asymmetric. Figure 7.11(b) shows a symmetric spectrum that was obtained after only 13 turns.

Bandpass filters are very important in the optics communication field and several applications have been proposed in the literature [30-32].

7.6 Summary

In this chapter the potentialities of the electric arc technique to produce devices other than long-period fibre gratings were highlighted. In particular, two novel applications were presented, the apodisation of fibre Bragg gratings and the inscription of sampled FBGs based on arc induced LPFGs. The fabrication of a bandpass filter based on a core mode blocker inserted between two LPFGs was also described.

In future work it would be interesting to have a better understanding of the formation of the sampled FBGs. Further work is also required to understand the implications of writing the FBG at the ends or in the middle of the LPFG. Besides the physical location, the choice of the resonance wavelengths of both gratings is also important. The improvement of the apodisation process may also be pursued. Bandpass filters are very promising devices and therefore, special attention should be paid to their optimised fabrication as well as applications.

References

[1] D.L. Bisbee. *Splicing Silica Fibers with an Electric-Arc.* Applied Optics **15**(3): 796-798, 1976.

[2] I. Hatakeyama and H. Tsuchiya. *Fusion Splices for Optical Fibers by Discharge Heating.* Applied Optics **17**(12): 1959-1964, 1978.

[3] A. Ishikura, Y. Kato, and M. Miyauchi. *Taper Splice Method for Single-Mode Fibers.* Applied Optics **25**(19): 3460-3465, 1986.

[4] H.N. Lin, U. Lewlomphaisarl, S.H. Chen, L.J. Lee, and D.P. Tsai. *Controllable fabrication of bent near-field optical fiber probes by electric arc heating.* Review of Scientific Instruments **69**(11): 3843-3845, 1998.

[5] F.M. Araújo. *Redes de Bragg em Fibra Óptica*, in *PhD. Thesis*. Universidade do Porto. 225-231 & 359-360, 1999

[6] K. Morishita and D. Yamamoto. *Fused fiber couplers wavelength-flattened by arc discharge*. in *Proceedings of 2005 IEEE/LEOS Workshop on Fibre And Optical Passive Components*: 187-191, 2005.

[7] V.I. Karpov, M.V. Grekov, E.M. Dianov, K.M. Golant, S.A. Vasiliev, O.I. Medvedkov, and R.R. Khrapko. *Mode-field converters and long-period gratings fabricated by thermo-diffusion in nitrogen-doped silica-core fibers*. in *Proceedings of 1998 Optical Fiber Communications Conference*: 279-280, 1998.

[8] K. Shiraishi, Y. Aizawa, and S. Kawakami. *Beam Expanding Fiber Using Thermal-Diffusion of the Dopant.* Journal of Lightwave Technology **8**(8): 1151-1161, 1990.

[9] E.M. Dianov, V.I. Karpov, M.V. Grekov, K.M. Golant, S.A. Vasiliev, O.I. Medvedkov, and R.R. Khrapko. *Thermo-induced long-period fibre gratings*. in *IOCC-ECOC 97 - 11th International Conference on Integrated Optics and Optical Fibre Communications / 23rd European Conference on Optical Communications, Vol 2*: 53-56, 1997.

[10] S.G. Kosinski and A.M. Vengsarkar. *Splice-based long-period fiber gratings*. in *Proceedings of 1998 Optical Fiber Communications Conference*: 278-279, 1998.

[11] G. Humbert and A. Malki. *High performance bandpass filters based on electric arc-induced pi-shifted long-period fibre gratings.* Electronics Letters **39**(21): 1506-1507, 2003.

[12] R. Falate, O. Frazao, G. Rego, J.L. Fabris, and J.L. Santos. *Refractometric Sensor Based on a Phase-Shifted Long Period Fiber Grating.* Applied Optics **45** (21): 5066-5072, 2006.

[13] G. Rego, R. Romero, O. Frazão, P.V.S. Marques, and H.M. Salgado. *Apodisation of uniform Fibre Bragg Gratings using electric arc discharges*. in *Proceedings of 2002 IEEE/LEOS Workshop on Fibre and Optical Passive Components*: 13-16, 2002.

[14] R. Romero, O. Frazão, G. Rego, P.V.S. Marques, and H.M. Salgado. *Sampled Fibre Bragg Gratings Fabrication using an Electric Arc and their Applications*. in *Proceedings of 2002 Course on Photosensitivity in Optical Waveguides and Glasses*: paper 43/WA5, 2002.

[15] J. Albert, K.O. Hill, B. Malo, S. Theriault, F. Bilodeau, D.C. Johnson, and L.E. Erickson. *Apodization of the Spectral Response of Fiber Bragg Gratings Using a Phase Mask with Variable Diffraction Efficiency.* Electronics Letters **31**(3): 222-223, 1995.

[16] J. Albert, K.O. Hill, D.C. Johnson, F. Bilodeau, and M. Rooks. *Moire phase masks for automatic pure apodisation of fibre Bragg gratings.* Electronics Letters **32**(4): 222-223, 1996.

[17] R. Kashyap, A. Swanton, and D.J. Armes. *Simple technique for apodising chirped and unchirped fibre Bragg gratings.* Electronics Letters **32**(13): 1226-1228, 1996.

[18] P.Y. Cortes, F. Ouellette, and S. LaRochelle. *Intrinsic apodisation of Bragg gratings written using UV-pulse interferometry.* Electronics Letters **34**(4): 396-397, 1998.

[19] T. Erdogan. *Fiber grating spectra.* Journal of Lightwave Technology **15**(8): 1277-1294, 1997.

[20] V. Mizrahi and J.E. Sipe. *Optical-Properties of Photosensitive Fiber Phase Gratings.* Journal of Lightwave Technology **11**(10): 1513-1517, 1993.

[21] B.J. Eggleton, P.A. Krug, L. Poladian, and F. Ouellette. *Long Periodic Superstructure Bragg Gratings in Optical Fibers.* Electronics Letters **30**(19): 1620-1622, 1994.

[22] M. Ibsen, M.K. Durkin, M.J. Cole, and R.I. Laming. *Sinc-sampled fiber Bragg gratings for identical multiple wavelength operation.* IEEE Photonics Technology Letters **10**(6): 842-844, 1998.

[23] C.Y. Lin, G.W. Chern, and L.A. Wang. *Periodical corrugated structure for forming sampled fiber Bragg grating and long-period fiber grating with tunable coupling strength.* Journal of Lightwave Technology **19**(8): 1212-1220, 2001.

[24] D.S. Starodubov, V. Grubsky, and J. Feinberg. *All-fiber bandpass filter with adjustable transmission using cladding-mode coupling.* IEEE Photonics Technology Letters **10**(11): 1590-1592, 1998.

[25] Y.G. Han, S.H. Kim, S.B. Lee, U.C. Paek, and Y. Chung. *Development of core mode blocker with H-2-loaded Ge-B codoped fibres.* Electronics Letters **39**(15): 1107-1108, 2003.

[26] Y. Shuto, S. Yanagi, S. Asakawa, M. Kobayashi, and R. Nagase. *Simulation of fiber fuse phenomenon in single-mode optical fibers.* Journal of Lightwave Technology **21**(11): 2511-2517, 2003.

[27] R. Kashyap and K.J. Blow. *Observation of Catastrophic Self-Propelled Self-Focusing in Optical Fibers.* Electronics Letters **24**(1): 47-49, 1988.

[28] T.E. Dimmick, D.A. Satorius, and G.L. Burdge. *All-fiber acousto-optic tunable bandpass filter*. in *Proceedings of 2001 Optical Fiber Communications Conference*: Paper WJ3, 2001.

[29] S. Choi, T.J. Eom, J.W. Yu, B.H. Lee, and K. Oh. *Novel all-fiber bandpass filter based on hollow optical fiber.* IEEE Photonics Technology Letters **14**(12): 1701-1703, 2002.

[30] S. Choi, T.J. Eom, Y. Jung, B.H. Lee, J.W. Lee, and K. Oh. *Broad-band tunable all-fiber bandpass filter based on hollow optical fiber and long-period grating pair.* IEEE Photonics Technology Letters **17**(1): 115-117, 2005.

[31] S. Choi, K. Oh, W. Shin, C.S. Park, U.C. Paek, K.J. Park, Y.C. Chung, G.Y. Kim, and Y.G. Lee. *Novel mode converter based on hollow optical fiber for gigabit LAN communication.* IEEE Photonics Technology Letters **14**(2): 248-250, 2002.

[32] Y. Han, S. Kim, and S. Lee. *Flexibly tunable multichannel filter and bandpass filter based on long-period fiber gratings.* Optics Express **12**(9): 1902-1907, 2004.

8

Applications of arc-induced gratings in optical communications and sensing

8.1 Introduction

In previous chapters we have described the technique by which gratings are induced by arc discharges in optical fibres, followed by a fully characterisation of the influence of the fabrication parameters on their spectra and on the sensitivity to changes of distinct physical parameters. Along this thesis several properties of arc-induced gratings were highlighted, being therefore the moment to discuss some of their applications.

In this chapter it will be presented several applications of long-period fibre gratings (LPFGs) in the optical communications and fibre sensing fields. In the former, special attention will be paid to the equalization of the gain curve of erbium-doped fibre amplifiers (EDFAs) and to suppression of amplified spontaneous emission in Er/Yb fibre lasers. In the latter, several sensor heads able to discriminate between temperature and strain will be described. Measurement of the refractive index of the surrounding medium based on LPFGs is also presented. Finally, a potential and important application of gratings fabricated in pure-silica-core fibres for monitoring structural integrity in nuclear facilities is also discussed.

8.2 Applications of arc-induced LPFGs

In Chapter 5 it was presented the thermal behaviour of gratings written in Ge-free fibres. There, it was verified that the resonance wavelengths of LPFGs arc-induced in those fibres, in particular, in Al doped and Er/Al co-doped fibres, show a linear dependence on temperature up to 700 ºC. This fact is very important in optical communications for compensation of temperature drifts and for wavelength tuning in amplifiers and fibre lasers. On the other hand, in the sensing domain it fits the most important requirement of temperature sensors up to 700

ºC. It should be stressed that gratings produced by the electric arc technique have a huge potential to be used as high temperature sensors.

In the past three years other applications of arc-induced gratings have been demonstrated. In optics communications they can perform optical filtering in Er/Yb fibre lasers, gain equalization in EDFAs [1] and as bandpass filters in coarse wavelength division multiplexing (CWDM) applications [2]. As a result of their properties there is a wide range of applications in the sensing field. LPFGs can be used as spectral filters for wavelength to amplitude conversion in a FBG interrogation scheme [3], or as variable attenuators in fibre optic intensity sensors [4], they can perform simultaneous measurement of physical parameters such as micro-displacement [5], temperature and strain [6, 7] or be used as torsion sensors (Soohee In *et al.*, Korea) [8]. They have been also employed in the monitoring of fuel quality (Falate *et al.*, Brazil) [9] and in water salinity measurements [10].

8.3 LPFGs applications in optical communications

The permanent development of optical communications demands for the constant enhancement of fibre lasers and amplifiers, as well as the optical components associated needed to improve system characteristics. Gain flattening filters and amplified spontaneous emission (ASE) filters in erbium doped fibre amplifiers, tuning of the output wavelength of a fibre laser and band rejection filters are some examples of applications where LPFGs can be applied with success.

8.3.1 Filters for Er/Yb fibre lasers

It is well known that one of the most used optical fibres for achieving gain is the erbium doped fibre (EDF), since its operating wavelength coincides with the third window for optical fibre communications around 1550 nm. In some cases, the use of a co-dopant, like ytterbium (Yb^{3+}), can bring benefits to the desired application. For example, the erbium/ytterbium system broadens the choice of pump source in Er^{3+} doped optical amplifiers because Yb^{3+} exhibits a broad absorption band between 800 and 1100 nm [11]. In this system, the optical pumping is based on the $Yb(^2F_{7/2})\rightarrow Yb(^2F_{5/2})$ absorption, arising this way the Er^{3+} pumping from energy transfer from Yb^{3+} to Er^{3+} : $Yb(^2F_{5/2})$ to $Er(^4I_{11/2})$. However, if the rate of multiphonon relaxation process $Er(^4I_{11/2})\rightarrow Er(^4I_{13/2})$ is not fast enough, a back transfer process from $Er(^4I_{11/2})$ to $Yb(^2F_{5/2})$ may occur. Thus, undesirable emission at around 1064 nm can happen, due to the energy levels of Yb^{3+}. In these cases, to maintain a good performance

of the device, it can be used filters that have a high transmission loss centred at 1064 nm, a wide bandwidth and low loss at both wavelengths of 980 and 1550 nm, the optimum pumping wavelength for avoiding the excited state absorption (ESA) effect and the emission wavelength, respectively. In this section it is shown that LPFGs fabricated using the electric-arc technique provide an adequate solution to this problem of designing optical filters with complex characteristics.

Gratings produced using the electric arc technique at short wavelengths puts forward several problems. Usually, fibres are multimode for those wavelengths and therefore the filters on them are very sensitive to bending (even to microbends during their inscription) making difficult to control the background loss. Furthermore, the well-known process of increasing the tension or the current to widen a spectrum or to have a higher transmission loss also results in an increased background loss. Moreover, a technical problem arises when periods of about 240 μm are required since in those cases we are working almost in the limit of the technique. This, in turn reduces the reproducibility since high tensions need to be used to increase the coupling strength. Therefore, transposing what is known about the writing of LPFGs in the third telecommunication window to this particular case is not straightforward.

Gratings were fabricated using the setup described in Appendix A.4. Although several fibres were tested for LPFGs inscription only the DSF from Corning revealed appropriate characteristics. Gratings with low background loss (< 0.3 dB) at the wavelengths of interest were obtained. However, their transmission loss and bandwidth (FWHM) were often lower than 10 dB and less than 10 nm, respectively. Figure 8.1(a) shows the spectrum of one of those gratings (T = 72.7 g, I < 10 mA, t = 0.8 s, Λ = 238 μm) centred at 1060.9 nm, with a transmission loss of about 13.5 dB and a bandwidth of approximately 8.5 nm. The loss at 980 nm was negligible and at 1550 nm was lower than 0.2 dB.

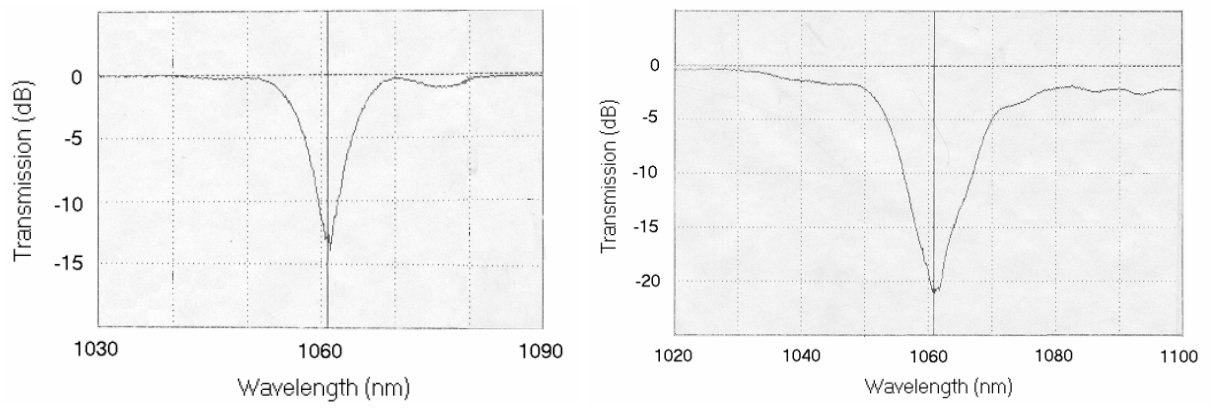

(a) (b)

Figure 8.1 – (a) Transmission spectrum of a 238-μm grating; (b) Spectrum of two concatenated chirped gratings.

In order to increase the bandwidth and the transmission loss two chirped gratings (T = 36.3 g, I < 12 mA, t = 1.5 s) were written. The period of the first grating was changed between 242.5 and 247.5 μm in steps of 0.2 μm starting at 245.0 (it was first increased, from centre wavelength towards longer wavelengths: 245.0 → 247.5 → 242.5 → 245.0). The period of the second was chirped from centre wavelength toward lower wavelengths (247.5 ± 2.5 μm, 0.2 μm: 247.5 → 245.0→ 250.0 → 247.5). Figure 8.1(b) shows the spectrum of the concatenated gratings. The filter has a resonant wavelength centred at 1060.9 nm with a transmission loss higher than 20 dB and a bandwidth of approximately 20 nm. The loss at 980 and 1550 nm was lower than 0.6 and 1.0 dB, respectively.

To improve the above results a multi-grating filter was produced, that is, a filter composed of several gratings with different periods. This filter possesses nine consecutive gratings of 15 periods each, ranging from 241 to 249 μm. The period differs by 1.0 μm from sub-grating to sub-grating. The resultant spectrum is shown in Figure 8.2. As it can be seen the resonant wavelength is centred at 1062.6 nm, its strength and bandwidth is, respectively, ~13 dB and ~19 nm. The background loss is lower than 0.7 dB. Apart from the common parameters to the electric arc technique (tension, current and time), there are several others that can affect the final spectrum of the filter such as the number of sub-gratings, its length, period and chirp. All these parameters can be modified from sub-grating to sub-grating and even gaps can be included in between. Moreover, a different number of discharges can be produced in the same physical region of the fibre as in an apodisation scheme. The complexity of this approach demands a better knowledge of the interplay between these variables and therefore further investigations are required. This powerful tool can lead to remarkable results in applications such as the fabrication of special filters, as the one discussed above, as well as in the gain equalization of amplifiers.

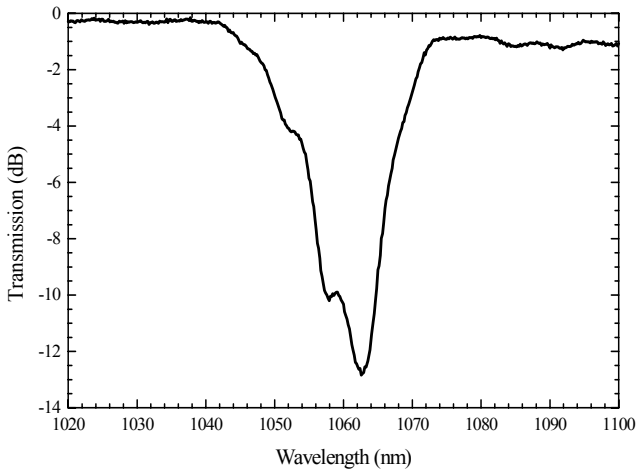

Figure 8.2 – Spectrum of a multi-grating filter.

8.3.2 EDFAs gain equalization

The gain flattening of EDFAs has been a research issue in recent years with the development of high capacity WDM optical communication systems. For single channel systems, the gain variation is not a problem. However, as the number of channels increases, the transmission problem arises because a conventional EDFA has intrinsic non-uniform gain. They typically present gain peaking at about 1530 nm and the useful gain bandwidth may be reduced to less than 10 nm. The gain curve of an EDFA depends on a large number of device parameters such as erbium-ion concentration, amplifier length, core radius and pump power. To increase the gain-bandwidth of an amplified lightwave system several methods can be used [12], but equalizing optical filters operating as spectrally selective loss elements appear to be the best candidates [13].

In this section it will be described the use of arc-induced LPFGs to flatten the spectrum of an EDFA and of an EDF source. In the former case, a single LPFG was fabricated with 57 periods of 611 μm, using a current of about 9 mA during 1.7 s and a mass of 5.1 g (setup described in Appendix A.4).

To observe the effect of the implemented gain-flattening filter on the EDFA gain spectrum, the setup presented in Figure 8.3 was used. Two WDM channels were inserted at the EDFA input (Figure 8.4(a)) that are unequally amplified by the EDFA (Figure 8.4(c)), due to its non-uniform gain curve in the considered band (Figure 8.4(b)). Before equalization, the EDFA gain excursion is approximately 15 dB, from 1524 nm to 1551 nm (27 nm bandwidth). Using the fabricated LPFG (see transmission spectrum in Figure 8.4(d)), the gain ripple over that bandwidth is reduced to approximately 3 dB, and the two WDM channels are similarly amplified (Figure 8.5).

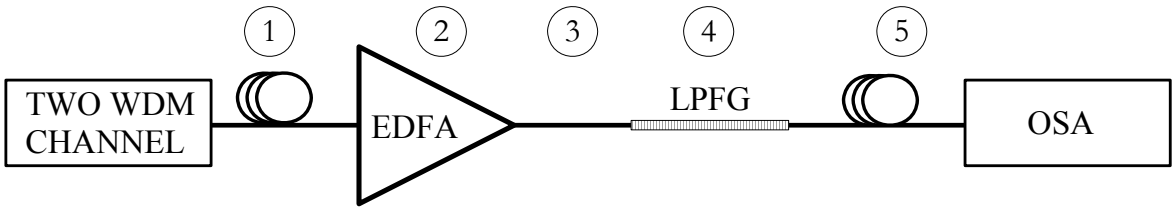

Figure 8.3 – Setup used to verify the EDFA gain equalisation.

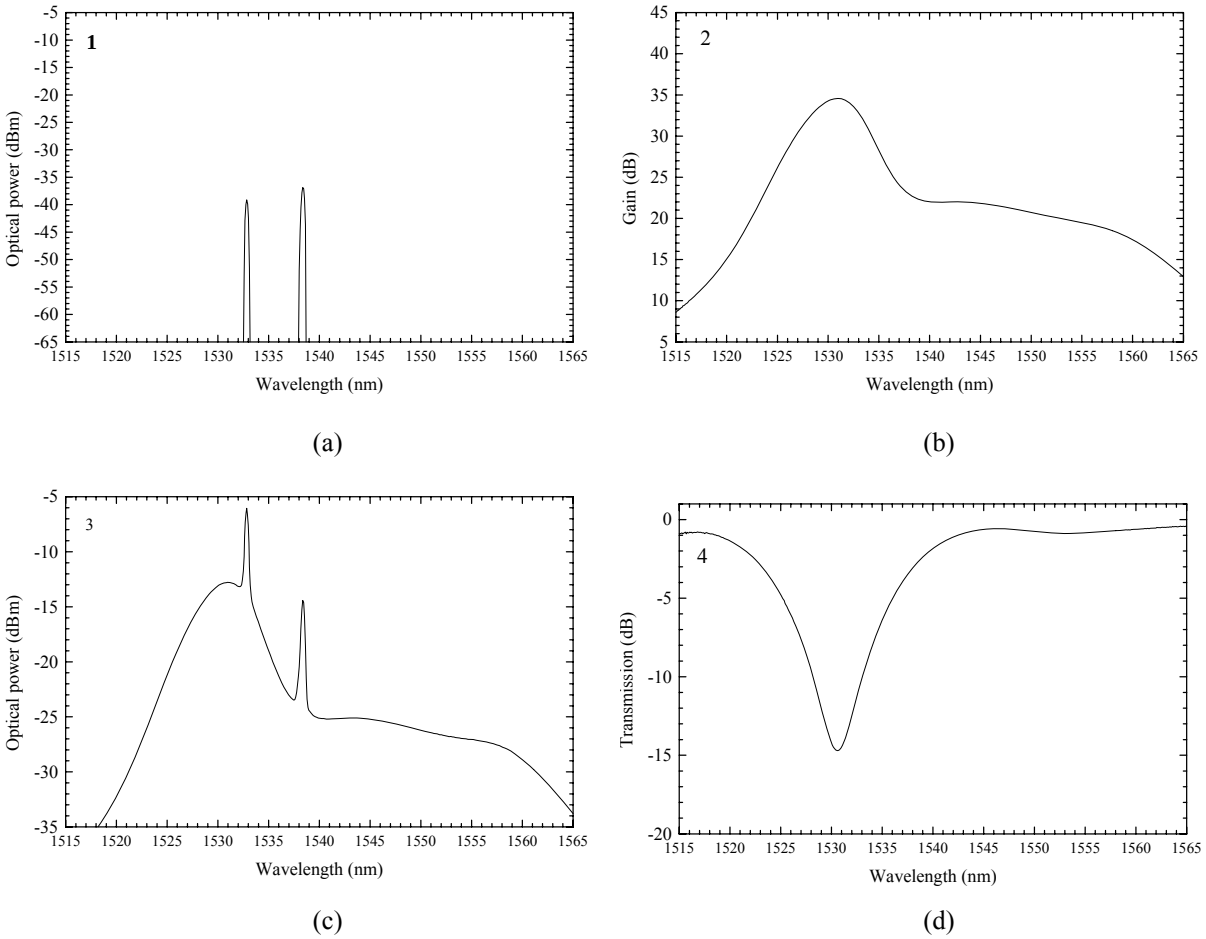

Figure 8.4 – Optical spectra (a): 1 – Input; (c): 3 – EDFA output (without equalization); (b): 2 – commercial EDFA; (d): 4 – implemented LPFG along the setup.

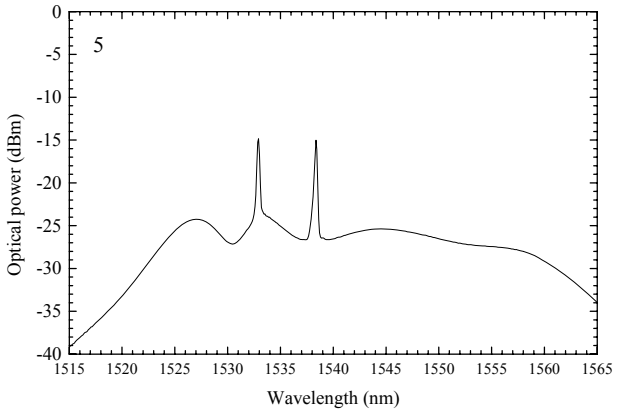

Figure 8.5 – Optical spectrum: 5 – Output (after equalization).

In the case of the EDF source, gratings were written in the Siecor fibre using the setup described in Appendix A.2, where periods between 585 μm and 615 μm were chosen in order to obtain wavelength selective filters suitable for gain equalization of EDFAs. The reproducibility obtained was better than 3 nm. To achieve gratings with a bandwidth of about 8 nm, the tension and the current need to be set to lower values, 1.4 g and 8.5 mA,

respectively. However, the number of electric discharges required to produce gratings with a transmission loss of about 8 dB is higher than 120. On the other hand, for gratings with a bandwidth of about 25-30 nm, those parameters can increase to 5.1 g and 9.0 mA, and therefore the number of discharges can go down to about 60.

The application of a Gaussian fitting to the EDF source emission spectrum resulted in the necessity to have three gratings to fulfil the spectral equalization requirement. One grating centred at 1532.2 nm with a bandwidth of 6 nm and a transmission loss of about 7 dB. The other two gratings centred at 1550.8 nm and 1559.5 nm, with a bandwidth of 14 nm and 8 nm**,** and a transmission loss of about 6 dB and 3 dB, respectively (Figure 8.6). Nevertheless, we have used only two gratings one centred at about 1533 nm and the other positioned around 1555 nm. Figure 8.7 and Figure 8.8 show typical spectral response of the gratings and the evolution of the gain curve during the growth of those gratings.

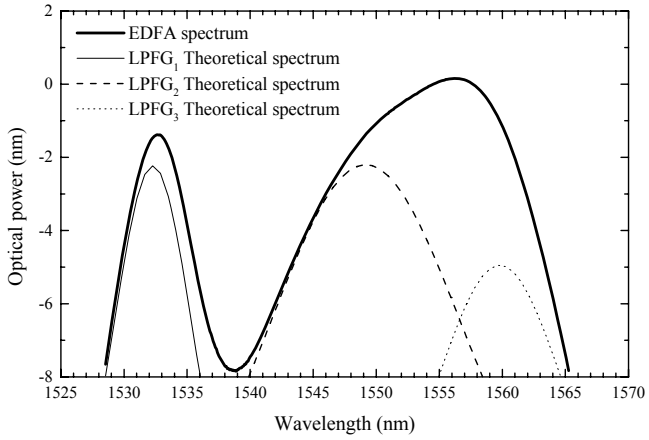

Figure 8.6 – Gaussian fitting to the EDFA gain curve.

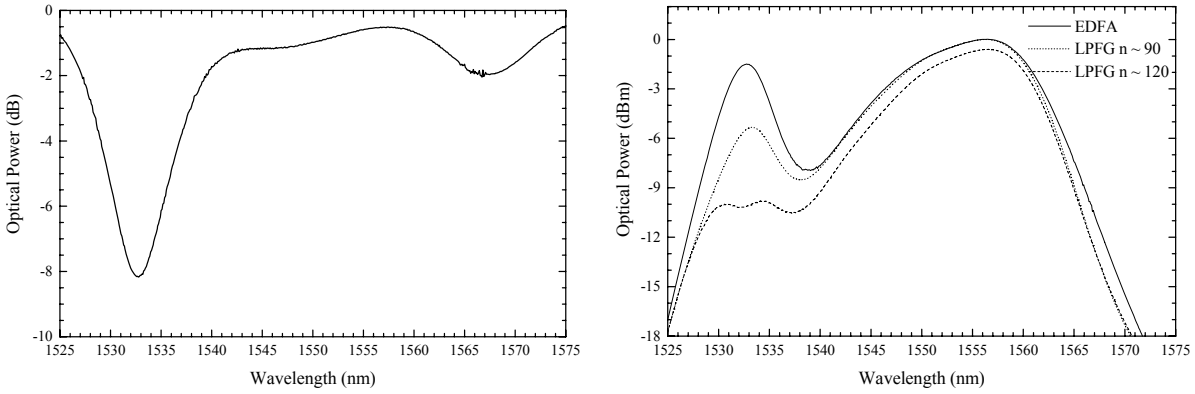

(a) (b)

Figure 8.7 – (a) Spectral response of a chirped grating with 150 periods between 587 and 588 μm. A mass of 1.4 g and a current of 8.5 mA were used; (b) Evolution of the gain curve with the number of arc discharges used to produce the grating centred at 1533 nm.

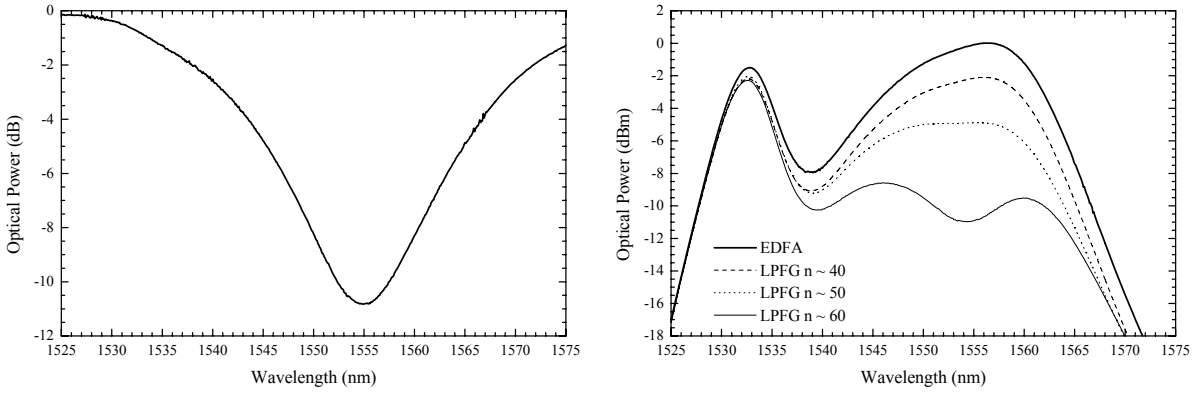

(a) (b)

Figure 8.8 – (a) Spectral response of the grating with 40 periods of 602 μm using a current of 8.5 mA and a mass of 5.1 g; (b) The gain curve dependence on the number of perturbations of the grating centred at 1555 nm.

After concatenation of the two gratings, one grating (1.4 g, 8.5 mA, 588 μm, 110) centred at 1532.9 nm with a bandwidth of approximately 8 nm and a transmission loss of 9 dB, and the other grating (5.1 g, 9.0 mA, 605 μm, 60) centred at 1554.4 nm with a bandwidth of about 28 nm and a transmission loss of 9 dB, the flattened spectrum shown in Figure 8.9 with a bandwidth of about 35 nm (1529-1564 nm) and a fluctuation < 2 dB was obtained. LPFGs are known to be very sensitive to bending and therefore this feature can be used to modify slightly the gratings shape.

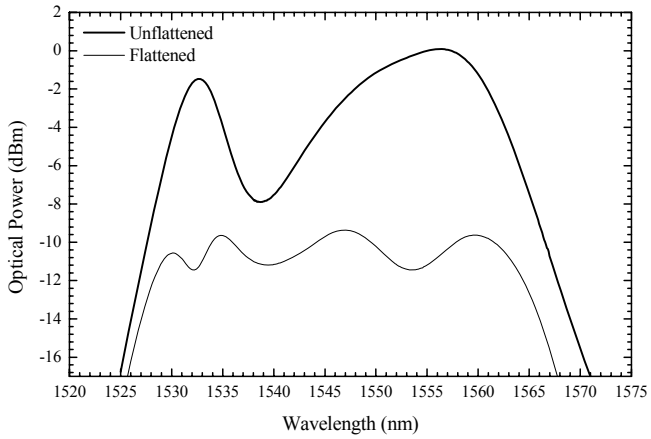

Figure 8.9 –EDF source with its emission spectrum flattened.

In order to further improve the gain ripple there are two approaches: one involves the writing of LPFGs with low transmission loss (< 3 dB) and narrow bandwidth (< 6 nm), i. e., weak gratings. These requirements were fulfilled by a 400 μm-LPFG written in a Corning dispersion-shifted-fibre, whose core is doped with 12 mol% of Ge, using a weight of 1.4 g and arc discharges of 9 mA during 1 s each. Figure 8.10 shows the growth of the peak-loss of

this grating, positioned at about 1547 nm, as the number of arc discharges is increased in steps of 50 up to 150. The evolution of the "third peak" of the flattened spectrum (Figure 8.10) with the increasing strength of this new grating is also shown. As it can be seen, due to the low growth rate of the grating there is a good control of the equalization process. Therefore, by increasing the number of weak gratings it is possible to obtain gain equalization with low ripple, although, at the cost of ending up with a long filter. The second approach consists on a better fitting to the initial EDFA gain curve what can be accomplished by increasing the bandwidth of the gratings using multi-grating filters. Afterwards, if necessary, weak gratings can also be concatenated. The combination of these two kinds of gratings seems to be very promising for gain flattening.

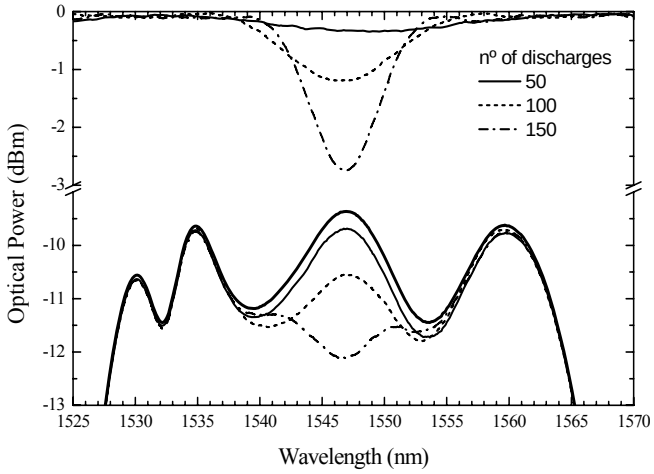

Figure 8.10 – Evolution of the transmission spectrum of the weak grating with the number of arc discharges and the correspondent change of the EDF flattened spectrum.

It should be mentioned that the obtained results are, in general, not as good as the ones published in literature by other authors. In a former work by Tachibana *et al.* [14], gain flattening (accompanied by an increase of its average value) was achieved through the use of a single grating mechanically induced in the active fibre. Recently, based on a similar technique further improvement on the gain characteristics of a double-pass two-stage EDFA was presented [15]. However, as far as gain flattening relying on LPFGs is concerned, better results were obtained through the concatenation of UV-induced gratings after the EDFA or in between two sections of the active fibre [16-18]. The well known sensitivity characteristics [19] of LPFGs also enable a better dynamic gain control as compared to reversible gratings. Therefore, it is expected that the writing of gratings in the active fibre, besides gain flattening improvement, would also enhance the gain characteristics of the EDFA [20]. This would be accomplished by a judiciously inscription of a distributed LPFG along the gain region such that it prevents the building up of the amplified spontaneous emission at ~1.53 μm, being

therefore the population inversion available at other wavelengths resulting in an overall increase of the gain level. Moreover, it would avoid splices loss and could, in principle, allow performing the grating for gain equalization in real time.

Finally, it is known that the use of an aluminosilicate glass host enhances the performance of EDFAs [21]. However, Ge-free Er-doped fibres demand for writing techniques, other than UV-irradiation, to fabricate permanent gratings. Recently [22], we have arc-induced LPFGs in Al^{3+} doped and Er^{3+}/Al^{3+} co-doped fibres. Therefore, it is expected that state-of-the-art EDFAs gain flatteners be achieved in a near future.

8.4 LPFGs applications in optical fibre sensing

Long-period fibre gratings are very sensitive to a multitude of physical parameters such as temperature, strain, pressure, bending, torsion and refractive index of the surrounding medium and therefore, they can be used for detection of changes on the values of those parameters. In this section we shall be focused on three particular applications. First, since these gratings are sensitive to several parameters that may act at the same time, it is important to implement sensor heads able to discriminate the effect of each distinct physical parameter. The second example deals with the intrinsic enhanced sensitivity of LPFGs to changes of external index of refraction. This ability can be used, for instance, to monitor water salinity. Finally, the possibility of using arc-induced gratings in pure-silica-core fibres to perform sensing of physical parameters in the presence of ionising radiation will be briefly discussed.

8.4.1 Simultaneous measurement of temperature and strain

Fibre Bragg grating (FBG)- based sensors for simultaneous measurement of strain and temperature, include FBGs written in Hi-Bi fibres [23], in fibres with different diameter [24] or dopants [25], in association with long period fibre gratings [26] or in a superstructure configuration [27]. In this section we start by presenting an innovative sensor head that works in reflection and comprises a UV-induced FBG written on top of an arc-induced LPFG leading to a SFBG. Afterwards, we will be focused on sensor heads based exclusively on gratings produced by arc discharges.

LPFGs have been used as sensing elements in simultaneous measurement of temperature and strain [28-31]. Potential drawbacks of the proposed sensing schemes are the requirement for two optical sources [28], the use of polarized light [29] and/or polarization maintaining fibres [30] and the need for two distinct fibre types [31]. Recently, it was

demonstrated that the response of arc-induced gratings to applied strain and temperature could be controlled by changing the fabrication parameters [6]. Based on the properties of those gratings, a sensor head comprising two concatenated LPFGs was assembled to perform temperature and strain measurements. However, to avoid recoupling between the two consecutive gratings, an index matching gel was used, which limits the range of the working temperature. A possibility to surpass this problem can be achieved through the recoating of the region between the gratings, but this is a risky alternative since this process can break the fibre. Another disadvantage of this technique is the overall length of the sensing head which could be undesirable for some applications. Below it will be discussed a way to solve these problems.

Sampled fibre Bragg grating

A new configuration of optical fibre sensor, for simultaneous measurement of strain and temperature, was developed taking advantage of the special spectral characteristics of a sampled FBG. The sensing head uses the combined response of both SFBG and LPFG.

The experimental setup used for characterisation of the sensor head is shown in Figure 8.11(b). An erbium-doped broadband source was used to illuminate the sensing head through a standard 3 dB coupler. This sensor head was then placed on the thermoelectric cooler (TEC)

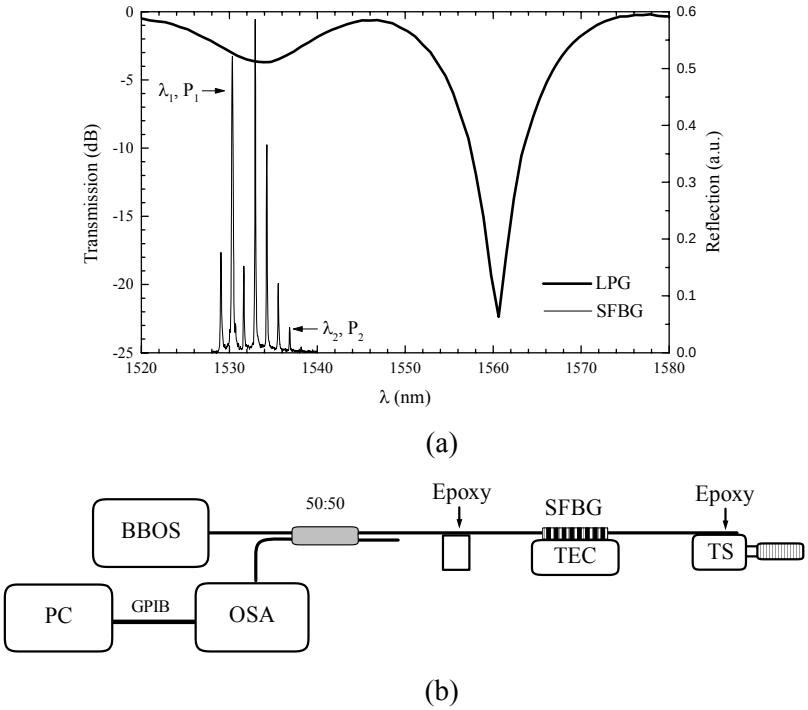

Figure 8.11 – (a) Spectral response of the SFBG and LPG and (b) experimental setup for sensing head characterisation (BBOS - Broadband Optical Source; OSA - Optical Spectrum Analyser; PC - Personal Computer; TEC - Thermoelectric Cooler; TS - Translation Stage).

and simultaneously subjected to temperature and axial strain variation. All measurements were provided by an OSA and a computer data acquisition system (LabView) for flexibility in data display processing and storage.

To characterise the sensing head, the reflected power (P_1, P_2) and the resonance wavelength of the two reflection peaks of the SFBG localized around λ_1 = 1530 nm and λ_2 = 1537 nm (see Figure 8.11(a)), were monitored for different values of applied strain and temperature. Figure 8.12(a)-(b) show the dependence of the wavelength (λ_2) and of the reflected power ($R = P_1/P_2$) on strain and temperature. From these results it can be observed that, while the resonant wavelengths of the SFBG increase with both temperature and strain, the ratio $R = P_1/P_2$ increases with temperature and decreases with strain (R depends on the relative position of the higher order resonance of the LPFG and of the λ_1, λ_2 signatures). The reason for this behaviour is that the FBG and LPFG structures have different responses to the applied strain and temperature. The temperature sensitivity of the LPFG is approximately six times higher than that of a FBG, whereas the strain sensitivities of these two fibre structures have different slope signs. Note that as discussed in Chapter 5, the strain sensitivity of the cladding modes can be either positive or negative.

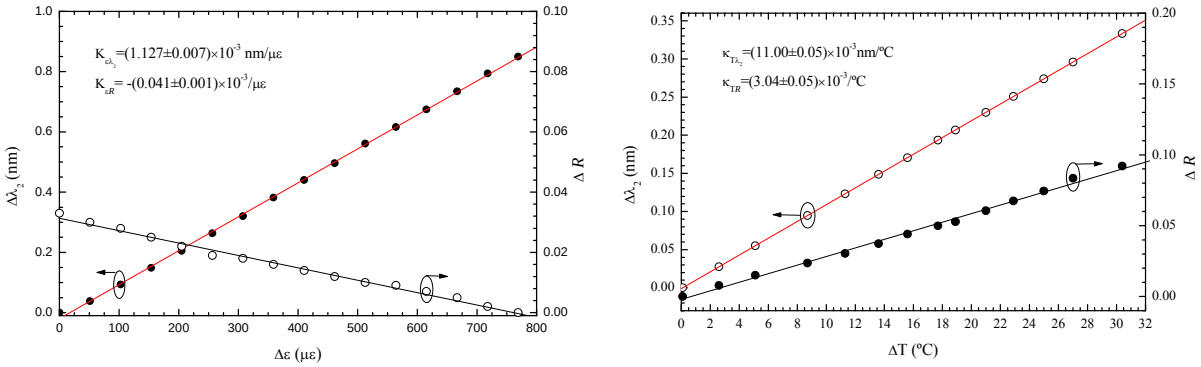

(a) (b)

Figure 8.12 – (a) Strain response of the sensing head (at constant temperature). (b) Temperature response of the sensing head (constant strain).

The experimental results allows one to write a well conditioned system of two equations for ΔT and $\Delta\varepsilon$ given in matrix form in Equation (8.1), where the matrix coefficients are the slopes of the linear fit that connect ΔT and $\Delta\varepsilon$ with ΔR and $\Delta\lambda_2$, respectively.

$$\begin{bmatrix}\Delta T\\ \Delta\varepsilon\end{bmatrix} = 257.93\begin{bmatrix}1.127 & 0.041\\ -11.00 & 3.04\end{bmatrix}\begin{bmatrix}\Delta R\\ \Delta\lambda_2\end{bmatrix} \tag{8.1}$$

The system resolution was determined when the sensing head was simultaneously subjected to strain and temperature changes. The rms deviations were found to be ± 0.32 ºC and ± 5.4 με for temperature and strain measurements, respectively (Figure 8.13).

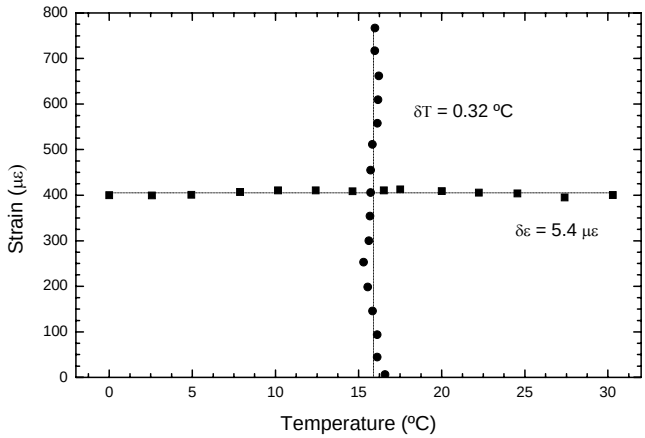

Figure 8.13 – Sensor output as determined by Equation (8.1).

Concatenation of two LPFGs written in the same fibre

To implement the sensor head, the previous study presented in chapter 5 on the influence of the fabrication parameters on the strain and temperature sensitivities was taken into account. Based on that study, two gratings LPFG#5 (T = 22.8 g, I = 9 mA, t = 1 s, 540 μm, N = 35) and

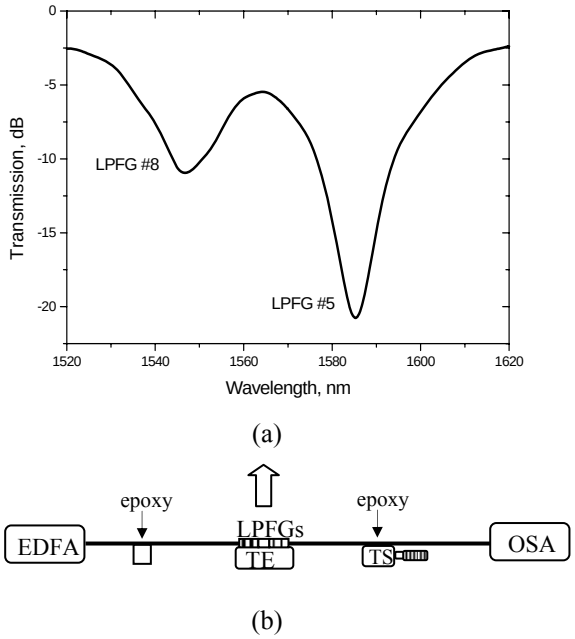

Figure 8.14 –Grating transmission spectrum and experimental setup.
(a) Close-up of the two resonances under measurement.
(b) Experimental setup for characterization of the sensing head.
TEC: thermoelectric cooler; TS: translation stage.

LPFG#8 (T = 5.1 g, I = 10 mA, t = 1 s, 540 μm, N = 40) were written in the SMF28 fibre using different fabrication parameters. Afterwards, they were concatenated and the region in between the two was immersed in index matching gel, to avoid that power from the cladding modes could be coupled again into the core by the second grating. Figure 8.14(a) shows the transmission spectrum of the two concatenated gratings.

The proposed technique for simultaneous strain and temperature determination is based on the measurement of the resonant wavelengths of the two LPFGs. The experimental setup used is shown in Figure 8.14(b). To calibrate the system, strain in the range 0-2000 με was applied at constant temperature and, by keeping the strain constant, temperature was changed in the range of 23-45 ºC (the maximum value was limited by the gel thermal resistance; the higher limit of the temperature range can be easily extended by recoating the fibre in between the gratings instead of using the index matching gel). The corresponding calibration results are presented in Figure 8.15. From the data in this figure (the slopes of the linear fittings), the matrix Equation (8.2) that allows the simultaneous measurement of strain and temperature can be written as

$$\begin{bmatrix} \Delta T \\ \Delta \varepsilon \end{bmatrix} = 0.10 \begin{bmatrix} -0.08 & 0.26 \\ -53.7 & 53.2 \end{bmatrix} \begin{bmatrix} \Delta \lambda_1 \\ \Delta \lambda_2 \end{bmatrix} \tag{8.2}$$

where $\Delta\lambda_1$ and $\Delta\lambda_2$ are expressed in pm, ΔT in ºC and $\Delta\varepsilon$ in με.

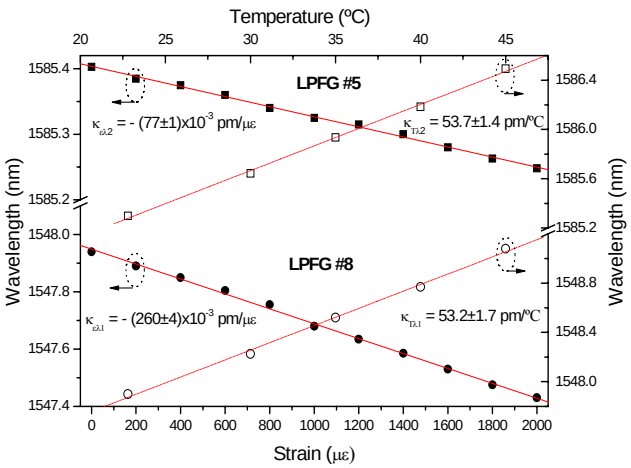

Figure 8.15 – Strain and temperature responses of the sensor head.

The system resolution was estimated directly from the calibration procedure. The *rms* deviations corresponding to temperature and strain were found to be ± 0.1 ºC and ± 41 με, respectively (Figure 8.16).

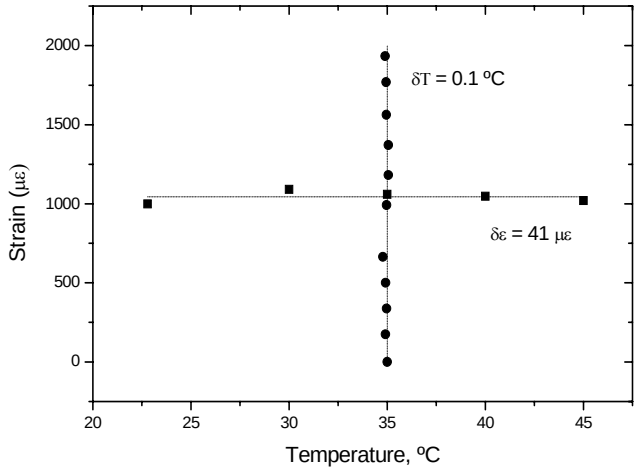

Figure 8.16 – Sensor output as determined by Equation (8.2).

Concatenation of two LPFGs written in different fibres: A case study

In order to improve the results presented in the previous section, some modifications of the sensor head were introduced. First, gratings were written in two different fibres such that the LPFGs would show well distinct responses to applied temperature and strain. Second, the region in between the concatenated gratings was recoated in order to extend the temperature range. It is interesting to note that despite the good linear dependence obtained for the change of the resonant wavelengths with strain and temperature, the error in the measurements of the proposed interrogation scheme was unexpectedly high and therefore it deserves a closer look.

One grating was written in the SMF-28 fibre (T = 22.8 g, I = 9 mA, t = 1 s, 540 μm, N = 40) and the other in the Fibrecore B/Ge co-doped fibre (T = 22.8 g, I = 8.5 mA, t = 0.5 s, 415 μm, N = 42). The spectra of the two concatenated gratings are shown in Figure 8.17.

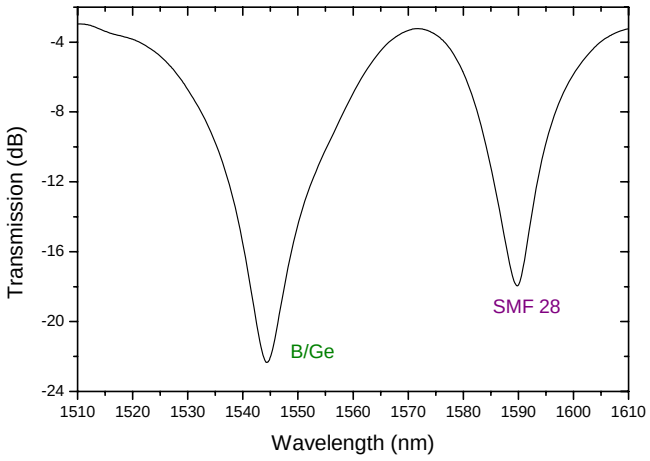

Figure 8.17 – Transmission spectra of the two concatenated gratings.

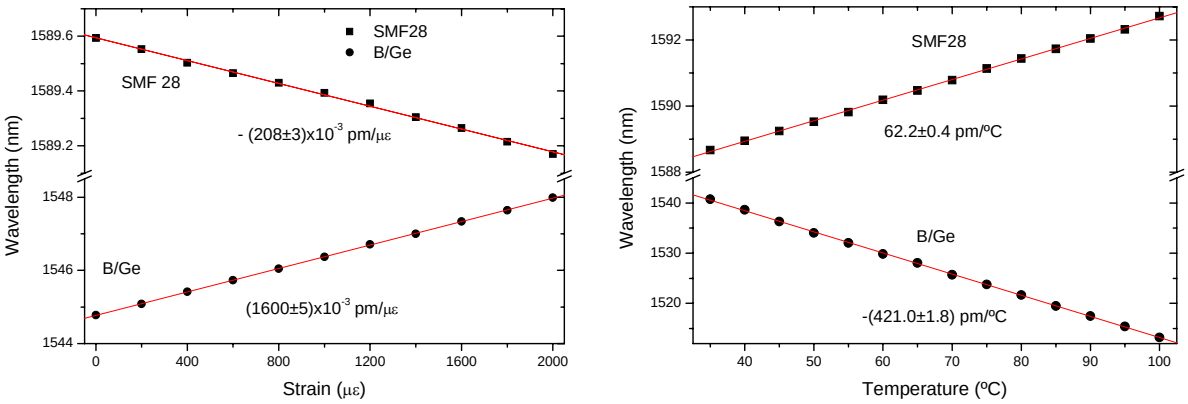

(a) (b)

Figure 8.18 – (a) Strain response of the sensing head (at constant temperature); (b) Temperature response of the sensing head (constant strain).

The response of the sensor head to applied strain and temperature is shown in Figure 8.18. The slopes of the linear fittings are used in the matrix Equation (8.3) that can be written as

$$\begin{bmatrix} \Delta T \\ \Delta \varepsilon \end{bmatrix} = -83.7x10^{-3} \begin{bmatrix} -0.208 & -1.6 \\ -62.2 & -421.0 \end{bmatrix} \begin{bmatrix} \Delta\lambda_1 \\ \Delta\lambda_2 \end{bmatrix} \tag{8.3}$$

where $\Delta\lambda_1$ and $\Delta\lambda_2$ are expressed in pm, ΔT in ºC and $\Delta\varepsilon$ in με.

The system resolution was estimated directly from the calibration procedure. As seen in Figure 8.19 this sensor is not suitable for the simultaneous measurement of temperature and strain. Although the error in the determination of the matrix coefficients is within 1.5%, the error in the calculation of the matrix determinant is quite high, above 20%. The performance of this sensor could be anticipated by using the expressions for the maximum error associated with the determination of temperature and strain [32, 33]. In conclusion, the choice of two

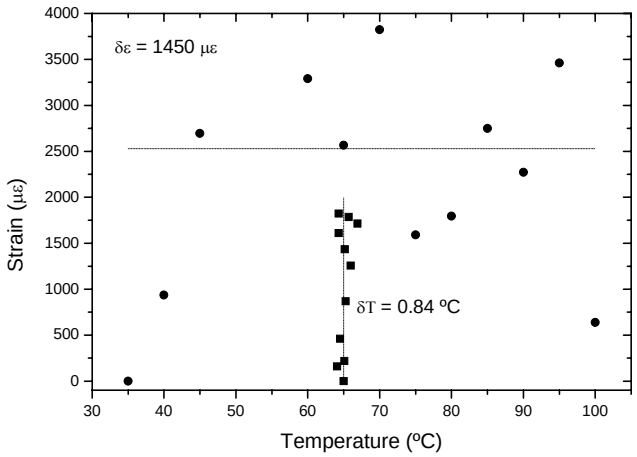

Figure 8.19 – Sensor output as determined by Equation (8.3).

gratings with completely different sensitivities to the parameters to be measured may not be the best option to implement a sensor.

LPFG with two distinct sections

In this section it is presented a compact sensor head which overcomes the previous drawbacks. The sensor consists of a LPFG with two sections written consecutively in the Corning SMF-28 fibre, i.e., without physical separation in between, which have the same period and different fabrication parameters. The bases of this sensor are the unique properties of gratings produced by the electric arc technique as discussed in Chapter 5.

To implement the sensor head, a LPFG was arc-induced in the SMF-28 fibre, and the fabrication parameters being chosen according to the requirement of having two neighbour resonant wavelengths around 1.55 μm and exhibiting different sensitivities to strain and temperature. Figure 8.20 shows the transmission spectrum of the grating after the writing process of each section. Following the inscription of the first section (T = 22.8 g, I = 9 mA, t = 1 s, Λ = 540 μm and N = 15), the writing parameters were modified and the second section (T = 1.2 g, I = 11 mA, t = 1 s, Λ = 540 μm and N = 40) was written without any physical separation.

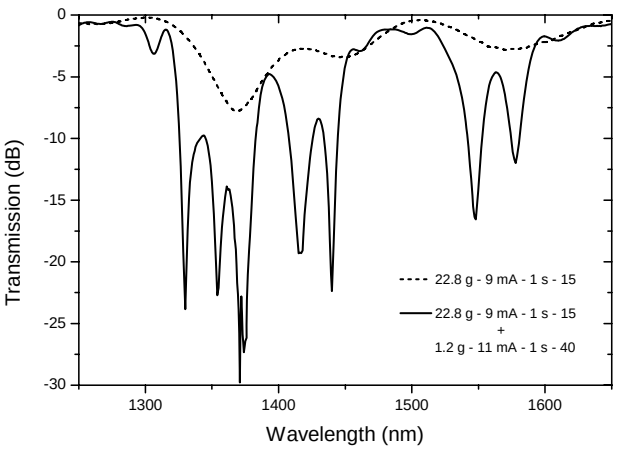

Figure 8.20 –Evolution of the grating spectrum during the fabrication process.

The proposed technique for simultaneous strain and temperature determination is based on the wavelength shift measurement of the two central wavelength resonances, shown in Figure 8.21, when temperature or strain is changed. The resonance at longer wavelength corresponds to the one obtained during the writing of the first section which continue to evolve afterwards, whilst the resonance at shorter wavelength appears due to the second section. During the writing process the strength of the first peak increases, followed by a spectral broadening and finally this resonance starts to split in two, being the short

wavelength resonance, which is the consequence of the second grating section, the last to appear. To calibrate the system, strain in the range of 0-1600 με was applied in steps of 200 με at constant temperature, and by keeping the strain constant the temperature was changed in the range of 22-110 ºC, in steps of 10 ºC. At each step, the transmission spectrum of the grating was recorded using an OSA set to a resolution of 0.1 nm, the light being supplied by the noise spectrum of an EDFA, from Photonetics. The corresponding calibration results are presented in Figure 8.22(a)-(b). It is interesting to note that the resonance at a longer wavelength is insensitive to strain. This result may reflect some interplay between the two resonances, as expected in the case of a phase shift grating. Also important is the fact that the dependence of the resonance wavelengths on temperature becomes increasingly parabolic with the increase of the electric arc current. This non-linear dependence, up to ~700 ºC, was discussed in Chapter 5.

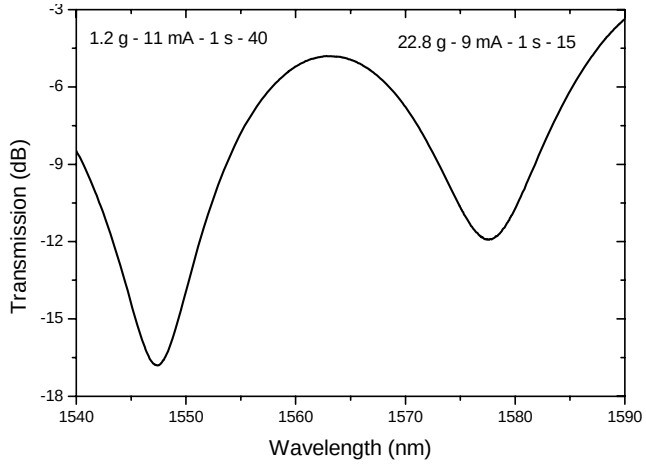

Figure 8.21 –Grating transmission spectrum showing the two resonances under measurement.

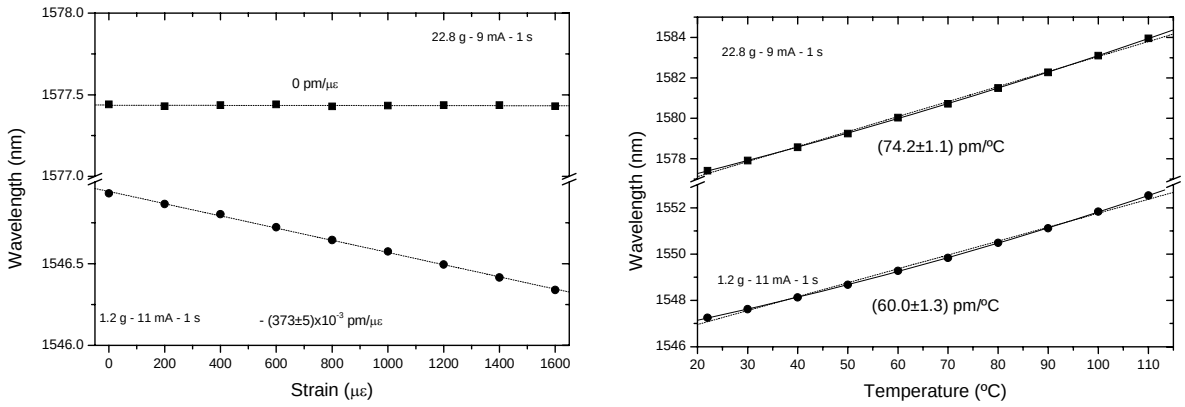

(a) (b)

Figure 8.22 – (a) Strain and (b) temperature response of the sensing head.

In what follows, a linear dependence is assumed to calculate the matrix coefficients [28]. From the results obtained (the slopes of the linear fittings), the matrix Equation (8.4) that allows the simultaneous measurement of strain and temperature can be written as

$$\begin{bmatrix} \Delta T \\ \Delta \varepsilon \end{bmatrix} = 36.1\times10^{-3} \begin{bmatrix} 0 & 0.373 \\ -74.2 & 59.8 \end{bmatrix} \begin{bmatrix} \Delta\lambda_1 \\ \Delta\lambda_2 \end{bmatrix} \tag{8.4}$$

where $\Delta\lambda_1$ and $\Delta\lambda_2$ are expressed in pm, ΔT in ºC and $\Delta\varepsilon$ in με.

To improve the system performance, corrections were further made in order to compensate for deviations between linear and quadratic behaviour. To execute this, the quadratic and the linear equations for the temperature responses of both resonances are taken. For each temperature change, a correction factor, which consists of the difference between the quadratic and the linear functions, is subtracted from the original wavelength values, enabling more precise measurand information. It should be noticed that by a proper compensation of the quadratic behaviour, this sensor can operate at temperatures as high as 700 ºC, only limited by the beginning of stress relaxation. Higher temperatures may be reached if fibre annealing is performed after the grating inscription. The system resolution was estimated directly from the calibration procedure. The *rms* deviations corresponding to temperature and strain were found to be ± 0.2 ºC and ± 35 με, respectively (Figure 8.23).

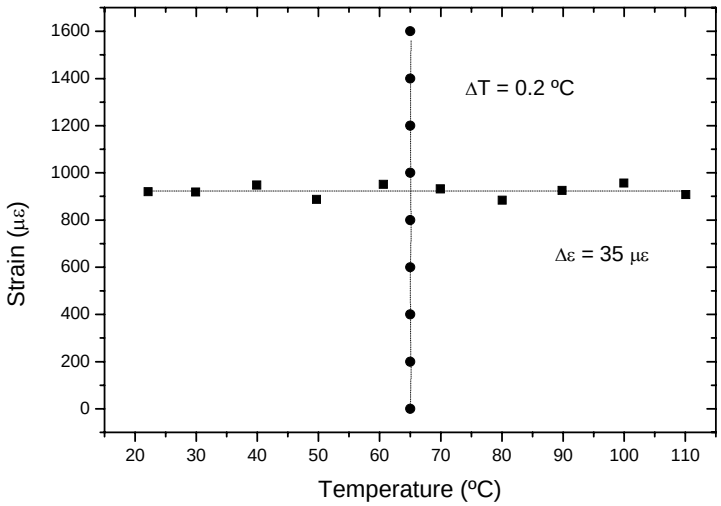

Figure 8.23 – Sensor output as determined by Equation (8.4), after compensation for the quadratic behaviour.

8.4.2 Refractive index measurement

In nowadays life there is an increasing demand for monitoring the water quality for several reasons, including public health. There is a large variety of physical and chemical methods

and related techniques to gather information with that objective. One of them that have proved to be highly effective is the precise determination of water refractive index, which changes depending on the biochemical composition of water. As an example, the degree of water salinity can be accurately determined by measuring the refractive index. Up to recently the precise determination of this parameter could only be performed by delivering water samples to the laboratory. This is a costly, time consuming process and not susceptible to real time monitoring. Therefore, it was natural to consider the utilization of optical fibre technology in view of its favourable characteristics: potential high readout sensitivity, remote measurement and multiplexing capability. In particular, LPFGs are devices with spectral characteristics highly sensitive to the surrounding environment and, therefore, to its refractive index. This happens because LPFGs are very prone to changes of the external medium since the effective refractive index of the cladding modes depends on the difference between the cladding and ambient refractive indexes [19, 34]. The sensitivity to refractive index changes increases with the reduction of that difference. Therefore, pure-silica-core fibres, where the cladding is doped with fluorine in order to decrease its refractive index, have an intrinsic advantage over standard fibres. Moreover, has shown in Chapter 5 the temperature sensitivity of arc-induced gratings written in pure-silica-core fibres is lower than the ones correspondent to LPFGs written in other type of fibres. This fact may be helpful in the reduction of potential cross-sensitivity problems, as they may arise in the configuration proposed in J. H. Chong *et al.* [35], since there gratings were written in a fibre with a very high sensitivity to temperature (typically 10 times higher than in pure-silica-core fibres). Further increases in refractive index sensitivity, besides a proper choice of the order of the cladding mode resonance, can be obtained through etching of the fibre cladding or by concatenation of two LPFGs in a Mach-Zehnder topology.

In this section we present results of the simulation of salinity measurements in water by using LPFGs arc-induced in pure-silica-core fibres. To assess the performance of the fabricated gratings for precise refractive index measurement, three samples containing mixtures of distilled water and ethylene glycol were prepared such that their respective refractive indexes fall in the 1.3325-1.3385 range. The lowest value corresponds to that of distilled water measured using an Abbe refractometer with a sodium lamp (589 nm). The refractive indexes of all samples at 1550 nm were calculated using the Cauchy equation being the respective parameters determined by further illuminating the refractometer with the Helium-Neon (632.8 nm) and Argon (514 nm) lasers [36].

In order to perform the refractive index measurements, fibres were kept under a tension of 22.8 g to avoid bending of the gratings. The noise spectrum of an EDFA and an OSA set to a resolution of 0.05 nm, were used to register the gratings spectra in the vicinity of a

particular resonance. The spectra were recorded for gratings on air, embedded in water and in the three water-glycol mixture samples (n_1 = 1.3231, n_2 = 1.3246 and n_3 = 1.3271). Careful has to be taken while exchanging the liquids to avoid contamination and to guaranty no temperature drift. Figure 8.24 and Figure 8.25 show the change that occurs in the transmission band of the grating induced in the Oxford Fibre, for different external fluids and its respective resonant wavelength shift with their correspondent refractive indexes. As it can be seen, the shift is linear for the small range of interest. The results for the three fibres investigated are summarised in Table I (the air-water change was already analysed in Chapter 5).

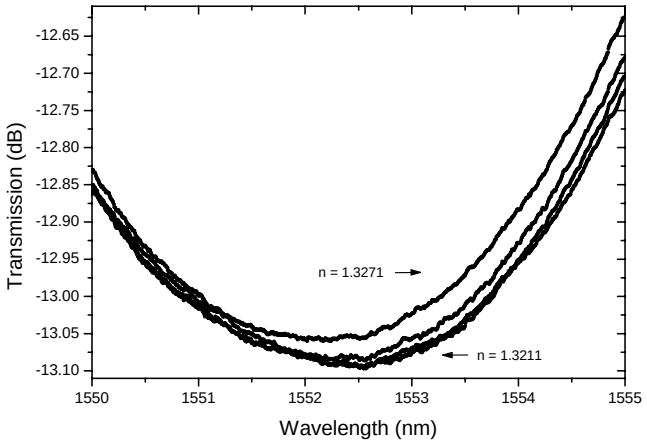

Figure 8.24 – Transmission of the resonant band of the grating written in the Oxford fibre for different fluids.

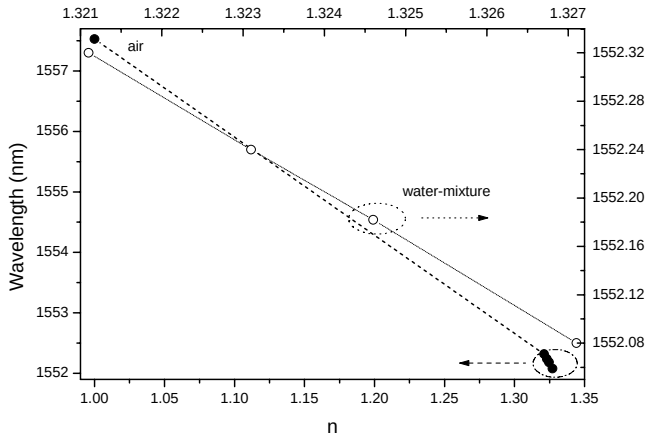

Figure 8.25 – Resonant wavelength (grating written in the Oxford fibre) for several external refractive indexes.

TABLE I. Resonant wavelength shift upon changes of the surrounding refractive index.

	Δλ/nm	
Medium / Fibre	Air-water 1-1.3211	Water-mixture 1.3211-1.3271
SiO_2-125 μm	5.21	0.24
SiO_2-150 μm	8.96	0.11
SMF28-125 μm	2.34	0.10

Note that for the small range of interest, corresponding to refractive index values of distilled water and sea-water, the SiO_2 fibre with standard dimensions revealed to be twice effective. More modest values were achieved with the standard fibre despite the monitoring of a higher order cladding mode. For comparison, the Bragg wavelength shift of a grating written in a strongly etched fibre was only ~50 pm for the same $6x10^{-3}$ change in the refractive index [36]. As far as the gratings refractive index sensitivity is concerned, a better understanding of the achieved results may require the study of leaky mode propagation in these peculiar fibre structures.

The sensitivity of arc-induced gratings to changes of ambient refractive index was investigated. It was found that LPFGs written in pure-silica-core fibres possess higher sensitivity compared with those induced in standard fibres. Sensitivities up to 40 nm/RIU (RIU = refractive index unity) were obtained. Further increase in gratings response can be achieved using higher order cladding modes. Etching of the fibre cladding and/or concatenating two LPFGs also lead to improvements of the above result. Therefore, a sensor head based on gratings arc-induced in pure-silica-core fibres can perform the precise measurement of water solutions refractive index, which permits a large spectrum of applications, as for example the measurement of salinity in water.

8.4.3 Sensors for radiation environments

In Chapter 5 it was presented results on the influence of γ-radiation on the spectra and on the sensitivity of gratings arc-induced in. It was found that total radiation doses up to 0.5 MGy has negligible effect on their spectra and also on their sensitivity to temperature and strain. Furthermore, gratings arc-induced in theses fibres show a temperature sensitivity about 2 to 3 times lower than the ones induced in standard fibres. On the other hand, the strain sensitivity is about 10 times higher. Therefore, gratings arc-induced in pure-silica-core fibres are very promising to perform structural integrity of nuclear facilities.

The simplest scheme for a sensor comprises the use of a single LPFG [37]. In this case the signal is detected in transmission, which sometimes is a drawback since this requires access to both ends of the fibre. In order to overcome this problem some configurations working in reflection can be suggested (in all cases a coupler will be needed to detect the reflection signal). For instance, a radiation-resistance mirror can be deposited on the fibre-end after the LPFG. A combination of a LPFG and Bragg gratings can also be used [38]. Two approaches are available for writing the Bragg gratings. One way is to write them directly in the OH-flooded SiO_2-core fibre using 193 nm UV-radiation [39], or by exposing the fibre to 267 nm femtosecond radiation [40]. The other is to splice the pure-silica-core fibre, containing the LPFG, with a short piece of a N-doped fibre [41] or a standard fibre without any kind of pre- or post-treatment [42], where Bragg gratings were previously written.

In conclusion, the nowadays requirement for other non pollutant sources of energy demands for more research regarding safety issues concerned to nuclear facilities. Therefore, the implementation and characterisation of sensor heads able to perform multi-parameter measurement under γ-radiation is clearly an important goal.

8.5 Summary

In this chapter were presented several applications of arc-induced gratings, namely, as an amplified spontaneous emission filter for Er/Yb fibre lasers and in the gain curve equalization of EDFAs, both in the optical communications domain. Regarding the sensing field, the simultaneous measurement of temperature and strain was the main example. The use of LPFGs for salinity measurements and for structural monitoring of nuclear facilities was also discussed.

Arc-induced gratings possess unique properties that can be employed in the development of new devices. In future work gain equalization of EDFAs through the writing of gratings in the active fibre should be investigated. The development of sensors to perform measurement of physical parameters up to 700 ºC can be easily obtained. A fully characterisation of the performance of high temperature sensors is required. However, a topic that should be pursued is the implementation of a sensor head for radiation environments.

References

[1] G. Rego, M. Melo, J.L. Santos, and H.M. Salgado. *Optical filters for fibre lasers and amplifiers*. in *London Communications Symposium 2002, Proceedings*: 49-52, 2002.

[2] G. Humbert and A. Malki. *High performance bandpass filters based on electric arc-induced pi-shifted long-period fibre gratings.* Electronics Letters **39**(21): 1506-1507, 2003.

[3] S. Abad, F.M. Araujo, L.A. Ferreira, J.L. Santos, and M. Lopez-Amo. *Bragg-grating interrogation scheme using spectral filtering and amplitude-to-phase optical conversion*. in *OFS 2002: 15th Optical Fiber Sensors Conference Technical Digest*: 103-106, 2002.

[4] J. Baptista, S. Abad, G. Rego, L. Ferreira, F. Araujo, J. Santos, and A. Lage. *Wavelength multiplexing of frequency-based self-referenced fiber optic intensity sensors.* Optical Engineering **43**(3): 702-707, 2004.

[5] S. Cazacu, J.M. Martins, G. Rego, S.F. Santos, J.L. Santos, and J.M. Baptista. *Micro-displacement measurement using a long period fiber grating in a self-referenced fiber optic intensity sensor*. in *2004 IEEE Leos Annual Meeting Conference Proceedings, Vols 1 And 2*: 262-263, 2004.

[6] G. Rego, P.V.S. Marques, H.M. Salgado, and J.L. Santos. *Simultaneous measurement of temperature and strain based on arc-induced long-period fibre gratings.* Electronics Letters **41**(2): 60-62, 2005.

[7] R. Romero, O. Frazão, G. Rego, P.V.S. Marques, and H.M. Salgado. *Sampled Fibre Bragg Gratings Fabrication using an Electric Arc and their Applications*. in *Proceedings of 2002 Course on Photosensitivity in Optical Waveguides and Glasses*: paper 43/WA5, 2002.

[8] S. In, C. Chung, and H. Lee. *The resonance wavelength-tuning characteristic of the arc-induced LPFGs by diameter modulation*. in *OFS 2002: 15th Optical Fiber Sensors Conference Technical Digest*: 131-134, 2002.

[9] R. Falate, R.C. Kamikawachi, M. Muller, H.J. Kalinowski, and J.L. Fabris. *Fiber optic sensors for hydrocarbon detection.* Sensors and Actuators B-Chemical **105**(2): 430-436, 2005.

[10] G.M. Rego, J.L. Santos, and H.M. Salgado. *Refractive index measurement with long-period gratings arc-induced in pure-silica-core fibres.* Optics Communications **259**(2): 598-602, 2006.

[11] W.L. Barnes, S.B. Poole, J.E. Townsend, L. Reekie, D.J. Taylor, and D.N. Payne. *Er3+ - Yb3+ and Er3+ Doped Fiber Lasers.* Journal of Lightwave Technology **7**(10): 1461-1465, 1989.

[12] C.R. Giles. *Lightwave applications of fiber Bragg gratings.* Journal of Lightwave Technology **15**(8): 1391-1404, 1997.

[13] A. Vengsarkar, P. Lemaire, J. Judkins, V. Bhatia, T. Erdogan, and J. Sipe. *Long-period fiber gratings as band-rejection filters.* Journal of Lightwave Technology **14**(1): 58-65, 1996.

[14] M. Tachibana, R.I. Laming, P.R. Morkel, and D.N. Payne. *Erbium-Doped Fiber Amplifier with Flattened Gain Spectrum.* IEEE Photonics Technology Letters **3**(2): 118-120, 1991.

[15] I. Sohn and J. Song. *Gain flattened and improved double-pass two-stage EDFA using microbending long-period fiber gratings.* Optics Communications **236**(1-3): 141-144, 2004.

[16] A.M. Vengsarkar, J.R. Pedrazzani, J.B. Judkins, P.J. Lemaire, N.S. Bergano, and C.R. Davidson. *Long-period fiber-grating-based gain equalizers.* Optics Letters **21**(5): 336-338, 1996.

[17] M. Harumoto, M. Shigehara, and H. Suganuma. *Gain-flattening filter using long-period fiber gratings.* Journal of Lightwave Technology **20**(6): 1027-1033, 2002.

[18] P.F. Wysocki, J.B. Judkins, R.P. Espindola, M. Andrejco, and A.M. Vengsarkar. *Broad-band erbium-doped fiber amplifier flattened beyond 40 nm using long-period grating filter.* IEEE Photonics Technology Letters **9**(10): 1343-1345, 1997.

[19] S.W. James and R.P. Tatam. *Optical fibre long-period grating sensors: Characteristics and application.* Measurement Science & Technology **14**(5): R49-R61, 2003.

[20] R. Singh, Sunanda, and E. Sharma. *Gain flattening by long period gratings in erbium doped fibers.* Optics Communications **240**(1-3): 123-132, 2004.

[21] E. Desurvire, in *Erbium-doped fiber amplifiers: principles and applications*. John Wiley & Sons, New York: 207-255, 1994

[22] G. Rego, R. Falate, J.L. Santos, H.M. Salgado, J.L. Fabris, S.L. Semjonov, and E.M. Dianov. *Arc-induced long-period gratings in aluminosilicate glass fibers.* Optics Letters **30**(16): 2065-2067, 2005.

[23] L.A. Ferreira, F.M. Araujo, J.L. Santos, and F. Farahi. *Simultaneous measurement of strain and temperature using interferometrically interrogated fiber Bragg grating sensors.* Optical Engineering **39**(8): 2226-2234, 2000.

[24] S.W. James, M.L. Dockney, and R.P. Tatam. *Simultaneous independent temperature and strain measurement using in-fibre Bragg grating sensors.* Electronics Letters **32**(12): 1133-1134, 1996.

[25] P.M. Cavaleiro, F.M. Araujo, L.A. Ferreira, J.L. Santos, and F. Farahi. *Simultaneous measurement of strain and temperature using Bragg gratings written in germanosilicate and boron-codoped germanosilicate fibers.* IEEE Photonics Technology Letters **11**(12): 1635-1637, 1999.

[26] H.J. Patrick, G.M. Williams, A.D. Kersey, J.R. Pedrazzani, and A.M. Vengsarkar. *Hybrid fiber Bragg grating/long period fiber grating sensor for strain/temperature discrimination.* IEEE Photonics Technology Letters **8**(9): 1223-1225, 1996.

[27] B.O. Guan, H.Y. Tam, X.M. Tao, and X.Y. Dong. *Simultaneous strain and temperature measurement using a superstructure fiber Bragg grating.* IEEE Photonics Technology Letters **12**(6): 675-677, 2000.

[28] V. Bhatia, D. Campbell, R.O. Claus, and A.M. Vengsarkar. *Simultaneous strain and temperature measurement with long-period gratings.* Optics Letters **22**(9): 648-650, 1997.

[29] O. Frazão, G. Rego, F.M. Araujo, L.A. Ferreira, H.M. Salgado, and J.L. Santos. *Simultaneous measurement of strain and temperature based on polarization loss properties of are-induced long period gratings*. in *Second European Workshop on Optical Fibre Sensors: Proceedings*: 168-171, 2004.

[30] K.J. Han, Y.W. Lee, J. Kwon, S. Roh, J. Jung, and B. Lee. *Simultaneous measurement of strain and temperature incorporating a long-period fiber grating inscribed on a polarization-maintaining fiber.* IEEE Photonics Technology Letters **16**(9): 2114-2116, 2004.

[31] Y.G. Han, S.B. Lee, C.S. Kim, J.U. Kang, Y. Chung, and U.C. Paek. *Simultaneous measurement of temperature and strain using dual long-period fiber gratings with controlled temperature and strain sensitivities.* Optics Express **11**(5): 476-481, 2003.

[32] W. Jin, W.C. Michie, G. Thursby, M. Konstantaki, and B. Culshaw. *Geometric representation of errors in measurements of strain and temperature.* Optical Engineering **36**(8): 2272-2278, 1997.

[33] W. Jin, W.C. Michie, G. Thursby, M. Konstantaki, and B. Culshaw. *Simultaneous measurement of strain and temperature: Error analysis.* Optical Engineering **36**(2): 598-609, 1997.

[34] H. Patrick, A. Kersey, and F. Bucholtz. *Analysis of the response of long period fiber gratings to external index of refraction.* Journal of Lightwave Technology **16**(9): 1606-1612, 1998.

[35] J.H. Chong, P. Shum, H. Haryono, A. Yohana, M.K. Rao, C. Lu, and Y.N. Zhu. *Measurements of refractive index sensitivity using long-period grating refractometer.* Optics Communications **229**(1-6): 65-69, 2004.

[36] D.A. Pereira, O. Frazão, and J.L. Santos. *Fiber Bragg grating sensing system for simultaneous measurement of salinity and temperature.* Optical Engineering **43**(2): 299-304, 2004.

[37] V. Bhatia and A.M. Vengsarkar. *Optical fiber long-period grating sensors.* Optics Letters **21**(9): 692-694, 1996.

[38] O. Frazão, R. Romero, G. Rego, P.V.S. Marques, H.M. Salgado, and J.L. Santos. *Sampled fibre Bragg grating sensors for simultaneous strain and temperature measurement.* Electronics Letters **38**(14): 693-695, 2002.

[39] J. Albert, M. Fokine, and W. Margullis. *Grating formation in pure silica-core fibers*. in *Proceedings of the Bragg Gratings, Photosensitivity and Poling in Glass Waveguides Conference*: paper BThC9-1, 2001.

[40] K.A. Zagorulko, P.G. Kryukov, Y.V. Larionov, A.A. Rybaltovsky, and E.M. Dianov. *Fabrication of fiber Bragg gratings with 267 nm femtosecond radiation.* Optics Express **12**(24): 5996-6001, 2004.

[41] S.A. Vasiliev, E.M. Dianov, K.M. Golant, O.I. Medvedkov, A.L. Tomashuk, V.I. Karpov, M.V. Grekov, A.S. Kurkov, B. Leconte, and P. Niay. *Performance of Bragg and long-period gratings written in N- and Ge-doped silica fibers under gamma-radiation.* IEEE Transactions on Nuclear Science **45**(3): 1580-1583, 1998.

[42] A.F. Fernandez, B. Brichard, P. Borgermans, F. Berghmans, M. Decreton, P. Megret, M. Blondel, and A. Delchambre. *Fibre Bragg grating temperature sensors for harsh nuclear environments*. in *OFS 2002: 15th Optical Fiber Sensors Conference Technical Digest*: 63-66, 2002.

9

Conclusions

In this thesis the fabrication through electric arc discharges of long-period fibre gratings and their applications in optical communications and sensing fields was presented.

The theoretical background required for the understanding of the formation of long-period fibre gratings was given. The mechanisms that have been proposed in literature for the formation of arc-induced gratings were also discussed. In particular, the effect of stress relaxation was addressed. The tomographic stress profiles of these gratings were recorded for the first time and calculations on the effect of geometrical changes were presented.

The fibre temperature is a key parameter for the understanding of the underlying mechanism responsible for formation of arc-induced gratings. Therefore, two methods to estimate the temperature reached by the fibre whilst being submitted to electric arc discharges were presented. One method is based on the blackbody radiation and the other on electrically insulated thermocouples assembled in situ. Both methods points toward a temperature value in the range of 1300 ºC to 1400 ºC for the typical arc current value of 9 mA used during gratings inscription. The latter technique was submitted to the Portuguese patent institute.

The process of writing long-period gratings using the electric arc technique was described. During this work several setups were implemented in order to improve the fabrication method. In particular, great effort was put in the attempt to increase the reproducibility and flexibility of the technique. The main problem in this task was the stability of the power supply. In any case, several useful fibre optical components were produced by these prototypes, as described in Chapters 8 and 9.

The influence of the fabrication parameters on the characteristics and properties of arc-induced gratings was discussed. It was found that by changing the fabrication parameters it is possible to control the spectra of the gratings, as well as, the resonant wavelengths and transmission loss, but also to modify the sensitivity of the gratings to physical parameters, such as, temperature and strain. This important property of the electric arc technique has not been demonstrated, so far, by any other technique.

The thermal behaviour of the gratings that were fabricated was also investigated. Two main properties were demonstrated. First, arc-induced gratings exhibit high temperature stability. Second, the ones inscribed in Ge-free fibres, in particular, in Er/Al co-doped fibres

show a linear behaviour on temperature up to 700 ºC. These results are extremely important in what concerns sensing of physical parameters from room temperature up to high temperatures.

The effect of gamma radiation on the properties of gratings arc-induced in pure-silica-core fibres was also studied for the first time, and the results obtained enabled one to conclude that those gratings are very promising to perform sensing in radiation environments.

A new technique to mechanically induce long-period fibre gratings was presented. A fully characterisation of the gratings that were actually produced was given. The polarisation dependent loss of these gratings was discussed and a simple birefringence compensation method was studied. Two applications of these gratings were also analysed. One, as an EDFA gain equalizer and the other, as a tunable filter in sensing schemes to interrogate FBGs where the dynamic range of the physical parameters under measurement can vary considerably.

Other devices fabricated with the electric arc technique, such as, phase shifted fibre Bragg gratings and long-period gratings were also briefly discussed. Special attention was given to the apodisation of fibre Bragg gratings and to the fabrication of sampled fibre Bragg gratings, comprising the writing of a fibre Bragg grating on top of an arc-induced long-period grating. These interactions between UV-radiation and arc discharges were investigated for the first time showing interesting results. The fabrication of core mode blockers based on the splicing of short pieces of silica capillaries was also studied. It should be stressed that these blockers are very important for the achievement of bandpass filters relying on two LPFGs.

Finally, several applications of arc-induced gratings in optical communications and sensing were presented. In the former field, the equalization of the gain curve of erbium-doped fibre amplifiers and the suppression of amplified spontaneous emission in Er/Yb fibre lasers was discussed. In the latter, the measurement of the refractive index of the surrounding medium relying on LPFGs induced in pure-silica-core fibres was presented. Several sensor heads able to discriminate between temperature and strain were also developed. A sensor head based on a single long-period grating having two sections fabricated with different parameters deserves specific mention.

The research summarised above gives indications of topics requiring further investigation. In this thesis, a large number of topics were investigated and therefore, some might require in fact a more detailed study. In particular, the improvement of the power supply for the new infrastructure is an important issue, since that will allow the fabrication of more complex optical components. This is also important to carry on further research concerning the apodisation of FBGs and the fabrication of sampled FBGs. In addition, investigation on the interactions between arc-discharges and UV-radiation might also help in the understanding of the former. Specifically, the measurement of the refractive index change

caused by the arc discharges might be achieved using Fabry-Perot cavities or Mach-Zenhder topologies in addition to the information provided by a profilometer. A list of research topics raised within this work and requiring further investigation follows:

- A better control and understanding on the dependence of the sensitivity of the gratings with the fabrication parameters is required. A detailed analysis on the sensitivity of arc-induced gratings to bending, torsion and load is needed.
- More accurate PDL measurements of arc-induced gratings and also the measurement of the PDL of phase-shifted LPFGs is important.
- The knowledge of the formation mechanisms should be pursued.
- In order to understand some of the peculiar spectra of arc-induced LPFGs a closer look on both simulations and theory might be needed.
- Studies on the effects of gamma radiation on arc-induced LPFGs and on FBGs induced by one of the available techniques.

The electric arc technique is a quite new technology and as such, some of the properties of the technique and of the gratings produced only recently have been discovered. Therefore, it is expected that in a near future new devices based on arc discharges will appear. From this work there are several applications of arc-induced gratings that can be anticipated, namely:

- EDFAs gain flattening through the writing of gratings in Er/Al co-doped fibres.
- A temperature sensor based on a phase-shift LPFG written in an Al-doped fibre.
- Bandpass filters to limit LEDs spectra when they are used as the light source of intensity sensor schemes.
- Salinity measurement based on phase-shift LPFGs induced in pure-silica-core fibres.
- The development of a sensor based on a sampled FBG to perform multi-parameter measurement under ionising radiation.
- Finally, long-period grating assisted fibre couplers are very promising devices where the arc discharge technology might play a fundamental role.

Appendices

A. Setups used for LPFGs fabrication

B. Electrodes' polishing

C. Software

D. Patent submitted

A

Setups used for LPFGs fabrication

This appendix describes briefly the five setups that have been used in UOSE to inscribe gratings using the electric arc technique. The first setup was implemented by Oleg Okhtnikov in late 1999. Basically, it consisted of the BICC fusion splicer to produce the arc discharges, a motorized translation stage (MTS) to displace the fibre, a pulley and a X-Y-Z platform to align the fibre. This setup allowed for the manual fabrication of the LPFGs and was not straightforward to align.

A.1 Setup by O. Okhotnikov (2000)

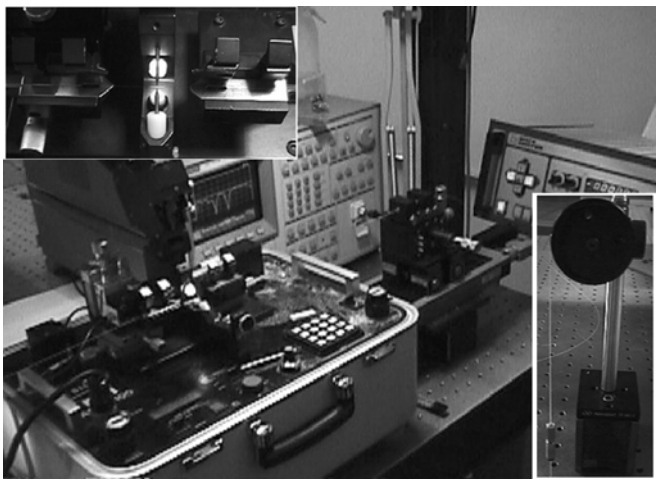

Figure A1 – Photograph of the first setup: manual fabrication process and not straightforward to align.

It was soon realized that the whole process needed to be computer controlled. That required some modifications in the splicer machine, that task was performed by Filipe Pinto and Alberto Maia. Some changes were also made in order to improve the alignment, however the solution found revealed to be mechanically unstable.

A.2 Version2 (2001)

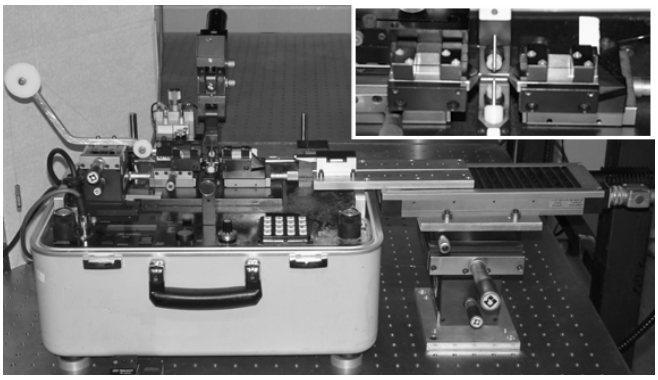

Figure A2 – Photograph of the second setup: computer controlled but mechanically unstable.

The previous drawbacks were overcome by the current setup. The MTS is now on top of two translation and rotation stages that enable a good alignment of the fibre. The main disadvantage of this setup is that it does not allow for changes of the arc parameters in a straightforward way from discharge to discharge limiting the flexibility of the technique.

A.3 Current setup (2002)

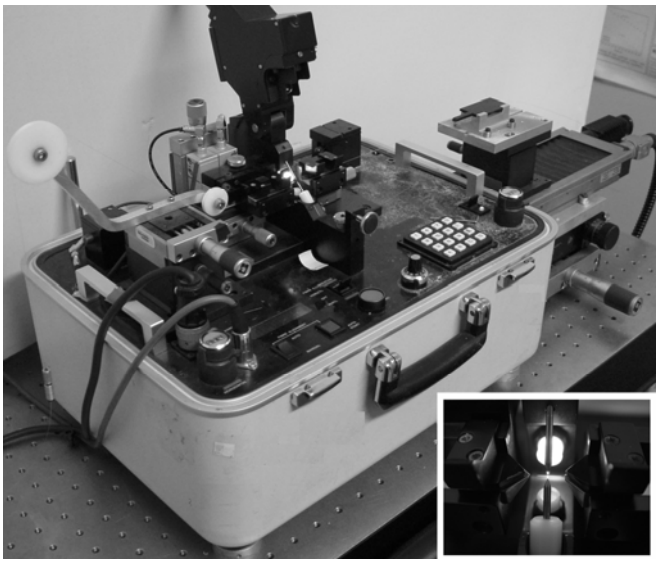

Figure A3 – Photograph of the current setup: not versatile for changes of arc parameters during gratings writing.

In paralel, the search for higher flexibility and reproducibility led us to the development of two prototypes. The first was proposed by Francisco Araújo and was implemented in collaboration with two technicians: Joaquim Cardoso and Ernesto Pinheiro. This machine enabled the fabrication of several useful devices as demonstrated troughout this work. However, the arc exhibited some instability and it was also difficult to align.

A.4 Setup by F. M. Araújo (2001)

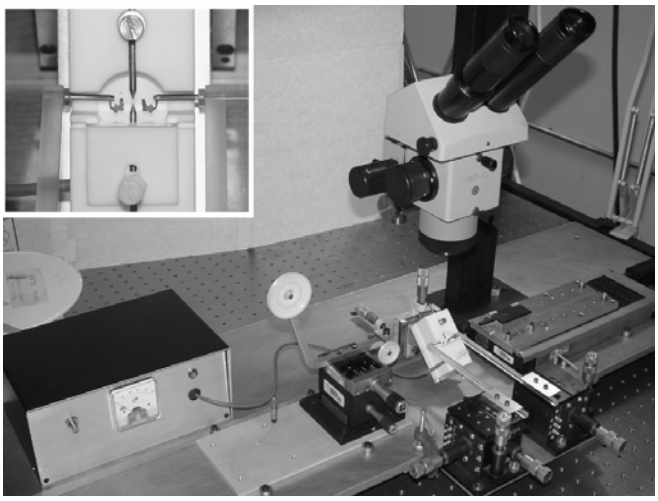

Figure A4 – Photograph of an alternative setup: instability of the arc and difficult to align.

Finally, I have also proposed and implemented a new setup. Its main characteristics are the ease to perform fibre alignment due to the central block that contains two v-groove set the main one being close to the discharge position and identical to the ones used in standard fusion splicers. The different blocks possess the degrees of freedom that enable a correct relative position between the arc discharge and the fibre. The robustness of the four blocks and the amount of metal pieces that had to be designed and fabricated are well patented in the Figure A5. The problem with this setup is again the stability of the power supply despite the several configurations used: DC and AC, with and without rectification. Once solved, this setup will enhance the reproducibility, but mainly, will enable the flexibility that we were headed for.

A.5 New setup (2003)

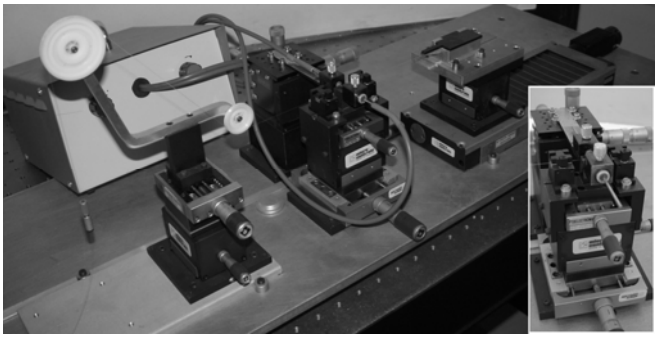

Figure A5 – Photograph of the setup under development: arc discharge unstable.

B

Electrodes' polishing

B.1 Introduction

The electrodes degrade during the arc discharges due to oxidation or to contamination by dust or silica particles that adhere to its tip. Therefore, after some use they need to be replaced. An apparatus to polish the electrodes was developed in our unit by Francisco Carpinteiro. The electrodes are made of 2 mm diameter tungsten rods with a small amount of thorium (2%). They are cut to the required length and the tip angle can be changed from ~20º to ~45º by altering the angle between the electrode and the diamond polishing material. The smaller the angle the higher the energy density and the faster the degradation occurs. Figure B1 shows the machine used to polish the electrodes. The support of the electrodes can be repositioned to define new tip angles. During the polishing both the diamond polisher and the electrodes are rotating.

Figure B1 – Photograph of the electrode's polishing apparatus.

To guarantee smoothness of the electrodes, a final step is performed in which the electrodes, tip and cone, are polished with sandpaper #800 (Figure B2). Prior to their replacement in the splicing machine they are carefully cleaned with alcohol.

Figure B2 – Photograph of the apparatus used in the final step of the polishing process.

C

Software

C.1 LPFGs fabrication using the BICC fusion splicer

Several LabView programs were written, in collaboration with Francisco Araújo, Miguel Melo and in particular with João Ferreira, to control the fabrication of arc-induced gratings using the different setups. The programs allow for the fabrication of simple and more complex LPFGs structures, inclusive for the inscription of multi-gratings and chirped gratings for which the period changes. LabView code was also written for the apodisation of FBGs, to control the tunable laser and a multimeter in the case of the sampled FBGs and for the measurement of the fibre temperature by controlling the fusion splicer and a multimeter. As an example, the code used to control the LPFGs fabrication using the BICC splicer is listed below (subroutines are not included).

Front Panel

Diagrams

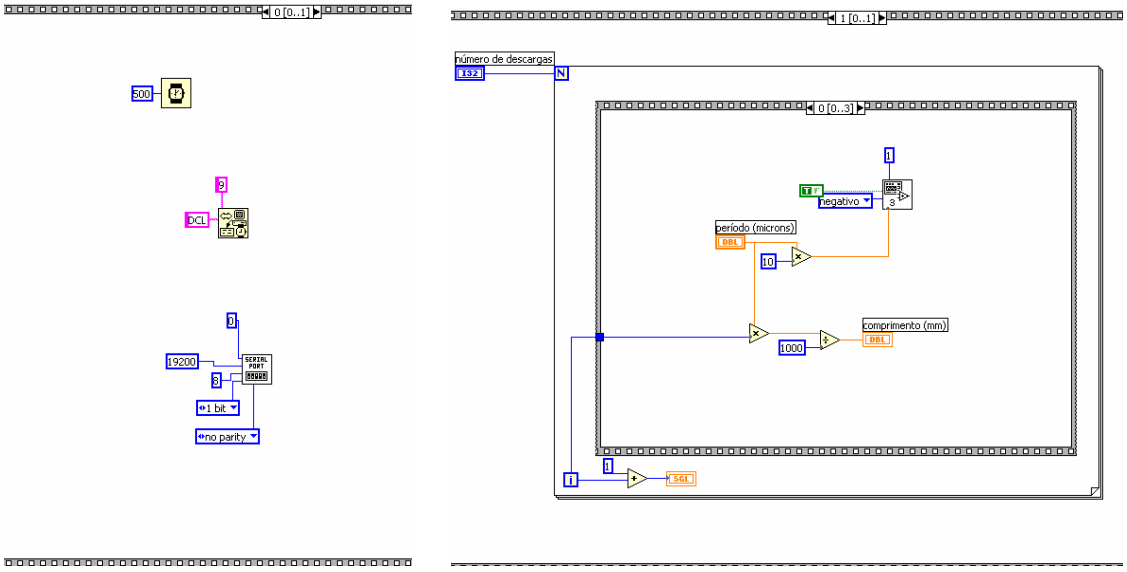

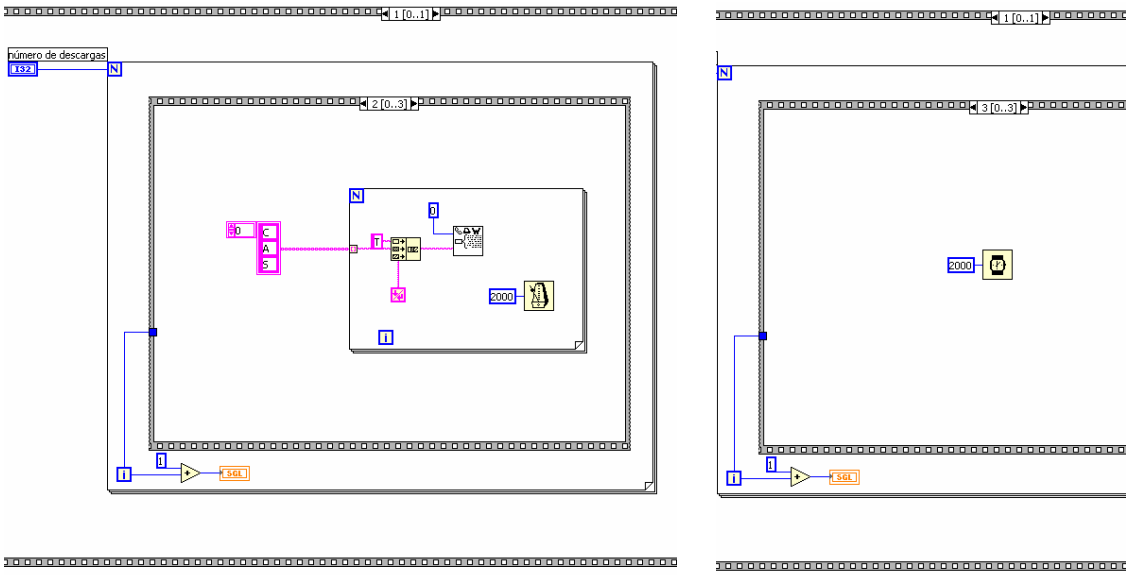

C.2 Estimation of the temperature profile in the fibre

Regarding the determination of the fibre temperature during an arc discharge several software programs were also written. For the measurement based on the blackbody a MatLab program radiation was written to control the Cronin spectrometer (by José Luís Costa). Another MatLab program written in collaboration with Henrique Salgado was used to simulate the temperature profile in the fibre. Finally, for the measurement of the fibre temperature using the thermocouples a program in FlexPDE was written in collaboration with Bernd Schröder and Luís Belchior. This program estimates the temperature profile in the fibre by solving the differential equation involving heat transfer in the system and by fitting the solution to the experimental results obtained for the different thermocouples. The code for the latter is listed below.

```
TITLE   'TC simulation Stationary PDE'
SELECT     errlim=1e-20    nodelimit=8000     ngrid=1
COORDINATES   XCYLINDER(Z,R)
VARIABLES   temp( range=1000)

{flux = -2.45e8; gap = 950um; d0 = 5um; k_air = 0.09; k_Pt = 98.4; k_Pt-Rh = 84.5}

DEFINITIONS
  R0=12.5e-6    R1=25e-6    R2=28e-6   R3=62.5e-6 R4=475.0e-6  Lz=1e-2    k=91.5   d0=5.0e-6
vx=1     h=0
          { Velocity }
  heat=0     tempi=1000  tempa=0 tempb=0   t0=4.998e-3
  fluxd_x=-k*dz(temp)     fluxd_y=-k*dr(temp)
  fluxd=vector( fluxd_x, fluxd_y)     fluxdm=magnitude( fluxd)
  fluxd0= -2.45e8*[ ustep( vx*t0+d0- z)- ustep( vx*t0- z) ]

s = 5.67E-8   e = 1.9*exp(-temp/552)+0.056
hair = 55.91+0.3249*((temp+300.0)/2.0)-1.164e-4*((temp+300.0)/2.0)^2

temp_Pt =   479.6 + (2*2.23942/Pi)*1.89e-3/(4*(z- Lz/2)^2+(1.89e-3)^2)
temp_Pt1 = 500.0 + (2*1.90168/Pi)*1.65e-3/(4*(z- Lz/2)^2+(1.65e-3)^2)


EQUATIONS
   div( fluxd)=heat

BOUNDARIES
region 'domain'
start (0,0)  natural(temp)=0
   line to (Lz,0)
value(temp)=300
   line to (Lz,R4)
natural(temp)=hair*(temp-300) + s*e*(temp^4 - 300^4)
   line to (Lz/2+d0/2,R4)
natural(temp)=fluxd0 line to (Lz/2-d0/2,R4)
natural(temp)=hair*(temp-300) + s*e*(temp^4 - 300^4) line to (0,R4)
value(temp)=300
   line to finish
{
region 'air gap2' k=3.84e-3+7.66e-5*temp-1.54e-8*temp^2
start (0,R3)   line to (Lz,R3)
   line to (Lz,R4)
   line to (0, R4)
   line to finish
}
region 'fiber' k = 0.78-0.054*exp((temp+379)/354)+0.165*exp((temp+379)/405)
{region 'fiber' k = 5.17}

start (0,R2)    line to (Lz,R2)
   line to (Lz,R3)
   line to (0, R3)
   line to finish

region 'air gap1' k=3.84e-3+7.66e-5*temp-1.54e-8*temp^2
{region 'air gap1' k=0.078}
start (0,R1)   line to (Lz,R1)
```

```
   line to (Lz,R2)
   line to (0, R2)
   line to finish

region 'air gap2' k=0.09
start (0,R3)   line to (Lz,R3)
   line to (Lz,R4)
   line to (0, R4)
   line to finish

region 'Pt' k=98.4
start (0,0)   line to (Lz/2,0)
   line to (Lz/2,R1)
   line to (0, R1)
   line to finish

region 'Pt_PtRh' k=84.5
start (Lz/2,0)   line to (Lz,0)
   line to (Lz, R1)
   line to (Lz/2, R1)
   line to finish


PLOTS

elevation( temp,temp_Pt,temp_Pt1) from (4e-3,R1) to (6e-3,R1)
elevation( temp,temp_Pt,temp_Pt1) from (0,R1) to (Lz,R1)

elevation( temp) from (4e-3,R2) to (6e-3,R2)
elevation( temp) from (4e-3,R3) to (6e-3,R3)
elevation( temp) from (0,R3) to (Lz,R3)

contour( temp) painted  zoom (4.0e-3,0, 2.0e-3,R4)
surface( temp)     vector( fluxd) norm
grid(z,r)
grid(z,r) zoom (4.0e-3,0, 2.0e-3,R4)
vector( fluxd) norm zoom (3.0e-3,0, 4.0e-3,R4)
elevation( temp,temp_Pt) from (2e-3,R1) to (8e-3,R1)

elevation( -normal(fluxd)) from (4e-3,R4) to (6e-3,R4)
elevation( -normal(fluxd)) from (0,0) to (0,R3)

END 23847
```

D

Patent submitted

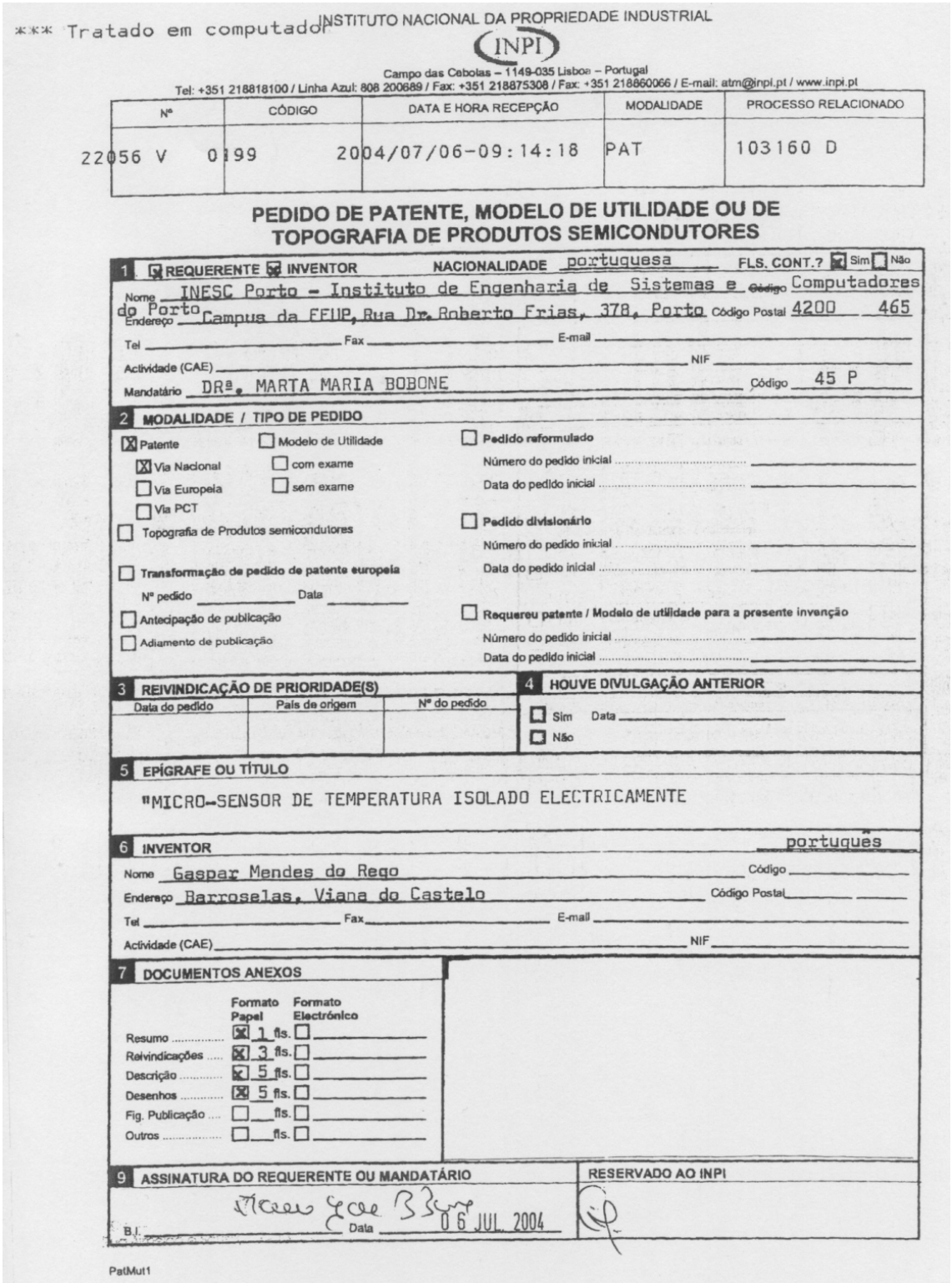

*** Tratado em computador

INSTITUTO NACIONAL DA PROPRIEDADE INDUSTRIAL

INPI

Campo das Cebolas – 1149-035 Lisboa – Portugal

Tel: +351 218818100 / Linha Azul: 808 200689 / Fax: +351 218875308 / Fax: +351 218860066 / E-mail: atm@inpi.pt / www.inpi.pt

Nº	CÓDIGO	DATA E HORA RECEPÇÃO	MODALIDADE	PROCESSO RELACIONADO
22056 V 0199		2004/07/06-09:14:18	PAT	103160 D

PEDIDO DE PATENTE, MODELO DE UTILIDADE OU DE TOPOGRAFIA DE PRODUTOS SEMICONDUTORES

1 ☒ REQUERENTE ☒ INVENTOR NACIONALIDADE portuguesa FLS. CONT.? ☒ Sim ☐ Não

Nome INESC Porto - Instituto de Engenharia de Sistemas e Computadores do Porto Código

Endereço Campus da FEUP, Rua Dr. Roberto Frias, 378, Porto Código Postal 4200 465

Tel ____ Fax ____ E-mail ____

Actividade (CAE) ____ NIF ____

Mandatário DRª. MARTA MARIA BOBONE Código 45 P

2 MODALIDADE / TIPO DE PEDIDO

☒ Patente ☐ Modelo de Utilidade

☒ Via Nacional ☐ com exame

☐ Via Europeia ☐ sem exame

☐ Via PCT

☐ Topografia de Produtos semicondutores

☐ **Transformação de pedido de patente europeia**

Nº pedido ____ Data ____

☐ Antecipação de publicação

☐ Adiamento de publicação

☐ **Pedido reformulado**

Número do pedido inicial ____

Data do pedido inicial ____

☐ **Pedido divisionário**

Número do pedido inicial ____

Data do pedido inicial ____

☐ **Requereu patente / Modelo de utilidade para a presente invenção**

Número do pedido inicial ____

Data do pedido inicial ____

3 REIVINDICAÇÃO DE PRIORIDADE(S)

Data do pedido	País de origem	Nº do pedido

4 HOUVE DIVULGAÇÃO ANTERIOR

☐ Sim Data ____

☐ Não

5 EPÍGRAFE OU TÍTULO

"MICRO-SENSOR DE TEMPERATURA ISOLADO ELECTRICAMENTE

6 INVENTOR português

Nome Gaspar Mendes do Rego Código ____

Endereço Barroselas, Viana do Castelo Código Postal ____

Tel ____ Fax ____ E-mail ____

Actividade (CAE) ____ NIF ____

7 DOCUMENTOS ANEXOS

	Formato Papel	Formato Electrónico
Resumo	☒ 1 fls.	☐
Reivindicações	☒ 3 fls.	☐
Descrição	☒ 5 fls.	☐
Desenhos	☒ 5 fls.	☐
Fig. Publicação	☐ fls.	☐
Outros	☐ fls.	☐

9 ASSINATURA DO REQUERENTE OU MANDATÁRIO

B.I. ____ Data 06 JUL. 2004

RESERVADO AO INPI

PatMut1

INSTITUTO NACIONAL DA PROPRIEDADE INDUSTRIAL

*** Tratado em computador

Campo das Cebolas – 1149-035 Lisboa – Portugal
Tel: +351 218818100 / Linha Azul: 808 200689 / Fax: +351 218875308 / Fax: +351 218860066 / E-mail: atm@inpi.pt / www.inpi.pt

Nº	CÓDIGO	DATA E HORA RECEPÇÃO	MODALIDADE	PROCESSO RELACIONADO
22056 V	0199	2004/07/06-09:14:18	PAT	103160 D

FOLHA DE CONTINUAÇÃO PARA REQUERENTES E/OU INVENTORES

1 ☑ REQUERENTE ☐ INVENTOR — NACIONALIDADE portuguesa

Nome Escola Superior de Tecnologia e Gestão, Instituto ~~Código~~ Politécnico de Viana do Castelo

Endereço Av. do Atlântico, Viana do Castelo Código Postal 4900 348

Tel ____ Fax ____ E-mail ____

Actividade (CAE) ____ NIF ____

2 ☐ REQUERENTE ☑ INVENTOR — NACIONALIDADE português

Nome Luis Manuel das Neves Belchior Faia dos Santos Código ____

Endereço Porto Código Postal ____

Tel ____ Fax ____ E-mail ____

Actividade (CAE) ____ NIF ____

3 ☐ REQUERENTE ☑ INVENTOR — NACIONALIDADE alemão

Nome Bernd Schroder Código ____

Endereço Porto Código Postal ____

Tel ____ Fax ____ E-mail ____

Actividade (CAE) ____ NIF ____

4 ☐ REQUERENTE ☑ INVENTOR — NACIONALIDADE português

Nome Paulo Vicente da Silva Marques Código ____

Endereço Valongo Código Postal ____

Tel ____ Fax ____ E-mail ____

Actividade (CAE) ____ NIF ____

5 ☐ REQUERENTE ☑ INVENTOR — NACIONALIDADE português

Nome Henrique Manuel de Castro Faria Salgado Código ____

Endereço Porto Código Postal ____

Tel ____ Fax ____ E-mail ____

Actividade (CAE) ____ NIF ____

6 ASSINATURA DO REQUERENTE OU MANDATÁRIO

06 JUL. 2004

B.I. ____ Data ____

RESERVADO AO INPI

INSTITUTO NACIONAL DA PROPRIEDADE INDUSTRIAL

*** Tratado em computador

Campo das Cebolas – 1149-035 Lisboa – Portugal
Tel: +351 218818100 / Linha Azul: 808 200689 / Fax: +351 218875308 / Fax: +351 218860066 / E-mail: atm@inpi.pt / www.inpi.pt

Nº	CÓDIGO	DATA E HORA RECEPÇÃO	MODALIDADE	PROCESSO RELACIONADO
22056 V	0199	2004/07/06-09:14:18	PAT	103160 D

FOLHA DE CONTINUAÇÃO PARA REQUERENTES E/OU INVENTORES

1 ☐ REQUERENTE ☒ INVENTOR — NACIONALIDADE portuguêS

Nome José Luis Campos de Oliveira Santos — Código

Endereço Vila do Conde — Código Postal

Tel — Fax — E-mail

Actividade (CAE) — NIF

2 ☐ REQUERENTE ☐ INVENTOR — NACIONALIDADE

Nome — Código

Endereço — Código Postal

Tel — Fax — E-mail

Actividade (CAE) — NIF

3 ☐ REQUERENTE ☐ INVENTOR — NACIONALIDADE

Nome — Código

Endereço — Código Postal

Tel — Fax — E-mail

Actividade (CAE) — NIF

4 ☐ REQUERENTE ☐ INVENTOR — NACIONALIDADE

Nome — Código

Endereço — Código Postal

Tel — Fax — E-mail

Actividade (CAE) — NIF

5 ☐ REQUERENTE ☐ INVENTOR — NACIONALIDADE

Nome — Código

Endereço — Código Postal

Tel — Fax — E-mail

Actividade (CAE) — NIF

6 ASSINATURA DO REQUERENTE OU MANDATÁRIO

B.I. — Data 06 JUL. 2004

RESERVADO AO INPI

RESUMO

MICRO-SENSOR DE TEMPERATURA ISOLADO ELECTRICAMENTE

A presente invenção descreve a fabricação de um micro-sensor de temperatura isolado electricamente, de dimensões reduzidas. O dispositivo é apresentado em duas configurações distintas. Na primeira, o termopar (1) é fabricado no interior de um capilar de sílica (2) por aplicação de descargas eléctricas (3) na região onde ocorre o contacto (4) topo-a-topo dos dois fios metálicos. A segunda configuração permite a fabricação prévia do termopar (5), pela técnica do contacto adjacente dos dois fios metálicos, antes deste ser inserido numa estrutura em sílica contendo dois ou mais orifícios, como por exemplo, numa *Twin-Hole-Fiber* (6). A extremidade contendo a junção do termopar é posteriormente selada por aplicação de calor, por meio de uma chama, ou descarga eléctrica ou outra. As configurações apresentadas, após calibração do respectivo termopar e posterior tratamento dos dados relativos às transferências de calor no sistema, permitem, entre outras aplicações, a medição de temperatura em sistemas de dimensões reduzidas e em sistemas em que exista um elevado gradiente de temperatura, como na medição da temperatura de amostras enquanto submetidas a descargas eléctricas.

REQUERENTES

INESC Porto, Instituto de Engenharia de Sistemas e Computadores do Porto, Instituição Portuguesa, com sede no Campus da FEUP, Rua Dr. Roberto Frias, nº 378, 4200-465 Porto.

Escola Superior de Tecnologia e Gestão, Instituto Politécnico de Viana de Castelo, Instituição Portuguesa, Av. do Atlântico, 4900-348 Viana do Castelo

AUTORES

Gaspar Mendes do Rego, Português, residente em Barroselas, Viana do Castelo. Luís Manuel das Neves Belchior Faia dos Santos, Português, residente no Porto. Bernd Schröder, Alemão, residente no Porto. Paulo Vicente da Silva Marques, Português, residente em Valongo. Henrique Manuel de Castro Faria Salgado, Português, residente no Porto. José Luís Campos de Oliveira Santos, Português, residente em Mindelo, Vila do Conde.

EPÍGRAFE

MICRO-SENSOR DE TEMPERATURA ISOLADO ELECTRICAMENTE

DESCRIÇÃO

MICRO-SENSOR DE TEMPERATURA ISOLADO ELECTRICAMENTE

Campo de Invenção

A presente invenção insere-se na área da instrumentação e medidas e diz respeito à realização de um sensor de temperatura isolado electricamente e de dimensões micrométricas. O sensor de temperatura compreende um termopar fabricado por aplicação de descargas eléctricas na zona de contacto dos fios metálicos, inseridos previamente num capilar de sílica.

Antecedentes de Investigação

A razão da presente invenção prende-se com a necessidade de determinar a temperatura de uma fibra óptica quando submetida a uma descarga eléctrica. Refira-se que a temperatura é um parâmetro importante na fabricação de dispositivos passivos em fibra óptica, nomeadamente, redes de período longo, qualquer que seja a técnica utilizada. No caso da técnica do arco eléctrico, a impossibilidade de utilização de um termopar sem isolamento eléctrico e cujas dimensões permitam a preservação das condições de descarga conduziram à fabricação do termopar no interior de um capilar de sílica, com

dimensões semelhantes às de uma fibra óptica cujo material predominante é também a sílica. Note-se que a fabricação de um termopar, que satisfaça os requisitos anteriores, por qualquer uma das técnicas conhecidas é extremamente difícil.

Estado da técnica

Os autores não encontraram nenhuma referência bibliográfica ou patente que descreva o sensor de temperatura proposto.

A presente invenção consiste num sensor micrométrico isolado electricamente que permite a medição da temperatura e/ou a sua distribuição em objectos de dimensões reduzidas sujeitos a temperaturas elevadas.

Descrição Sumária da invenção

A Figura 1 representa o micro-sensor de temperatura, o qual é fabricado aplicando descargas eléctricas (3) na região de contacto (4) entre os dois fios que formam o termopar (1) e que foram inseridos previamente num capilar de sílica (2).

A Figura 2 representa o termopar (5) numa configuração mais comum inserido numa *Twin-Hole-Fiber* (6) que lhe confere o isolamento eléctrico.

A Figura 3 mostra a resposta do sensor de temperatura a uma descarga eléctrica efectuada na junção do termopar (4) (de menor intensidade do que as utilizadas na sua própria fabricação).

A figura 4 mostra a distribuição axial de temperatura no termopar, obtida efectuando descargas eléctricas ao longo do termopar em ambos os lados da junção.

A figura 5 mostra o perfil de temperatura no capilar calculado com base na resolução das equações referentes às transferências de calor envolvidas no sistema arco/termopar/capilar.

Descrição Sumária das Figuras

Figura 1 – A Figura 1 representa o termopar fabricado no interior de um capilar de sílica.

Figura 2 - A Figura 2 representa o termopar, numa configuração standard, inserido numa *Twin-Hole-Fiber*.

Figura 3 - A Figura 3 mostra a evolução temporal da tensão no termopar correspondente a uma descarga eléctrica efectuada sobre a respectiva junção.

Figura 4 - A Figura 4 mostra a distribuição longitudinal de temperatura registada pelo termopar referenciada à posição zero onde se efectua a descarga.

Figura 5 - A Figura 5 mostra o perfil longitudinal de temperatura no capilar (referenciada à posição zero onde se efectua a descarga).

Descrição Detalhada

A Figura 1 apresenta o esquema do micro-sensor de temperatura cuja fabricação consiste na introdução dos fios do termopar (1) num capilar em sílica (2) e posterior aplicação de descargas eléctricas (3) na zona de contacto (4) entre os dois fios metálicos a fim de se produzir a fusão localizada dos dois materiais. É possível fabricar o termopar antes de o introduzir no capilar desde que as dimensões da junção do termopar sejam inferiores às do diâmetro interno do capilar. Se se pretender mapear termicamente e em tempo real uma superfície, plana ou curva, é possível recorrer ao agrupamento de vários destes sensores ou mesmo inseri-los individualmente numa estrutura contendo diversos orifícios, por forma a garantir uma geometria compatível com a superfície alvo de medição.

A Figura 2 mostra um termopar numa configuração clássica, com controlo das dimensões da respectiva junção, que foi introduzido numa *Twin-Hole-fiber* após remoção do material existente entre os dois orifícios. Posteriormente, procedeu-se ao isolamento eléctrico do termopar aplicando descargas eléctricas na extremidade da fibra provocando a sua fusão e o respectivo colapso local dos dois capilares. Este tipo de fibra tem dimensões típicas da ordem dos 400 micrómetros de diâmetro e possui dois orifícios com diâmetros entre 100 a 150 micrómetros. Por conseguinte, o sensor de temperatura resultante tem dimensões superiores ao da figura 1, sendo no entanto mecanicamente mais robusto. Relativamente ao mapeamento térmico de superfícies, esta configuração permite igualmente essa possibilidade quer por agrupamento de vários sensores quer por inserção dos termopares em orifícios (dois orifícios por termopar) existentes numa estrutura em sílica apropriada.

A Figura 3 mostra o resultado de se submeter o termopar isolado, representado na figura 1, a uma descarga eléctrica de 9 miliamperes efectuada sobre a junção e com a duração de 3 segundos. O termopar utilizado é do tipo S e os fios de platina e de platina (90%)/ródio(10%) que o constituem possuem um diâmetro de 50 micrómetros. O capilar de sílica, que confere o isolamento eléctrico, tem dimensões internas e externas de 56 e 125 micrómetros, respectivamente. Atendendo aos resultados obtidos verifica-se que neste sistema o tempo de resposta é inferior a 1 segundo.

A Figura 4 mostra a distribuição de temperatura ao longo de um termopar do tipo S, cujos fios possuem um diâmetro de 25 micrómetros, resultante da aplicação de descargas eléctricas, de 9 miliamperes durante 3 segundos, em diferentes posições axiais do termopar em ambos os lados da junção. A tensão registada foi posteriormente convertida para temperatura usando a função de referência para os termopares do tipo S baseados nas normas ITS-90 [G. W. Burns et al. (1993) "*Temperature-Electromotive Force Reference Functions and Tables for the Letter-Designated Thermocouple Types Based on the ITS-90*", NIST Monograph 175].

Na Figura 5 está representado o perfil de temperatura no capilar de 56/125 micrómetros, obtido numericamente por resolução de um modelo de transferência de calor em que se faz uso dos resultados experimentais referentes ao termopar do tipo S e apresentados na Figura 4.

Os micro-sensores de temperatura isolados electricamente nas diferentes configurações apresentadas permitem a medição da temperatura do material que confere o isolamento eléctrico quando sujeito a uma descarga eléctrica. Esta medição permite inferir o valor da temperatura em materiais maciços como seja a situação de uma fibra óptica. O procedimento é ainda extensível ao caso do aquecimento do material ser efectuado por outras fontes de energia, como por exemplo via radiação laser.

Na área das comunicações ópticas, e em particular, nas máquinas de fusão de fibras ópticas, estes sistemas de medida permitem igualmente uma calibração universal destas unidades recorrendo ao parâmetro temperatura e não ao parâmetro corrente eléctrica, que é actualmente usada e que tem como grande desvantagem, entre outros factores, a dependência na configuração dos eléctrodos, onde ocorre a descarga eléctrica.

De uma forma geral estes sensores isolados electricamente têm dimensões reduzidas (podendo ser inferiores a um décimo de milímetro) e permitem a medição numa gama

alargada de temperaturas, pelo que o campo de aplicações apresenta-se transversal às várias áreas da ciência e da tecnologia.

REIVINDICAÇÕES

1. Micro-sensor de temperatura isolado electricamente, caracterizado por ser constituído por um termopar (1 ou 5) consistindo em dois fios metálicos, com junção topo a topo, dispostos axialmente no interior de uma estrutura em sílica (2) ou de outro material dieléctrico apropriado; ou consistindo em dois fios metálicos adjacentes (configuração clássica) inseridos numa *Twin-Hole-Fiber* (6).

2. Micro-sensor de temperatura isolado electricamente, de acordo com a reivindicação 1, caracterizado por ser constituído por um termopar (1) fabricado por aplicação de descargas eléctricas (3) na zona de contacto topo a topo (4) dos fios metálicos, previamente inseridos num capilar de sílica (2).

3. Micro-sensor de temperatura isolado electricamente, de acordo com a reivindicação 1, caracterizado por ser constituído por um termopar (5) fabricado por aplicação de descargas eléctricas na zona de contacto adjacente dos fios metálicos, previamente inseridos numa *Twin-Hole-Fiber* (6).

4. Micro-sensor de temperatura isolado electricamente, de acordo com as reivindicações 1 a 3, caracterizado por ser constituído por vários termopares inseridos numa estrutura em sílica com diversos orifícios.

5. Micro-sensor de temperatura isolado electricamente, de acordo com as reivindicações 1 a 4, caracterizado por permitir o agrupamento de vários sensores.

6. Micro-sensor de temperatura isolado electricamente, de acordo com as reivindicações 1 a 5, caracterizado por permitir a medição da temperatura desde

temperaturas criogénicas até uma temperatura que em princípio será superior a 1500 ºC e cuja limitação será imposta pelo material do termopar (e.g. calibração e/ou ponto de fusão) ou do seu encapsulamento (ponto de fusão/amolecimento).

7. Micro-sensor de temperatura isolado electricamente, de acordo com as reivindicações 1 a 6, caracterizado por permitir a medição da temperatura ou a sua distribuição numa escala micrométrica.

8. Micro-sensor de temperatura isolado electricamente, de acordo com as reivindicações 1 a 7, caracterizado por permitir a medição da temperatura de uma fibra óptica enquanto submetida a uma descarga eléctrica.

9. Micro-sensor de temperatura isolado electricamente, de acordo com as reivindicações 1 a 7, caracterizado por permitir a medição da temperatura de uma fibra óptica enquanto submetida a radiação proveniente de qualquer tipo de laser.

10. Micro-sensor de temperatura isolado electricamente, de acordo com as reivindicações 1 a 7, caracterizado pelo facto de permitir o ajuste dos parâmetros que controlam a descarga eléctrica de uma máquina de fusão de fibras ópticas (calibração universal).

FIGURAS

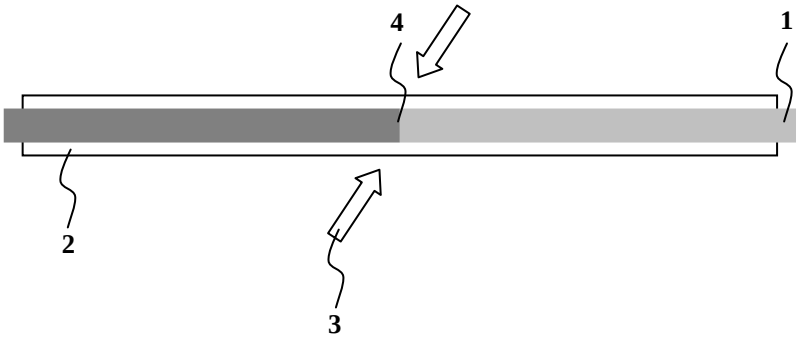

Figura 1

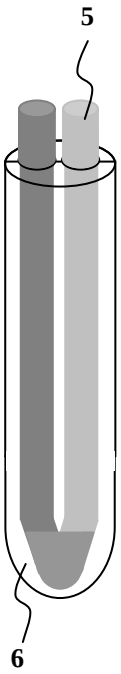

Figura 2

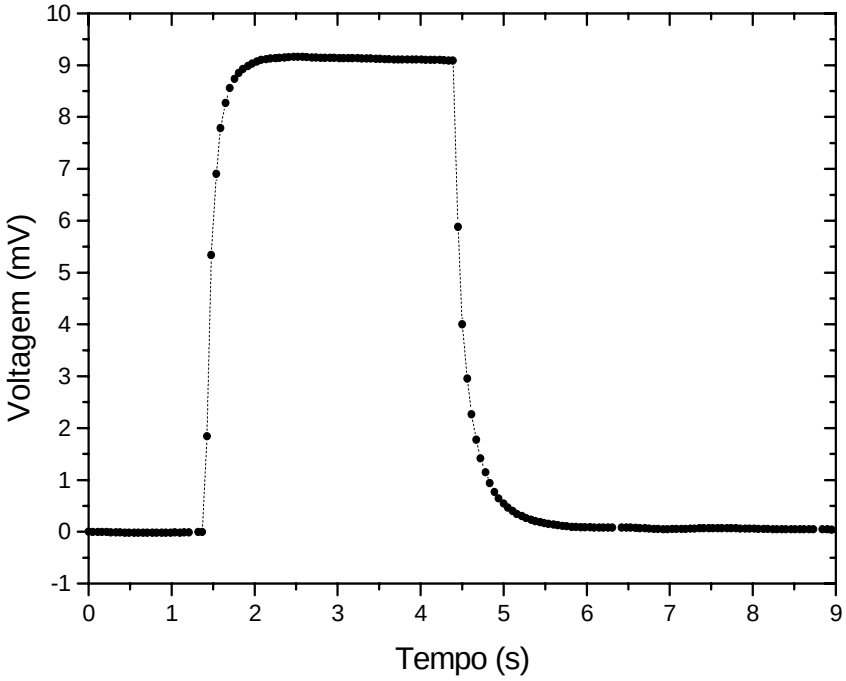

Figura 3

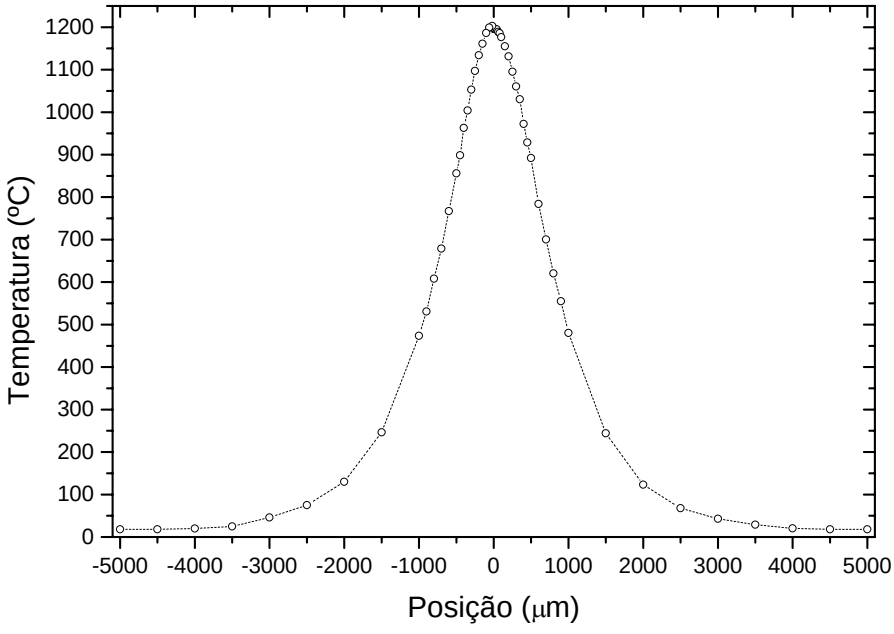

Figura 4

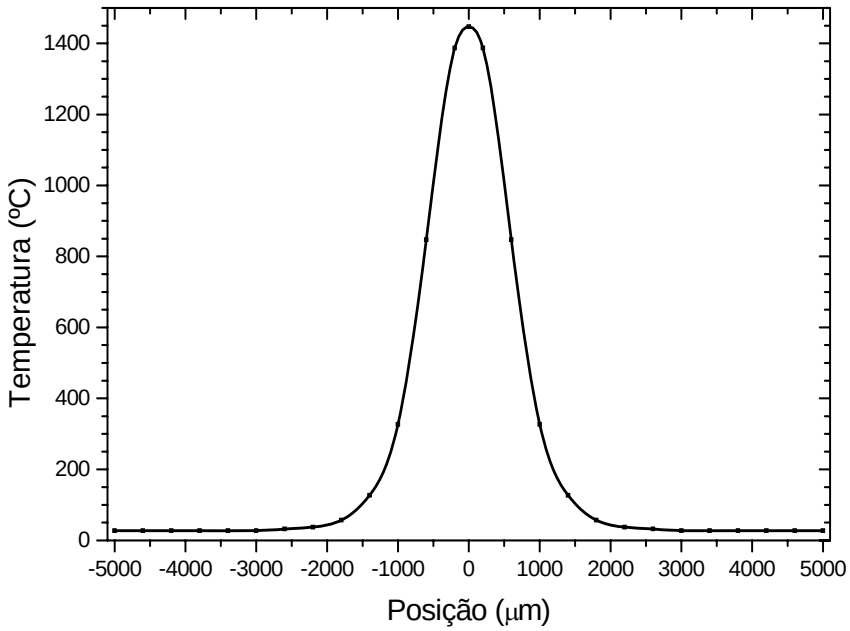
Temperatura (ºC)
1400
1200
1000
800
600
400
200
0
-5000
-4000
-3000
-2000
-1000
0
1000
2000
3000
4000
5000
Posição (μm)

Figura 5